The Influence of African Easterly Waves on Atlantic Tropical Cyclone Activity

Erica M. Staehling

A Dissertation
Presented to the Faculty
of Princeton University
in Candidacy for the Degree
of Doctor of Philosophy

Recommended for Acceptance
by the Program in
Atmospheric and Oceanic Sciences
Advisor: Isaac M. Held

January 2015

Abstract

A high-resolution global atmospheric model is used to disentangle the relationship between African easterly waves (AEWs) and Atlantic tropical storms (TCs) from the large-scale environmental factors that may obscure their connection. Since the two most cited references on AEW interannual variability in relation to TC activity draw conflicting conclusions about the historical relationship, and the AEW counts in each study do not show agreement on historical variability, novel analysis procedures are developed to produce consistent AEW and TC count statistics for the historical record using reanalysis products. This reanalysis-derived historical record is used to legitimize the model for the study of AEWs, which is subsequently utilized to investigate the relationship between AEWs and TCs.

The internal variability of the relationship between AEW and TC count, including the sensitivity to ENSO phase and annual trends, and the interplay between environmental factors, AEW activity, and TC activity are probed using three sets of simulations: 1) climatological simulations, consisting of three ensemble members forced with historical seasonally and annually varying SST; 2) simulations with interannually invariant forcing, including a control simulation with climatological mean SST and a perpetual La Niña simulation with composite SST from strong La Niña years; 3) perturbed simulations, in which the large-scale environment is drastically altered through the manipulation of African albedo.

Since variability exists in AEW count that is unexplained by known indicators of large-scale environmental favorability, across all simulations and multiple timescales, it is unlikely that the ubiquitous covariance between AEW and TC count is simply a response to environmental factors. The statistically significant correlations between AEW and TC statistics suggest that AEW variability accounts for a portion of the observed variability in TC count not due to known environmental factors, since there is unexplained variance in AEW count, and both individual years and aggregated

model runs with more (fewer) AEWs also tend to have more (fewer) TCs. It is argued that while half of the covariance between AEW and TC count interannually is mediated by the large-scale environment, the other half can be attributed to stochastic AEW variability.

Acknowledgements

Well, it was a long and winding road, but here we are. I would like to thank...

The usual suspects: my advisor, **Isaac Held**; my dissertation committee members, **Stephan Fueglistaler**, **Stephen Garner**, and **Robert Hart**. This dissertation benefited greatly from your collective guidance and expertise, it has truly been an honor to work with you all. Also, special thanks to **Ming Zhao** and **Sergey Malyshev**, for their practical help with the numerical modeling.

The Princeton AOS faculty, especially **Sonya Legg**, for convincing me to persevere, and **Anand Gnanadesikan**, for being a valuable committee member during the semester of my general exam (and unrelatedly, for prompting me to exchange phone numbers with my now husband, way back when in 2007). Also the Princeton AOS students with whom I overlapped, especially **Amanda O'Rourke**, **Lauren Padilla**, and **Peng Xie**, who are wonderful friends, officemates, and scientists.

All of my mentors, past and present. The Bucknell Physics Department, especially my undergraduate academic advisor, **Martin Ligare**, for supporting my education and encouraging me to pursue graduate studies. My undergraduate research advisor and friend, **James Cho**, who made me the scientist I am today and has provided ongoing support and encouragement. My current supervisor, **Ellen Granger**, for allowing me the flexibility to complete my dissertation, from research topic selection in 2012 to writing these acknowledgements, all while working full-time in the Office of Science Teaching Activities at the Florida State University.

My counselors, formal and informal. **Suraiya Baluch**, for helping me be a survivor in difficult circumstances. Life coach extraordinaire, fellow activite, and friend, **Barbara Shoplock**. My close friends and fellow scientists, **Melisa Yashinski**, **Elaine Pranski**, and **Sarah Strazzo**. And who rescued whom, **Chloe (Staehling) Truchelut**? I never would have made it through year three without my loyal canine companion Chloe and her inexhaustible zest for life.

Finally, all of my big crazy family, but especially my parents, **Pete Staehling** and **Susan (Kahl) Staehling**. Thank you for raising me to think critically and make my own decisions, and for being supportive along the way. Last, but certainly not least... my synoptic meteorology consultant, live-in copy editor, and ever-zany husband, **Ryan Truchelut**, who was always there to remind me to follow my HEART. Thank you for being my "life partner" in the truest sense of the term, through this and everything. I cannot wait to see where the next phase takes us and what new adventures are in store. Awkward and upward!

This dissertation is dedicated to

Esther Helen Studier Staehling

February 7, 1916 - September 20, 2013

Table of Contents

Chapter 1

Introduction

1.1 Motivation

Most hurricane damage in the United States is owed to the rare and often difficult to predict events in which high intensity tropical cyclones (TCs) make landfall (Landsea, 1993; Emanuel, 2011). While much of the year-to-year variance in total hurricane activity can be anticipated given adequate information about the large-scale environment (Emanuel et al., 2008; Knutson et al., 2007), storm intensity, duration, frequency, and thus destructive potential varies with genesis location (Kossin et al., 2010). Kossin et al. (2010) found that storms that form in the region sensitive to African Easterly Wave (AEW) fluctuations tend to be very intense, long-lived, and destructive, so there is cause to believe that AEW-spawned tropical storms are of special import to the United States.

Avila et al. (2000) separated "African years" from "non-African years" based on the percentage of storms that originated from AEWs for the 30-year period from 1967-1997 and found that the destructive potential of storms is larger for African than non-African years. Furthermore, Landsea (1993) found that over 80% of intense hurricanes originate from AEWs, compared to 60% of tropical storms and moderate hurricanes. Unfortunately, AEW variability is poorly understood and the extent to which AEW variability impacts hurricane activity is debated in the literature, as some

authors have suggested a correlation exists between AEW activity and Atlantic TC activity (Thorncroft and Hodges, 2001; Frank and Roundy, 2006; Hopsch et al., 2007; Belanger et al., 2010), while others found little to no independent correlation (Avila et al., 2000; Goldenberg et al., 2001; Caron and Jones, 2011).

This dissertation does not attempt to predict AEW variability or to understand the mechanisms of tropical cyclogenesis, but instead focuses on constraining the extent to which the nature of Atlantic TC activity is dependent on the variability of AEWs. Others have tried to address this issue, but previous attempts have been restricted to historical analyses, reanalyses, or limited regional modeling studies, and have been unable to cleanly disentangle the relationship between AEWs and TCs from the large-scale environmental factors that often obscure the role of AEWs (see Section 1.2.2). With the recent developments in high resolution atmospheric models producing reliable TC simulations (see Sections 1.2.3), it is now possible to 1) establish previously unavailable information on the internal atmospheric variability of the AEW-TC relationship by comparing multiple model realizations with observed sea surface temperature (SST) used as the lower boundary condition, 2) remove annual SST variations to explore the sensitivity of AEW and TC activity to altered seasonally-varying SST, and 3) perturb the large-scale environment beyond the realm of the present day climate to examine the relationship between the environment, AEW activity, and TC activity. In order to understand whether TCs and AEWs simply respond to the same large-scale environmental factors or AEWs take a more active role in TC variability, this work endeavors to isolate and examine the importance of AEW activity using a TC-permitting global atmospheric model.

1.2 Past Work

This section reviews relevant past literature, beginning with what is known about AEWs themselves, including their observed characteristics as well as the current understanding of their dynamics (Section 1.2.1). Next, past works exploring the potential connections (or lack of connection) between Africa, AEWs, and TCs are considered (Section 1.2.2). This is followed by an overview of TC-permitting models (Section 1.2.3), beginning with a discussion of the strengths and limitations of high-resolution atmosphere-only models in general, and then highlighting successful past studies of TCs using the National Oceanic and Atmospheric Administration's (NOAA) Geophysical Fluid Dynamics Laboratory's (GFDL) High Resolution Atmospheric Model (HiRAM).

1.2.1 Properties and Variability of AEWs

African Easterly Wave Characteristics

The characteristics of AEWs have been examined with a variety of methods, including composite techniques (Carlson, 1969b; Reed and Recker, 1971; Burpee, 1974; Reed et al., 1977; Norquist et al., 1977; Thompson et al., 1979; Duvel, 1990; Diedhiou et al., 1999; Kiladis et al., 2006; Aiyyer and Thorncroft, 2006; Hopsch et al., 2010; Peng et al., 2011; Agudelo et al., 2011), spectral techniques (Burpee, 1972, 1974; Albignat and Reed, 1980; Nitta and Takayabu, 1985; Reed et al., 1988b; Lau and Lau, 1990; Duvel, 1990; Thorncroft and Rowell, 1998; Pytharoulis and Thorncroft, 1999; Mekonnen et al., 2006; Frank and Roundy, 2006), and synoptic case studies (Carlson, 1969a; Frank, 1970; Reed et al., 1988a; Avila and Clark, 1989; Avila and Pasch, 1992; Pytharoulis and Thorncroft, 1999; Avila et al., 2000; Karyampudi and Pierce, 2002; Berry and Thorncroft, 2005; Ross and Krishnamurti, 2007; Zawislak and Zipser, 2010; Bain et al., 2011), using datasets from observations, field campaigns,

operational analyses, reanalysis products, and modeling techniques. A cursory review of selected past studies is provided in this section.

AEWs form over tropical Africa and then propagate westward into the open Atlantic. The first systematic study of AEWs utilized synoptic analysis of early satellite images and rawinsonde data (Carlson, 1969a,b), finding a wavelength of 1300 mi (about 2000 km), a period of 3.2 days, and a westward speed that varied from 12 to 20 kt (about 6 to 11 m s^{-1}), but the source region of the disturbances was not determined. Burpee (1972, 1974) went on to identify a mid-tropospheric easterly jet as an important player in the origin of the disturbances, using both statistical and compositing methods to uncover a horizontal wavelength of 3100-3800 km and a period of 3-5 days.

The extensive observational program GATE (GARP Atlantic Tropical Experiment) was launched in the mid-1970s, providing temporally and spatially rich data from the AEW region of interest for the first time and corroborating previous estimates of wavelength and phase speed. GATE began in June of 1974, included three observing periods of three weeks each, and covered a large experimental area from 10°S to 20°N and 100°W to 60°E by coordinating both ship and land observing networks (Kuettner, 1974). Several authors presented summaries of observations from GATE (Reed et al., 1977; Norquist et al., 1977; Thompson et al., 1979; Greenfield and Fein, 1979; Albignat and Reed, 1980), with a general consensus that AEWs have a wavelength between 2000 and 4000 km, an easterly phase speed of about 8 m s^{-1}, and are typically found around 15°N. Using the GATE dataset and a compositing method, Reed et al. (1977) found that the wavelength and period of AEWs is longer over land (2700km and 3.7 days) than over the ocean (2200km and 3.2 days), but the wave speed is about the same in both regions.

GATE remains a landmark field campaign and has shaped the modern understanding of the general structure of AEWs, but questions on the difference between

developing and non-developing AEWs remained. The aim of the JET2000 project (Thorncroft et al., 2003) was to address unanswered questions on AEW evolution and propagation. Unfortunately, JET2000 lasted less than a week (in comparison with 100 days of GATE), and although it was launched during the climatologically active period during late August, conditions were markedly drier and AEWs were weaker and less coherent than had been hoped. The next major campaign took place in 2006, the downstream extension of the international African Monsoon Multidisciplinary Analyses (AMMA) experiment, the National Aeronautics and Space Administration (NASA) AMMA (NAMMA) (Zipser et al., 2009). NAMMA endeavored to address the questions of which AEWs become TCs and what role the Saharan Air Layer (SAL) plays, collecting extensive data on seven AEWs, two that developed into TCs, three that bore some connection to future TCs but not as cleanly, and two that never developed beyond the wave stage.

Beyond satellite observations and field campaigns, studies examining operational analysis (Nitta and Takayabu, 1985; Reed et al., 1988a,b; Duvel, 1990; Lau and Lau, 1990; Pytharoulis and Thorncroft, 1999; Thorncroft and Hodges, 2001; Karyampudi and Pierce, 2002; Fink and Reiner, 2003; Berry and Thorncroft, 2005; Ross and Krishnamurti, 2007; Peng et al., 2011) and reanalysis products (Diedhiou et al., 1999; Fink et al., 2004; Matthews, 2004; Chen, 2006; Kiladis et al., 2006; Mekonnen et al., 2006; Hopsch et al., 2007; Fink et al., 2010; Hopsch et al., 2010; Leroux et al., 2010; Agudelo et al., 2011; Ventrice et al., 2011) also provide insight into AEW structure and dynamics. While resolution is not generally sufficient to shed further light on the wave characteristics discussed above, select reanalysis and operational analysis studies are discussed further in the following section in the context of wave dynamics, where they are more apt to aid our understanding.

Finally, many idealized modeling studies have examined the structure and lifecycle of AEWs. Hall et al. (2006) provided a useful summary table of AEW characteristics

from previous idealized studies (Rennick, 1976; Simmons, 1977; Mass, 1979; Kwon, 1989; Chang, 1993; Thorncroft and Hoskins, 1994a,b; Thorncroft, 1995; Paradis et al., 1995; Grist et al., 2002), in which maximum wind speeds range from 10 to 23 m s^{-1}, growth rates range from 0.25 to 0.88 day^{-1}, periods range from 2.2 to 5.3 days, wavelengths range from 2000 to 3900 km, and phase speeds ranged from 7.5 to 15.8 m s^{-1}.

There is some debate in the literature about interannual variability in AEW frequency. Avila et al. (2000) compiled thirty-one years of operational data (1967-1997), and while they noted variation from year to year in AEW count, they argued that the variation is "probably not significant" and might be due to changes in observational methods. In an earlier work Avila and Clark (1989) went as far as to claim there has been an "almost constant number of African waves per year," while on the other hand several studies claim that there has been "marked interannual variability" in African Easterly Wave activity (Thorncroft and Rowell, 1998; Thorncroft and Hodges, 2001; Hopsch et al., 2007). The interannual variability of AEW frequency is discussed further in the context of its potential impact on the frequency on TCs in Section 1.2.2 and the datasets published by Avila et al. (2000) and Thorncroft and Hodges (2001) are revisited in Section 3.1.

The African Easterly Jet and Wave Dynamics

Using early upper air data, Burpee (1972) was the first to show that AEWs are associated with a midtropospheric easterly jet in the baroclinic zone of the Sahel (apparent in Figure 1.1 at 600mb around 15°N), and he further showed that this jet satisfies the Charney and Stern (1962) instability criterion. Burpee (1972) also found that perturbations (AEWs) forming along this jet undergo mixed baroclinic-barotropic wave growth (with horizontal and vertical zonal shear acting as equal sources of energy) and are unlike typical tropical disturbances, which he attributed

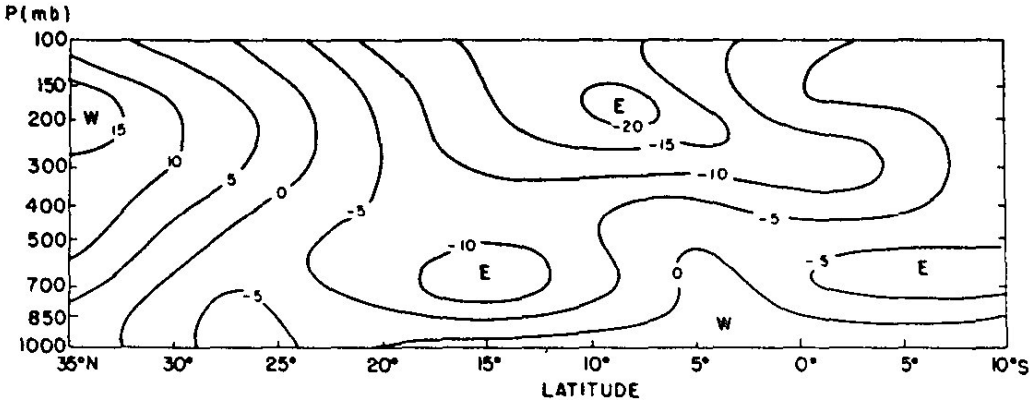

Figure 1.1: Reproduced from Burpee (1972), meridional cross-section at 5°E of zonal wind averaged for August. The 600mb easterly jet at about 15°N with a peak strength of 12-15 m/s is referred to as the African Easterly Jet by both Thorncroft and Hoskins (1994a) and Burpee (1972), and will be referred to as AEJ_N throughout this paper. The 200mb jet closer to 10°N is identified as a remnant of the Indian monsoon jet by Burpee (1972), is referred to as the Tropical Easterly Jet by Thorncroft and Hoskins (1994a), and will be referred to as AEJ_S throughout this paper.

to the fact that the monthly mean surface temperature of North Africa changes by 10°C in only 10° of latitude. The jet from whence AEWs come is often referred to as the African Easterly Jet (AEJ), although this can be a bit misleading, as modern analysis has revealed two distinct latitudes of AEW formation (Nitta and Takayabu, 1985; Reed et al., 1988a; Lau and Lau, 1990; Ross, 1991; Thorncroft and Hoskins, 1994a; Thorncroft and Hodges, 2001; Fink and Reiner, 2003; Fink et al., 2004; Chen, 2006; Hopsch et al., 2007; Ross and Krishnamurti, 2007; Chen et al., 2008).

Burpee (1974) noted that in a general sense, the vertical structure of the waves varies such that the meridional wind tilts in the opposite direction to the mean zonal shear, consistent with positive baroclinic energy conversion. This point was later nuanced by Reed et al. (1977) and Albignat and Reed (1980), who found similar structure at 15°N, but found less vertical tilt equatorward. Thorncroft (1995) suggests that this may be due to weaker baroclinicity and stronger latent heating effects at lower latitudes.

Revisiting the plot of the meridional cross-section of zonal wind at 5°E from a typical August from Burpee (1972), Thorncroft and Hoskins (1994a) make the distinction between what they referred to as the "African Easterly Jet" or AEJ and the "Tropical Easterly Jet" or TEJ (see Figure 1.1). The northern track, which Thorncroft and Hoskins (1994a) labeled the AEJ and will henceforth be called AEJ_N, consists of the types of eddies with the characteristic ascent of warm and dry air over surface troughs as are commonly found in arid zones (Lau and Lau, 1990). On the other hand, the southern storm track, which coincides with the latitude of the TEJ from Thorncroft and Hoskins (1994a) and will henceforth be called AEJ_S, is associated with moist convective systems and coincides with the climatologically rainy zone (Lau and Lau, 1990). Disturbances from these two regions are known to interact and sometimes merge in the Atlantic (Reed et al., 1977; Thorncroft and Hoskins, 1994a; Ross and Krishnamurti, 2007).

AEWs often have complicated structures, sometimes being multicentered, with one low-level circulation center to the north and another mid-tropospheric center to the south (Reed et al., 1977; Pytharoulis and Thorncroft, 1999). Using a manual method to identify and track AEWs for 1998 and 1999 in ECMWF analysis, Fink and Reiner (2003) found that only 12 of 81 "AEWs" over Africa were not accompanied by a second vorticity center. Fink et al. (2004) coined the term "simultaneous twin vortices" to describe these pairs, and revisited the GATE period through ERA-40 to focus on the dynamics of waves propagating along AEJ_N. They found that AEWs on the northern track are almost always accompanied by an AEW on the southern track for at least part of their lifetime, and that during the GATE period only 2 out of 18 pairs of AEWs merged.

In contrast, Chen (2006) found a population ratio of 2.5 northern to 1 southern AEW in an analysis of ECMWF reanalysis from 1991-2000, but the tracking methodology, although still manual, differed from that of Fink and Reiner (2003). Looking

closely at the two years the studies have in common (1998 and 1999), the reported counts cannot easily be reconciled. Fink et al. (2004) found 36 (32) northern (southern) AEWs in May-October 1998 and 41 (41) northern (southern) AEWs in 1999, and through analysis of synoptic maps the authors argued that the northern and southern waves are usually coherent features. Chen (2006) found 38 (8) northern (southern) AEWs in June-September 1998 and 31 (16) northern (southern) AEWs in 1999, concluding that the two types of waves seem to be independent of each other. How one defines an AEW and how the line is drawn between waves associated with the northern or southern storm track has a strong effect on the conclusions drawn.

While there is agreement in the literature that the AEJ_N and AEJ_S are distinct (although not necessarily independent) over land, whether they "merge" over the ocean is debated and in some ways is a semantic argument. Some authors concluded that the jets themselves essentially merge over the open ocean (Reed et al., 1988b; Duvel, 1990), but Nitta and Takayabu (1985) found that although the waves following the two tracks seemed to be coupled and individual disturbances do at times merge, there was no merger of the two tracks, and waves from AEJ_S propagated farther into the Atlantic. Ross and Krishnamurti (2007) found that mergers of vorticity centers occur but are not common, and more often the tracks of AEWs tend to converge to a similar latitude without the individual vorticity centers actually merging.

There are also notable differences between AEW growth and development over land and over the ocean. From composite analysis from the GATE dataset (Reed et al., 1977), Norquist et al. (1977) first suggested that diabatic effects may play an important role in strengthening AEWs over land in west Africa, but not over the open ocean. Thompson et al. (1979) asserted that over the ocean, AEWs grow through barotropic energy conversion and are actually weakened by baroclinic energy conversion and latent heat release. However, as Albignat and Reed (1980) found, AEWs grow primarily over land, with the principal growth region being well inland

(0-10°E) and a secondary growth region present near the coast, so by the time waves reach the western coast of Africa, nonlinear effects have likely tapered.

In idealized studies of the linear instability of the AEJ, Thorncroft and Hoskins (1994a) and later Paradis et al. (1995) found that without diabatic effects, AEWs are dominated by barotropic energy conversions, so they concluded that latent heating increases the baroclinic relative to barotropic energy conversion in AEW formation and growth, and thus diabatic effects are important in determining synoptic structure of AEWs. In a follow-up nonlinear lifecycle study, Thorncroft and Hoskins (1994b) confirmed that AEWs are initially fueled by barotropic energy conversion and later grow through baroclinic energy conversion.

Latent heating may not only be important in influencing the growth and synoptic structure of AEWs—there is some suggestion that localized latent heating in the entrance region of the AEJ may serve to initiate disturbances downstream (Berry and Thorncroft, 2005; Mekonnen et al., 2006; Thorncroft et al., 2008). Along with latent heating, Leroux et al. (2011) suggest that there may also be remote dynamical precursors. Hall et al. (2006) first put forward the notion that AEW-formation may require a finite amplitude trigger, because they found that even a low level of surface damping has a stabilizing effect in idealized simulations, and thus the AEJ may be stable or only weakly unstable. The findings of Hsieh and Cook (2008) support the idea that jet instability is not sufficient to induce significant convection, so it is likely that the jet sustains waves in their decaying stage but is unable to initiate waves without some kind of convective precursor. This so-called "trigger hypothesis" has been studied as an alternative to the classical explanation that AEWs result from the AEJ itself being unstable, but Leroux and Hall (2009) found that even if one assumes a finite amplitude precursor is required, AEW formation is still extremely sensitive to intraseasonal variations in the AEJ itself.

While AEWs weaken the AEJ by fluxing easterly momentum away from the jet (Thorncroft and Hoskins, 1994a), diabatically forced meridional circulations, namely dry convection in the Sahara and moist convection in the intertropical convergence zone (ITCZ), are thought to maintain it (Karyampudi and Carlson, 1988; Thorncroft and Blackburn, 1999). Cook (1999) posits that the AEJ forms over West Africa as a result of strong meridional soil gradients, because in a series of general circulation model (GCM) experiments, positive temperature gradients associated with solar irradiation, SSTs, or clouds were not large enough to produce an easterly jet without realistic soil moisture gradients. Although it is clear that the AEJ and AEWs are dynamically linked, Hsieh and Cook (2005) found that AEW generation may be more dependent on the strength of the ITCZ than the strength of the AEJ. The relationship between the AEJ and AEWs is rather complicated, and this is taken a step further in the next section in considering how TCs fit into the picture.

1.2.2 Connections between Africa, AEWs, and TCs

By the late 1960s it was already clear that many hurricanes and tropical storms develop from African disturbances (Carlson, 1969a). Unfortunately, the question of whether the count of AEWs varies substantially interannually is somewhat unsettled (see Section 1.2.1), let alone the question of whether any AEW variability might affect TC variability on seasonal or interannual scales. Some authors maintain that there is no independent connection between AEW variability and TC variability, others suggest an indirect connection (e.g., subject to large-scale environmental factors or mediated by African rainfall variability), and still other authors claim a direct connection between AEW and TC variability.

Rather than looking at aggregate interannual variability, some studies emphasize the importance of the structure or intensity of individual AEWs (Kwon and Mak, 1990; Zipser et al., 2009; Zawislak and Zipser, 2010; Hopsch et al., 2010; Agudelo

et al., 2011; Peng et al., 2011), but this dissertation is not framed in terms of isolating differences between developing versus non-developing AEWs and so these issues are not addressed in detail here. The idea that AEW intensity might be more important than frequency is consistent with the "finite-amplitude precursor idea" of Emanuel (1989), but while an individual AEW's structure or intensity may impact its ability to develop into a TC, the focus of this dissertation is on addressing the influence AEWs have on TC activity in an aggregate sense.

There is also some debate as to which or whether both AEW storm tracks (AEJ_N and AEJ_S) have a strong connection to Atlantic TC formation, but part of the discrepancy comes from accounting differences in discerning between northern and southern waves and whether one counts the percentage of TCs that formed from AEWs or the percentage of AEWs that become TCs. Thorncroft and Hodges (2001) found that AEWs from the southern storm track tend to make the largest contribution to hurricane formation. On the other hand, Chen et al. (2008) found that in their analysis of 1979-2006 reanalysis products, northern AEWs seed 32% of Atlantic TCs, while southern AEWs seed 26%, but given the 2.5:1 population ratio of northern to southern AEWs found in that dataset (Chen, 2006), the conversion rate of southern AEWs to tropical cyclones is twice as effective as that of their northern counterparts. Finally, Fink et al. (2004) found that most AEWs come in pairs, which would make the above distinction moot to some extent. Regardless, Kossin et al. (2010) explained that disturbances traveling along the northern storm track are less effective at initiating cyclogenesis, because they need to make it farther west before intensifying and are thus more likely to encounter hostile environments before developing. In support of the idea that fewer northern AEWs have the chance to initialize cyclogenesis, Hopsch et al. (2007) noted that about 75% of the southern AEWs continue to the main development region (MDR), but only about 20% of northerly AEWs make it.

Setting the details of structure, intensity, and type (northern or southern) aside, oft-cited opposition to the potential connection between AEW and TC variability was put forth by Avila (Avila and Clark, 1989; Avila and Pasch, 1992; Avila et al., 2000). Avila's historical tabulations of manually tracked tropical systems have shown that "African years" (years in which at least 70% of TCs originated from AEWs) have a higher destructive potential than "non-African years" (in which no more than 50% of TCs originated from AEWs). Despite a standard deviation of 12% of the average value in May-November AEW count for 1967-1997 (see Section 3.1.1), the authors maintain that the AEW count remains functionally constant from year-to-year. Based on this supposition, Avila et al. (2000) argue that the large-scale environment must play the most important role for storm development, since the number of AEWs remains fairly constant from year-to-year and non-African years are anecdotally found to correspond with strong El Niño episodes, which provide a hostile environment and do not permit AEWs to grow. That is, the number of storms developing from AEWs varies drastically, but since the authors believe that the number of AEWs does not, the number of AEWs must be unrelated to the number of TCs that ultimately form. The data on which this argument is based is revisited in Section 3.1.1.

Caron and Jones (2011) also concluded that large-scale environmental factors are more important than AEWs in determining how many TCs originate from African disturbances, but not because AEW activity levels are constant. Caron et al. (2010) and Caron and Jones (2011) extended a Canadian regional model to the tropics, and in tuning various model parameters (e.g., resolution, downscaling technique, lateral boundary conditions, regional domain size) they noted variations in both AEW and TC activity in the Atlantic. While Caron et al. (2010) found that it is essential to capture the frequency and intensity of AEWs in order to simulate TC activity in the MDR, in a follow-up study Caron and Jones (2011) concluded that the potential correlation between AEW and TC activity could not be disentangled from changes in

genesis potential index (GPI) in the MDR. They instead ascribed coincidental variation in AEW activity and TC activity to differences in the large-scale environment, specifically high mid-tropospheric humidity creating an environment more favorable for moist convection. Furthermore, in simulations with reduced AEW activity, Caron and Jones (2011) did not see a reduction in the total number of TCs so much as a shift in the dominant region of cyclogenesis, namely from the MDR to the subtropics.

Aside from SST influences in general, some authors have suggested that the SAL and the Madden-Julian Oscillation (MJO) also supersede the importance of AEW variability. Dunion and Velden (2004) found that the SAL has a stabilizing effect due to enhanced vertical wind shear and warm dry air, which may inhibit the growth of the many TC "seedlings" (i.e., AEWs). Ventrice et al. (2011) found that the MJO seems to modulate AEW activity as well as TC frequency. However, they posit that the MJO might modulate tropical cyclone activity by first modulating variability in AEWs as well as large-scale environmental impacts, concluding that the MJO influences AEW activity directly by enhancing or suppressing convection locally over Africa as well as altering characteristics of the AEJ.

There is some suggestion in the literature of another indirect indicator of an AEW-TC relationship, evident in African rainfall statistics. Thorncroft and Rowell (1998) noticed marked interannual variability in AEW activity that is positively correlated with seasonal mean rainfall in the Guinea Coastal region in a GCM with realistic interannual seasonal rainfall variability. Through dry linear instability calculations, Grist et al. (2002) confirmed that the basic state of composite winds from wet years compared with dry years results in a shift in the preferred strength and period of AEWs. In the 1990s several authors noted a strong correlation between African rainfall and TC activity (Landsea and Gray, 1992; Goldenberg and Shapiro, 1996), so taken together with the notion that AEWs and African rainfall are related, this could be interpreted as evidence of a link between AEWs and TCs. On the other hand,

Thorncroft and Hodges (2001) did not find a simple relationship between AEW variability and West Sahel rainfall variability, and starting in the mid-1990s, it seems that the correlation between African rainfall and TCs also began to deteriorate (Aiyyer and Thorncroft, 2006; Fink et al., 2010).

Aiyyer and Thorncroft (2006) examined the relationships of the El Niño-Southern Oscillation (ENSO) index and Sahel precipitation with Atlantic shear, finding the ENSO-shear correlation to have strengthened since the mid-1990s but the Sahel-shear correlation to have weakened. Empirical orthogonal function (EOF) analysis of the Atlantic shear shows interannual variability (the first EOF) to be highly correlated with ENSO, while multidecadal evolution (the second EOF) is correlated with Sahel precipitation. Both EOFs explain about 16% of the variability of TC activity in the MDR. Fink et al. (2010) found that the correlation between West African precipitation and overall TC activity in the Atlantic is weaker in years when the MDR is more conducive to development. They speculated that SST variability can supersede the impacts of African rainfall, but when conditions in the MDR are marginal, the amplitude of AEWs and degree of organization becomes critical.

Thorncroft and Hodges (2001) claimed that there is a direct correlation post-1985 between AEW activity and Atlantic TC activity, but this is based on a "visual inspection" of somewhat limited data. They suggested that TC activity may be influenced by the number of AEWs with significant low-level amplitudes that leave the West African coast, not simply by the total number of AEWs, so they counted positive relative vorticity centers leaving the coast of Africa in May through October in ECMWF analyses. Hopsch et al. (2007) extended this work from 20 (1979-1998) to 45 (1958-2002) years using ECMWF reanalysis and found that the positive correlation Thorncroft and Hodges (2001) had found is not significant on an interannual timescale.

Like Thorncroft and Hodges (2001), Hopsch et al. (2007) kept track of AEW storm tracks (diagnosing and tracking coherent structures in the vorticity field), but also considered synoptic AEW activity (diagnosed with 2-6 day filtered meridional wind variance at 850 hPa). While the storm track measure does not correlate with TC activity on a year-to-year basis, there is correlation in low-frequency variability. The authors did find strong correlation between TC interannual variability and the synoptic measure. These studies are revisited briefly in Sections 3.1.2 and 3.1.3.

There is further support for a direct relationship between AEW and Atlantic TC interannual variability from both observational evidence and modeled variability. Using composite spectral analysis of outgoing longwave radiation (OLR) in a global study of tropical waves of various temporal and physical scales (Rossby-gravity waves, tropical depressions-type or easterly waves, equatorial Rossby waves, Kelvin waves, and the MJO), Frank and Roundy (2006) found that cyclogenesis coincides with above average AEW activity. Belanger et al. (2010) developed a monthly forecast system and found that part of the model skill comes from correctly capturing the frequency of AEWs–25% of the variance in TC activity predicted is associated with the intraseasonal variability of the frequency of AEWs.

The results of these past works highlight the strong sensitivity to the diagnostic method for determining AEW activity. Additionally, historical analyses only provide fairly short climatologies and do not provide a very clean sense of the "spread" or natural variability. While the relationship between African precipitation, AEWs, and TCs is anything but simple, the goal of this dissertation is to determine the extent to which AEW activity itself affects TC activity, beyond changes in the large-scale environment, in a TC-resolving model.

1.2.3 TC-Permitting Models

Various types of "TC-permitting models," including regional scale (Knutson et al., 1998, 2008; Emanuel et al., 2008; Garner et al., 2009; Caron et al., 2010; Caron and Jones, 2011) as well as global scale models (Vitart et al., 1997; Vitart, 2006; Oouchi et al., 2006; Bengtsson et al., 2007a,b; LaRow et al., 2008; Gualdi et al., 2008; Sugi et al., 2009; Satoh et al., 2011; Held and Zhao, 2011; Murakami et al., 2012; Manganello et al., 2012), have gained popularity in recent years, owing to their utility in TC-related research areas from seasonal forecasting to global climate change. Some studies have included coupling with an ocean (Vitart, 2006; Gualdi et al., 2008), but due to computational costs most are atmosphere-only. Since this dissertation itself employs a high-resolution atmosphere-only model, this section begins with a discussion of the known strengths and limitations of such models in general, followed by a summary of past studies of TCs using GFDL's HiRAM in particular.

Fidelity of High-Resolution Atmosphere-Only Models

High-resolution atmosphere-only models (AGCMs) are an unmatched tool, allowing for the manipulation and disentanglement of complicated factors that can obscure understanding of TC variability. The ability to produce multiple model realizations also provides a sense of the natural variability of the climate system that cannot be extracted from the single realization that is the historical record. However, there are some limitations that have been explored in past studies that must be acknowledged.

The main concern in high-resolution atmosphere-only models is the lack of atmosphere-ocean feedback. Bender et al. (1993) explored the effects of ocean feedbacks on an idealized TC vortex embedded in both easterly and westerly basic flows. They found that the decrease in SST that is induced by a TC itself has a significant impact on the ultimate storm intensity by reducing the total heat flux into the storm, and there is more SST cooling the slower an idealized storm moves. They also found

that ocean interaction has more limited effects on the track of the storm, but does turn the storm more north and east in cases with weak easterly or no background east/west flow. Schade and Emanuel (1999) corroborated that a lack of oceanic feedback may lead to stronger storms by comparing a fully coupled axisymmetric hurricane model to an uncoupled model with constant and horizontally uniform SSTs, finding that SST feedback can cut the intensity of an idealized hurricane in half compared with a storm modeled over a constant SST.

A lack of SST-feedback may have other indirect effects that influence TCs. Waliser et al. (1999) found that when comparing simulations with a coupled slab ocean mixed layer in the tropics to simulations forced with specified SSTs, even though the coupled model produces very small SST perturbations (0.10-0.15°C), the decoupling dulls the intraseasonal variability of the MJO. Similarly, Douville (2005) found that the transient response of the Indian summer monsoon in fully coupled models is not accurately captured in atmosphere-only models with prescribed SSTs, and he cautioned that the lack of SST feedback can adversely affect both intraseasonal and interannual timescales in atmosphere-only simulations in the context of climate change time-slice experiments. That said, Douville (2005) also noted that AGCMs can be a useful tool for determining the extent to which SSTs contribute to atmospheric variability.

Although the lack of SST coupling may produce stronger storms (Bender et al., 1993; Schade and Emanuel, 1999), modeled storms are known to have lower intensities and wider expanse than observed storms due to the constraints of resolution (Bengtsson et al., 2007a,b). Walsh et al. (2007) stressed the importance of resolution-dependent criteria for TC detection if one wishes to compare simulated cyclogenesis with climatological cyclogenesis. This is important to bear in mind when setting thresholds to distinguish between tropical storm intensities and is taken into consideration in Section 2.2.2.

Resolution dependence plays out in another way: the parametrization of sub grid-scale processes can influence modeled TC intensity and genesis frequency. In HiRAM simulations, Zhao et al. (2012) found that TC frequency and intensity are sensitive to two model parameters in particular, the horizontal cumulus mixing rate and the strength of damping of horizontal divergence. Increasing the former, there is a sharp increase and then decrease in global storm frequency, and a monotonic increase in storm intensity. Increasing the latter, there is a monotonic increase in frequency with no change in intensity. While these parameters can play a strong role in total TC count, one hopes that holding these parameters fixed across simulations, interannual variability and perturbations from a control case will be meaningful.

While simulations of TC intensity leave something to be desired across the board and sub-grid-scale processes can tip the balance, there is hope that models with unrealistic distributions of TC intensity can still produce reliable results in terms of TC frequency (Zhao et al., 2009). As Zhao et al. (2009) suggest, the best way to judge the value of uncoupled models in TC research is by examining the quality of their simulated interannual variability. The following section does just that by reviewing past studies of model TCs produced by HiRAM simulations.

GFDL's HiRAM

The technical details of the version of HiRAM used in this dissertation can be found in Section 2.1.2. This section focuses on the results of past TC studies using HiRAM.

Zhao et al. (2009) compared tracks, total counts per basin, and seasonal cycles of hurricane strength storms from an ensemble of four 1981-2005 control simulations of HiRAM forced with Hadley Centre Global Sea Ice and Sea Surface Temperature (HadISST) dataset (Rayner et al., 2003), with observations from the International Best Track Archive for Climate Stewardship (IBTrACS) (Knapp et al., 2010). There are some regional discrepancies with observations, but the modeled count, seasonal

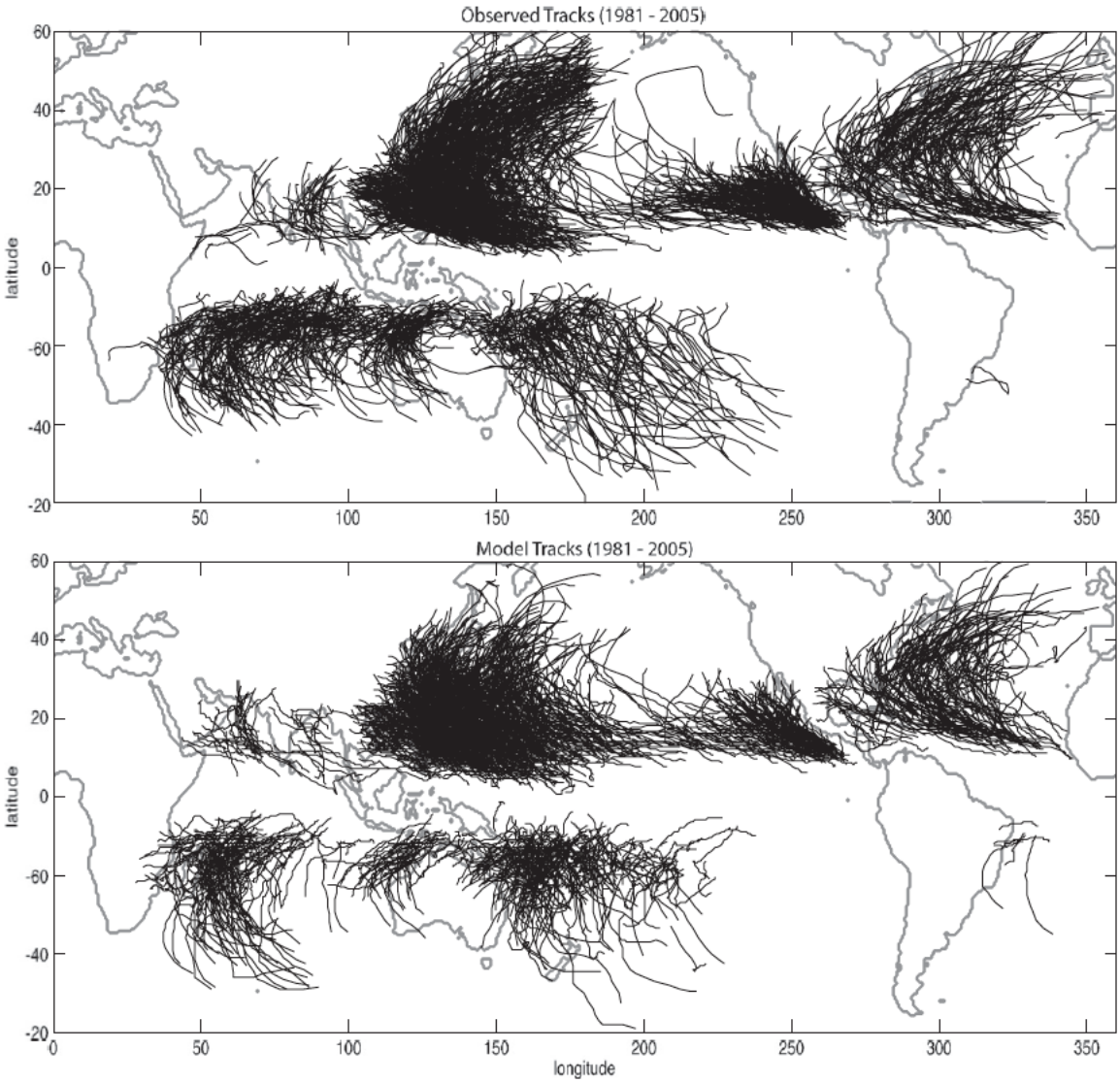

Figure 1.2: Reproduced from Zhao et al. (2009), a comparison of observed (top) and model-simulated (bottom) TC tracks from 1981 to 2005 using GFDL's HiRAM forced with HadISSTs (Rayner et al., 2003).

cycle, and interannual variability in the North Atlantic matches the observed counts well. Figure 1.2 shows a comparison of observed tracks from 1981-2005 and model-simulated TC tracks from one of the ensemble members for that same period.

As expected in a model of this resolution (approximately 50 km), the distribution of storm intensity is not a good match with observations, but this does not seem to affect the fidelity of modeled hurricane frequency. The observed and model-

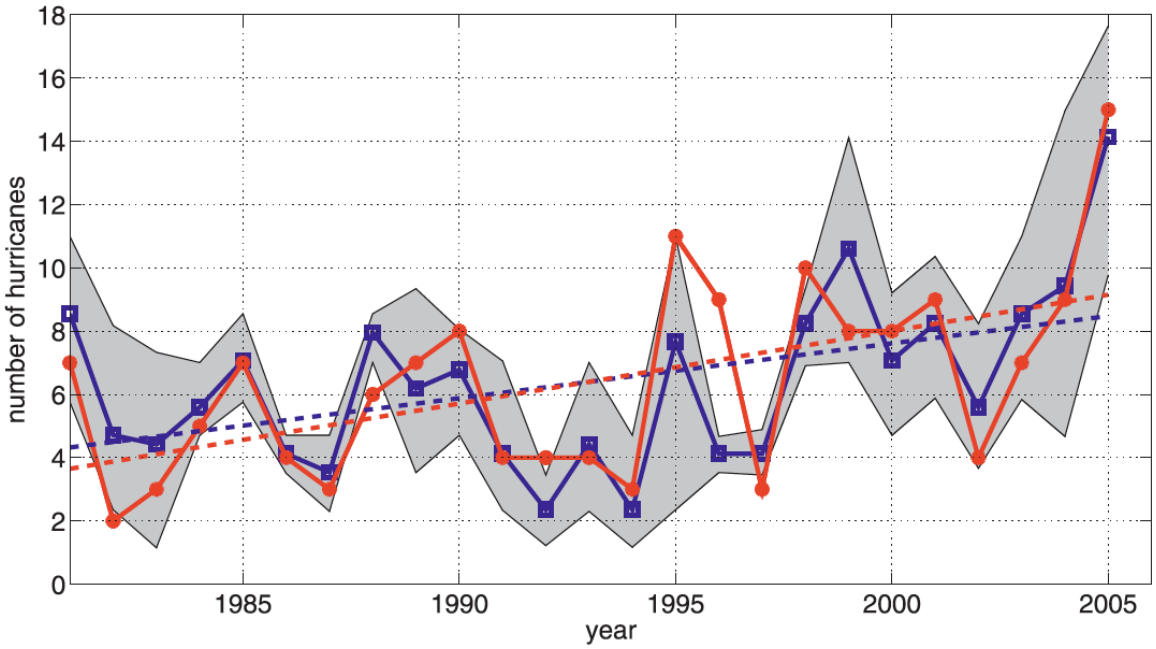

Figure 1.3: Reproduced from Zhao et al. (2009), a comparison of observed (red) and ensemble mean (blue) interannual variation in hurricane count for the North Atlantic from 1981 to 2005 using IBTrACS observations (Kruk et al., 2010) and GFDL's HiRAM forced with HadISSTs to produce the integrations of four ensemble members. The shaded area shows the simulated maximum and minimum count from the four-member ensemble. The modeled counts are normalized by a time-independent multiplicative factor (1.17) to match the total observed number of storms. Dotted lines show the observed and modeled linear trends.

simulated interannual variability of hurricane count in the North Atlantic is shown in Figure 1.3. To highlight the model's ability to capture interannual variability, the authors normalized the modeled counts with a time-independent multiplicative factor (1.17) to match the total observed storm count. The ensemble mean has a correlation coefficient of 0.83 with IBTrACs in the Atlantic, which the authors interpreted as evidence that factors not transmitted through SST must not be as crucial in determining interseasonal variability in hurricane count in the Atlantic.

Zhao et al. (2009) also went on to examine a climate change scenario, forced with prescribed seasonally varying SST with no interannual variability. SST climate change perturbations were obtained from coupled climate simulations and were then added to

base climatological SST to force the atmospheric model. The authors discovered that storm count has notable sensitivity to the choice of base climatological SST, as well as to the differences between the SST change predicted by the various coupled climate simulations. The authors were able to attribute these differences to differences in Atlantic "relative SST," defined as the average temperature in the MDR of the basin minus the global average tropical SST. A difference of as little as 0.15°C in relative SST leads to a substantial difference in storm count. In other words, the authors found that the amount of warming in the tropical Atlantic compared to the tropical Pacific is correlated with the change in Atlantic TC frequency across the simulations.

Two additional HiRAM studies addressed the nature of shifts in TC count in changing climates. First, Held and Zhao (2011) compared the effects of uniformly increasing all SSTs by 2K and doubling atmospheric CO_2 content, both independently and in combination. They found that either doubling atmospheric CO_2 or increasing SST by 2 K separately each results in a 10% decrease in global TC frequency, and a 20% decrease when the two effects are combined. Second, Zhao and Held (2012) was an extension of Zhao et al. (2009), examining a total of ten global warming experiments, eight using SST anomalies from different coupled models, one from an average over 18 different coupled models, and one in which climatological SSTs were uniformly warmed by 2 K. Although there is sizable intermodel spread in the magnitude and sign of TC genesis frequency response to climate change, this study provided additional support for the importance of relative SST globally (although relative SST is a better predictor of TC count perturbations in some basins than in others).

Finally, HiRAM has been used to answer questions of the predictability of seasonal hurricane activity. Zhao et al. (2010) computed the global SST anomaly field for the month of June in each year from 1982-2008 using the mean of the years 1982-2005 to define the anomaly, then integrated from June 1 through the end of December for

each year after adding the anomaly to the climatological mean SST for each month. Compared to the scenarios forced by observed SSTs (Zhao et al., 2009), the decline in skill from allowing June anomalies to persist is largely attributed to missing the seasonal evolution of relative SST. In other words, this study provides further evidence that on both seasonal and interannual timescales, SSTs provide most of the skill in capturing hurricane count variability.

HiRAM has proved a useful tool for many applications, successfully reproducing the interannual variability in TC count of the past several decades (Zhao et al., 2009), allowing exploration of potential changes in TC count under future climate scenarios (Zhao et al., 2009; Held and Zhao, 2011; Zhao and Held, 2012), providing insight into the types of seasonally-evolving SST patterns that are important to predict for accurate seasonal forecasting (Zhao et al., 2010), and generally advancing understanding of environmental controls on TC frequency. These characteristics make it ideal for use in this dissertation.

1.3 Dissertation Overview

This opening chapter has provided motivation for studying the relationship between AEWs and Atlantic TCs, summarized past work toward understanding the characteristics and dynamics of AEWs and the intricate relationship between Africa and Atlantic TCs, and asserted the relevance and past successes of TC-resolving models. The stage has been set to utilize GFDL's HiRAM to shed further light on the relationship between AEWs and Atlantic TCs.

Chapter 2 opens with an explanation of the experimental design in Section 2.1, including specifications of the reanalysis products (Section 2.1.1) and model simulations (Section 2.1.2). The analysis tools used throughout the study are described in Section 2.2, including details of the diagnosis of large-scale environmental favora-

bility using a genesis potential index (Section 2.2.1) and the method of quantifying AEW and TC activity with a hybrid manual-automated TC-AEW tracking algorithm (Section 2.2.2). The methodological choices made are justified and validated in Section 2.3.

The core results follow in Chapters 3 through 6. First, the historical record is revisited in Chapter 3, to clarify the relationship between AEW and TC activity. Data from previous studies are analyzed and compared (Section 3.1), the present tracking methodology is applied to reanalysis data to produce an updated historical record (Section 3.2), and the past and current studies of climatological AEW data are summarized (Section 3.3). Once the historical record is clarified, it is used to legitimize the model for the study of AEWs in Chapter 4, exploring the reliability of the model-produced seasonal cycle of AEW and TC count statistics (Section 4.1), power spectra and statistical measures of AEW activity (Section 4.2), large-scale environment (Section 4.3), interannual variability of AEW and TC count statistics (Section 4.4), and relationship between environmental factors, AEW activity, and TC activity (Section 4.5).

After being shown to adequately capture AEW and TC activity, in Chapter 5 the model is used to isolate the internal variability of AEW activity by removing the effects of interannual variation in SST. The climatological simulations from Chapter 4 are briefly revisited (Section 5.1), then interannually invariant simulations are considered (Sections 5.2 and 5.3), followed by a summary (Section 5.4). In the process, the relevance of ENSO is discussed in the context of a control simulation forced by climatologically averaged SSTs, and an experimental simulation forced by composited SSTs from strong La Niña years.

Next, the large-scale environment is perturbed beyond current climatological variability to examine how changes in AEW activity and overall environmental favorability interact and affect TC activity in Chapter 6. This is accomplished through the

systematic variation of the surface albedo of Africa, the role of which is discussed in Section 6.1. In a suite of four simulations, the albedo of Africa is prescribed as uniform, with varying magnitude. These simulations are analyzed to help disentangle the impacts of large-scale favorability and AEW count on TC count in Section 6.2, and a summary of the results of the perturbed simulations is presented in Section 6.3.

The model results from Chapters 4 through 6 are considered holistically in Chapter 7, to show consistency between the previous chapters and to quantify the relationship between AEW and TC count, both interannually (Section 7.1) and climatologically (Section 7.2). Finally, the dissertation closes with conclusions in Chapter 8, including a summary of the key findings (Section 8.1) and recommendations for future work (Section 8.2).

Chapter 2

Methodology

This chapter opens with an introduction of the overarching conceptual framework of this dissertation, and then the methodology used throughout is detailed and justified.

The goals of this study are reviewed and the overall experimental design is outlined in Section 2.1, followed by details of the reanalysis product used to study the historical record (Section 2.1.1) and the specifications of the model and modeling techniques (Section 2.1.2) used to probe the relationship between AEWs and TCs. Section 2.2 provides an overview of the specific analytical techniques and tools employed, defining the genesis potential index used to diagnose large-scale environmental favorability (Section 2.2.1) and detailing the hybrid manual-automated tracking method used to quantify AEW and TC activity (Section 2.2.2).

Finally, Section 2.3 provides justification for the methodological choices made, considering the fidelity of the reanalysis selected (Section 2.3.1), the relevance of the particular choice of genesis potential index (Section 2.3.2), and the validity of the newly-developed tracking algorithm (Section 2.3.3).

2.1 Experimental Design

This dissertation is designed to elucidate several distinct facets of the AEW-TC relationship. The first goal, which will be addressed in Chapters 3 and 4, is to clarify the

historical record of AEW activity and use it to legitimize the model for further study of the AEW-TC relationship, by comparing historical model realizations against the historical record. The former is accomplished by revisiting past studies and using novel analysis techniques to establish a historical record of AEW and TC activity. The model realizations are then compared with the historical record in terms of the large-scale conditions, the seasonal cycle of AEWs and TCs, spectral measures of AEW activity, interannual variability, and the relationship between AEWs and TCs.

Through these first two chapters of results, the second goal is also addressed: providing evidence toward settling the debate about whether or not AEW and TC activity are indeed historically correlated. Questions raised in Chapter 4 about the importance of interannual variation in SST in the historical record are explored in Chapter 5, addressing the third goal: isolating the internal variability of the modeled AEW activity and its relationship with TC activity in the absence of large-scale environmental differences. The fourth and final goal is to disentangle the effects of large-scale environmental favorability and AEW activity on TC activity in more extreme cases than the climatological record affords, by perturbing the environment and manipulating AEW activity in Chapter 6, addressing the complex relationship between AEWs, the large-scale environment, and TCs.

To meet these goals, the historical record as captured by reanalysis and three separate sets of simulations are analyzed here. The technical details of the model and the manipulation techniques used in this dissertation are spelled out in greater detail in Section 2.1.2, but first the three central sets of simulations are described in general terms to provide a conceptual framework.

The first set of simulations, referred to as **"the climatological simulations"** throughout the rest of this dissertation, is a historical ensemble, consisting of three ensemble members (H1, H2, and H3). Each ensemble member models the 27-year period from 1982-2009, with observed seasonally and annually varying SSTs used as

the lower boundary condition. Ensembles take advantage of the ability of models to produce multiple realizations over the same time period. This expands the dataset and provides for a better estimate of the significance of potential trends and correlations, while also allowing quantification of the internal variability of the atmospheric system. The climatological simulations are analyzed primarily in Chapter 4 and are revisited in Chapter 5.

For the next two sets of simulations, collectively referred to as "the manipulated simulations," each set includes a control simulation along with experimental simulation(s). For both of these sets of manipulated simulations, **"the control simulation"** is a 20-year experiment forced by interannually invariant mean SSTs, averaged from 1982-2005. In other words, the prescribed SSTs in the control vary seasonally, but do not change from year to year. Other model parameters remain the same as those of the climatological simulations.

This control is first paired with an experimental simulation forced with composite La Niña SSTs (averaged for the strongest La Niña years, see Appendix B), referred to as **"the perpetual La Niña simulation"** throughout the rest of this dissertation. Aside from the change in prescribed SSTs, all other model parameters are held fixed, and the perpetual La Niña simulation is also a 20-year experiment. The perpetual La Niña simulation is analyzed in Chapter 5.

Finally, the third set of simulations has the same control experiment, this time paired with four 20-year experimental simulations with uniform African albedo, numbered 1 through 4. Aside from the difference in African albedo, all other model parameters are the same as for the control. These are referred to as **"the uniform albedo simulations"** or "the perturbed simulations" throughout the rest of this dissertation. These simulations are analyzed in Chapter 6.

Information about the reanalysis (Sections 2.1.1) and model (Section 2.1.2) follow, including general specifications and details of the manipulation techniques used to produce the suites of simulations mentioned above.

2.1.1 Revisiting AEW Historical Record Using Reanalysis

The primary reanalysis product used throughout this study is the NCEP-DOE AMIP-II reanalysis (Kanamitsu et al., 2002), henceforth referred to as NCEP-NCAR II. This reanalysis is an updated version of an earlier NCEP-NCAR reanalysis (Kalnay et al., 1996; Kistler et al., 2001), and was selected due to its availability and wide use. While still having its limitations, NCEP-NCAR II includes several key improvements relative to NCEP-NCAR I that are especially relevant to this study. Pertinent updates and limitations are discussed below, and the adequacy of NCEP-NCAR II for studying AEWs is explored further in Section 2.3.1.

The resolution is the same as the original NCEP-NCAR reanalysis, with a horizontal spectral truncation of T62 (i.e., 210 km at the equator), 28 vertical levels, and 6-hourly output. NCEP-NCAR II incorporates precipitation observations through NCEP/CPC global precipitation analysis (Xie and Arkin, 1997) to improve soil moisture fidelity, rather than simply using the model-generated precipitation. The desert albedo was also improved globally using the algorithm of Briegleb et al. (1986), and especially over the Sahara, which may have relevance for the AEJ and AEW dynamics. To minimize the introduction of artificial signals due to changes in observing systems, only the years 1979-2012 are considered (Trenberth et al., 2001). It should be noted that additional raw observational data was added after 1993 (Kanamitsu et al., 2002), so any trends that might surface in the data may be circumspect.

2.1.2 Using HiRAM to Explore the AEW-TC Relationship

The version of HiRAM used in this dissertation is the same as the version used for GFDL's contribution to the Fifth Assessment Report of the Intergovernmental Panel on Climate Change (IPCC AR5). This version is referred to as HiRAM2.2 and was also used by Zhao et al. (2012), who verified that it produced TC statistics consistent with those of earlier model versions. The technical specifications used in this study are summarized below, followed by the details of model manipulation methods, specifically, changes implemented to the prescribed SSTs as a lower boundary condition and the African albedo.

HiRAM Specifications

HiRAM is built upon GFDL's atmospheric model version 2.1 (AM2.1) (Anderson et al., 2004), but with a finer resolution, a different dynamical core, modified moist physics, and a modified convective closure. Without alterations to the moist physics and convective closure, AM2.1 produces an excessively calm Atlantic (Zhao et al., 2009). Some of the key features of HiRAM2.2 are detailed below.

- **Dynamical Core:** Uses a finite-volume core on a cubed-sphere grid topology (Putman and Lin, 2007), which has exceptional grid uniformity and eliminates the need for flux-form semi-Lagrangian extensions for transport processes as well as the need for polar Fourier filtering for fast waves. Updated to improve efficiency and stability by Zhao et al. (2012).

- **Horizontal Resolution:** There are 180×180 grid points on each face of the cube. This means that the size of the model grid varies from 43.5 to 61.6 km (about 0.5° or 50 km resolution).

- **Vertical Resolution:** Includes 32 vertical levels, with higher density of levels near the tropopause than in AM2.1.

- **Cloud Scheme:** Details of the convective closure and diagnostic cloud fraction scheme assuming a subgrid-scale distribution of total water can be found in Appendix A of Zhao et al. (2009). There was a minor retuning of this parameterization by Zhao et al. (2012) to achieve top-of-atmosphere radiative balance after updates were made to the dynamical core.

- **Land Model:** Uses GFDL's LM2 (GFDL Global Atmospheric Model Development Team, 2004). The climatological simulations include dynamic vegetation, improved representations of vegetation reception of snow and rain, water phase change in soil and snow pack, water storage and flow through global river network. In the manipulated simulations, the albedo is prescribed and the vegetation is static.

Sea Surface Temperature

For the interannually and seasonally varying climatological simulations, observed SSTs from the HadISST dataset (Rayner et al., 2003) are used as the lower boundary condition. Only the years 1982-2009 are examined here because of a potential inhomogeneity in observations between 1981 and 1982 in the HadISST dataset.

In all of the manipulated simulations, SSTs vary seasonally but do not change year-to-year. The control experiment for both manipulated simulation sets and all of the uniform albedo experiments are 20-year simulations forced by climatologically average SSTs. The average is calculated from years 1982-2005 of the HadISST dataset, resulting in a seasonally varying climatological SSTs with no interannual variability.

The SSTs from the strongest La Niña years (1985, 1988, 1998, 1999, and 2000) are averaged and used as the lower boundary condition for the 20-year perpetual La Niña simulation. These years were chosen using the NOAA/NWS Cold and Warm Episodes by Season (2014) Oceanic Niño Index (ONI) chart as a reference. Specifically, years for which both the July-August-September ONI and August-September-October ONI

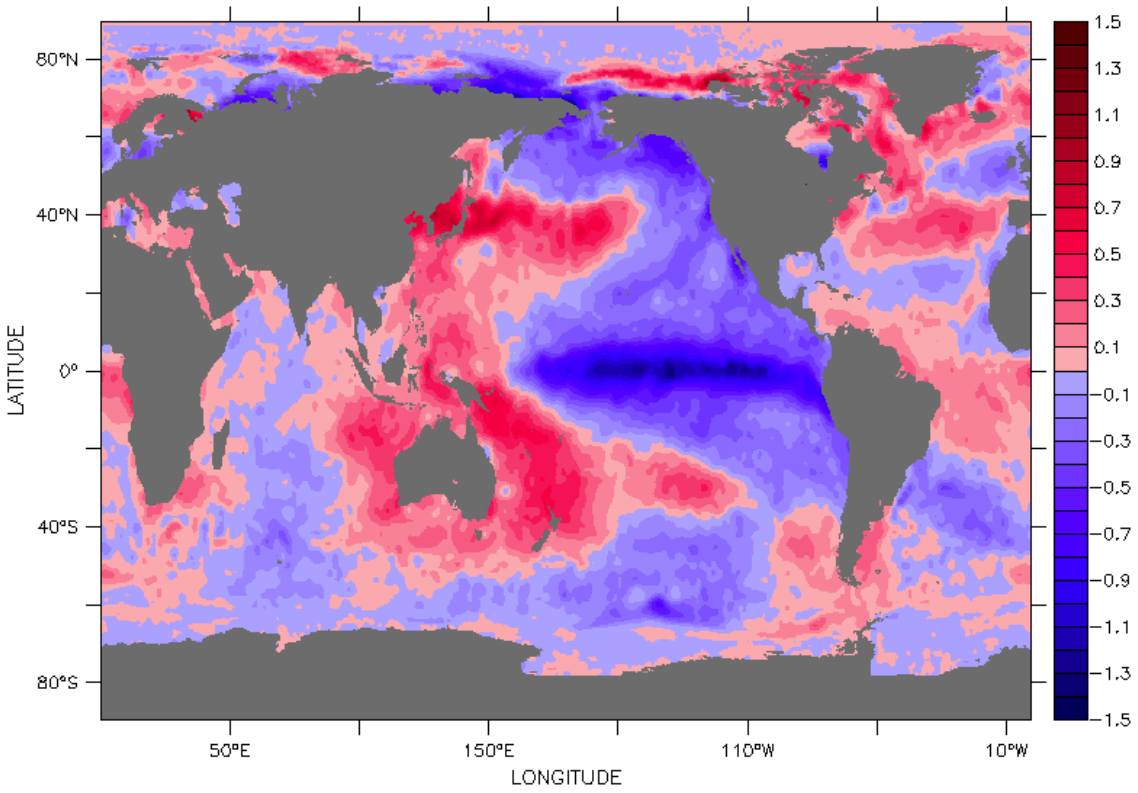

Figure 2.1: La Niña minus climatological SSTs for the months of August through October at 1 degree resolution, calculated using the Hadley Centre Global Sea Ice and Sea Surface Temperature (HadISST) dataset (Rayner et al., 2003). Land is shown in grey.

were both less than -0.5 were included in the composite. For more information on the ENSO classification scheme used throughout this dissertation, see Appendix B.

The mean SSTs from the control simulation are subtracted from the La Niña composite to obtain the La Niña SST anomaly. The resulting average SST anomaly for the months of August through October is shown in Figure 2.1. The SST anomaly in Figure 2.1 reveals characteristic La Niña features, such as cooler ocean temperatures across the east-central equatorial Pacific.

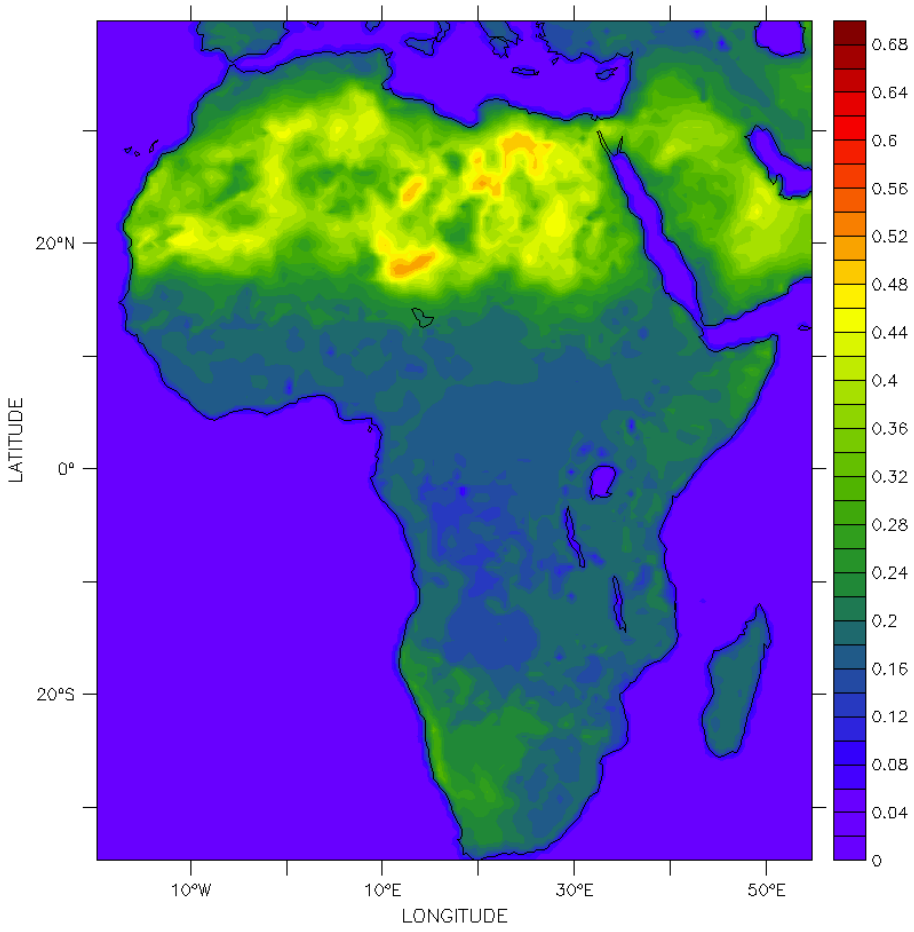

Figure 2.2: Average African surface albedo for the months of August through October.

African Albedo

For simulations in the climatological ensemble, the control simulation, and the perpetual La Niña simulation, albedo is prescribed to be realistic over Africa (GFDL Global Atmospheric Model Development Team, 2004). The average African albedo for the months of August through October is shown in Figure 2.2.

Figure 2.2 shows *total* surface albedo, i.e., the ratio of mean upward to downward shortwave radiation at the surface, and is therefore a function of the near-infrared (NIR) and the visible (VIS) incoming radiation and reflectance. To manipulate the albedo for the purposes of the uniform albedo simulations, it is necessary to consider these NIR and VIS albedo components separately.

(a) Near Infrared Surface Albedo

(b) Visible Surface Albedo

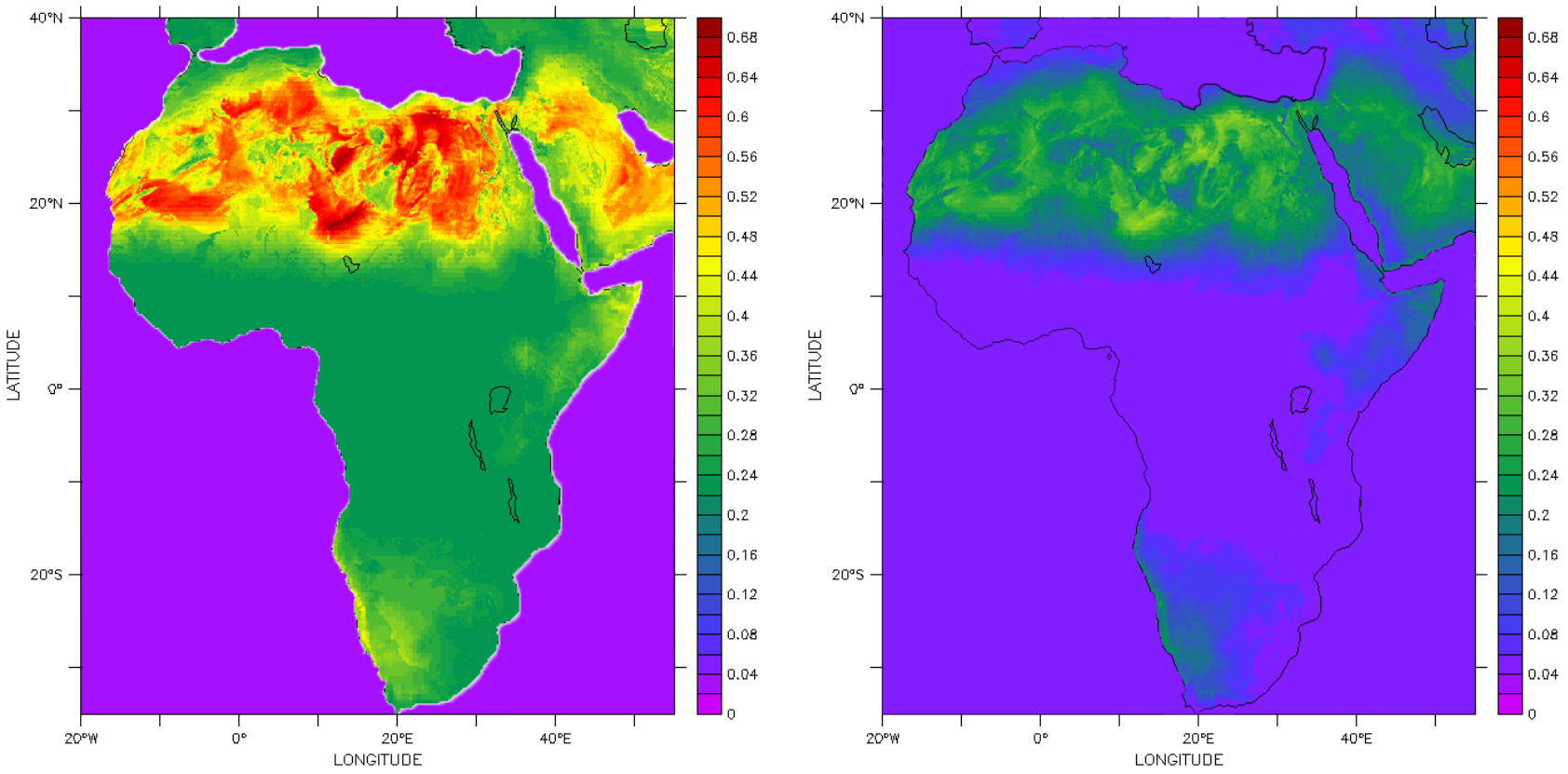

Figure 2.3: Isotropic surface albedo from MODIS data (Schaaf et al., 2002), obtained through personal communication (Malyshev, 2014), broken down into (a) near-infrared (NIR), and (b) visible (VIS) components.

The NIR and VIS components of the isotropic albedo are shown separately in Figure 2.3 for MODIS data (Schaaf et al., 2002), obtained through personal communication (Malyshev, 2014). Through visual inspection of these albedos, a ratio of 2:1 for NIR to VIS albedo appears reasonable, and is therefore used when prescribing the NIR and VIS albedo for the uniform albedo simulations. Because approximately half of the incoming solar radiation is visible and half is near-infrared on average, the total albedo can be estimated from the average of the NIR and VIS albedo parameters. Albedo parameters for the uniform albedo simulations are given in Table 2.1, and these simulations are subsequently referenced by their "Total Albedo."

Table 2.1: Uniform Albedo Simulation Isotropic Albedo Parameters

Simulation	**Isotropic VIS**	**Isotropic NIR**	**Total Albedo**
uniform albedo 1	0.05	0.10	**7.5%**
uniform albedo 2	0.10	0.20	**15%**
uniform albedo 3	0.20	0.40	**30%**
uniform albedo 4	0.30	0.60	**45%**

For the uniform albedo simulations, the isotropic African albedo is prescribed to be uniform over the entire continent and the land type is prescribed to be homogenous. Because the soil albedo also has a weak dependency on the azimuth angle, the total albedo is not completely uniform, and does vary latitudinally with the seasons (Schaaf et al., 2002) and geographically with the variation in the diffuse to direct ratio of solar radiation.

2.2 Analysis Tools

Two analytical tools that are used throughout this dissertation warrant an extended introduction. First, the concept of a genesis potential index (GPI) is reviewed and the version of GPI used throughout this work is defined in Section 2.2.2. Next, the

method of quantifying AEW and TC activity is detailed in Section 2.2.2. For further justification of these methodological choices, consult Sections 2.3.2 and 2.3.3.

As mentioned in Section 1.2.2, the conflicting results of past works highlight the strong sensitivity of the inferred AEW-TC relationship to the diagnostic method and thresholds for detecting AEW activity. A diverse array of tracking techniques have been used in past studies, including statistical, manual, and automated algorithms, each with its own limitations and strengths. Section 2.2.2 provides a short literature review of these past techniques and then details the hybrid manual-automated method used throughout this study.

2.2.1 Genesis Potential Index

Motivated by the seminal work of Gray (1979), Emanuel and Nolan (2004) presented a genesis index, typically referred to as the Genesis Potential Index (GPI), which is used throughout this study and given by

$$\mathrm{GPI} = |10^5\eta|^{3/2}\left(\frac{\mathcal{H}}{50}\right)^3\left(\frac{V_{\mathrm{pot}}}{70}\right)^3(1+0.1V_{\mathrm{shear}})^{-2}, \tag{2.1}$$

where η is the absolute vorticity at 850 mb in units of s^{-1}, $\mathcal{H}$ is the relative humidity at 600 mb in units of percent, V_{pot} is the potential intensity in units of m s^{-1}, and V_{shear} is the magnitude of the vertical wind shear between 850 and 200 mb in units of m s^{-1}. The potential intensity (V_{pot}; Bister and Emanuel, 2002) is the theoretically maximum wind speed sustainable given the convectively available potential energy, and is calculated from SST, sea level pressure (SLP), and the vertical profile of temperature and specific humidity at each grid point, using a publicly available script (Emanuel, 2014).

A refinement of the index from Gray (1979), GPI was developed starting from a large set of environmental variables that have been previously shown to have skill in

predicting TC variability, but variables that might not have broad application beyond the current climate conditions were avoided. The index was trained on NCEP-NCAR reanalysis (Kalnay et al., 1996) for 1950 through 2004 using a combination of multiple regression and common sense to select a suitable combination of predictors, combining monthly averages of large-scale environmental indicators into one powerful index.

This index is typically averaged over some region of interest, such as an entire basin or hemisphere, to quantify the expected level of TC activity given the environmental parameters. Emanuel and Nolan (2004) showed that the index has skill in reproducing monthly mean storm count in the northern and southern hemispheres, and Camargo et al. (2007a) further detailed the development of the index and used it to determine which environmental factors communicate the influence of ENSO on TC activity.

Since interest in creating empirical indices for genesis was revived by Emanuel and Nolan (2004), there have been several publications that either investigate the effectiveness of or attempt to improve upon this definition of GPI (Camargo et al., 2007a,b, 2009; Emanuel, 2010; Tippett et al., 2011; McGauley and Nolan, 2011; Bruyère et al., 2012). This is an area of active research and there is not currently a consensus on which measure of genesis potential is best suited for the purposes of this study–diagnosing the favorability of the large-scale atmosphere. Because subsequent studies that have attempted to improve the prediction of the likelihood of genesis begin from GPI as defined above by Emanuel and Nolan (2004), and the index has been widely used since its development, this incarnation of GPI is used throughout this study. The rationale behind this decision and potential limitations are discussed further in Section 2.3.2.

Throughout this study, GPI is calculated from interannually averaged monthly mean reanalysis and model fields. Spatial maps of GPI are shown for various purposes (see Figures 4.7, 5.8, 6.4, and 6.6), and averages of both GPI and its individual components (vorticity, relative humidity, potential intensity, and shear) are taken

over the MDR (10°N to 20°N; 20°W to 80°W) and the entire Atlantic basin (5°N to 45°N; between the coasts of the United States and Africa), which are used as measures of environmental favorability.

2.2.2 Hybrid Manual-Automated Tracking Algorithm

AEWs are challenging to identify and track, because unlike TCs, there are no agreed-upon structure or amplitude thresholds that determine whether a disturbance should be classified as an AEW. As past studies have shown, AEWs often have complicated structures (Pytharoulis and Thorncroft, 1999) and vary drastically in strength (Hopsch et al., 2007; Zawislak and Zipser, 2010), which can cause tracking algorithms to systematically exclude certain types of AEWs (Bain et al., 2011). In examining past studies, it is self-evident that the method of AEW tracking has an impact on the ultimate conclusions drawn (see Sections 1.2.2 and 3.1). Past techniques used to track AEWs fall into three categories: statistical (Burpee, 1972, 1974; Albignat and Reed, 1980; Lau and Lau, 1990; Duvel, 1990; Thorncroft and Rowell, 1998; Diedhiou et al., 1999; Ventrice et al., 2011), automated (Thorncroft and Hodges, 2001; Hopsch et al., 2007; Caron et al., 2010; Agudelo et al., 2011; Bain et al., 2014), or manual (Carlson, 1969a,b; Reed et al., 1988a; Avila and Clark, 1989; Avila et al., 2000; Fink and Reiner, 2003; Fink et al., 2004; Chen, 2006; Ross and Krishnamurti, 2007; Kerns et al., 2008; Zawislak and Zipser, 2010; Snyder et al., 2010).

Statistical tracking methods often utilize power spectra and band-pass filtering, which aggregate and smooth results, leaving certain potentially interesting details difficult to recover. These methods are appropriate for applications when the details of individual waves are less important and the focus is on aggregate variability in smooth fields. To address the questions raised in this study, it is important to more precisely assess interannual variability, and to discern which and how many individual AEWs develop into TCs and how many TCs were spawned by AEWs. For this reason,

statistical approaches are not compatible with the primary goals of this study, but are used to corroborate the fidelity of the hybrid manual-automated tracking algorithm in Section 2.2.2.

Automated tracking methods can be appealingly efficient, but the varied characteristics of AEWs cause complications. Thorncroft and Hodges (2001) were the first to develop an automated tracking system for use with AEWs, from the feature tracking algorithm of Hodges (1995), to objectively trace closed relative vorticity maxima at two atmospheric levels that exceeded a threshold value, had a lifetime of more than 2 days, and travelled at least 10° zonally in reanalysis data. This method results in fewer AEWs and greater interannual variability than studies employing other methods, e.g., Avila et al. (2000), and the authors report that it is less reliable in interpreting AEWs with multiple vorticity centers or distinguishing between AEWs and mesoscale convective systems.

Agudelo et al. (2011) describe a fundamentally different algorithm specifically designed for AEWs. This method claims to capture all waves moving into the Atlantic ocean, even if a wave is only evident at a single level or for a single variable. However, the algorithm's complexity and simultaneous utilization of a large number of fields make it unwieldy for use on typical model output. On the other hand, Bain et al. (2014) use a manual-inspired automated method, utilizing object-oriented image processing to identify propagating waves from Hovmöller diagrams in the manner a human technician employing a manual method might. Although Bain presents a computationally efficient and reliable method, it only provides details on AEW count and does not track developing vorticity centers. In order to preclude false positives when taking the AEW record and matching it with the TC record, it would be difficult to completely eliminate the human technician. Despite some promising progress in the literature, automated tracking methods are not suitable for this study, given the necessity of reliably matching individual AEWs with particular TCs.

Manual tracking methods are employed almost exclusively in early studies of AEW variability, and there has been a recent resurgence of manual methods in the literature. Unlike feature-tracking automated analyses, early independent manual analyses exhibit good agreement (Fink et al., 2004). Many recent manual methods incorporate multiple steps to locate and verify AEWs, such as examining Hovmöller diagrams of vorticity and wind anomalies, streamline maps, and band-pass filtered relative vorticity. Because AEWs are difficult to reliably track using automated methods and the goals of this dissertation require that more information be retained than is available from statistical methods, a manual method of AEW detection and classification is detailed below and used in this study.

Although it is argued above that manual analysis may be a necessary inconvenience in AEW tracking and TC-AEW matching, automated TC trackers are more reliable, owing to the well-defined structure and intensity thresholds of TCs. An automated method has already been developed and validated for tracking TCs in HiRAM (Zhao et al., 2009, 2012), so an automated TC-tracker is used throughout this study. A general description of the automated TC-tracking algorithm is provided below. The results of these two detection methods are matched *a posteriori* to determine which TCs were spawned by AEWs, as well as which AEWs became TCs. This matching procedure is also described below.

While the previous studies detailed above show that tracking methodology does indeed have an impact on the ultimate conclusions drawn, especially when it comes to AEW frequency, Bain et al. (2014) argue that "the self-consistency of any method is perhaps more important than the comparison with other methods as long as the feature characteristics are broadly similar." For that reason, the methods detailed below are consistently applied to all experimental cases. First the manual detection of AEWs is described, followed by details of the automated detection of TCs, and the

general techniques used to manually match the AEW and TC datasets. Finally, the section closes with a case study.

Manual Detection of AEWs

A manual method is employed to detect AEWs in model simulations. Namely, Hövmoller diagrams of average meridional winds at 850 mb, averaged from 10°N to 20°N, between 15°W and 30°W, from June through November (i.e., hurricane season) are generated and analyzed (e.g., Figure 2.4), and when necessary, corroborated by daily synoptic maps of 850 mb vorticity (e.g., Figure 2.5). Averaging between 10°N and 20°N captures signatures of waves propagating along both the AEJ_N and AEJ_S without double-counting potential "simultaneous twin vortices" (Fink et al., 2004). Although averaging may cause some weak waves to be excluded from the count, previous studies have indicated a significant positive relationship between wave amplitude and subsequent development (Thorncroft and Hodges, 2001; Agudelo et al., 2011).

In order to qualify as an AEW and be counted for the purposes of this study, an area of positive meridional wind (the trailing edge of a wave) must be evident at the eastern boundary of the domain of the Hövmoller diagram and propagate to the western boundary without significant interruption. This ensures waves are of African origin, since the coast of Africa is around 15°W between 10°N and 20°N, and that waves make it to the MDR, giving them a chance to develop into TCs, and thus making them relevant to this study. This requirement is relaxed for marginal cases, in which coherent waves travel out of the range averaged to produce the Hövmoller diagrams (i.e., north of 20°N or south of 10°N) during part of their lifetime. So long as a coherent positive vorticity signal is observed to propagate westward in contemporaneous synoptic maps, these features are also counted.

Figure 2.4 is an example Hövmoller diagram generated to manually identify and count AEWs for each year of every HiRAM model run. This particular example comes

from 1988 in climatological simulation H2, and is representative of a typical year in which some but not all AEWs develop into TCs, and some but not all TCs have their origins in AEWs. The terminus of each wave counted is denoted with an open circle, and a filled circle with yellow border denotes waves that develop into tropical storms. The labels W1, W2, and W3 correspond to the vorticity centers labeled in Figure 2.5.

In 1988 of climatological simulation H2, there were two AEWs in June, four in July, six in August, five in September, five in October, and two in November. A total of eight of these twenty-four AEWs developed into tropical storms in this model year.

Automated Detection of Atlantic TCs

Output from the tropical cyclone detection and tracking algorithm described in Zhao et al. (2009) and Zhao et al. (2012) is used with the help and permission of the authors to identify Atlantic tropical storm origins, which are in turn used to manually diagnose whether or not each model-produced tropical storm is AEW-induced. The algorithm is briefly described below, but full details can be found in the original papers (Zhao et al., 2009, 2012), including more information about sensitivity to parameter choices.

The algorithm first locates all maxima in 850 mb relative vorticity greater than 1.6×10^{-4} s^{-1} that also coincide with a local minimum in sea level pressure and a warm-core, both located within 2° of each vorticity maximum. These "potential storms" are then subjected to trajectory analysis, in which the snapshots of the features located in the first step are linked together into trajectories. Any potential storms that do not belong to a trajectory that lasts 3 days or longer and has a maximum surface wind speed greater than 17 m s^{-1} during at least three days is deleted from the record.

Note that while the model underestimates storm winds due to its relatively coarse spatial and temporal resolutions (see Section 2.1.2), this is compensated for by an overestimation due to the fact that the "surface" level in the model is located higher in the atmosphere than that used in observationally based records, such as IBTrACS

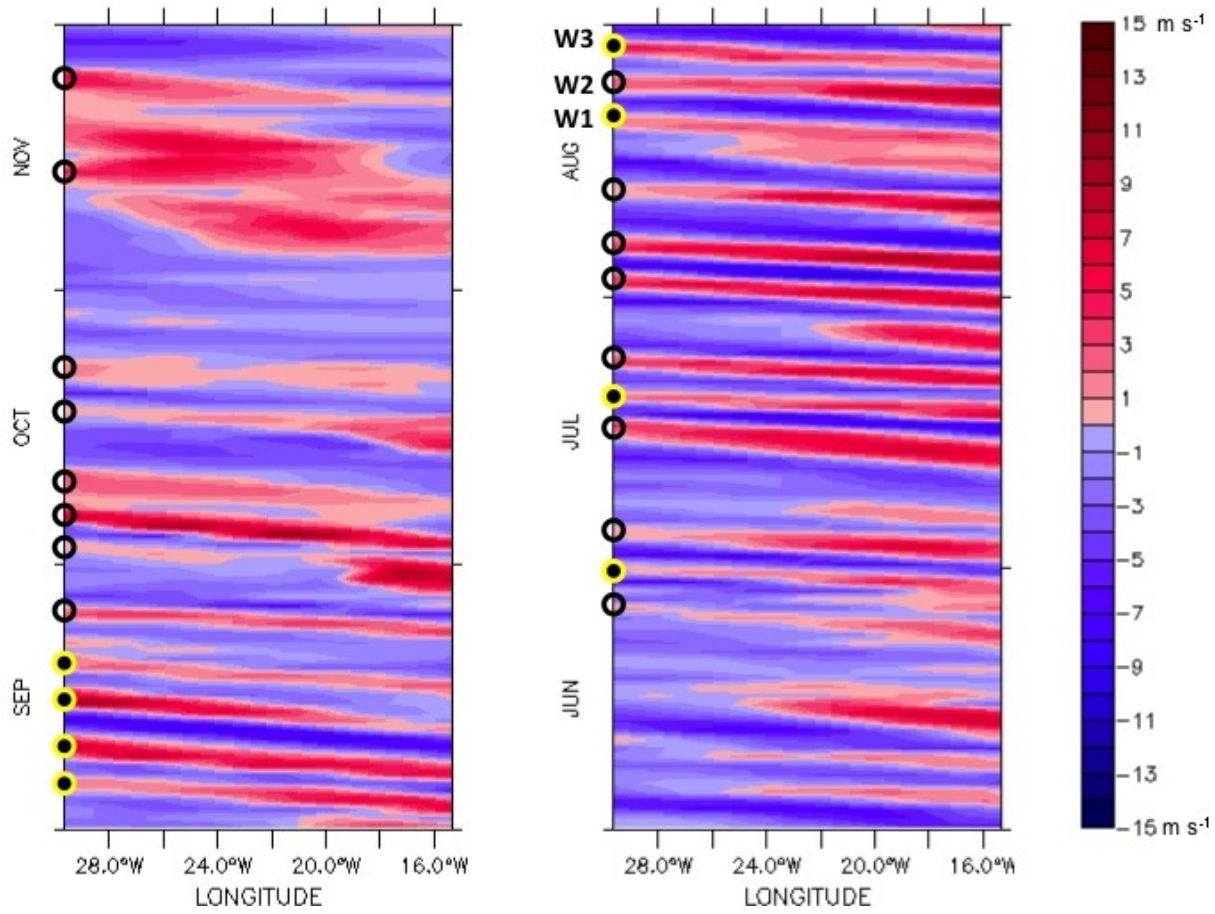

Figure 2.4: Meridional winds at 850 mb, averaged from 10 to 20°N, between 15 and 30°W, from June through November. AEWs are visible as areas of positive meridional winds (red) that began at the eastern boundary of the domain and propagate to the western boundary. Plots like this were generated for each year of every HiRAM model run, but this example is from 1988 of the climatological simulation H2. The terminus of each wave counted is denoted with an open circle, and a filled circle with yellow border denotes waves that developed into tropical storms. The labels W1, W2, and W3 correspond to the vorticity centers labeled in Figure 2.5.

(Kruk et al., 2010). These two effects roughly cancel out, addressing the concerns originally raised by Walsh et al. (2007) about modeled storm intensities. In this dissertation, all intensities of cyclones detected by the algorithm are included, and are referred to interchangeably as "tropical storms" and "TCs," regardless of strength.

The tracker outputs details (e.g., year, month, day, hour, longitude, latitude, wind speed, vorticity maximum, central pressure) of all remaining storms that made it through the trajectory analysis, both as snapshots in time and also grouped together into contiguous tracks. For the purposes of this study, the trajectory origins output by the algorithm are utilized. In the case of the historical reanalysis, the IBTrACS database (Knapp et al., 2010) is used instead of the automated TC detection algorithm output. Starting from the tropical storm origins as determined by the algorithm or IBTrACS, each vorticity center is manually tracked backward in time using synoptic maps to determine whether or not it emerged from the coast of Africa. More details on the matching of tropical storms and AEWs follow.

Manual Matching of AEW and TC Datasets

Given the Hövmoller diagrams from the manual AEW tracker (e.g., Figure 2.4) and the list of tropical storm origin points from the automated TC tracker, the two datasets are matched through manual analysis of synoptic maps of 850 mb relative vorticity (e.g., Figure 2.5). This process is first described generally, followed by an illustrative case study.

Synoptic maps of 850 mb vorticity are produced daily from May 1 through November 30 for every year of every simulation. Each vorticity map covers the region from 100 to 15°W and 0 to 45°N. The maps are colorized so that positive vorticities from 0 to 1.0×10^{-4} s^{-1} are shown in increasingly dark reds, and negative vorticities from 0 to -1.0 $\times$ 10^{-4} s^{-1} are shown in increasingly dark blues. Since the threshold for tropical storm relative vorticity in the automated tracker is 1.6×10^{-4} s^{-1}, tropical

storm strength vorticities present as white space, making them straightforward to match with the automated tracker output.

Tropical storm origins diagnosed by the automated TC tracker are located on the relevant daily synoptic map by latitude and longitude, and then are manually traced back in time by examining and matching earlier daily synoptic maps. Each storm is traced backward in time individually, one storm at a time. Even at times before each feature has reached tropical storm strength, it is common to see an associated region of positive vorticity present that is traveling westward and/or northward in time.

Whether or not a given storm has African origins (i.e., can be traced back to a region of positive vorticity originating on the African coast) is systematically noted, as well as the date that the storm crossed out of the domain of the associated Hövmoller diagram (i.e., north of 20°N or west of 30°W) if it did indeed have African origins. It would be exceedingly difficult to perform this type of analysis with an automated tracker, as AEWs and the regions of positive vorticity associated with them often do not have well-defined structures and present at various strengths and degrees of coherence. However, it is relatively simple for a technician with a trained eye to "follow" AEWs as they travel across the Atlantic.

The recorded date and the synoptic tracking allow an AEW associated with a tropical storm to be marked on the relevant Hövmoller diagram as having developed into a TC, with no ambiguity. Sometimes more than one TC originates from the same AEW, either because the wave was multi-centered or a storm dissipated and then re-intensified. Many of the TCs identified by the tracker did indeed dissipate and re-intensify, but are clearly connected in time by a surviving region of positive relative vorticity. It is not uncommon for this to happen in the real world, e.g., Humberto in 2013 (Landsea and Blake, 2014). In these cases, each intensification is counted as a new origin point by the tracking algorithm.

The converse, one TC originating from multiple AEWs, occurs rarely. This presents as very occasional merger events of two separate AEWs. Mergers are readily distinguished from multi-centered AEWs, because they initially present as temporally separated bands of positive meridional winds on the associated Hövmoller diagram.

For consistency, AEWs are simply tallied as developing or non-developing, and tropical storms as having African origins or not, regardless of whether there was more then one storm or more than one associated AEW. The matching method detailed in this section produces a dataset of monthly AEW counts, developing AEW counts, TC counts, and African TC counts.

Case Study of Manual Matching Technique

To elucidate the procedure described above, a representative case study is presented here. The data for this case study come from the year 1988 in climatological simulation H2, a typical year in which some but not all AEWs developed into TCs, and some but not all TCs had their origins in AEWs. Specifically, synoptic 850 mb vorticity maps from August 18 through August 29, 1988 are shown in Figure 2.5. In this period of time, two tropical storms formed: one that had African origins, and one that originated from a mid-latitude frontal system.

The daily plots in Figure 2.5 should be read chronologically from left to right, top to bottom (note the date in white on the upper left corner of each plot). The 850 mb vorticity over water is shown in filled color contours, with land overlaid in gray. There are three AEWs labeled sequentially, W1, W2, and W3, each of which is also labeled on the corresponding Hövmoller diagram from Figure 2.4.

On August 19, a wave can be seen leaving the coast of Africa, which is labeled W1 in yellow. W1 crosses 30°W around August 20 and moves westward for several days, beginning to curve northward around August 26, and eventually developing into a tropical storm on August 29, labeled TS1 in yellow. In diagnosing the origins

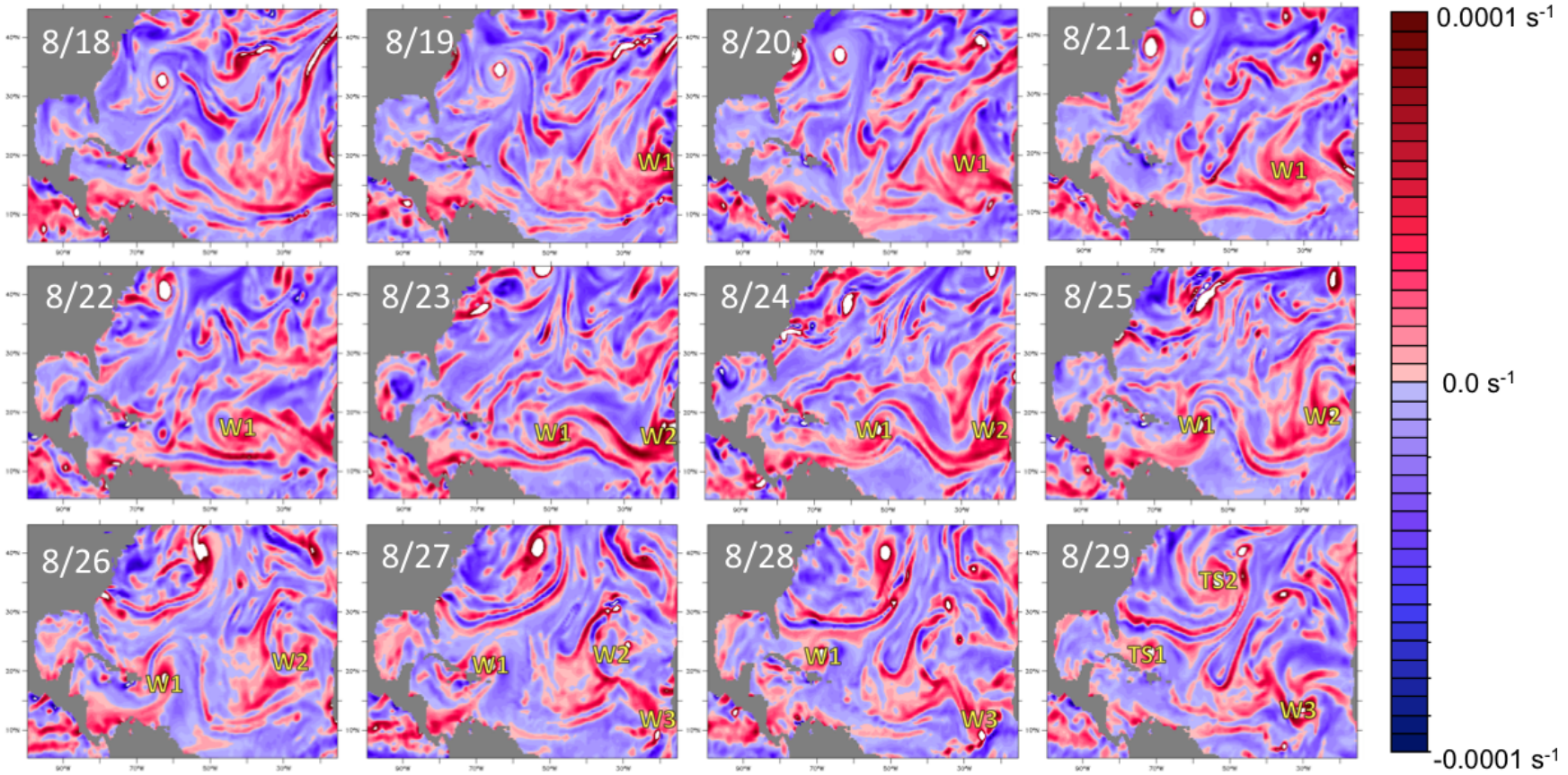

Figure 2.5: Maps of 850 mb vorticity for August 18 through August 29, 1988 from climatological simulation H2, from 100°W to 50°W, 0°N to 45°N, with land overlaid in grey. Plots are shown daily in chronological order, starting in the upper left corner (note the date label over the United States in white). Three AEWs are labeled in yellow outlined with black (W1, W2, W3). On August 29, two tropical storms form and are also labeled, one of African origins (TS1), the other not (TS2).

of TS1, the associated positive vorticity center was tracked *backward* in time from August 29, and was seen to cross 30°W around August 20, two days after having left Africa on August 19. Thus, TS1 is said to be of African origins and W1 is said to be a developing AEW.

A second tropical storm forms on August 29 as well, labeled TS2 in yellow. However, following the positive vorticity center associated with TS2 back in time shows that it did not originate from Africa. Instead, this tropical storm developed out of a mid-latitude frontal system. As expected, tropical storms in the model that were not seeded by AEWs owe their origins to either mid-latitude frontal systems, random ITCZ convection that is unassociated with an AEW, or to the orographic influence of islands.

Two other AEWs are present over the range of dates shown in Figure 2.5. A second AEW is apparent at the coast of Africa on August 23, labeled W2 in yellow. However, this wave curves north much more quickly, and dissipates by the end of this time series. A third AEW (W3) forms near the end of this case study, on August 27, crossing 30°W around August 29. Although not shown in Figure 2.5, this wave also eventually develops into a tropical storm.

2.3 Justification of Methodological Choices

This section provides justification for some of the methods used in this research, comparing the selected reanalysis to an alternative in Section 2.3.1, considering the strengths, limitations, and relevance of the particular choice of genesis potential index in Section 2.3.2, and validating the tracking algorithm against spectral metrics and official reports in Section 2.3.3.

2.3.1 Reanalysis Fidelity

Although NCEP-NCAR II is an improvement over the original NCEP-NCAR reanalysis (Kalnay et al., 1996), correcting several errors and incorporating upgrades, it is self-admittedly not "a next-generation reanalysis" (Kanamitsu et al., 2002). This might raise concerns about its adequacy in reproducing AEW statistics, which are addressed here through comparison with the ERA-Interim reanalysis (Dee et al., 2011).

ERA-Interim has the advantage of being both "next-generation" and having been produced by an entirely separate institute. Despite known inconsistencies between reanalyses, especially in the tropics (Trenberth et al., 2001), NCEP-NCAR II (Kanamitsu et al., 2002) and ERA-Interim (Dee et al., 2011) reanalyses show good agreement in their representation of AEWs as measured using the present analytical tools, specifically in Hovmöller diagrams of 850 mb meridional winds and synoptic maps of 850 mb relative vorticity.

The year 2008 was selected for a random check and detailed comparison of the two reanalyses. Applying the tracking methodology detailed in Section 2.2.2 yields not only identical counts for AEWs and developing AEWs, but one-to-one agreement for individual events. As shown in Figure 2.6, there is remarkable agreement between the two reanalyses when comparing Hövmoller diagrams. Note that climatological simulation H1 is also shown in Figure 2.6, to demonstrate that the model produces realistic AEW signals that resemble those of the reanalyses, but there is no expectation that individual events from the model should correspond to events in history, since the model's atmosphere is freely evolving.

In the year examined and partially shown in Figure 2.6, there are some "marginal cases" (see Section 2.2.2) of AEWs that are more pronounced in one of the reanalyses than the other (e.g., in mid-July, areas of positive vorticity that seem that they may have either dissipated or left the domain before reaching the western boundary in the ERA-Interim plot more clearly make it to the MDR in the NCEP-NCAR II plot).

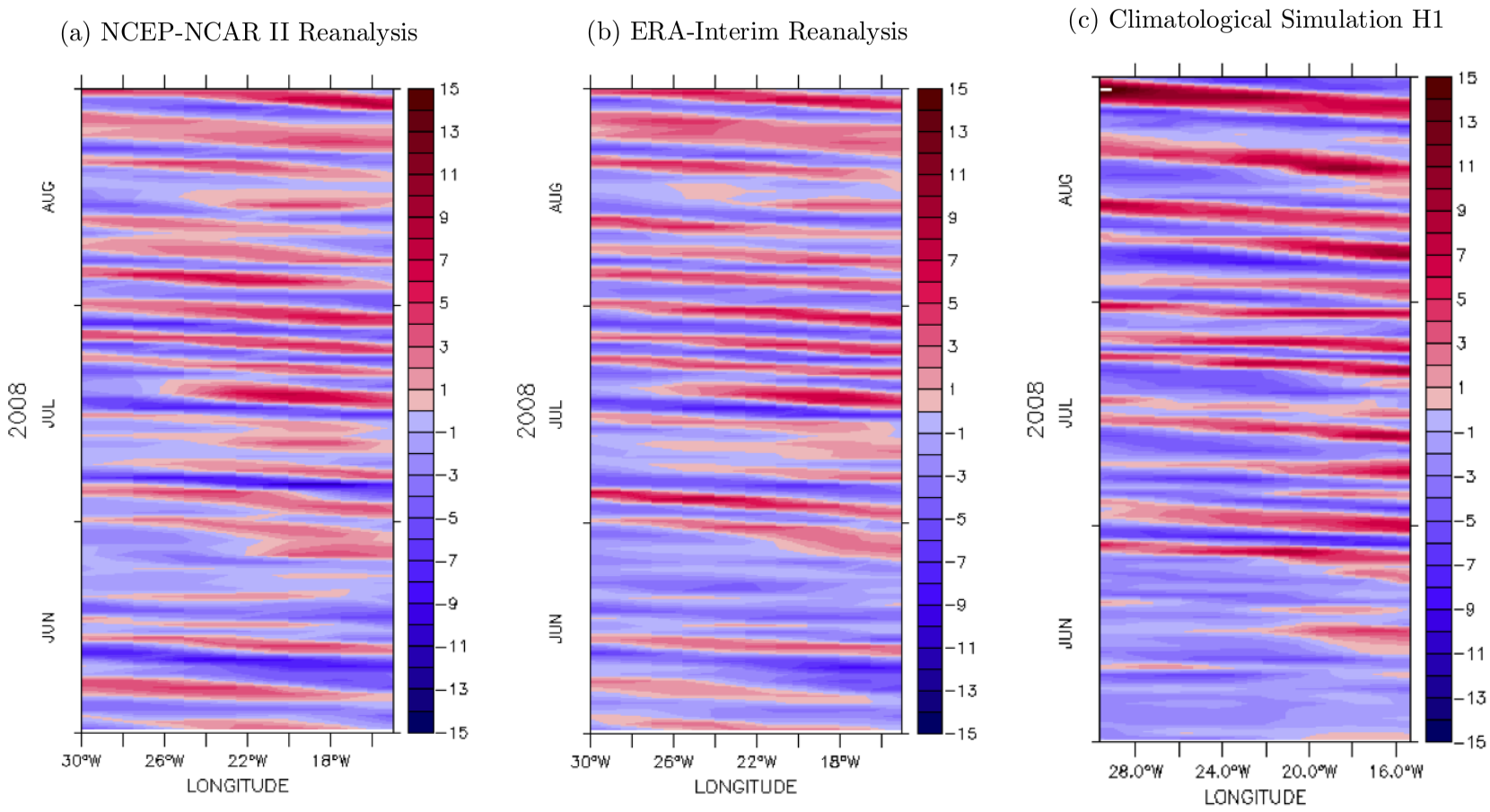

Figure 2.6: Meridional winds at 850 mb, averaged from 10 to 20°N, between 15 and 30°W, from June through August, for (a) NCEP-NCAR II Reanalysis (Kanamitsu et al., 2002), (b) ERA-Interim Reanalysis (Dee et al., 2011), and (c) the climatological simulation H1. As in Figure 2.4, AEWs are visible as areas of positive meridional winds (red) that begin at the eastern boundary of the domain and propagate to the western boundary.

However, in the tracking procedure implemented, such a marginal case triggers the verification of the disturbance in synoptic maps of 850 mb vorticity, to check if a coherent positive vorticity signal can be seen to continue to propagate westward. For this reason, the ultimate count statistics produced by the tracking methodology as applied to each reanalysis agree for the year 2008.

The synoptic vorticity maps may appear to show poorer agreement than the Hövmoller plots at first glance. This is because NCEP-NCAR II has lower resolution and thus tends to be characterized by more muted signals that are less spatially intricate when compared to ERA-Interim (for an example, see Figure 2.7). However, at least in the year 2008, the features required for AEW tracking are adequately resolved for the purposes of this study. For example, Figure 2.7 shows the 850 mb vorticity for August 1, 2008 in each reanalysis. In both the NCEP-NCAR II and ERA-Interim representations, the AEW that clearly manifests at the end of July in the Hövmoller diagrams is shown crossing 30°W. Although NCEP-NCAR II admittedly shows less detail in the vorticity field, it is of sufficient resolution to track a disturbance as it propagates and determine if it is associated with a downstream TC genesis event.

It is possible that other years may fare less favorably in a side-by-side comparison, and the rare discrepancies mentioned in Section 2.3.3, which compares the entire historical record produced using NCEP-NCAR II to National Hurricane Center Tropical Cyclone Reports, may be due to issues of resolution. Since the reanalyses were only directly compared for one year, it would be interesting to quantify the level of variation between different reanalyses, along the lines of Schenkel and Hart (2012). Since the agreement between NCEP-NCAR II and ERA-Interim demonstrated in this section is adequate to inspire sufficient confidence in a historical record produced using the present methodology applied to NCEP-NCAR II to address the goals set forth in Section 2.1, a more detailed intercomparison of representations of AEWs in various reanalyses is left for future work.

(a) NCEP-NCAR II Reanalysis (b) ERA-Interim Reanalysis

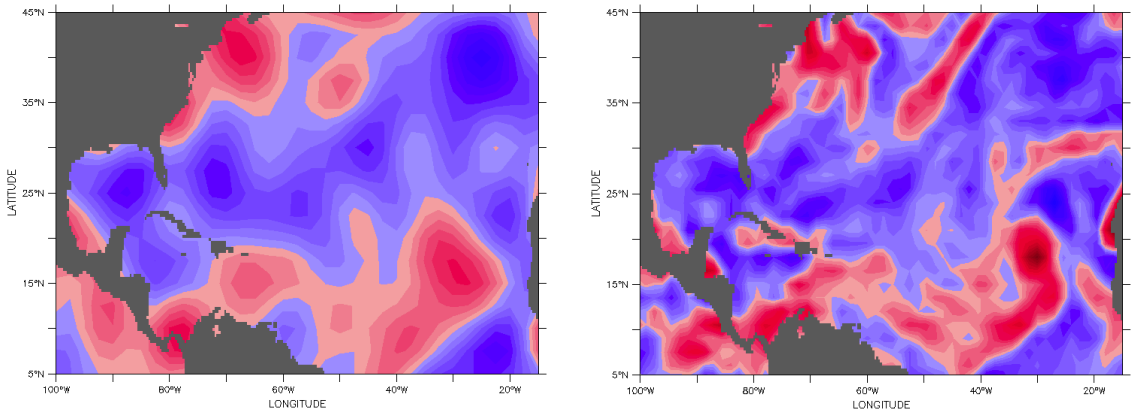

Figure 2.7: Relative vorticity at 850mb on August 1, 2008, for (a) NCEP-NCAR II Reanalysis (Kanamitsu et al., 2002), and (b) ERA-Interim Reanalysis (Dee et al., 2011). Note: scale identical to that of Figure 2.5, i.e., dark red is 0.0001 s^{-1}, dark blue is -0.0001 s^{-1}.

2.3.2 Relevance of Genesis Potential Index Choice

In general, GPI serves two purposes in this study: (1) providing an intuitive feel for changes between different model simulations though visual inspection of spatial plots, and (2) identifying various large-scale predictors of favorability (i.e., spatially averaged total GPI, as well as each of its constituent components: absolute vorticity, relative humidity, potential intensity, and shear) and quantifying their relative importance in comparison to AEW count in the uniform albedo simulations. A key reason the Emanuel and Nolan (2004) GPI is employed in this study is that these goals do not necessarily align with those of more recently developed measures of the likelihood of cyclogenesis. Additionally, as explained in Section 2.2.1, the index is in wide use and most updated indices use it as a starting point.

Gray (1979) was the first to introduce an empirical index to link large-scale environmental parameters to the likelihood of genesis, and there has been a resurgence of interest in such indices in recent years (Emanuel and Nolan, 2004; Sall et al., 2006; Camargo et al., 2007a,b; Bye and Keay, 2008; Emanuel, 2010; Tippett et al., 2011;

McGauley and Nolan, 2011; Bruyère et al., 2012). Genesis potential indices have a wide variety of contemporary uses, and have garnered attention as a proxy for changes in the number of TCs in changing climates, specifically in situations where only large-scale fields are available due to computational limits (Ryan et al., 1992; Royer et al., 1998; Camargo et al., 2007b). This is not the situation here, as the model used throughout this study reproduces realistic TC activity and variability dynamically (see Section 1.2.3). Therefore it is not necessary to use an index to statistically down-scale in order to surmise the TC frequency.

The notion of a "genesis index" may also be thought of as a useful way to diagnose the favorability of the large-scale environment in an average sense, to determine whether changes observed in TC frequency are due to environmental favorability or changes in the number of "seeds," such as AEWs. GPI, the genesis index used here and defined in Section 2.2.1, is well-suited to this purpose, as it has previously been used to explore the relative importance of various environmental factors and assess the large-scale favorability for TCs (Camargo et al., 2007a, 2009). While there have been many proposed improvements to GPI, these improvements have not focused on accurately diagnosing the large-scale favorability, but instead on producing reliable estimates of TC frequency at various temporal and spatial scales, for various purposes. In the process of tuning to these applications, such studies make assumptions that are not necessarily relevant to this investigation, e.g., McGauley and Nolan (2011) build in the assumption that "seeds for cyclogenesis (preexisting disturbances) remain somewhat fixed in frequency for a given period of time and location."

Caron and Jones (2011) used Emanuel and Nolan's GPI to argue that changes in TC count associated with changes in AEW activity were likely due to the large-scale environment and not the AEWs themselves, by correlating average TC count with GPI and its constituent components and comparing the correlation strength to that between TC count and AEW activity as measured by Sahel wind variance (which may

be problematic, as discussed in Section 2.3.3). In a sense, a goal of this work is to test and reevaluate the conclusions drawn by Caron and Jones (2011), as it seems possible their findings were influenced by their choice of metric to characterize AEW activity. It is logical to use the same definition of GPI as Caron and Jones (2011) in reevaluating their conclusion that AEW activity does not provide additional information beyond the large-scale favorability, so as not to change multiple variables.

Although there are multiple reasons to use the GPI given in Equation 2.1, there are some known limitations and shortcomings that must be considered. The original index set forth by Emanuel and Nolan (2004) does not have meaningful dimensions (Emanuel, 2010) and its derivation had a component of subjectivity that means it is not reproducible (Tippett et al., 2011). Bruyère et al. (2012) found that GPI is able to capture mean intraseasonal variation, but is much less skillful in reproducing interannual variability. Depending on the purpose, many authors have argued that the individual components of GPI (absolute vorticity, relative humidity, potential intensity, and/or shear) are more or less effective, or perhaps even flawed (Emanuel, 2010; Tippett et al., 2011; McGauley and Nolan, 2011; Bruyère et al., 2012). These conclusions may depend on differences in timescales, regions, or range of climates considered, and examining these discrepancies warrants further study.

Limitations aside, spatial plots of GPI calculated from monthly mean data fields capture changes between different simulations. Because there is still debate over which parameters are most important or relevant for diagnosing the large-scale favorability for TC formation, each component of GPI is considered separately whenever used quantitatively, namely in Chapter 6. Consideration of each component separately indicates that one of the most questioned parameters, relative humidity, may be the most relevant for these simulations (see Section 6.2). This lends further credence to the use of Emanuel and Nolan's GPI over more recently developed indices that

eliminate, replace, or minimize the dependence on relative humidity (Emanuel, 2010; Tippett et al., 2011; Bruyère et al., 2012).

2.3.3 Tracking Algorithm Validation

While the tracking algorithm detailed in Section 2.2.2 is rigorously defined and reproducible, any method that involves manual analysis is liable to have a component of subjectivity. To provide a different perspective and an independent validation of the tracking methodology, statistical measures of AEW activity are first considered, and then the historical record produced here is compared with National Hurricane Center (NHC) Tropical Cyclone (TC) Reports (NHC Data Archive, 2014).

It is worth noting that spatial maps and averages of the variance of meridional winds at 850 mb were also considered as an alternative measure of AEW activity, but were found to have no correlation with AEW count. Hopsch et al. (2007) also found that 2-6 day filtered meridional wind variance at 850 mb did not compare favorably with their measure of AEW count. For this reason, past studies that have used variance as a measure of AEW activity should be approached with caution, and it should be noted that simple variance does not seem to be a suitable substitute for AEW count.

Comparing AEW Counts with Statistical Measures of Activity

Following a similar approach as Lau and Lau (1990), who calculated power spectra for several regions of enhanced 850 mb relative vorticity variability, including the eastern Atlantic and western Africa, it is possible to produce power spectra that characterize AEW activity for each of the simulations considered in this study. Plots of power spectra for individual simulations are discussed in the relevant chapters, but here two key features of these spectra are considered as potential proxies for AEW activity: the spectral centroid and the percent power located in the 3-5 day band.

All spectra (see Figures 3.6, 4.3, and 6.3) are averaged interannually and presented as plots of the power density multiplied by frequency on a natural logarithm of frequency scale, as Zangvil (1977) showed that this area-conserving transformation was the most useful for visualizing and isolating dominant scales of activity. In this transformation, red noise appears as a horizontal line, and areas where there is significant departure from that line signal the dominant time scales of variability.

The power spectra and the corresponding spectral statistics were calculated from 1-10 day band-pass filtered 850 mb meridional winds, averaged between 10°N and 20°N, near the coast of Africa (15°W), from six-hourly data between August 1 and October 31. The meridional winds and the region chosen were selected to be easily physically relatable to the Hövmoller diagrams used to count AEW activity, and to be an objective measure of the character of the variance at the coast of Africa. The spectra are quite noisy for individual years, and were therefore averaged to produce a characteristic spectrum for each simulation.

The spectral centroid is selected as the first characteristic property of the spectra to be examined, because it is the weighted mean of the frequencies present in the signal, and indicates the "center of mass" or characteristic frequency of the spectrum:

$$\text{centroid (frequency)} = \frac{\sum \nu P(\nu)}{\sum P(\nu)}, \tag{2.2}$$

where ν is the frequency, $P(\nu)$ is the power as a function of frequency, and all frequencies in the 1 to 10 day bands are included in the sum. This represents the characteristic *frequency* of variability, which is converted to a *timescale* in days for each simulation (see Figure 2.8a), for easier interpretation of physical meaning. Decreasing centroid (timescale) typically corresponds to increasing AEW activity.

The second spectral characteristic considered is the percent power located in the 3-5 day band. This is calculated from the area under the curve between 3 and 5

days, divided by the area between 1 and 10 days. Figures 3.6, 4.3, and 6.3 show this graphically, plotting $\nu P(\nu)$ for the entire 1-10 day band, with the 3-5 day band highlighted in cyan. Activity characteristic of AEWs typically occurs in this band, and the fraction of the variability serves as a proxy for the total AEW power, compared to all scales of variability. Normalizing by total power allows for better comparison between models and reanalyses of varying resolutions. An increase in the percent power in the 3-5 day band typically corresponds to increasing AEW activity (see Figure 2.8b).

Both spectral measures show statistically significant (at the 97% level or higher) correlation with the AEW count as determined from the tracking algorithm (see Section 2.2.2) when considering all model simulations and the reanalysis. Correlating the count with spectral centroid yields a coefficient of determination of $R^2 = 0.501$ ($p = 0.02$). The count and percent power statistic have a correlation with $R^2 = 0.676$ ($p = 0.003$).

Inspecting the scatter plots in Figure 2.8, two points are obvious outliers: the NCEP-NCAR II reanalysis, and the fourth uniform albedo simulation. Removing these outliers, both spectral measures show statistically significant (at the 99% level or higher) correlation with the AEW count as determined from the tracking algorithm, with a coefficient of determination of $R^2 = 0.951$ ($p = 0.00004$) for the spectral centroid, and $R^2 = 0.812$ ($p = 0.002$) for the percent power metric. The reanalysis may be an outlier due to the difference in resolution, as shown in Figures 2.6 and 2.7 from Section 2.3.1. In the case of both outliers, one must consider the centroid and the percent power together to make sense of the change in AEW count.

From Figure 2.6, it is clear that the reanalysis exhibits a similar timescale of AEW variability to the model (and thus one would expect similar average count statistics), but Figure 2.7 shows that the overall activity is weaker and less defined. This is also apparent in the power spectrum itself–because of the coarser resolution

(a) Spectral Centroid

(b) Percent Power in 3-5 Day Spectral Band

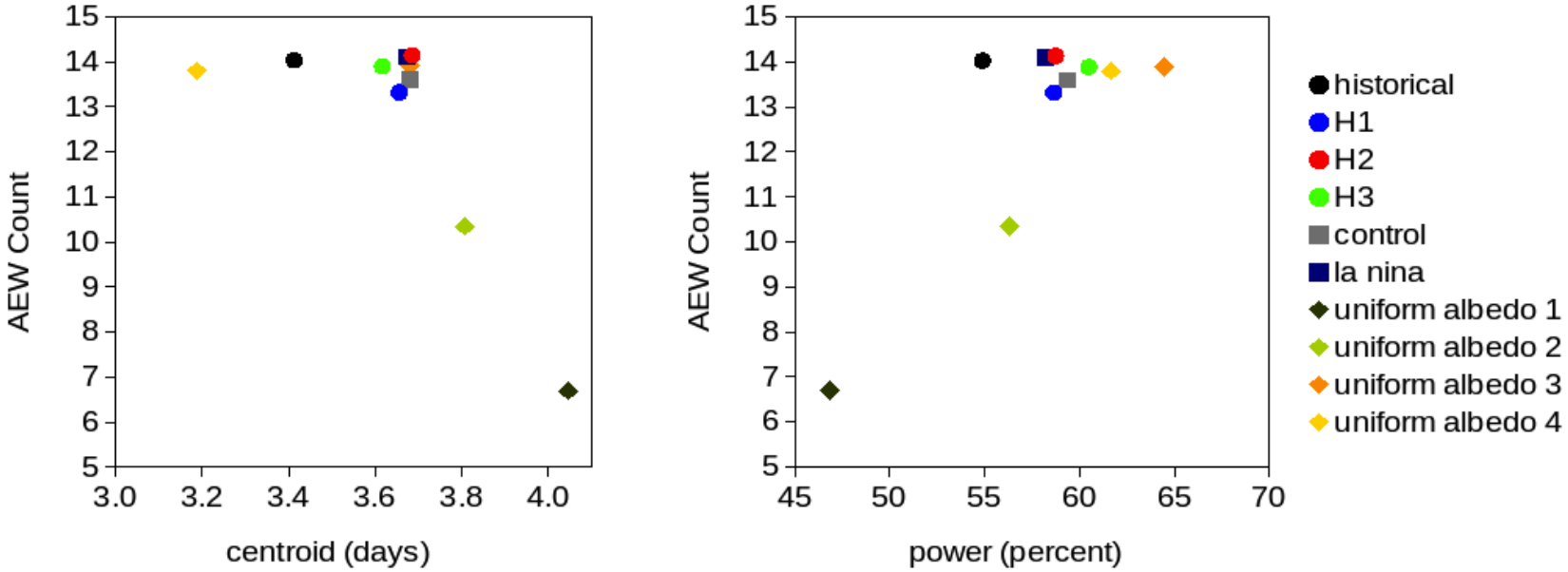

Figure 2.8: AEW count versus spectral statistics calculated for the NCEP-NCAR II reanalysis (historical) and for each of the model simulations (H1, H2, H3, control, la nina, uniform albedo 1, 2, 3, and 4), specifically (a) spectral centroid, and (b) percent power in the 3-5 day spectral band, for 1-10 day band-pass filtered 850 mb meridional wind, averaged between 10°N and 20°N, near the coast of Africa (15°W), from six-hourly data between August 1 and October 31.

in NCEP-NCAR II as compared with the model, the AEW band is less distinct (see Figure 4.3). Since the AEW band is less distinct, the statistics are more heavily influenced by the less relevant frequencies of variability and are therefore less reliable indicators of AEW activity.

This is also true in the fourth uniform albedo simulation, but for different reasons. The fourth uniform albedo simulation is characterized by strong shear over the eastern Atlantic, which may be responsible for the overall decrease in power. Note that the spectral centroid seems to indicate that the fourth uniform albedo simulation should have a much higher AEW count than the third, but the percent power implies that the fourth would have a similar but somewhat lower AEW count to the third. Using the manual tracking methodology, the two simulations have statistically indistinguishable AEW counts, which is not surprising when considering both the centroid and the percent power together.

In general, the spectral centroid and the percent power metrics typically agree on the magnitude and direction of the change in AEW activity between most model runs, and further agree with the AEW activity as diagnosed by count. However, the spectral centroid and the percent power each tells a slightly different story, and both must be considered jointly to parse physical meaning. It is difficult to represent a discrete phenomenon (e.g., event count) with continuous measures (e.g., spectral metrics, variance), so while spectral metrics can provide insight on the nature of the AEW activity, they do not replace count.

Confirming Historical TC Origins with Tropical Cyclone Reports

Further confirmation of the reliability of the manual-automated matching technique can be found in a curated archive of the synoptic origins for each Atlantic TC in the study period. The NHC has released an individual TC Report for every tropical storm since 1958, e.g., Landsea and Blake (2014), which contains "comprehensive

information on each storm, including synoptic history, meteorological statistics, casualties and damages, and the post-analysis best track" (NHC Data Archive, 2014). These reports are written by individual synopticians and are not completely uniform in methodology, but they are informed by all available operational fields and represent the authoritative account of each TC. Reports prior to 1988 are only available as scanned images and early reports are not always precise in their usage of terminology such as "tropical wave," but from these records it is possible to determine storm origins, specifically, whether or not an individual TC developed from or was influenced by an AEW.

After applying the AEW-TC counting methodology detailed in Section 2.2.2 to the historical reanalysis, diagnosing TC origins as described, the NHC report of each storm was reviewed to independently determine the official origins of every storm. For the 420 events between 1979 and 2012, there were only 25 cases where the reanalysis-derived dataset and the official reports disagreed on the origins of an individual TC. This means there was 94% agreement between the experimental method and "objective" reality, as presented by the NHC TC Reports, for TC origins.

Of these 25 disagreements, there were a total of 14 cases where the report attributed TC genesis to non-African origins, but the tracking methodology showed some connection to an AEW. These cases are likely due to varying standards for deciding whether an AEW was worth mentioning in the report, in cases such as when a TC forms during a merger of a frontal system and an AEW. On the other hand, there were 11 cases in which the report attributed storm genesis to an AEW, but evidence of this was not present in the reanalysis. As mentioned in Section 2.3.1, it is possible that some of these discrepancies could be due to NCEP-NCAR II's low resolution.

The level of agreement does not seem sensitive to the temporal definition of the hurricane season, with only 18 of the 322 events during August through October between 1979 and 2012 showing disagreement, again for 94% agreement. This high

degree of agreement lends credence to both the suitability of NCEP-NCAR II for studying the relationship between AEWs and TCs, and to the tracking algorithm itself.

Chapter 3

Results: Historical Record of African Easterly Wave Activity

As discussed in Sections 1.2.1 and 1.2.2, whether AEW count exhibits significant variation interannually has been debated, and the question of whether or to what extent that variability might influence TC activity remains open. In order to legitimize HiRAM for the purpose of studying AEW activity and variability, it is first necessary to clarify the historical record. In this chapter, past studies of the interannual variability of AEWs and TCs are revisited and compared (Section 3.1), then a new climatology of AEW activity from historical reanalysis is constructed using novel methods and compared with past studies (Section 3.2). Conclusions are drawn about the historical relationship between AEW and TC count, and results are summarized (Section 3.3).

3.1 Revisiting Past Studies

Avila et al. (2000) and Thorncroft and Hodges (2001) are often cited, respectively, in opposition to or in support of the notion that AEW activity and TC activity are correlated interannually. In addition to these two influential works, another relevant study is Hopsch et al. (2007), which used the technique developed in Thorncroft and Hodges (2001) to revisit and extend the historical record of AEW activity, ultimately

overturning the still-cited conclusion of the original work that AEW and TC count are correlated interannually.

Since the original studies did release annual counts, but did not necessarily include relevant statistics to make sense of the counts (relying primarily on anecdotal explanations and visual inspection), these counts are revisited and rigorous statistical tests are performed here. First, each study is considered separately (Sections 3.1.1, 3.1.2, and 3.1.3), and then the studies are compared to each other (Section 3.1.4). Since some of the arguments presented by the authors of the original studies were dependent on timeframe and/or ENSO phase, these statistical tests are performed on all years, all years after 1985, El Niño years only, La Niña years only, and neutral ENSO years (see Appendix B for details of the ENSO classification).

3.1.1 Data Published by Avila et al. (2000)

Avila et al. (2000) published a table of Atlantic tropical statistics for the 31 years between 1967 and 1997 (see their Table 1), including the number of waves, both the *total* number and *African* number of tropical systems, broken down into the categories of tropical depressions, tropical storms, and hurricanes, and the ratio of African to non-African systems for each year (TCs were counted as "African" if they developed from an AEW). Atlantic disturbances that emerged from the coast of Africa were tracked manually using synoptic analysis and counts were totaled for the months of May through November (MJJASON). The authors counted all systems that were identifiable in wind, pressure, or cloud patterns for multiple days, with no attempt to eliminate weaker systems.

In the original study, no explicit correlations were calculated and the idea that AEW variability might have any relationship to TC variability was summarily dismissed, since "year-to-year variation in the total number of waves is probably not significant because the process of identifying tropical waves has not been uniformly

applied over the years" (Avila et al., 2000). While this potential inhomogeneity was a reality in earlier works and should be taken into account, the methodology remained fairly consistent throughout publications in which the tables were updated (Avila and Clark, 1989; Avila and Pasch, 1992; Avila et al., 2000). For certain years in Avila et al. (2000) as well as in earlier studies, narratives were constructed by the authors to explain variance. For example, 1972, 1983, and 1997 were identified by the authors as "strong El Niño years," and also years in which there was an abnormally low number of African tropical storms relative to the total number of tropical storms.

Although there was no statistical analysis performed in the original study, the authors attributed much of the observed variability to ENSO variations, so when computing correlation coefficients, the phase of ENSO is taken into consideration (see Appendix B). The correlation coefficients between AEWs and tropical storms, and AEWs and hurricanes were calculated from the historical counts published by Avila et al. (2000) and are displayed in Figure 3.1. All years 1967-1997 are included in the "All" category (31 years), all years after 1985 in the "Post-1985" category (13 years), only years in which ENSO was in its positive phase in the "El Nino" category (9 years), only years in which ENSO was in the negative phase in the "La Nina" category (7 years), and finally all years in which the ENSO index was not strongly positive or negative in the "Neutral" category (21 years).

The statistical analysis suggests that ENSO phase may be a limiting factor in the correlation between AEWs and tropical systems, although this is tempered by small sample size. Considering all years together, all years post-1985, and El Niño years, there is no correlation between AEW and TC activity. Correlation coefficients are larger and skew positive for La Niña years, but this is not statistically significant. Since there are only seven La Niña years in the historical record, it is impossible to know if the lack of significance is due to the lack of a relationship, or simply small sample size.

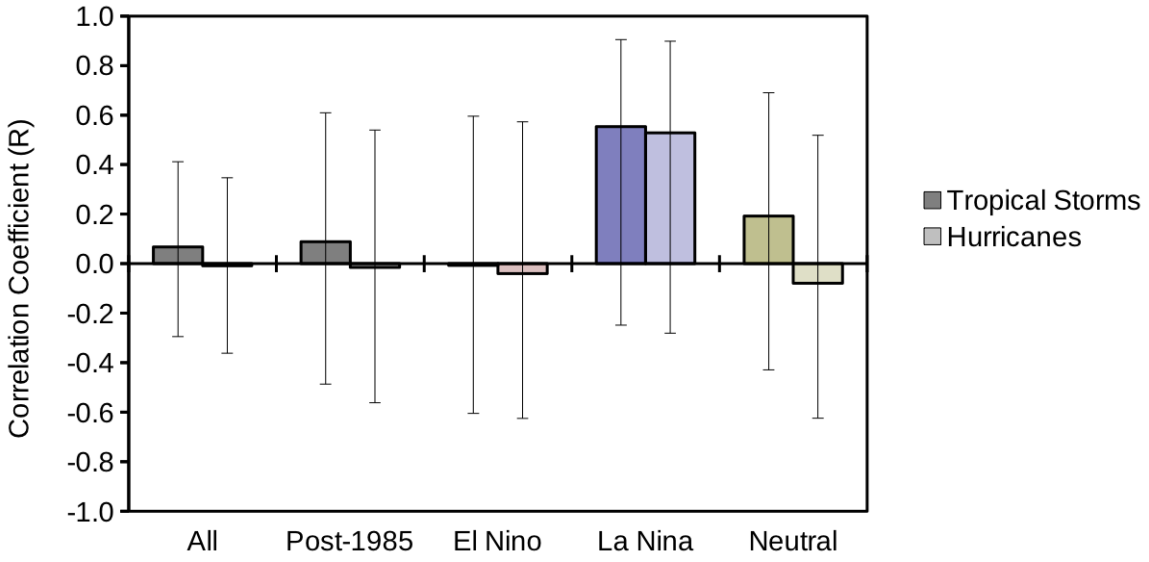

Figure 3.1: Correlation between TC counts and AEW counts calculated from data originally published by Avila et al. (2000). Includes Pearson's correlation coefficients (R-values) between annual (May through November) AEW counts and TC counts, with error bars denoting the 95% confidence intervals. AEW counts are correlated with both tropical storm counts (left) and hurricane counts (right) for all years (n=31, 1967-1997), all years post-1985 (n=13, 1985-1997), El Niño years only (n=11), La Niña years only (n=8), and neutral ENSO years (n=12).

A potential dependence on ENSO phase would not be wholly surprising, since El Niño years are characterized by hostile conditions in the MDR due to increased shear, and previous authors have suggested that this may trump any effect from AEW variability (see Section 1.2.2). Although there could be a difference in the *relationship between* AEW and TC count according to ENSO phase, there is not enough evidence to rule out the possibility that the average AEW *count* is the same regardless of ENSO phase, with an average of 62.0 waves in La Niña years and 57.1 waves in El Niño years (an unpaired Student's t-test returns $p = 0.11$), compared with an overall average of 60.7 waves per year. This lends some credence to the idea that "these waves are very persistent" and "[maintain] their identity and westward progression in spite of any hostile large-scale environment they might encounter" (Avila and Clark, 1989).

Despite the statement to the contrary in the original study, it seems that the AEW count in this dataset does exhibit interannual variability, with a standard deviation of over 11% of the mean. While the statistical analysis performed here of the counts published by Avila et al. (2000) suggests that AEW variability likely comes second to large-scale favorability, it also hints that there may be a weak correlation between AEW activity and TC activity in the absence of a strong El Niño.

3.1.2 Data Published by Thorncroft and Hodges (2001)

Although Thorncroft and Hodges (2001) are often cited in support of the claim that AEW and TC interannual variability are correlated, the original analysis was based on visual inspection and the quantitative correlations found in their data are weak at best. Part of this may be due to the small sample size, since the study only considered the 20 years from 1979 through 1998, but even the weak patterns found in these years do not hold when the same counting techniques were later used to extend the record (Hopsch et al., 2007). Potential reasons for this are discussed in Section 3.1.4, but one possible explanation involves the importance of the seasonal cycle. Therefore, it is important to note that Thorncroft and Hodges included systems from May through October (MJJASO).

As mentioned in Section 2.2.2, this was the first study to attempt to track AEWs using an automated system, tracing closed relative vorticity maxima that exceed a threshold value, last for 2 of more days, and travel at least 10° zonally in ECMWF reanalysis from 1979 to 1993 (Gibson, 1997) and ECMWF operational analyses between 1994 and 1998. Thorncroft and Hodges counted 850 mb waves in a box between 5°–15°N and 10°–20°W using the tracker output, and these counts are plotted along with named storm, hurricane, and intense hurricane counts for comparison in Figure 13 of the original study. The box was chosen because the authors found the southern storm track to be the most relevant to TC development and the northern track to have

comparatively little interannual variability. No statistical tests were performed in the original study, but a "visual inspection" indicated that "from 1985 onward there [was] a strong positive correlation" between AEW activity (850 mb wave counts) and TC activity.

To test these conclusions, values were manually transcribed from the plot in Figure 13 of Thorncroft and Hodges (2001) for analysis. Years are again grouped as described above in Section 3.1.1, to calculate correlation coefficients between AEW count and tropical storm count totals, and AEW count and hurricane count totals for the relevant months. Results are shown in Figure 3.2. All years 1979-1998 are included in the "All" category (20 years), only years after 1985 in the "All Post-1985" category (14 years), only years in which ENSO was in its positive phase in the "El Nino" category (6 years), only years in which ENSO was in the negative phase in the "La Nina" category (4 years), and finally all years in which the ENSO index was not strongly positive or negative in the "Neutral" category (10 years).

The small sample size makes it difficult to draw conclusions about the potential importance of the phase of ENSO in this dataset. The correlation coefficients in the La Niña bin are virtually meaningless, since there were only 4 years included and the confidence intervals are expansive. Although the reasons are unclear, the 1985-1998 correlation coefficients are significantly positive at the 95% confidence level, with both tropical storm and hurricane counts correlated with AEW count. Otherwise, there are no statistically significant correlations, and when revisited by Hopsch et al. (2007), the difference between the pre- and post-1985 relationship vanishes. This is discussed further in the next section.

The AEW count in this dataset exhibits strong interannual variability, with a standard deviation of 29% of the mean. There is not enough evidence to rule out the possibility that the average AEW count is the same regardless of ENSO phase, with an average of 14.5 waves in La Niña years and 12.0 waves in El Niño years (an

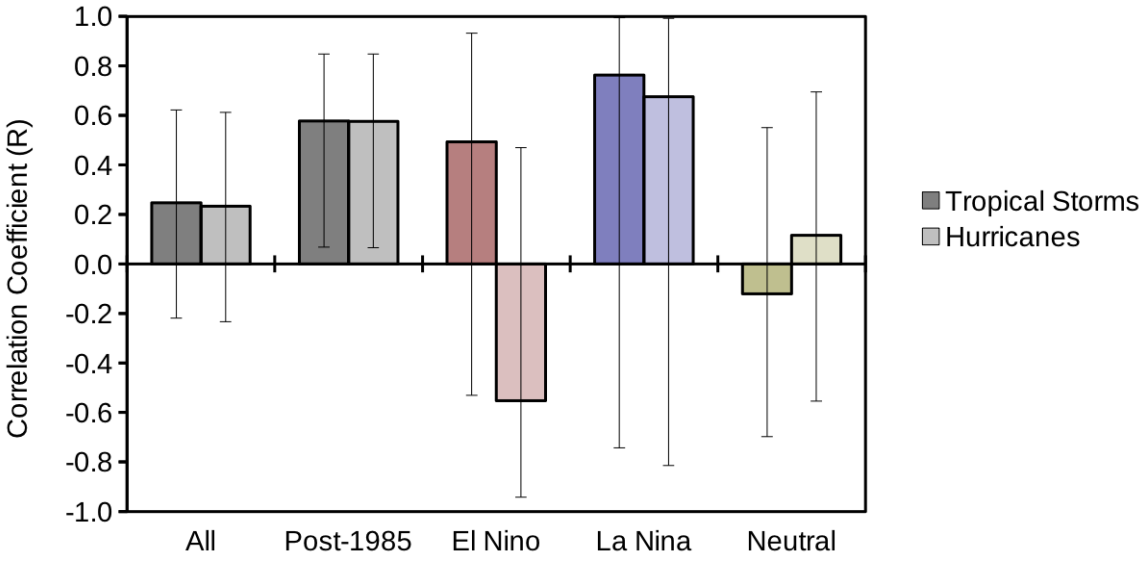

Figure 3.2: Correlation between TC counts and AEW counts calculated from data originally published by Thorncroft and Hodges (2001). Includes Pearson's correlation coefficients (R-values) between annual (May through October) AEW counts and TC counts, with error bars denoting the 95% confidence intervals. AEW counts are correlated with both tropical storm counts (left) and hurricane counts (right) for all years (n=20, 1979-1998), all years post-1985 (n=14, 1985-1998), El Niño years only (n=6), La Niña years only (n=4), and neutral ENSO years (n=10).

unpaired Student's t-test returns $p = 0.32$), compared with an overall average of 12.3 waves per year.

3.1.3 Data Published by Hopsch et al. (2007)

Hopsch et al. (2007) applied the automated tracking technique from Thorncroft and Hodges (2001) to July through October (JASO) data from ERA-40 (Uppala et al., 2005), whereas the original study combined May through October data from an earlier reanalysis (Gibson, 1997) with additional years from operational analysis. Like Thorncroft and Hodges (2001), Hopsch et al. (2007) found that the southern storm track is the most relevant for TC development and has significant seasonal and interannual variability, but unlike Thorncroft and Hodges, Hopsch et al. found that AEW counts were uncorrelated with TC activity interannually.

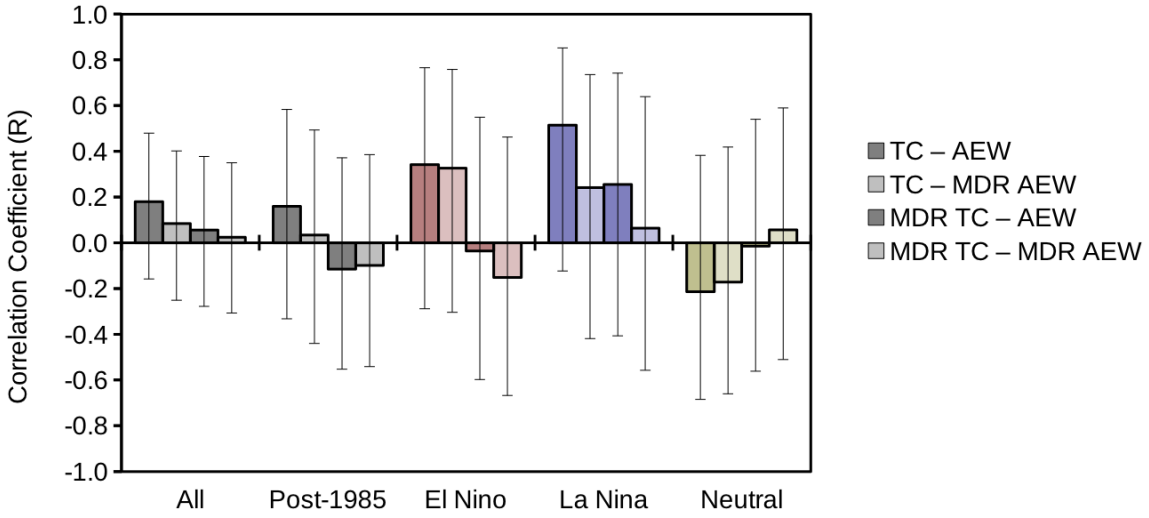

Figure 3.3: Correlation between TC counts and AEW counts calculated from data originally published by Hopsch et al. (2007). Includes Pearson's correlation coefficients (R-values) between annual (July through October) AEW counts and TC counts, with error bars denoting the 95% confidence intervals. Correlations are shown between TC and AEW counts (far left), TC counts and MDR AEW counts (center left), MDR TC counts and AEW counts (center right), and MDR TC and MDR AEW counts (far right) for all years (n=36, 1967-2002), all years post-1985 (n=18, 1985-2002), El Niño years only (n=12), La Niña years only (n=11), and neutral ENSO years (n=13).

To verify, values were manually transcribed from the plot in Figure 8 of Hopsch et al. (2007) for further analysis. Years are grouped as in the previous sections, with "All" encompassing the years 1967-2002 (36 years), "Post-1985" including 1985-2002 (18 years), "El Niño" including only strong positive ENSO phase years (12 years), "La Niña" including only negative ENSO years (11 years), and finally "Neutral" including the years with neither strongly positive nor strongly negative ENSO index (13 years). Hopsch et al. provided not only the counts of AEWs from the southern storm track (using roughly the same box as Thorncroft and Hodges, 9°–18°N and 10°–20°W) and TC counts, but also the number of TCs that formed in and the number of AEWs that reached the MDR (defined as 10°–20°N and 20°–80°W).

The correlation coefficients calculated from the historical counts published by Hopsch et al. (2007) are shown in Figure 3.3, including the correlation between the

TC count and AEW count from Hopsch et al. (2007), the total TC count and the MDR AEW count, the MDR TC count and the total AEW, and the MDR TC count and the MDR AEW count. In contrast to Thorncroft and Hodges (2001) and Figure 3.2, there is notably little difference between the AEW-TC relationships in the subset of post-1985 years when compared to the full timeseries. Despite this being a follow-up study to Thorncroft and Hodges (2001), Hopsch et al. (2007) did not have an explanation for this discrepancy, remarking:

> [W]*e found that* [the significant interannual AEW variability] *is not significantly correlated with Atlantic tropical cyclone activity. This disagrees with the suggestion made by TH01* [Thorncroft and Hodges, 2001], *that tropical cyclones may be weakly but positively correlated with the numbers of storms. In fact, even the short period in TH01 where there appeared to be a positive correlation (1985–98) is not reproduced in the present analysis. The reasons for the differences are not easy to determine, although it should be noted that TH01 used arguably a reanalysis product (ERA-15) that is not as good as the one used in the current study* [ERA-40], *together with operational analysis that included years where different assimilation systems were used and the resolution progressively increased. The best correlation with tropical cyclones in the TH01 study appeared to be exactly when the operational analyses were used* [four years, 1994-1998].

There is no significant correlation on an interannual scale in any of the combinations of TC and AEW counts shown in Figure 3.3. Hopsch et al. (2007) also considered low-frequency variation (11-year running mean count) and argued for a relationship, but the dataset is quite short to draw convincing conclusions from such low-frequency and small amplitude variation. Furthermore, there is not a clear argument why one would expect a running average to be physically meaningful, as there

is no evidence interannual count variation is not stochastic, and the choice of eleven years is arbitrary.

Hopsch et al. (2007) also argue that seasonal variation in TC and AEW count may be related, and further that AEW count may be more important than environmental factors. While the TC and AEW counts do share similar seasonal cycles, their argument that this is more important than the environment is flawed, as the authors were mistaken on the effect shear has on environmental favorability, arguing:

> *In contrast* [to the seasonal peak of AEW and TC count in September], *the tropospheric deep vertical shear shows no such peak in September suggestive of the fact that seasonal variations in storm* [AEW] *activity at the height of the tropical cyclone season may be more important than seasonal variations in the environment (measured in terms of shear).*

In the accompanying figure (their Figure 7), the 200-850 mb shear shows a clear minimum in September, which actually corresponds with *maximum* favorability (measured in terms of shear).

The AEW count in this dataset does exhibit strong interannual variability, with a standard deviation of 21% of the mean for all AEWs, and 29% of the mean for AEWs that make it to the MDR. There is no statistical difference between average AEW count when binning by ENSO phase, with an average of 15.3 waves in La Niña years and 15.1 waves in El Niño years (an unpaired Student's t-test returns $p = 0.88$), compared with an overall average of 15.2 waves per year total. Considering only the subset of waves that proceed to the MDR, there are an average of 9.6 waves in La Niña years and 9.9 waves in El Niño years (an unpaired Student's t-test returns $p = 0.80$), compared with an overall average of 10.1 waves annually between June and October.

3.1.4 Intercomparison of Past Studies

Since Avila et al. (2000), Thorncroft and Hodges (2001), and Hopsch et al. (2007) each set out to produce a historical climatology of AEW count that is relevant for comparison with annual TC counts, one might expect to find agreement in the interannual variability of AEW activity reported by each study. Surprisingly, the AEW counts from the 19 overlapping years of the two most-cited studies, Avila et al. (2000) and Thorncroft and Hodges (2001), exhibit no statistically significant correlation with each other, with a coefficient of determination of $R^2 < 0.01$. Perhaps this could be attributed to differences in methodology, since the authors used very different methods of enumerating AEW count. Yet despite Hopsch et al. (2007) having been a follow-up study to Thorncroft and Hodges (2001) and using an almost identical methodology, there is not a significant correlation in AEW counts across these two studies during the 20 overlapping years either, with a coefficient of determination of $R^2 = 0.03$.

Regardless of the original conclusions drawn by the authors, the data from Avila et al. (2000) does exhibit interannual variability and may hint at a weak connection between AEW activity and TC activity in the absence of a strong El Niño, despite no apparent statistically significant change in average AEW count with ENSO phase. Since this dependence of the AEW-TC relationship on ENSO phase is not present in other studies, it may be due to the peculiarities of the specific methodology the authors employed. The relationships uncovered in the statistical analysis are weak, with any potential signal likely masked by two methodological choices. Specifically, the authors: 1) counted anything remotely resembling an AEW, so weak systems and simultaneous twin vortices may have been overrepresented, and 2) defined the season of interest very broadly, as May 1 through November 30 (MJJASON).

On the other hand, Thorncroft and Hodges (2001) claimed to have uncovered a historical correlation between AEW count and TC count, especially for the short time period from 1985 through 1998. While the reported correlation was based on

visual inspection and the study wanted for quantitative statistics, there is indeed a statistically significant positive correlation present between the 1985-1998 AEW and TC counts from the original study. The authors did not suggest any physical explanation for the reported shift in the AEW-TC relationship after 1985, and the follow-up study from Hopsch et al. (2007) found that this post-1985 correlation is not actually reproducible, in that it is not present in an extended historical record created using similar methodology. However, the historical AEW records set forth by both Thorncroft and Hodges (2001) and Hopsch et al. (2007) do indeed exhibit marked interannual variability, stronger than that of Avila et al. (2000).

The drastically different average count yielded by each study is another symptom of the inconsistencies in the methodologies used. Where Avila et al. (2000) may have erred on the side of over-counting disturbances, Thorncroft and Hodges (2001) and Hopsch et al. (2007) systematically excluded certain waves, specifically those propagating along the AEJ_N and those lacking a closed vorticity contour, resulting in significantly lower AEW counts. Avila et al. (2000) found an average of 60.7 AEWs each year, compared with 12.3 for Thorncroft and Hodges (2001) and 15.2 for Hopsch et al. (2007). Avila et al. (2000) used manual synoptic analysis to count all AEWs for the months of May through November, while Thorncroft and Hodges (2001) and Hopsch et al. (2007) only considered AEWs identified by an automated tracker in a $10^\circ \times 10^\circ$ box that was designed to count AEWs propagating along the AEJ_S, for the months of May through October and July through October, respectively.

Despite Hopsch et al. (2007) totaling AEW counts for fewer months than Thorncroft and Hodges (2001) (JASO versus MJJASO), the former study reported higher average counts than the latter. While Hopsch et al. (2007) suggest that differences in AEW-TC correlations may be attributable to the difference in reanalysis products used between the two studies, and this argument could be extended to the differences in counts, the discrepancy in average count could also be due to their repositioning of

the AEW domain of interest from Thorncroft and Hodges (2001) or due to differences in the range of dates averaged (1967-2002 versus 1979-1998).

Along with the counting method, the variability of "total count" of AEWs is likely sensitive to the seasonal timeframe considered. Unfortunately, the past works discussed here did not provide monthly breakdowns of the AEW counts annually, so it is impossible to determine the relative importance of the differences in counting methodologies versus definitions of AEW seasons. Hopsch et al. (2007) found that AEWs seem to be more likely to develop into TCs in August and September, with roughly 40% of waves developing, compared to 0%, 12%, and 15% in June, July, and October. That, coupled with the fact that there tend to be many AEWs before the hurricane season begins in earnest, means the seasonal cycle is an important factor to consider when studying the relationship between AEWs and TCs.

Figure 3.4 shows a detailed comparison of the interannual variability of the AEW counts of the three different studies, including cross-study correlation coefficients and 95% confidence intervals, broken into the same categories for which each study's AEW counts were compared to TC counts in Figures 3.1, 3.2, and 3.3. There is no statistically significant correlation for AEW count between any of the three past studies detailed above, regardless of the timeframe or ENSO phase considered. This is likely due to the differences in counting methodology mentioned above.

Since there is no agreement between any of the major past works that examined AEW variability in order to test for correlation with interannual TC variability, either on the AEW historical record itself or on the conclusions drawn about the relationship between AEWs and TCs, it is necessary to establish a baseline historical record of AEW activity using reanalysis before moving on to analyze model results. To address this deficiency in the literature, the historical record produced by applying the methodology discussed in Section 2.2.2 to NCEP-NCAR II reanalysis data is presented in the next section.

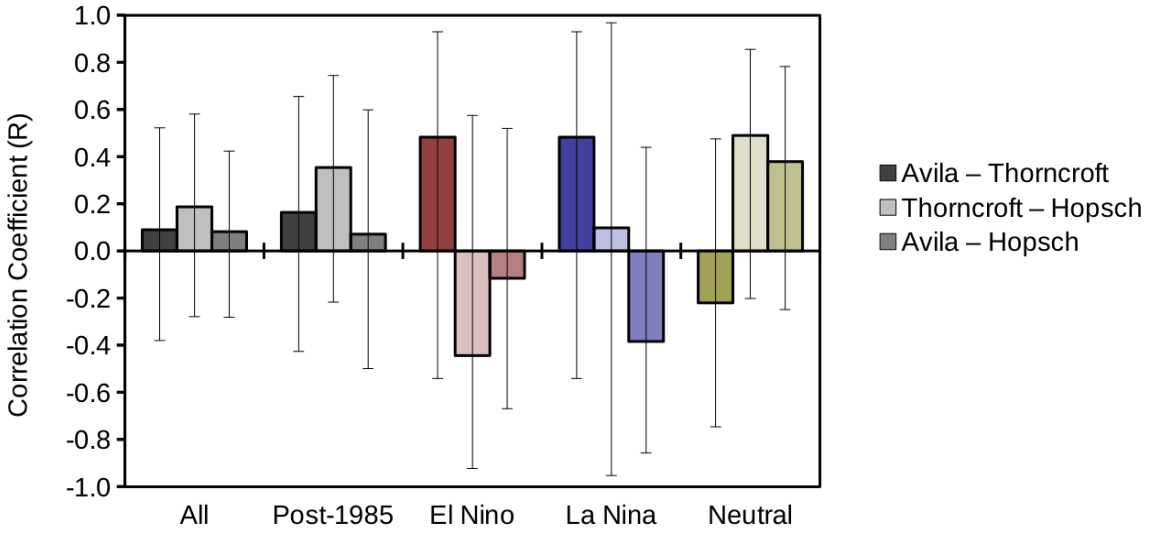

Figure 3.4: Correlation of AEW counts across studies, calculated from data originally published by Avila et al. (2000), Thorncroft and Hodges (2001), and Hopsch et al. (2007). Includes Pearson's correlation coefficients (R-values) between the annual AEW counts of each study, with error bars denoting the 95% confidence intervals. Total AEW counts for overlapping years are correlated between Avila et al. (2000) and Thorncroft and Hodges (2001) (left), Thorncroft and Hodges (2001) and Hopsch et al. (2007) (center), and Avila et al. (2000) and Hopsch et al. (2007) (right), for all overlapping years, all overlapping years post-1985, overlapping El Niño years only, overlapping La Niña years only, and overlapping neutral ENSO years.

3.2 Establishing Historical AEW Activity Using Reanalysis

The results of applying novel tracking techniques (described in Section 2.2.2) to NCEP-NCAR II reanalysis (described in Section 2.1.1) are presented here, producing a new climatological record of AEW activity from 1979 through 2012 to address the shortcomings of past studies (described in Section 3.1.4). Several aspects of this new historical record of AEW activity are detailed and compared with past studies where appropriate, including the seasonal cycles of AEW and TC count statistics (Section 3.2.1), the power spectrum and statistical measures of AEW activity (Section 3.2.2), and the interannual variability of AEW and TC count statistics and

potential correlations (Section 3.2.3). Finally, a multiple linear regression model of TC count is considered (Section 3.2.4).

3.2.1 Seasonal Cycle of Count Statistics

Few past studies of AEWs have reported AEW counts separately by month, but most studies that consider seasonal cycle agree that peak AEW activity typically occurs in August or September. In tracking closed vorticity contours, Thorncroft and Hodges (2001) found a strong peak in seasonal AEW activity in August at the 600 mb level, and in September at the 850 mb level. Using composite spectral analysis to perform a global analysis of OLR, Frank and Roundy (2006) found that tropical cyclones and AEWs have similar seasonal cycles. When Hopsch et al. (2007) analyzed 2- to 6-day filtered 850 mb meridional wind variance from reanalysis, AEW activity was elevated from July through October. Similarly, Agudelo et al. (2011) found that about 35% of the annual AEW activity occurred in the months of July through September, with peak activity in August.

As explained in Section 2.2.2, the present tracking methodology produces monthly counts of AEWs, developing AEWs, TCs, and African TCs. These monthly counts are averaged over all of the years of the reanalysis (1979-2012) and are plotted in Figure 3.5, along with 95% confidence intervals. The seasonal cycle of AEWs (Figure 3.5a) shows good agreement with past studies (Thorncroft and Hodges, 2001; Frank and Roundy, 2006; Hopsch et al., 2007; Agudelo et al., 2011), with AEW activity elevated July through October and peaking in August.

Although there are more AEWs in July than in October (see Figure 3.5a), relatively few of them mature into TCs, compared to the months of August through October (see Figure 3.5c). The environment becomes more favorable and hurricane season picks up somewhat abruptly in August (see Figure 3.5b), with August through October showing the most elevated TC activity on average. Because the focus of this

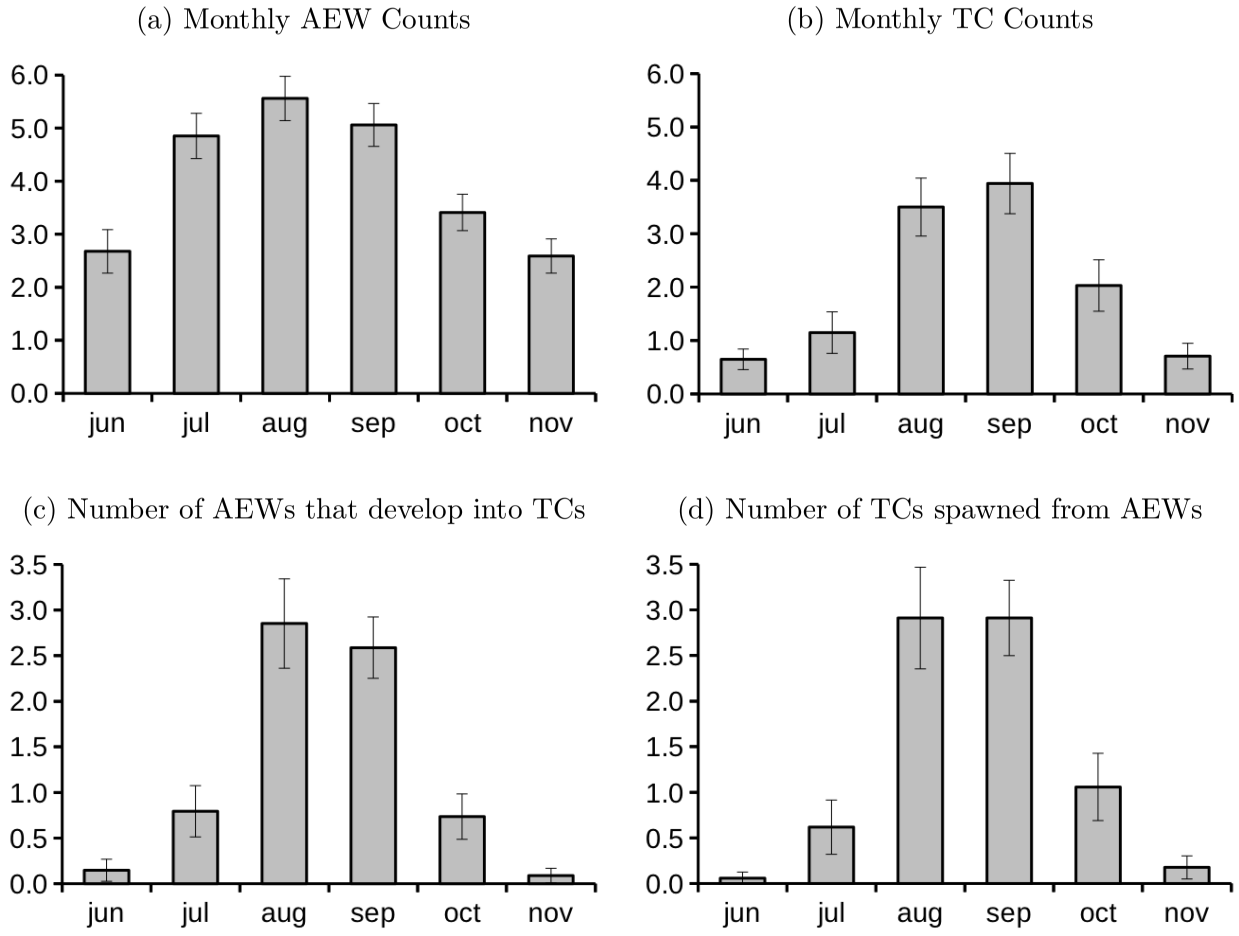

Figure 3.5: Average monthly counts of (a) AEWs, (b) TCs, (c) developing AEWs, and (d) African TCs, for the historical record as determined from NCEP-NCAR II reanalysis and IBTRaCS. Error bars denote 95% confidence intervals.

study is to compare AEW and TC variability, it is reasonable to select the months in which both AEW and TC activity are elevated for consideration. For this reason, total August through October (ASO) counts are subsequently referred to as "annual counts," unless otherwise specified.

3.2.2 Power Spectrum and AEW Statistical Measures

The statistical techniques discussed in Section 2.3.3 and used to validate the AEW counting methodology across all simulations were applied to the NCEP-NCAR II reanalysis data to produce a normalized power spectrum of 1-10 day band-pass filtered 850 mb meridional winds, averaged between 10°N and 20°N near the coast of Africa, from six-hourly data between August 1 and October 31, averaged for the years 1979-2012 (see Figure 3.6). The general shape of this spectrum compares favorably with similar spectral representations of AEWs from past studies (Albignat and Reed, 1980; Lau and Lau, 1990; Thorncroft and Rowell, 1998), with a period of maximum power of 3.4 days, a spectral centroid of 3.4 days, and 55% of the power located in the 3-5 day band. This provides further evidence that NCEP-NCAR II adequately captures AEW variability (see also Section 2.3.1) and is an objective check on the reasonability of the manual measure of AEW activity. This power spectrum is revisited in more detail in Section 4.2, in comparison with model-derived spectra.

3.2.3 Interannual Variability of Count Statistics

This section begins with a comparison of the interannual variability of AEW activity in the present study with that reported by Avila et al. (2000), Thorncroft and Hodges (2001), and Hopsch et al. (2007), and a discussion of the features that distinguish the present study from the existing literature. Once this context has been established, the dataset produced using the manual-automated tracking technique is examined

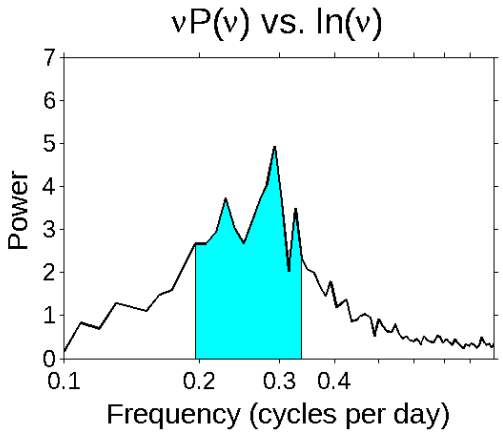

Figure 3.6: Normalized power spectrum of 1-10 day band-pass filtered meridional wind at 850mb, averaged between 10°N and 20°N, at the coast of Africa (15°W), for August 1 through October 31, averaged for 1972-2012 for NCEP-NCAR II reanalysis. The 3-5 day band is highlighted in cyan.

further, with a focus on the relationship between AEW activity and TC activity on seasonal timescales.

To compare the present annual count statistics with count statistics from the past studies discussed in Section 3.1 interannually, AEW counts were totaled for the months that overlap with each study and then correlation coefficients were calculated between these "annual counts" from the NCEP-NCAR II reanalysis and each of the past studies. It is worth noting that the definition of the season does not seem to have an extreme effect on the interannual variability of AEW count in the current study (this is discussed further below), but months were matched as closely as possible when comparing with each past study to minimize confounding variables. Although some past studies have included AEWs from May in their total seasonal counts, the current methodology only provides counts for June through November, since May is not technically part of hurricane season. Ultimately, the June through November NCEP-NCAR II counts were compared with the May through November counts from Avila et al. (2000), June though October with the May through October counts from

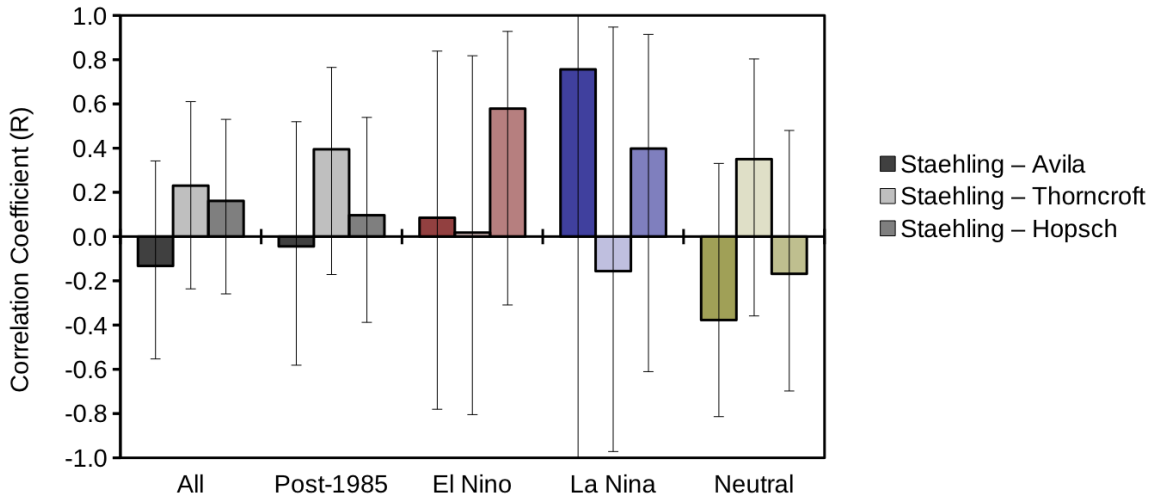

Figure 3.7: Correlation of AEW counts between the present study and past studies, calculated using data originally published by Avila et al. (2000), Thorncroft and Hodges (2001), and Hopsch et al. (2007). Includes Pearson's correlation coefficients (R-values) between the annual AEW counts of each study, with error bars denoting the 95% confidence intervals. Total AEW counts established in this study are correlated with Avila et al. (2000) (left), Thorncroft and Hodges (2001) (center), and Hopsch et al. (2007) (right), for all overlapping years, all overlapping years post-1985, overlapping El Niño years only, overlapping La Niña years only, and overlapping neutral ENSO years.

Thorncroft and Hodges (2001), and July through October with the corresponding counts from Hopsch et al. (2007).

No statistically significant correlation for AEW count between the present study and any of the three past studies was found, regardless of the timeframe or ENSO phase considered, as shown in Figure 3.7. This lack of agreement with past studies might be worrisome, except for the fact that none of the past studies agree with each other (recall Figure 3.4). It is impossible to make a value judgment on the accuracy of the current study based on its lack of agreement with irreconcilable past studies. Some possibilities are briefly discussed in Section 3.1.4, but without more details of the past studies than are publicly available, it is impossible to determine precisely why they differ from each other, or from the current study.

There are several relevant differences between the methodology used here and the methodology of past studies, including differences in the types of waves counted and the choice of months examined, which conceivably make the present dataset more compelling and relevant for addressing the problem at hand. As described in Section 2.2.2, the methodology used in this study was designed to target and count relevant AEWs, i.e., capturing signatures of strong waves propagating along both the AEJ_N and AEJ_S, without double-counting "simultaneous twin vortices" (Fink et al., 2004), and only counting waves that originated in Africa and make it to the MDR, giving these waves a chance to develop into TCs. While Avila et al. (2000) counted every Atlantic wave, perhaps double-counting "simultaneous twin vortices" and including weak transient systems in the process, Thorncroft and Hodges (2001) and Hopsch et al. (2007) systematically excluded certain waves, not only intentionally excluding waves propagating along the AEJ_N, but perhaps unintentionally excluding those that did not have a closed vorticity contour. These methodological differences are manifest in the very different annual counts for each study. Correcting for the number of months considered, the number of AEWs counted annually using the current methodology is significantly greater than for Thorncroft and Hodges (2001) and Hopsch et al. (2007), but is significantly fewer than for Avila et al. (2000).

As argued in Section 3.2.1, since the focus of this study is comparing AEW and TC variability, it is reasonable to consider only months in which both AEW and TC activity are elevated. This intentional choice means there is a better chance of locating a signal within the noise and determining if there is a relationship between AEWs and TCs, as AEW variability in months during which there are few or no TCs is less likely to have an impact on TC variability. On the other hand, both Avila et al. (2000) and Thorncroft and Hodges (2001) defined their season of interest very broadly, as MJJASON and MJJASO, respectively. Since the intercomparison of past studies in Section 3.1.4 indicated that there might be sensitivity to the definition of a

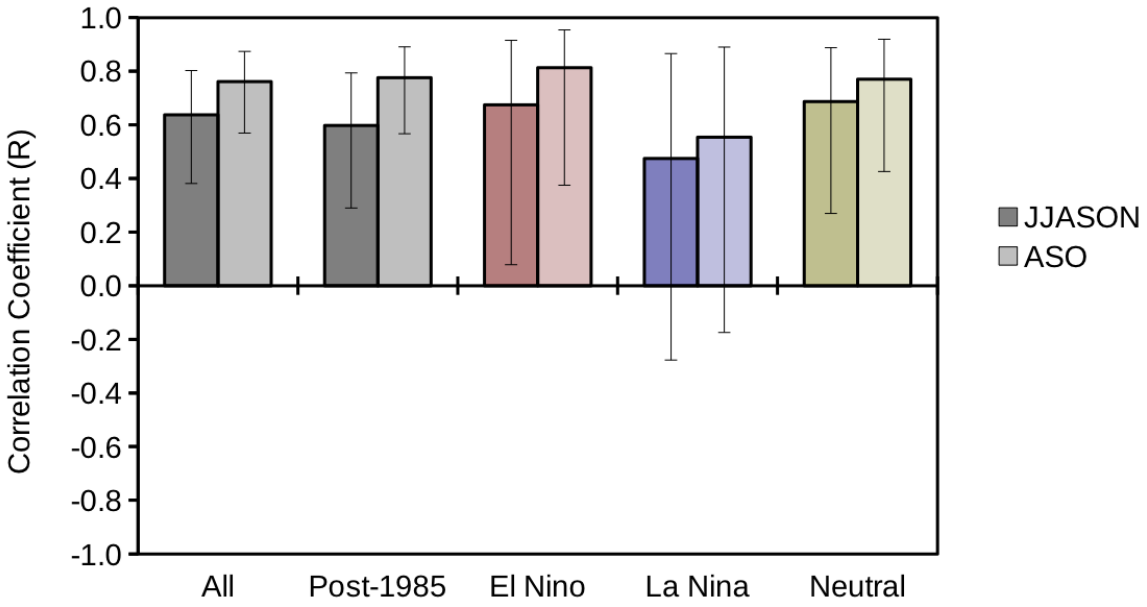

Figure 3.8: Correlation between TC counts and AEW counts from present study. Includes Pearson's correlation coefficients (R-values) between annual (defined two different ways) AEW counts and TC counts, with error bars denoting the 95% confidence intervals. TC and AEW counts are totaled for the months of June through November (JJASON, left) and August through October (ASO, right) and correlated for all years (n=34, 1979-2012), all years post-1985 (n=28, 1985-2012), El Niño years only (n=10), La Niña years only (n=9), and neutral ENSO years (n=15).

season, the AEW and TC counts produced using the current methodology as applied to NCEP-NCAR II are first correlated interannually for both the entire hurricane season (June 1 through November 31) and for the peak months of activity (August 1 through October 31), broken into the same categories for which past studies were examined and compared and shown in Figure 3.8.

While the correlations are unsurprisingly stronger for the months of elevated AEW and TC activity (ASO), even the seasonal totals (JJASON) of AEW and TC count show statistically significant positive correlation interannually in Figure 3.8. While the signal is stronger when isolating the months of elevated activity, the interannually variability does not seem strongly dependent on the definition of the season in the present study. This may or may not hold true in past studies, but does suggest that

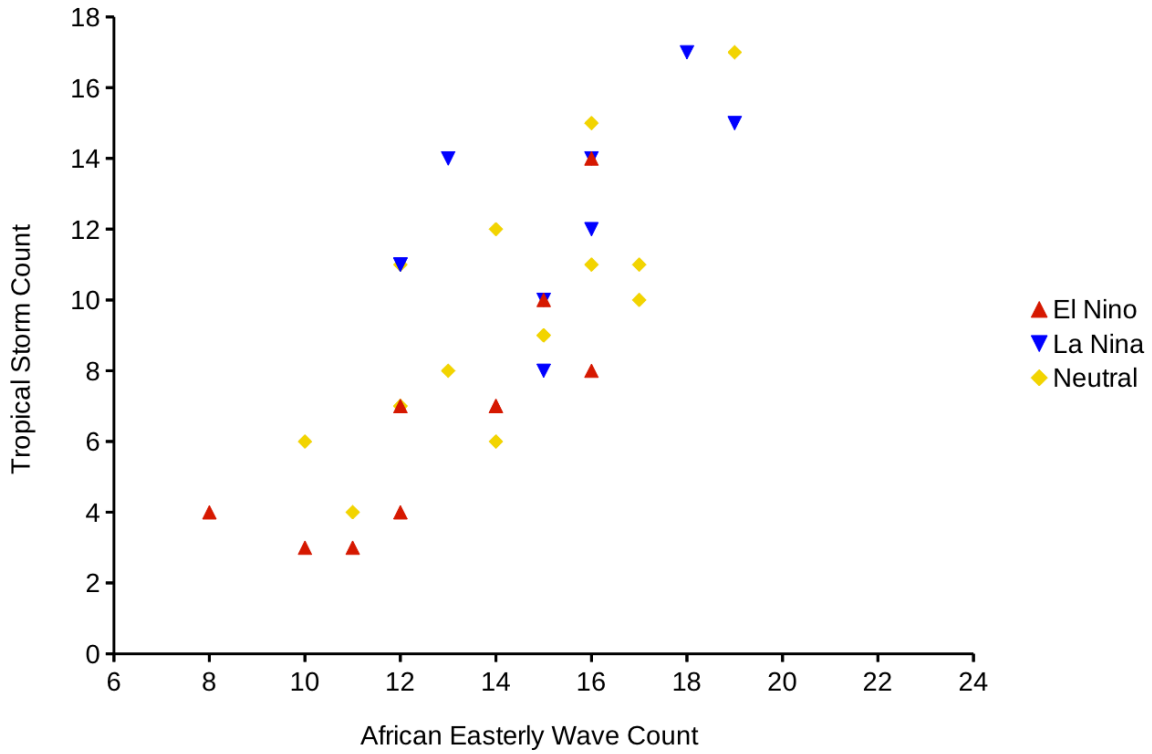

Figure 3.9: Scatterplot of annual total TC count versus AEW count for the months of August through October (ASO), as determined from NCEP-NCAR II reanalysis and IBTrACS. Each point is color-coded by the ENSO phase of the year, with El Niño years in red, La Niña years in blue, and neutral ENSO years in yellow.

the differences in counting methodology may be more important than the differences in the months considered when comparing studies. As in past studies, the AEW count in this newly-derived historical dataset does exhibit strong interannual variability, with a standard deviation of 18% of the mean, regardless of the definition of season (JJASON, JJASO, JASO, or ASO).

Figure 3.9 shows a scatterplot of annual (ASO) TC count versus AEW count for all years in the present reanalysis-derived historical record, with El Niño years plotted as red triangles, La Niña years as blue triangles, and neutral ENSO years as yellow diamonds (see Appendix B for definitions of the ENSO classifications). Contrary to the conclusion suggested in the analysis of the data from Avila et al. (2000) in Section 3.1.1, that correlation might be stronger in the absence of a strong El Niño,

the relationship between AEW count and TC count appears *weaker* in La Niña years than in El Niño years (see Figure 3.8 for correlation coefficients). This is likely an artifact of small sample size and is not conclusive, with only 9 La Niña years in the dataset. The importance of ENSO phase is revisited throughout this dissertation, particularly in Sections 3.2.4, 4.5, and 5.3.

3.2.4 Multiple Linear Regression Models of TC Count

As shown in Figure 3.8 of Section 3.2.3, there is a significant interannual correlation between annual (ASO) AEW count and TC count, with a 95% confidence interval of $0.569 < \mathrm{R} < 0.874$ ($\mathrm{R}^2 = 0.57$, $\mathrm{p} = 1.8 \times 10^{-7}$). Another way of expressing this result is that the measured AEW variability explains 57% of the variance in TC count. This is a significant result itself, providing the first quantitative evidence supporting the conclusions suggested by Thorncroft and Hodges (2001).

One could argue that this correlation is not causal and is instead mediated by external factors, and that perhaps AEW variability does not play an active role in influencing TC activity, but rather the AEW and TC counts are controlled by the same large-scale environmental factors. As suggested by Avila et al. (2000), changes in AEW activity could simply reflect changes in the phase of ENSO. To address this concern, stepwise linear models of TC count are constructed, using ENSO index (see Appendix B for details), AEW count, and the year as the set of predictors for multiple linear regression models. These three potential predictors were each tested separately, as well as in various combinations, producing the adjusted coefficients of determination and associated p-values shown below in Table 3.1. In this table, notation of the form $y \sim 1 + x_1 + x_2 + x_3$, where y is the predictand and x_i are predictors, is shorthand for the multiple linear regression model $y = C_0 + C_1 x_1 + C_2 x_2 + C_3 x_3$, where C_i are constants.

Table 3.1: Multiple Linear Regression of Historical TC Counts (1979-2012)

Linear Model	**Adjusted R^2**	**p-value**
TC $\sim$ 1 + AEW	0.566	1.8×10^{-7}
TC $\sim$ 1 + year	0.321	2.8×10^{-4}
TC $\sim$ 1 + ENSO	0.233	2.3×10^{-3}
TC $\sim$ 1 + year + ENSO	0.516	4.9×10^{-6}
TC $\sim$ 1 + year + ENSO + AEW	0.712	7.1×10^{-9}

The year, ENSO index, and AEW count each shows significant skill over a constant model in explaining TC count. As shown in Table 3.1, there is a statistically significant trend in the TC count data ($R^2 = 0.321$, $p = 2.8 \times 10^{-4}$), associated with an average slope of 0.23 additional TCs each year, which may be associated with the tendency for negative Atlantic Meridional Mode states prior to 1995 and positive thereafter (Kossin and Vimont, 2007). Of AEW count, year, and ENSO phase, AEW count explains the highest percentage of variance in TC count, and each individually explains 57%, 32%, and 23%, respectively. Together, year and ENSO index account for 52% of the variance in TC count ($R^2 = 0.516$, $p = 4.9 \times 10^{-6}$), but the addition of AEW count increases this to over 71% ($R^2 = 0.712$, $p = 7.1 \times 10^{-9}$). The p-value to accept AEW count as an additional predictor in the stepwise model is $p = 0.000053$, which demonstrates that it provides a statistically significant improvement over year and ENSO index alone.

Notably, there is no statistically significant covariance between AEW count and ENSO index ($R^2 = 0.079$, $p = 0.11$). There is a weak but statistically significant trend evident in AEW count, i.e., AEW count increases with time, with a slope of an average of 0.13 additional AEWs per year ($R^2 = 0.239$, $p = 0.0033$). This is worth noting, but since the AEW count was derived from reanalysis, as mentioned in Section 2.1.1, trends cannot be trusted at face value, due to discontinuities in assimilated observational data. (The trend in TC count, on the other hand, was not derived from the reanalysis, and therefore represents the ostensibly real trend present in IBTRaCS).

Finally, to estimate the contribution of AEW count to TC count variability beyond what is explained by ENSO phase and annual trends, both AEW count and TC count are detrended by ENSO phase and year, and the residuals are then correlated. Correlating these AEW and TC residuals yields a statistically significant relationship, with a 95% confidence interval of $0.368 < R < 0.797$ ($R^2 = 0.395$; $p = 7.0 \times 10^{-5}$). In other words, even when the effects of ENSO phase and annual trends are removed, AEW variability still explains approximately 40% of TC interannual variability. From this analysis, it is clear that AEW count provides skill above and beyond the large-scale conditions encapsulated in the ENSO index.

3.3 Summary and Discussion

While past studies have attempted to determine whether or not AEW and TC activity are correlated on interannual timescales, the methodologies employed have varied widely, resulting in inconsistent results. These inconsistencies have exacerbated the lack of consensus in the field, not only in terms of the relationship between AEWs and TCs, but of the characteristics of the historical AEW record itself. In an attempt to reconcile seemingly contradictory results, the climatological AEW count records published by Avila et al. (2000), Thorncroft and Hodges (2001), and Hopsch et al. (2007) were revisited, analyzed quantitatively, and compared in this chapter.

To address the deficiencies found in the literature, a historical record of AEW activity produced using a novel tracking technique was then compared to these past studies, described, and analyzed. Although it is impossible to determine the precise reasons for the discrepancies between the AEW historical record as produced in past and present studies without more details than are publicly available, some possible explanations were provided, and it was argued that the present dataset is more relevant and reliable for addressing the historical relationship between AEW and TC count.

Finally, conclusions were drawn about the relationship between AEW and TC activity using the updated historical record of AEW count. The findings about the historical AEW record produced by past studies and the context into which the present study fits, as well as the relationships between AEW and TC activity uncovered within the new historical record described here, are summarized below.

None of the AEW counts produced by any of the past studies examined (Avila et al., 2000; Thorncroft and Hodges, 2001; Hopsch et al., 2007) show any cross-study interannual correlation for overlapping years, regardless of the timeframe or ENSO phase considered. Since none of the past studies agree with each other on either AEW average count or interannual variability, it is impossible to use these studies to assess the accuracy of the current study, which in turn does not corroborate the annual AEW count or interannual AEW variability of any of the past studies. That said, there is good agreement between the seasonal cycle and spectral statistics of the present historical record with past studies (Albignat and Reed, 1980; Lau and Lau, 1990; Thorncroft and Rowell, 1998; Thorncroft and Hodges, 2001; Frank and Roundy, 2006; Hopsch et al., 2007; Agudelo et al., 2011). Since the present methodology accurately captures the seasonal cycle of AEWs while making provisions to count the most relevant waves over the most relevant months, there is cause to believe the historical record produced in the present study better describes the relevant variability of AEWs.

Although Hopsch et al. (2007) suggested that their counting methodology is sensitive to the choice of reanalysis/analysis product used, and that higher resolution reanalyses might be necessary to produce a reliable historical record of AEW activity, these potential limitations do not seem to be significant for the novel tracking techniques used here (recall Section 2.3.1). This may be attributable to methodological improvements that make the present dataset more robust for the purposes of addressing AEW variability and its relationship with TC variability on interannual

timescales. Since the present methodology includes provisions to track all strong AEWs, while avoiding double-counting simultaneous twin vortices and excluding systems that dissipate before reaching the MDR, the AEWs counted in this study are likely those that are most relevant to TC development.

Since Avila et al. (2000), Thorncroft and Hodges (2001), and Hopsch et al. (2007) did not provide monthly counts and there is some suggestion that the differences in their definitions of the AEW season of interest could have affected the transparency of any potential AEW-TC relationship present in their data, AEW and TC counts produced using the current methodology and the relationships therein were considered for both the entire hurricane season (JJASON) and the peak months of AEW and TC activity (ASO). In the present study, the correlations between AEW and TC count are stronger between ASO totals than JJASON totals, but both seasonal definitions result in statistically significant positive correlations interannually. This suggests that differences in counting methodologies between past studies might be more important than differences in the definition of the season. Although the interannual variability does not seem strongly dependent on the definition of season in the context of the present study, it makes sense to focus on the months for which both AEW and TC activity are elevated (ASO), during which there is a better chance of detecting a signal over the noise.

There is indeed a significant interannual correlation between annual (ASO) AEW count and TC count in the present historical data, in which AEW count variability ostensibly explains 57% of the variance in TC count. While Thorncroft and Hodges (2001) were the first to suggest such a linkage, this is the first rigorous quantitative evidence in support of this relationship. This strong correlation itself does not preclude the possibility that AEW and TC count are simply controlled by the same large-scale environmental factors. To address this concern, multiple linear regression was used to evaluate the relative importance of ENSO phase, annual trends, and AEW count

in stepwise linear models of TC count. AEW count was shown to provide significant skill over ENSO index and annual trends, both alone and together. When detrending AEW and TC count for ENSO index and annual trend, there is a statistically significant correlation between the residual AEW and TC counts. Effectively removing the impacts of ENSO phase and annual trend, AEW count still explains 40% of the TC interannual variability.

While it is clear that AEW count provides information on TC count apart from the large-scale conditions, there is more work to be done unpacking the potential importance of ENSO phase in modulating the relationship between AEW and TC variability. The relationship between AEWs and TCs in La Niña years is of especial interest, since there are hints of a potential dependence on ENSO phase that cannot be adequately resolved due to small sample size. To strengthen the conclusions drawn here and strengthen the case for a causal link between AEW and TC activity, it is necessary to isolate and study the importance of interannual variability in the favorability of the large-scale environment. These topics are addressed through model simulations in Chapter 5, once the model is compared against the historical record in Chapter 4.

Chapter 4

Results: Comparing HiRAM to the Historical Record

The methodological techniques outlined in Section 2.2.2 have been used to produce an updated historical record of AEW variability from NCEP-NCAR II reanalysis (Kanamitsu et al., 2002), which is described in detail in Chapter 3. The same techniques are applied to the climatological suite of HiRAM simulations in this chapter in order to compare the model-produced AEW activity to that of the reanalysis. This suite of climatological simulations consists of three ensemble members (H1, H2, and H3), each forced with observed seasonally and annually varying SSTs (Rayner et al., 2003) for the period from 1982 through 2009 (see Section 2.1 for more details). HiRAM has already been shown to reliably reproduce tropical storm statistics through past studies (see Section 1.2.3), so the main focus of this chapter is on demonstrating that the model adequately captures AEWs through comparison with the reanalysis-derived historical AEW record.

First, the modeled seasonal cycle of AEW and TC count statistics (Section 4.1) and statistical measures of AEW activity (Section 4.2) are examined and compared with the historical record. Since the results of Chapter 3 indicate that the large-scale environment likely plays some role in the relationship between AEW and TC variability, the large-scale environmental factors, including the GPI of the Atlantic basin and the strength of the AEJ, are examined in Section 4.3. Finally, the interannual

variability of AEW and TC count statistics (Section 4.4) and the connections between environmental factors, AEW activity, and TC activity (Section 4.5) are considered and compared with the reanalysis-derived historical record. The chapter closes with a summary of the reliability of the climatological simulations, and by extension, the validity of using HiRAM to study AEW and TC variability.

4.1 Seasonal Cycle of Count Statistics

The tracking methodology produces monthly counts of AEWs, developing AEWs, TCs, and African TCs (see Section 2.2.2), which are averaged over all of the years of the reanalysis (1979-2012) and over the years of interest in each of the climatological simulations (1982-2009). These average monthly counts are plotted in Figure 4.1, along with 95% confidence intervals. The climatological simulations are largely consistent with past studies of the AEW seasonal cycle (Thorncroft and Hodges, 2001; Frank and Roundy, 2006; Hopsch et al., 2007; Agudelo et al., 2011), with elevated AEW activity in the months of July through October, and show reasonable agreement with the reanalysis-derived historical record (see Section 3.2.1). The arguments made above in Section 3.2.1 concerning the months of interest still apply here. Namely, although there are more AEWs in July than in October (see Figure 4.1a), relatively few of them mature into TCs when compared to the months of August through October (see Figure 4.1c). As in Chapter 3, total counts for August through October (ASO) are hereafter referred to as "annual counts."

While the historical records derived from NCEP-NCAR II and the climatological simulation ensemble members may have slightly different seasonal cycles, with less of a distinct peak in AEW activity in August and stronger activity persisting through to October in the model-derived statistics (see Figure 4.1a and 4.1c), it is clear that the model captures the overlap in the peak AEW months and the peak TC

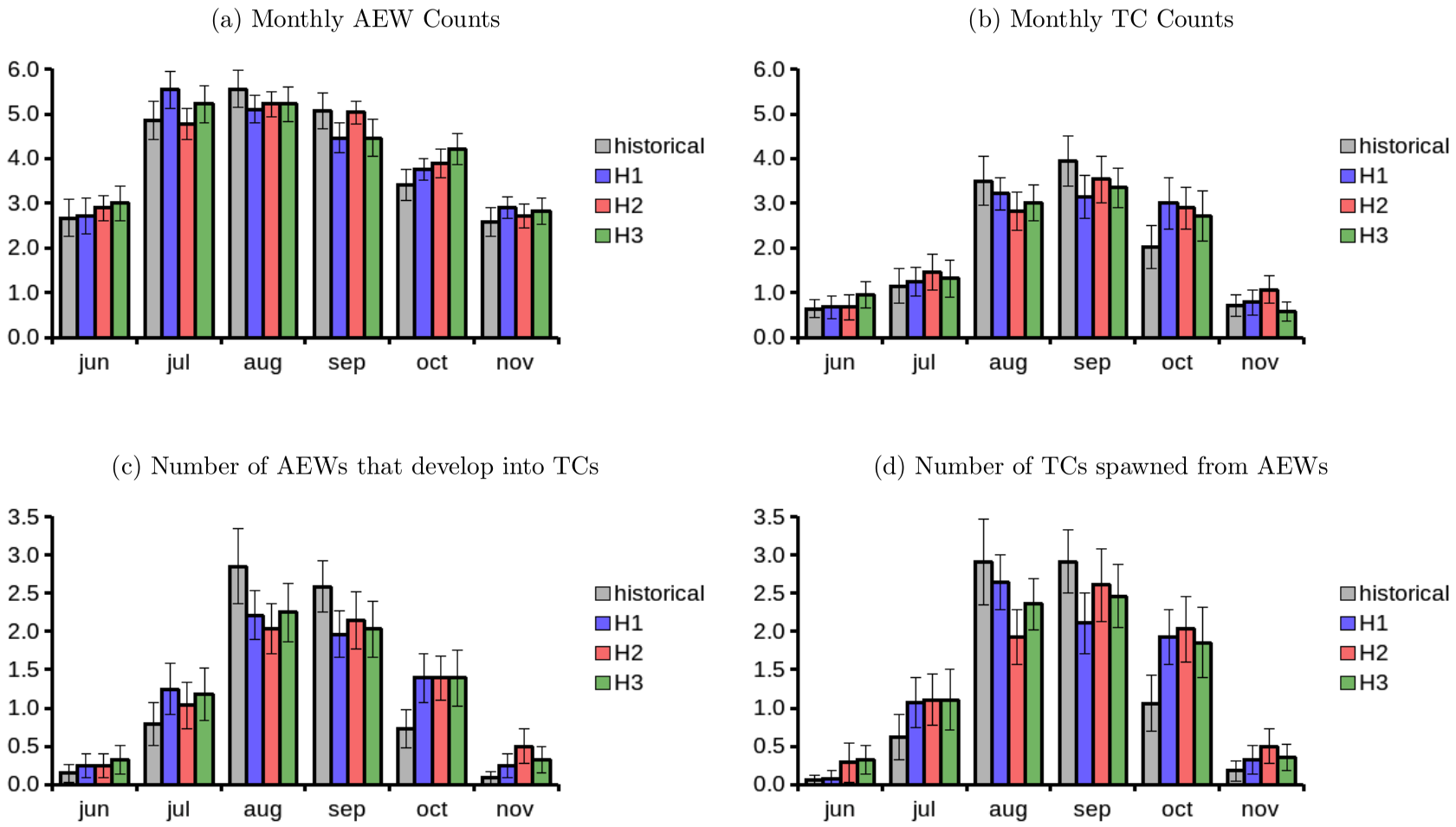

Figure 4.1: Average monthly counts of (a) AEWs, (b) TCs, (c) developing AEWs, and (d) African TCs, for the historical record (gray) as determined from NCEP-NCAR II reanalysis and IBTRaCS, and the climatological suite of HiRAM simulations (H1 in blue, H2 in red, and H3 in green). Error bars denote 95% confidence intervals.

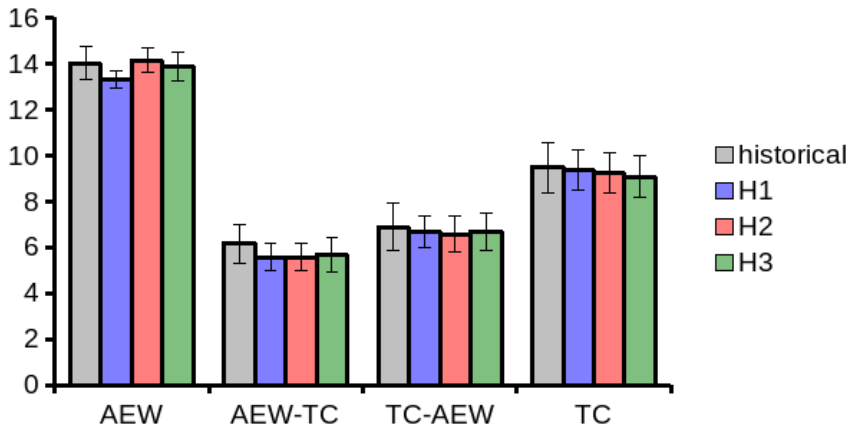

Figure 4.2: August through October average counts for African easterly waves (AEW), developing African easterly waves (AEW-TC), African tropical storms (TC-AEW), and all tropical storms (TC) for the historical record (gray) determined from NCEP-NCAR II reanalysis and IBTrACS, and each ensemble member of the climatological suite of HiRAM simulations (H1 in blue, H2 in red, and H3 in green). Error bars denote 95% confidence intervals.

months (see Figure 4.1a and 4.1b). Although there is some variation in peak month between ensemble members, monthly AEW counts consistently peak earlier than TC counts. Both AEW and TC counts are near their respective maxima in the late summer, from August through October (see Figure 4.1a and 4.1b), and this overlap is reflected in the monthly counts of developing AEWs (Figure 4.1c) and African TCs (Figure 4.1d). Note that the differences in Figures 4.1c and 4.1d arise due to the counting methodology, detailed in Section 2.2.2.

Despite some slight differences in the seasonal cycle between the reanalysis-derived and the modeled historical records, there is excellent agreement in annual total (ASO) count in all categories, including AEW count, developing AEW count, African TC count, and TC count (see Figure 4.2). This is evident from the overlapping 95% confidence intervals (see error bars in Figure 4.2), and also holds up in rigorous statistical testing. A Student's paired t-test returns p-values ranging from 0.29 to 0.96 when comparing the counts from the overlapping years of NCEP-NCAR II with each of the HiRAM ensemble members, indicating that there is no statistically significant dif-

ference between the reanalysis-derived average annual counts and the model-derived annual counts.

4.2 Power Spectra and AEW Statistical Measures

For comparison with Section 3.2.2, the statistical techniques discussed in Section 2.3.3 were applied to each ensemble member to produce power spectra of 1-10 day band-pass filtered 850 mb meridional winds, averaged between 10°N and 20°N near the coast of Africa, from six-hourly data between August 1 and October 31, averaged for the years 1982-2009. Figure 4.3 shows these raw spectra for the NCEP-NCAR II reanalysis and for the climatological ensemble members, with the 3-5 day band highlighted in cyan. The general shape of these spectra compares favorably with similar spectral representations of AEWs from past studies (Albignat and Reed, 1980; Lau and Lau, 1990; Thorncroft and Rowell, 1998), but note that the reanalysis-derived spectrum is more muted than the modeled spectra (see Figure 4.3a).

NCEP-NCAR II has less total power in the 1-10 day range in comparison with the climatological simulations, possibly due to differences in resolution. When normalizing by total power in the 1-10 day band, the spectra for the climatological ensemble members compare favorably with the NCEP-NCAR II spectrum by visual inspection (see Figure 4.4). This normalization does not affect the calculation of the centroid or the percent power in the 3-5 day band. There is some variation between the ensemble members, with the centroid ranging from 3.62 to 3.69 days, and the percent power ranging from 58.6% to 60.5%. These values are reasonably similar to the reanalysis-derived spectral statistics, for which the centroid is 3.41 days and 54.9% of the power is in the 3-5 day band. As suggested in Section 2.3.1, it would be interesting to produce a more detailed intercomparison of representations of AEWs

(a) NCEP-NCAR II

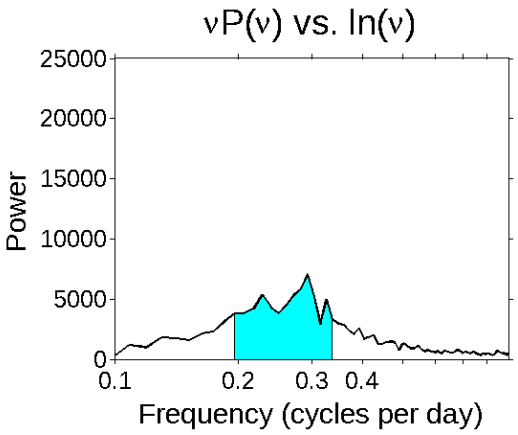

(b) H1

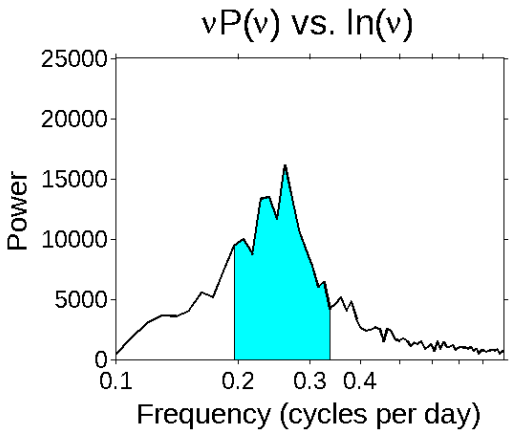

(c) H2

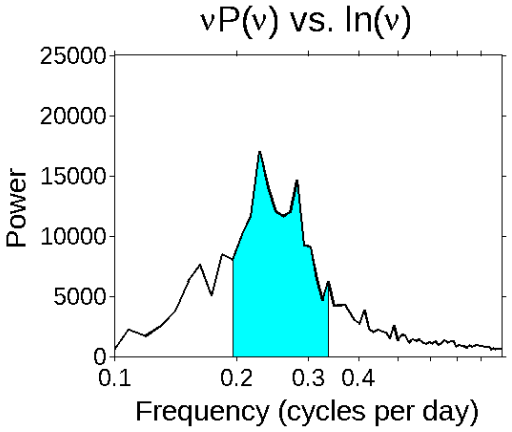

(d) H3

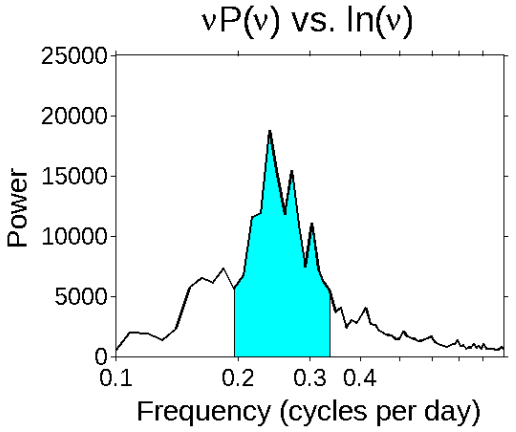

Figure 4.3: Power spectra of 1-10 day band-pass filtered meridional wind at 850mb, averaged between 10°N and 20°N, at the coast of Africa (15°W), for August 1 through October 31, for (a) NCEP-NCAR II reanalysis, and for the climatological model runs, (b) H1, (c) H2, and (d) H3. The 3-5 day bands are highlighted in cyan.

in various reanalyses, including the spectral representations, but this is left for future work.

4.3 Large-Scale Environmental Factors

While the climatological plots of NCEP-NCAR II fields do not necessarily represent reality and are likely flawed themselves, they are used as a baseline for comparison with the HiRAM climatological simulations here. Again, while it would be interesting to compare the relevant fields and measures of environmental favorability across various reanalyses, it is beyond the scope of this work. All climatological HiRAM plots in this section are derived from 30-year climatological fields (1979-2008), and NCEP-NCAR II plots are 34-year climatologies (1979-2012). All plots shown are annual (ASO) averages, including the 600 mb zonal wind, the precipitation rate, and the genesis potential index discussed below.

Figure 4.5 shows the zonal wind field at the level of the jet core (600 mb) for the reanalysis (a) and each of the climatological ensemble members (b-d). While there is some intra-ensemble variance, there is good agreement between the ensemble members on the approximate magnitude and location of the AEJ, which is about 9-10 m s^{-1} at its maximum around 15°N over Africa. The structure and magnitude of the zonal wind compare favorably with past studies that have included plots of zonal wind over Africa (Burpee, 1972; Cook, 1999; Leroux and Hall, 2009).

The NCEP-NCAR II jet core is marginally weaker and further south (see Figure 4.5), but the overall structure of the zonal wind is qualitatively similar to that of the model-derived fields. These plots also compare well with Figure 1 of Cook (1999), which includes average July zonal wind over Africa for both NCEP and EMCWF reanalyses, plotted at the respective level of the AEJ maximum. Cook (1999) provides an example of the degree of variation that can be observed in different reanalyses,

(a) NCEP-NCAR II

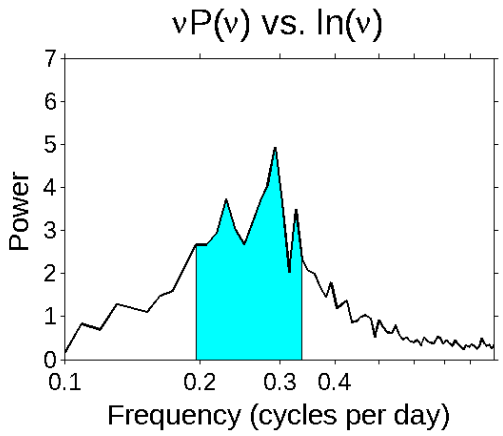

(b) H1

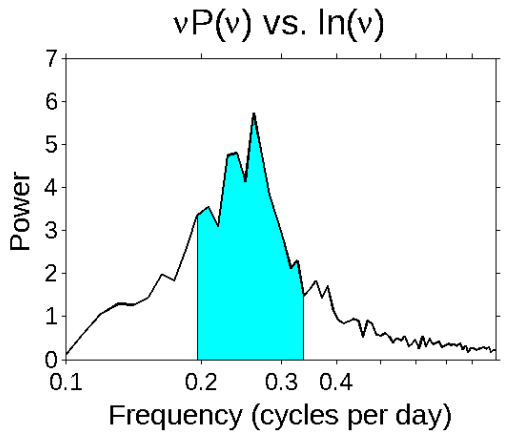

(c) H2

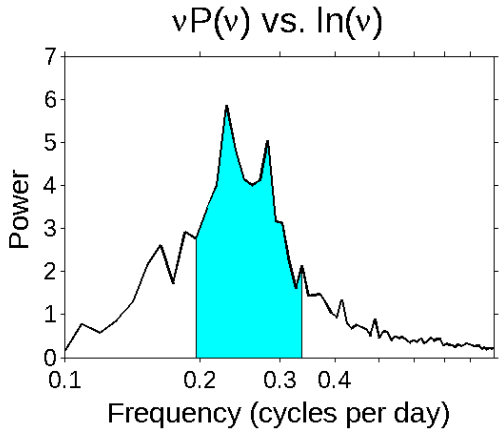

(d) H3

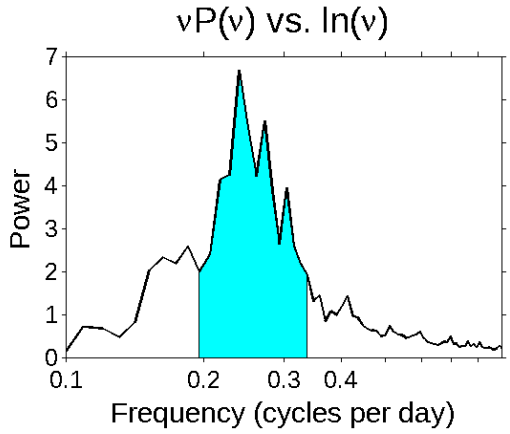

Figure 4.4: Normalized power spectra of 1-10 day band-pass filtered meridional wind at 850mb, averaged between 10°N and 20°N, at the coast of Africa (15°W), for August 1 through October 31, for (a) NCEP-NCAR II reanalysis, and for the climatological model runs, (b) H1, (c) H2, and (d) H3. The 3-5 day bands are highlighted in cyan.

(a) NCEP-NCAR II

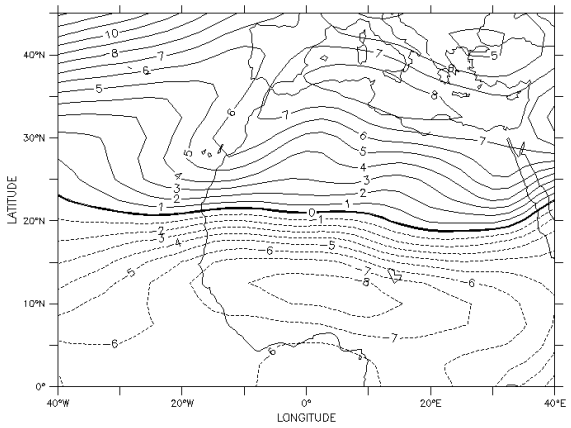

(b) H1

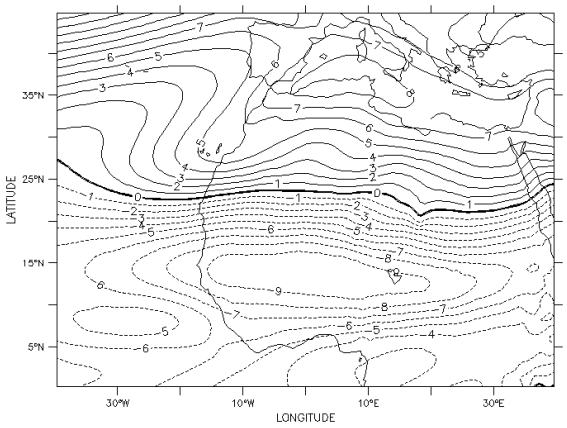

(c) H2

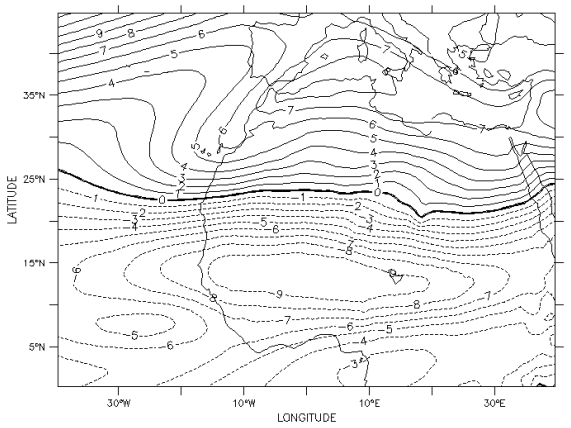

(d) H3

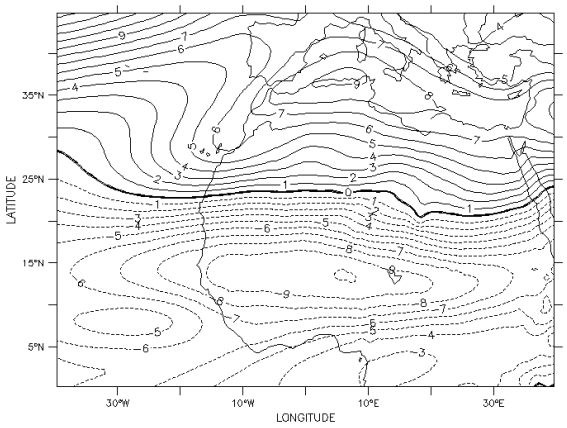

Figure 4.5: Climatological zonal wind at 600 mb, averaged for the months of August through October. Dashed contours indicate easterly winds, solid contours indicate westerly winds, and the contour interval is 1 m s^{-1}.

strengthening the argument that, despite differences between the NCEP-NCAR II and the HiRAM zonal winds, the AEJ is adequately captured by the model.

The average precipitation rate is shown in Figure 4.6 to give some indication of the strength and location of the ITCZ. The ITCZ may be relevant to the relationship between the AEJ, AEW activity, and TC activity, as suggested by Nicholson and Grist (2001) and Hsieh and Cook (2005), and this potential relationship is discussed in Chapter 6. The primary rainfall core is located off the coast of Africa, extending 20° into the Atlantic between 5° and 10°N, with secondary maxima over land, most notably just east of the Gulf of Guinea. The usefulness of the reanalysis-derived precipitation is known to be limited, since NCEP-NCAR II is not a next-generation reanalysis and does not explicitly assimilate rainfall data (Kanamitsu et al., 2002). Regardless, the reasonable qualitative agreement between the structure of the reanalysis-derived and model-derived precipitation rate fields is encouraging.

Finally, the genesis potential together with the spatial distribution of August through October genesis events is considered (see Figures 4.7 and 4.8). Genesis potential index (GPI) is defined in Section 2.2.1 as a measure of the large-scale favorability, diagnosed from absolute vorticity at 850 mb, relative humidity at 600 mb, potential intensity (Bister and Emanuel, 2002), and vertical wind shear between 850 and 200 mb, and is calculated from monthly mean fields averaged over all years of each climatology (Emanuel and Nolan, 2004). The genesis points, on the other hand, are only shown for the overlapping years (1982-2009), so as to provide a fair visual comparison of TC quantity. The average number of TCs per year ranges from 9.1 to 9.4 in the climatological simulations, compared with 9.1 in IBTrACS during the same time period.

In general, genesis events (Figure 4.8) tend to be roughly clustered in regions of elevated GPI (Figure 4.7) as expected. Examining the component fields separately, it appears that the differences between the reanalysis- and the model-derived GPI are

(a) NCEP-NCAR II

(b) H1

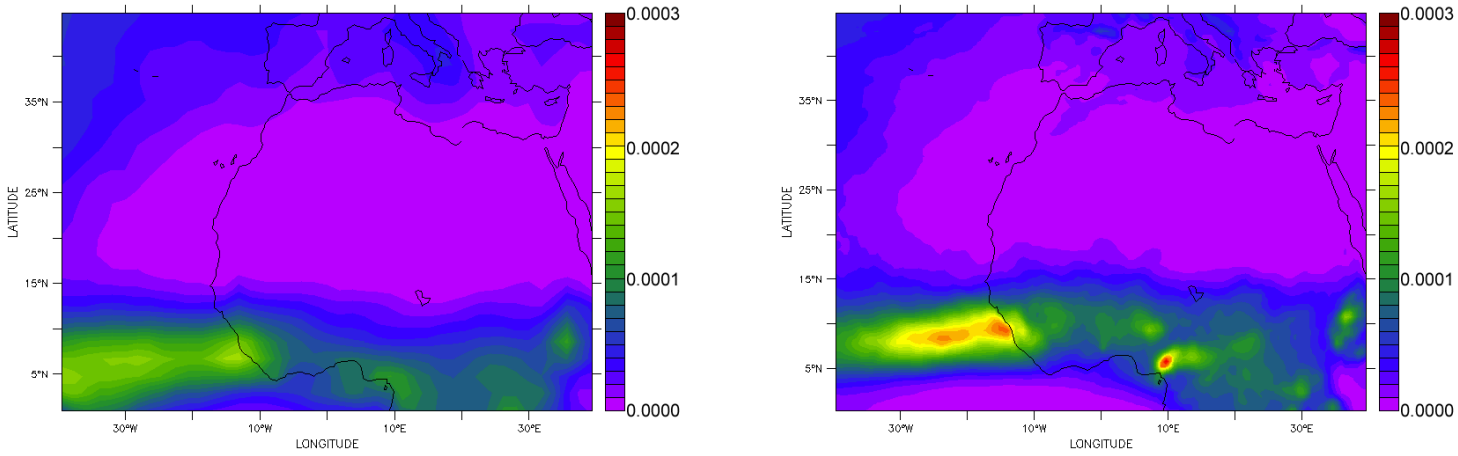

(c) H2

(d) H3

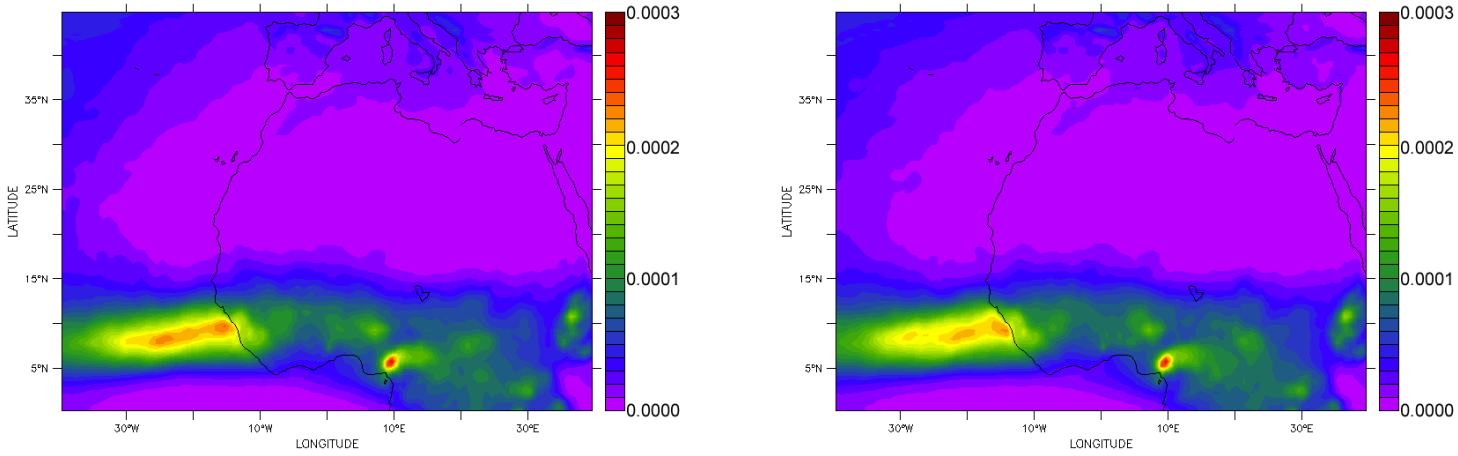

Figure 4.6: Precipitation rate, averaged August through October. Colorbar ranges from 0 to 0.0003 kg m^{-2} s^{-1}.

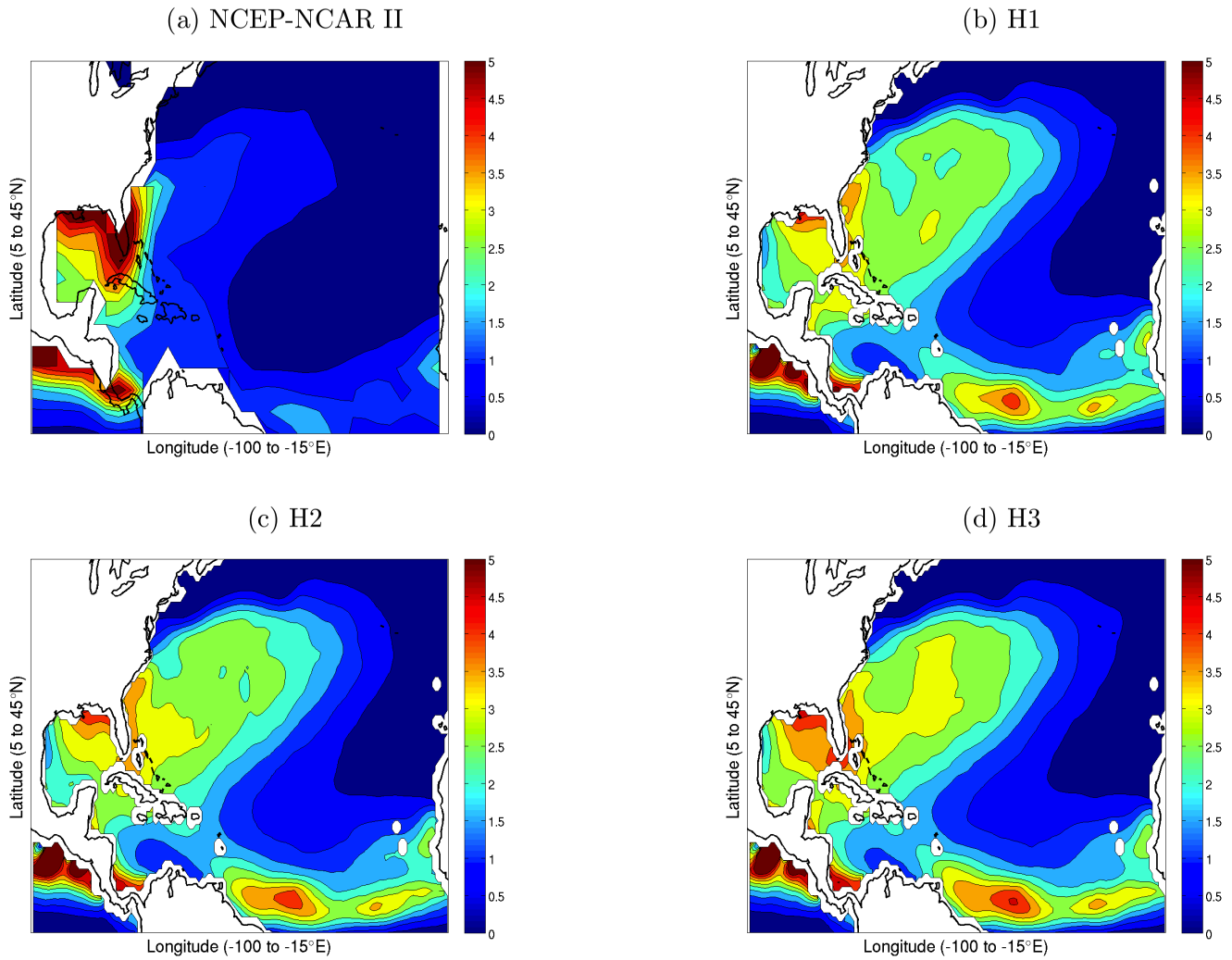

Figure 4.7: Average genesis potential index (Emanuel and Nolan, 2004) for the months of August through October, for (a) NCEP-NCAR II reanalysis, and for the climatological model runs, (b) H1, (c) H2, and (d) H3.

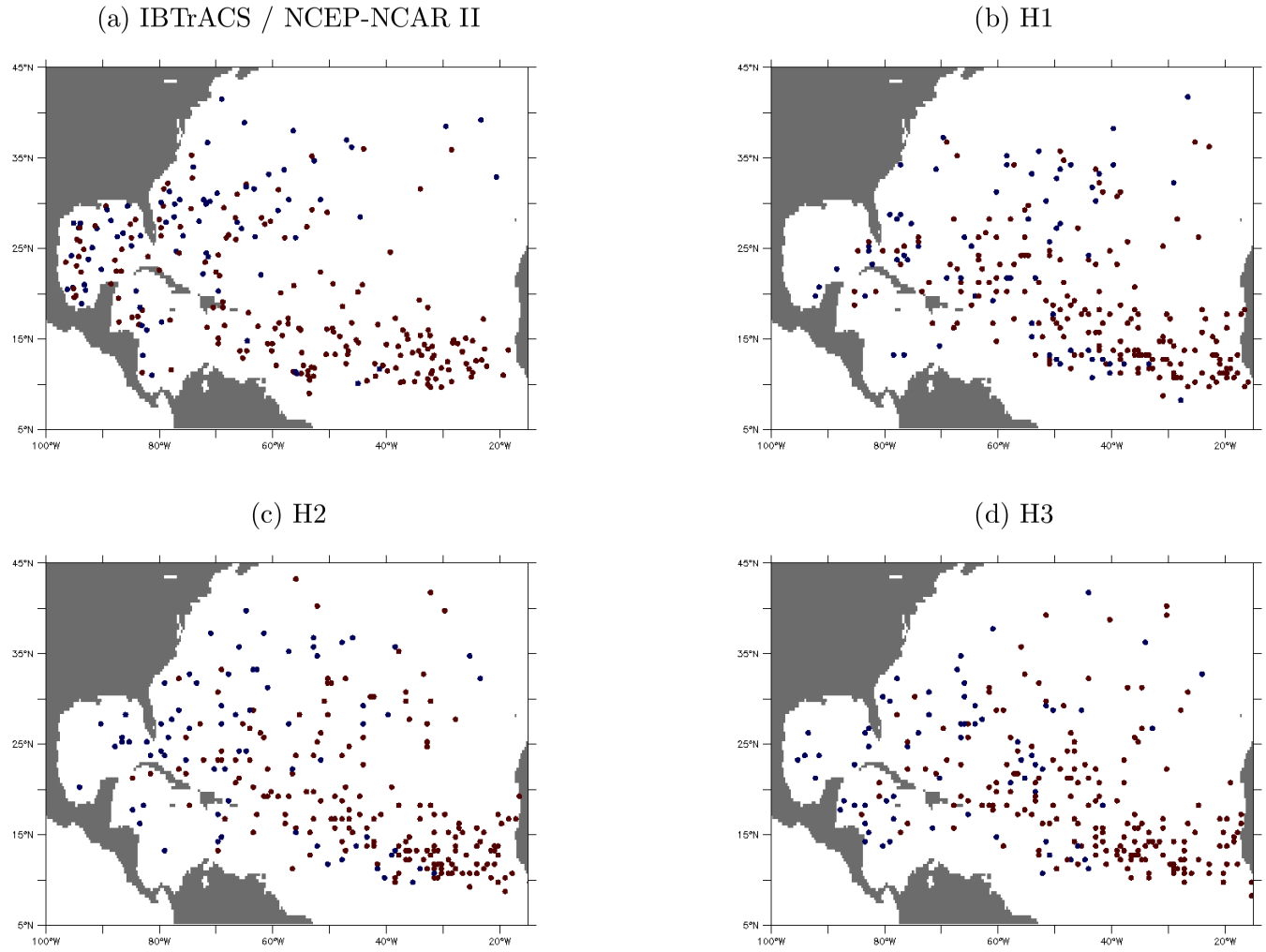

Figure 4.8: Tropical storm origins for the months of August through October and the years 1982-2009, for (a) the historical record (Knapp et al., 2010), and from the climatological model runs, (b) H1, (c) H2, and (d) H3. Genesis points of storms spawned by AEWs are shown as red dots, non-African storms as blue dots.

primarily due to the relative humidity, which is anomalously high over Florida and low over the MDR in NCEP-NCAR II. This is likely another artifact of the choice of reanalysis product, but it would be interesting to examine the sensitivity of GPI across various reanalyses to confirm.

In Figure 4.8, the genesis points are color-coded, with TCs spawned by AEWs in red, and non-African storms in blue. For Figure 4.8a, the genesis points themselves are taken from IBTrACS, but the storm origins were diagnosed using NCEP-NCAR II reanalysis. As noted in previous studies (Zhao et al., 2009), HiRAM produces anomalously few TCs in the Gulf of Mexico compared to the real world, but the origin plots compare favorably otherwise, including in the breakdown of African versus non-African storms. The percent of storms with African origins ranges from 71.4 to 73.6% for the climatological ensemble members, with 72.8% in the historical dataset.

While the favorable comparison between the historical and the modeled large-scale environment and genesis distribution is heartening, the best test of the adequacy of HiRAM for the study of AEW activity variability is the fidelity of the AEW record itself. This is explored in the following section and compared with the reanalysis-derived record.

4.4 Interannual Variability of Count Statistics

Figure 4.9 provides a comparison of the historical (from NCEP-NCAR II and IBTrACS) and the modeled (from climatological simulations H1, H2, and H3, see Section 2.1) AEW and TC count variability. The historical counts are shown in red, the modeled ensemble mean is shown in blue, and the shaded areas show the count range between the three ensemble members. In general, the interannual variability of the modeled AEW count is of a smaller magnitude than in the historical record, but the model does exhibit statistically significant covariance with the historical record.

(a) Annual African Easterly Wave Count

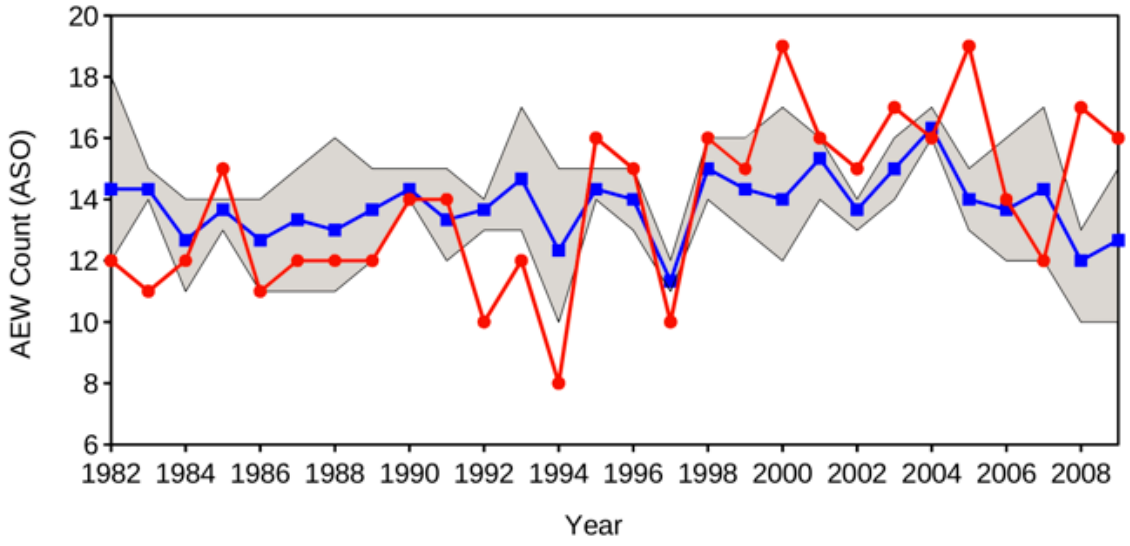

(b) Annual Tropical Storm Count

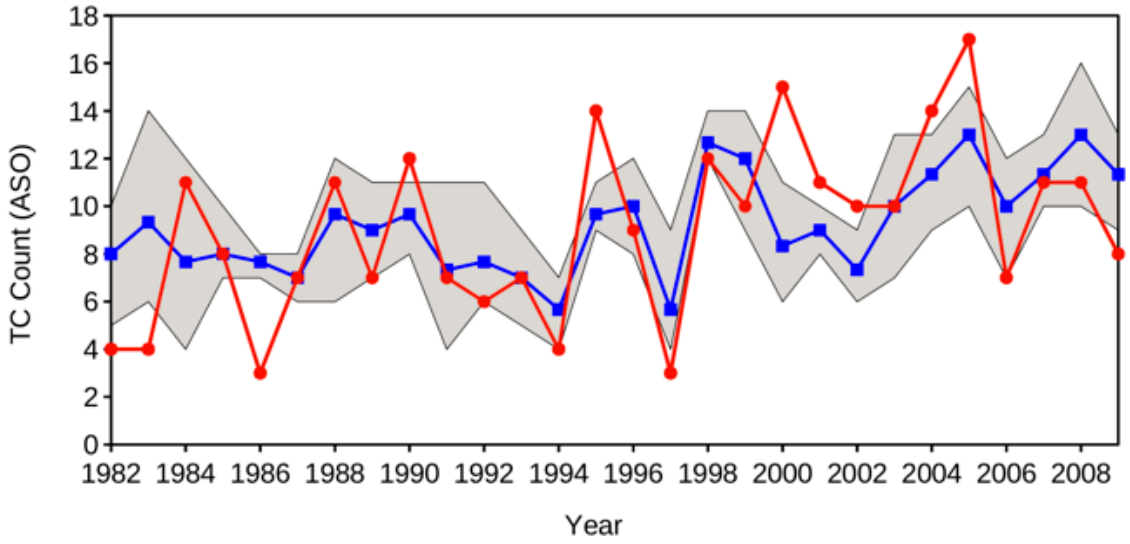

Figure 4.9: A comparison of historical (red) and modeled ensemble mean (blue) interannual variation in counts of (a) AEWs, and (b) TCs, summed for August through October (ASO) of each year. The historical records were determined from NCEP-NCAR II reanalysis and IBTRaCS, respectively. The shaded area shows the simulated maximum and minimum count from the three-member ensemble of simulations (H1, H2, H3).

While there is not a statistically significant correlation between individual climatological simulation ensemble members and the historical AEW variability, there is a notable correlation between the ensemble mean and the historical AEW variability. Correlating the historical and modeled ensemble mean AEW count interannually yields a coefficient of determination of $R^2 = 0.164$ ($p = 0.033$) and a 95% confidence interval of $0.037 < R < 0.676$. For comparison, the historical and modeled TC count yields a coefficient of determination of $R^2 = 0.387$ ($p = 0.00041$), a 95% confidence interval of $0.324 < R < 0.808$, and there is a statistically significant correlation between individual ensemble members and historical TC activity interannually.

The fact that the ensemble mean does show weak interannual correlation with the historical AEW record suggests that AEW activity is at least partially determined by the prescribed SST and thereby influenced by the large-scale environment in some way. However, since the correlation is much weaker between modeled and historical AEW counts than it is for TC counts, it seems that the large-scale environment exerts less control over AEW variability than it does TC variability in the model. Coupled with the lack of correlation between individual ensemble members and the historical record, this may imply that the internal variability of AEW activity is greater than TC variability. By extension, perhaps AEW variability explains a component of the TC variability that differs between ensemble members. This idea is revisited in Section 5.1.

As was apparent in the historical data in Section 3.2.3, there is also a direct relationship between ensemble mean AEW count and TC count in the simulations. In the next section, correlations between AEW count and TC count in individual ensemble members and between ensemble means are considered, along with the importance of ENSO phase and annual trends.

4.5 Multiple Linear Regression of TC Count

As mentioned above in Section 4.4, the climatological simulations do exhibit inter-annually correlated AEW and TC counts. Pooling all years from the three ensemble members together yields a coefficient of determination of $R^2 = 0.108$ ($p = 0.0023$), while the ensemble average AEW count and TC count yield a coefficient of determination of $R^2 = 0.128$ ($p = 0.062$). Regardless, the correlation between the AEW count and TC count in the model is weaker than the historical analog in Section 3.2.4, but is still statistically significant.

Again, one could argue that this correlation is not causal and is instead mediated by external factors. However, the results presented in Section 4.4 indicate that the AEW activity exhibits internal variability beyond what is determined by the large-scale environment through the prescribed SST. The notion that AEW activity may exhibit variability independent of the environment is expanded upon in Section 5.1 by considering the relationship between ensemble members, but is first subjected to the same analysis as in Section 3.2.4 here. Namely, stepwise linear models of TC count are constructed to determine the relative importance of ENSO index (see Appendix B for details), AEW count, and year as predictors of TC count in climatological simulations H1, H2, and H3.

As in Table 3.1, the three potential predictors of TC count were each tested separately, as well as in various combinations, producing the adjusted coefficients of determination and associated p-values shown below in Table 4.1. As in Section 3.2.4, notation of the form $y \sim 1 + x_1 + x_2 + x_3$, where y is the predictand and x_i are predictors, is shorthand for the multiple linear regression model $y = C_0 + C_1x_1 + C_2x_2 + C_3x_3$, where C_i are constants. Although there are statistically significant correlations, the associated lines of best fit are not necessarily well-constrained, due to the level of variability and relatively small sample size. This issue is revisited

in Section 7.1, where the interannual relationship between AEW and TC count is quantified.

Table 4.1: Multiple Linear Regression of Modeled TC Counts (1982-2009) for model runs H1, H2, and H3 (N=84)

Linear Model	**Adjusted R^2**	**p-value**
TC $\sim$ 1 + AEW	0.113	1.0×10^{-3}
TC $\sim$ 1 + year	0.158	1.1×10^{-4}
TC $\sim$ 1 + ENSO	0.116	8.8×10^{-4}
TC $\sim$ 1 + year + ENSO	0.273	9.2×10^{-7}
TC $\sim$ 1 + year + ENSO + AEW	0.339	6.4×10^{-8}

Pooling the years of the simulations together rather than considering only the ensemble mean is an intentional decision. When conducting similar analysis as that of Tables 3.1 and 4.1 for the ensemble average AEW and TC counts, the mean AEW count does *not* provide additional skill beyond the ENSO index and year. This is not surprising, as ensemble averaging helps bring the effects of the large-scale forcing to the forefront, while pooling all years together gives a better indication of the chaotic component of the model (Garner et al., 2009). Since the focus of this section is on the internal variability of the atmosphere and that is best captured by individual ensemble members, the remainder of the analysis in this chapter focuses on the pooled data rather than the ensemble mean.

As in Section 3.2.4, the year, ENSO index, and AEW count each shows significant skill over a constant model in explaining TC count variability. As shown in Table 4.1, there is a statistically significant trend in the TC count data ($R^2 = 0.158$, $p = 1.1 \times 10^{-4}$), associated with an average slope of 0.14 additional TCs each year, compared with 0.23 in the historical record. Of AEW count, year, and ENSO phase, the annual trend actually explains the highest percentage of variance in TC count, and each individually explains 11.3%, 15.8%, and 11.6%, respectively. Together, year and ENSO index account for 27.3% of the variance in TC count ($p = 9.2 \times 10^{-7}$), but the addition of AEW count increases this to 33.9% ($p = 6.4 \times 10^{-8}$). The p-value to

accept AEW count as an additional predictor in the stepwise model of TC count is $p = 0.0034$, which demonstrates that AEW count provides a statistically significant improvement over year and ENSO index alone.

As in the historical record, there is no statistically significant covariance between AEW count and ENSO index ($R^2 = 0.024$, $p = 0.060$), but the weak trend present in AEW count in the historical record is not present in the model ($R^2 = 0.006$, $p = 0.48$). This provides support to the claim made in Section 3.2.4 that the trend in AEW count in the reanalysis may be due to discontinuities in the assimilation of observational data, although it could still be a real trend that the model simply fails to capture.

Finally, again as in Section 3.2.4, both AEW count and TC count are detrended by ENSO phase and year, and the residuals are correlated to estimate the contribution of AEW count to TC count variability beyond what is explained by ENSO phase and annual trends. Correlating these AEW and TC residuals yields a statistically significant relationship, with a 95% confidence interval of $0.108 < R < 0.496$ ($R^2 = 0.099$; $p = 0.0035$). This effect is weaker in the simulations than it was for the historical record, but even when the effects of ENSO phase and annual trends are removed, AEW variability still explains approximately 10% of TC interannual variability in the model. From this analysis, it is clear that AEW count provides skill above and beyond the large-scale conditions encapsulated in the ENSO index in HiRAM, as it did in the historical record.

4.6 Summary

As demonstrated above, the climatological simulations show reasonable agreement with the historical record in terms of AEW and TC seasonality and interannual variability, and the model adequately captures the spectral signature of AEWs as well

as the large-scale structure of the AEJ and ITCZ. Although the climatological simulations produce annual AEW and TC counts that are statistically indistinguishable from the historical record on average, the modeled covariance between AEW and TC counts, while still statistically significant, is weaker than in the historical record.

The model statistics are similar to the historical record in many ways, but there are notable differences. The year, ENSO index, and AEW count each shows significant skill in explaining variance in TC count in stepwise linear models, but each explains less of the variance in the climatological simulations than in the historical record (compare Tables 3.1 and 4.1). Detrending both the AEW and TC counts for ENSO phase and annual trend, as in the reanalysis-derived historical record, the modeled residuals are significantly correlated. The modeled AEW residuals explain 10% of the TC residuals, which is statistically significant, though smaller in magnitude than what was found in the reanalysis-derived historical record (40%). Although there was a significant trend in the AEW count in the reanalysis-derived historical record, this was not present in the modeled record. This may be due to discontinuities in the assimilation of observational data in the reanalysis, or the trend could be real and the model could simply fail to capture it.

While the individual ensemble members do not exhibit statistically significant correlation with historical AEW variability, they do with historical TC variability. Both the ensemble average AEW and TC annual count do covary with the respective historical count. Since ensemble averaging helps isolate the effects of the large-scale forcing, this implies that AEW activity is at least partially determined by the prescribed SST, and thereby the large-scale environment, but to a lesser extent than TC activity. Since AEW activity exhibits marked variability distinct from that forced by the large-scale environment, it follows that the stochastic component of the AEW variability could be related to the portion of the TC variability unexplained by the large-scale environment. Along the same lines, AEW variability may explain a com-

ponent of the TC variability that differs between ensemble members. This is explored in the following chapter.

Given the above caveats, the model reliably captures the major features of the climatological AEW and TC record across multiple temporal and physical scales. Now that the ability of HiRAM to reasonably capture the relationship between AEWs and TCs has been shown via its agreement with the reanalysis-derived historical record, HiRAM is used exclusively in the next two chapters to further probe the AEW-TC relationship.

Chapter 5

Results: Isolating the Internal Variability of AEW Activity by Minimizing the Effects of Interannual Variation in SST

The results of Chapters 3 and 4 have provided preliminary evidence that there is a significant component of AEW activity that may be essentially stochastic, in that it is unexplained by the large-scale environment. This is noteworthy, because the stochastic AEW variability may explain a component of the TC variability that remains unexplained by known environmental factors. To isolate and study this stochastic component of AEW activity, first the climatological simulations are revisited in Section 5.1. Next the simulations with interannually invariant SSTs, the control simulation and the perpetual La Niña simulation, are described and analyzed in Sections 5.2 and 5.3. Finally, the results of isolating the internal variability of AEW activity are summarized in Section 5.4.

5.1 Revisiting the Climatological Simulations

Since ensembles provide multiple realizations over the same time period, they can be used to diagnose the internal variability of the atmospheric system. This internal variability is explored further here, first by considering the consistency across ensemble

members (Section 5.1.1) and then by considering the perturbations of each ensemble member from the ensemble mean (Section 5.1.2).

5.1.1 Consistency across Ensemble Members

As mentioned in Section 4.4, unlike the ensemble mean, individual ensemble member AEW counts are not correlated with historical AEW count interannually. Examining modeled AEW counts from different climatological ensemble members, there is no significant interannual correlation between ensemble member AEW counts, as shown in Figure 5.1 for both August through October (ASO) and June through November (JJASON) totals. This indicates that, at least in the model, AEW count exhibits variability that is independent from large-scale forcing, since each ensemble member is forced with identical SSTs. This behavior is distinct from that of TC count, for which there is strong correlation between ensemble members, since TC count does have a strong dependence on SSTs. AEW counts totaled for the months of August through October annually for each ensemble member are shown in Figure 5.2. The perturbations of ensemble member counts from the ensemble average are examined in Section 5.1.2.

Even in the absence of discernible interannual correlation between ensemble members, there is strong agreement in average annual count, for not only AEWs, but also developing AEWs, African TCs, and all TCs, as shown in Figure 5.3. While the AEW variability is not completely dependent on SST variability, and AEW count varies on a year-to-year basis, there is a well-defined climatological mean level of activity about which AEW count fluctuates. As is demonstrated below, this climatological mean does not seem sensitive to changes in ENSO phase (see Section 5.3), but can be perturbed through manipulation of the large-scale environment (see Chapter 6).

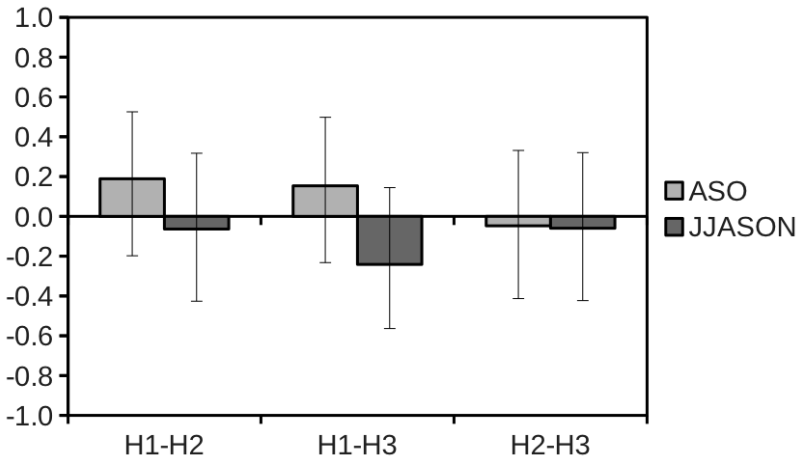

Figure 5.1: Correlation coefficients (R-values) of AEW count between different ensemble members (H1-H2, H1-H3, and H2-H3) for August through October total AEW counts (ASO, light grey) and June through November total AEW counts (JJASON, dark grey). Error bars denote 95% confidence intervals.

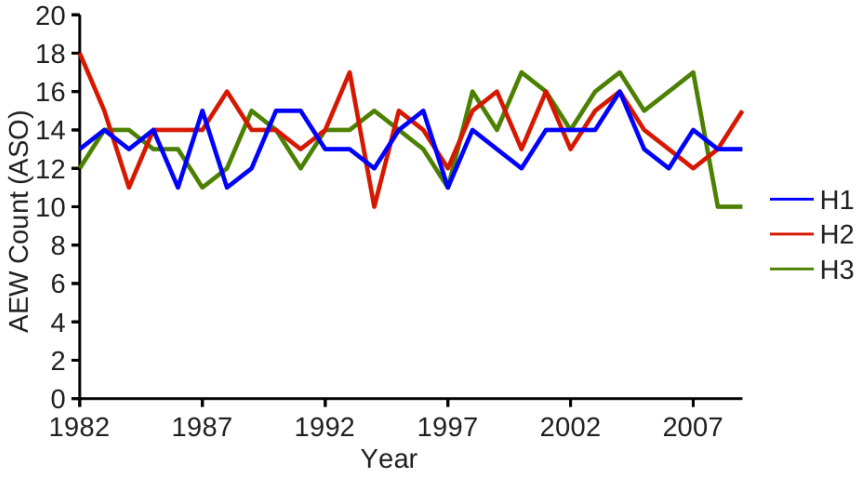

Figure 5.2: Modeled August through October annual African easterly wave count for each ensemble member of the climatological suite of HiRAM simulations (H1 in blue, H2 in red, and H3 in green).

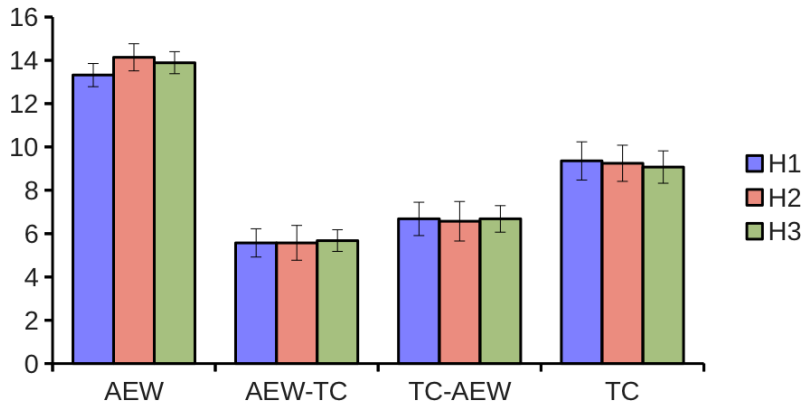

Figure 5.3: Modeled August through October average counts for African easterly waves (AEW), developing African easterly waves (AEW-TC), African tropical storms (TC-AEW), and all tropical storms (TC) for each ensemble member of the climatological suite of HiRAM simulations (H1 in blue, H2 in red, and H3 in green). Error bars denote 95% confidence intervals.

5.1.2 Perturbation from Ensemble Mean

Since the ensemble mean is the portion of the signal most influenced by the large-scale environment, isolating the perturbation from this ensemble mean provides an estimate of the variability that remains unexplained by the variability of the large-scale conditions. All three ensemble members were forced with the same SSTs and therefore had arguably similar large-scale environments by design. To isolate the stochastic component of the AEW and TC variability in the climatological ensemble members, perturbation counts for each ensemble member year are constructed by subtracting the annual ensemble mean.

This concept is formalized using the following notation:

$$\mathrm{AEW} = \overline{\mathrm{AEW}} + \mathrm{AEW}'$$

$$\mathrm{TC} = \overline{\mathrm{TC}} + \mathrm{TC}'$$

where the total AEW and TC counts of each ensemble member are broken into the sum of the ensemble average (denoted with an overbar) and the perturbation from

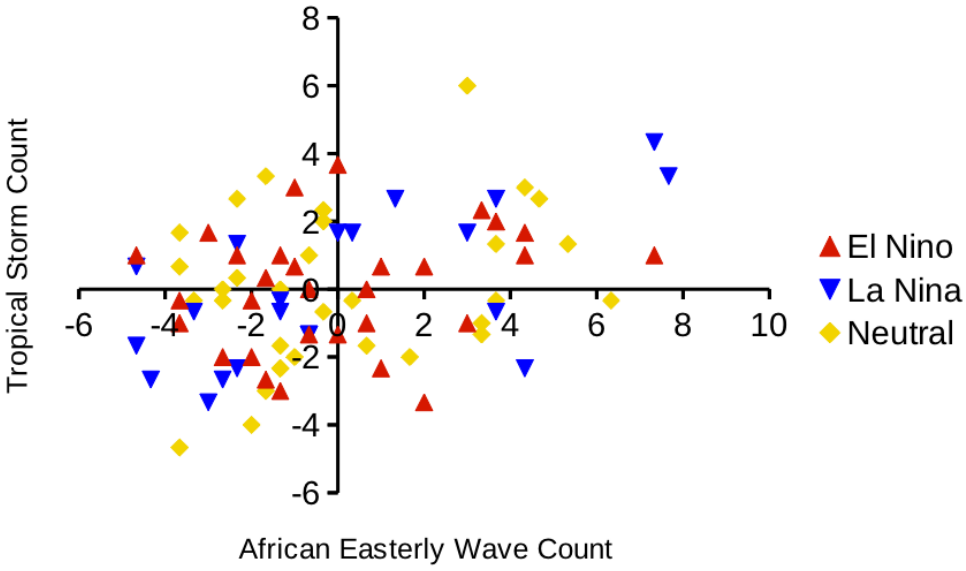

Figure 5.4: Scatterplot of the perturbation of each climatological model ensemble member (H1, H2, H3) from the ensemble mean annual TC count versus AEW count for the months of August through October (ASO). Each point is color-coded by the ENSO phase of the year, with El Niño years in red, La Niña years in blue, and neutral ENSO years in yellow.

that average (denoted with a prime). In this definition, both the ensemble average and the perturbation from that average are time-varying. The terms $\overline{\text{AEW}}$ and $\overline{\text{TC}}$ can be thought of as the variance due to the environmental variability, while AEW' and TC' can be thought of as the stochastic component of total variance.

As mentioned in Section 4.5, there is a statistically significant correlation between $\overline{\text{AEW}}$ and $\overline{\text{TC}}$ ($R^2 = 0.128$, $p = 0.062$), but when probing this relationship further using multiple linear regression, $\overline{\text{AEW}}$ does not provide additional skill beyond the ENSO index and year in predicting $\overline{\text{TC}}$. This supports the notion that the variance of the ensemble mean AEW count does not contain unique information beyond that forced by the large-scale environment.

The relationship between annual perturbation counts is shown in a scatterplot of TC' versus AEW' in Figure 5.4. The perturbation AEW and TC counts exhibit statistically significant covariance, with a 95% confidence interval of $0.171 < R <$

0.543 ($R^2 = 0.138$, $p = 0.00050$). About 14% of the variance in perturbation TC count is explained by the perturbation AEW count, and a least squares regression returns the following line of best fit:

$$TC' \approx 0.25 \cdot AEW'. \tag{5.1}$$

This can be interpreted to mean that the conversion rate for additional AEWs (above and beyond the average number purportedly determined by the large-scale environment) becoming TCs is 4:1 on average.

Another way to consider the internal variability of the model atmosphere is to remove the interannual variability in large-scale environmental factors as much as possible, by not only subtracting for the effects of the interannual variation as above, but by removing the interannual variation in SST entirely. The next section accomplishes this, by replacing the historical SSTs with climatologically average SSTs as a lower boundary condition.

5.2 Internal Variability of Simulations with Interannually Invariant SSTs

The control and perpetual La Niña simulations are each forced with composite SSTs that vary seasonally but do not change from year to year (see Section 2.1 for more details). The control simulation has the climatologically average SST from 1982-2005 as its lower boundary condition, and the perpetual La Niña simulation has composite SST from the strongest La Niña years (see Appendix B). Although there could still be some internal variation in large-scale favorability, the large-scale environment as encapsulated in the SSTs is effectively constant from year-to-year within each of these simulations. Even though these simulations are forced with interannually invariant SSTs, their modeled AEW and TC counts still exhibit marked variability. This

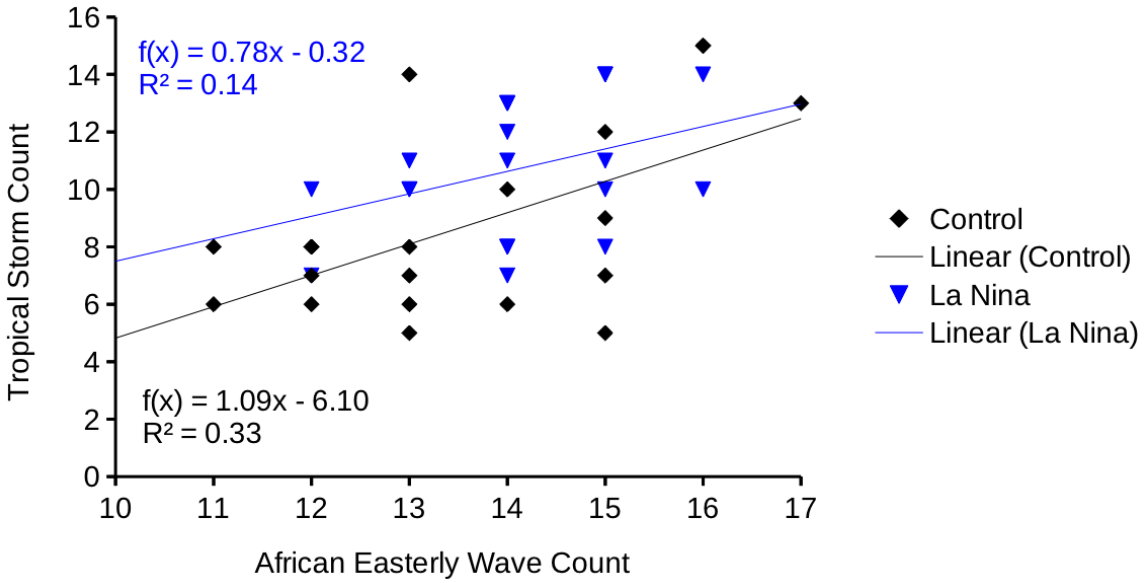

Figure 5.5: Scatterplot of annual TC count versus AEW count for the months of August through October (ASO) for the control simulation (black diamonds) and the perpetual La Niña simulation (blue triangles), along with the corresponding lines of best fit and coefficients of determination from least-squares linear regression.

variability is a measure of the internal atmospheric variability of the model, similar to the perturbation counts considered above in Section 5.1.2.

As is discussed further in Section 5.3, while there is a discernible increase in TC activity, there is no statistically significant difference in average AEW count from the control to the perpetual La Niña simulations. Further, there is no significant difference in the relationship between AEW and TC variability. In Figure 5.5, a scatterplot of annual (ASO) TC count versus AEW count, this manifests cleanly as a vertical shift from the control data (shown in black) to the perpetual La Niña data (shown in blue). While the coefficients of determination between the TC and AEW counts may appear to be different for the control simulation ($R^2 = 0.329$, $p = 0.0081$) and the perpetual La Niña simulation ($R^2 = 0.142$, $p = 0.10$), there is significant overlap in the confidence intervals and the two are not statistically distinguishable.

While the two simulations have indistinguishable AEW counts on average, for the same number of AEWs, there are typically more TCs in the perpetual La Niña

simulation than in the control simulation. Another way to interpret this is that the baseline TC activity level is higher in La Niña conditions than average environmental conditions due to increased large-scale favorability, but the interannual variability is similarly affected by the AEW count variance. These simulations are further unpacked in the following section.

5.3 Control and Perpetual La Niña Simulation Comparison

Past studies and present climatological analysis indicate that ENSO phase may play a role in modulating the relationship between AEW and TC variability. There are hints in Chapter 3 that La Niña years in particular could exhibit anomalous AEW-TC correlations, and although the sample sizes are too small to resolve any potential dependence, this motivates the study of a perpetual La Niña simulation in comparison to a climatological control. The internal variability of the atmosphere in the control and perpetual La Niña simulations, especially the covariance of AEW and TC count, is discussed above in Section 5.2. In this section, the aggregate statistics for these simulations are compared to evaluate the impacts of ENSO phase on the large-scale environment, AEW count, and TC count. Aggregate count statistics and spectral statistics are examined in Section 5.3.1. Section 5.3.2 provides a comparison of large-scale environmental factors, including GPI and the associated spatial distribution of genesis events. The significance of ENSO phase in light of these results is briefly discussed in Section 5.3.3.

5.3.1 Count Statistics

Figure 5.6 shows averaged monthly AEW counts, TC counts, developing AEW counts, and African TC counts for the perpetual La Niña and the control simulations. There

is no significant difference in AEW count seasonal cycle between the experimental and the control simulations. While there is a difference in the magnitude of the signal for the La Niña TC counts, developing AEW counts, and African TC counts, the general shape of the seasonal cycle remains unchanged for all counts.

Summing these counts for the months of August through October, the differences between the perpetual La Niña and control simulations are readily apparent in Figure 5.7. A Student's t-test between La Niña and control AEW counts returns a p-value of $p = 0.39$, revealing that there is no significant change in the number of AEWs for perpetual La Niña conditions with over 95% confidence. As expected, there is an increase in the number of TCs under La Niña conditions ($p = 0.064$). The perpetual La Niña simulation also shows a significant increase in the number of developing AEWs ($p = 0.051$) and African TCs ($p = 0.032$) relative to the control.

Not only is the AEW count indistinguishable between these two model simulations, but the control and La Niña simulations have very similar spectral signatures of AEW activity as well. The 1-10 day band-pass filtered 850 mb meridional winds averaged between 10°N and 20°N near the coast of Africa from August 1 through October 31 (see Section 2.3.3) are used to verify the level of AEW activity. The control and La Niña simulation spectra are not shown here, as they do not exhibit notable differences from climatology, but the climatological spectra are shown in Figure 4.3.

Each simulation has spectral statistics that fall within the range of variation exhibited by the climatological ensemble members (see Figure 2.8). Specifically, the centroid for the control simulation is 3.68 days, the La Niña simulation is 3.67 days, and the centroids for the climatological ensemble members (H1, H2, H3) are between 3.62 and 3.69 days. Similarly, the difference between the percent of the power in the 3-5 day band for the control and the perpetual La Niña simulations is less than the variability exhibited by the climatological ensemble members, with 59.4% in the control, 58.2% in the perpetual La Niña simulation, and 58.6% to 60.5% in the

(a) Average Monthly AEW Counts

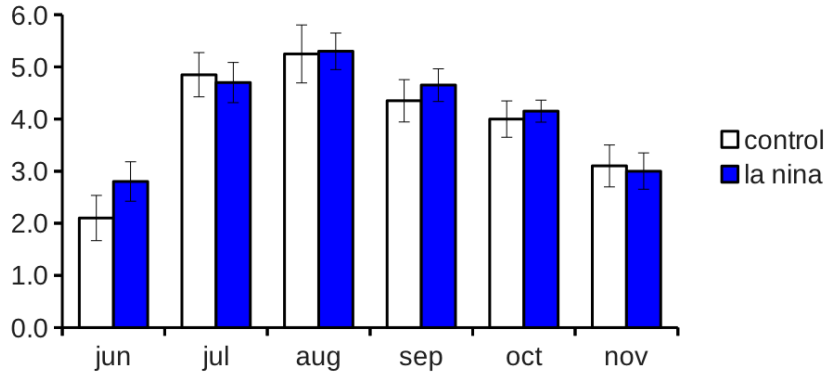

(b) Average Monthly TC Counts

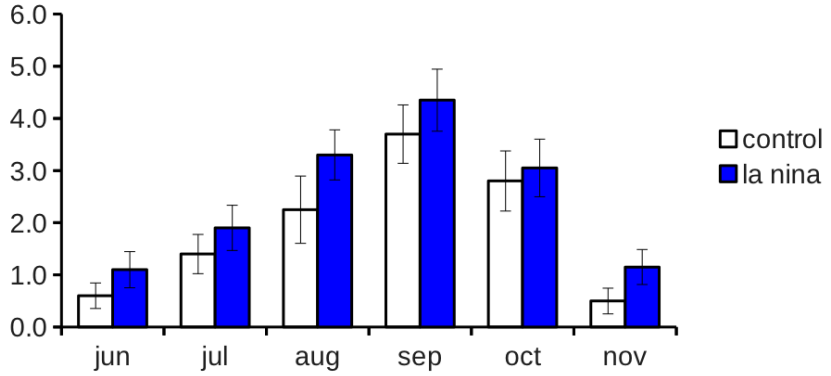

(c) Average Number of AEWs that develop into TCs

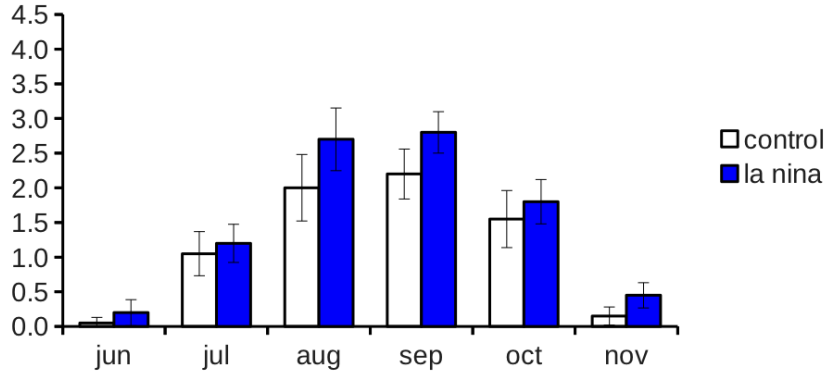

(d) Average Number of TCs spawned from AEWs

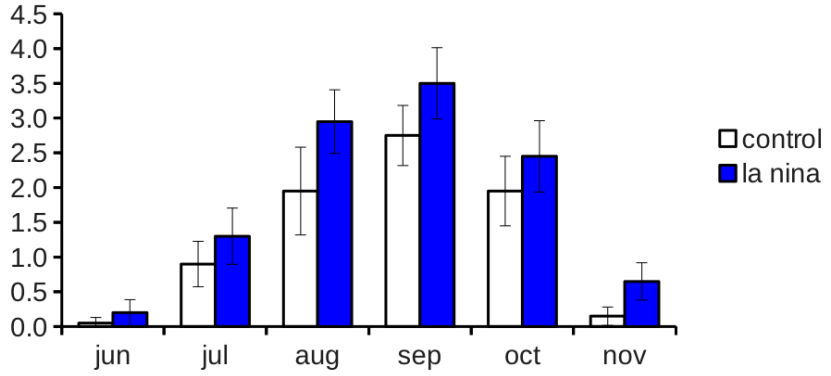

Figure 5.6: Average monthly counts of (a) AEWs, (b) TCs, (c) developing AEWs, and (d) African TCs, for the perpetual La Niña simulation (blue) and the associated control simulation (white). Error bars denote 95% confidence intervals.

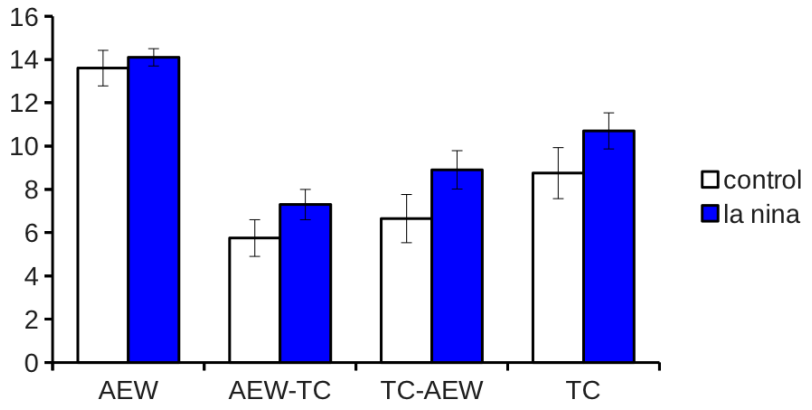

Figure 5.7: Modeled August through October average counts for African easterly waves (AEW), developing African easterly waves (AEW-TC), African tropical storms (TC-AEW), and all tropical storms (TC) for the perpetual La Niña simulation (blue) and the associated control simulation (white). Error bars denote 95% confidence intervals.

climatological ensemble. Since the difference in spectral statistics between climatological ensemble members is larger than between the control and perpetual La Niña simulations, there is no detectable difference between the La Niña and the control simulations' AEW activity as diagnosed by spectral characteristics.

5.3.2 Large-Scale Environmental Factors

Unsurprisingly, the the large-scale environment is more favorable for development in the perpetual La Niña simulation in comparison with the control. Figure 5.8 includes the La Niña simulation GPI calculated from monthly mean fields (a), the control simulation GPI (b), and the difference between the two (c). For more information on the calculation of GPI, see Section 2.2.1. The GPI anomaly in Figure 5.8c exhibits good agreement with Figure 6b of Camargo et al. (2007a), which also shows the ASO La Niña GPI anomaly, calculated from NCEP Reanalysis data for the years 1950-2005. As in the historical data examined by Camargo et al. (2007a), there is a well-defined net increase in GPI in the Atlantic basin in association with modeled La Niña conditions.

(a) La Niña GPI

(b) Control GPI

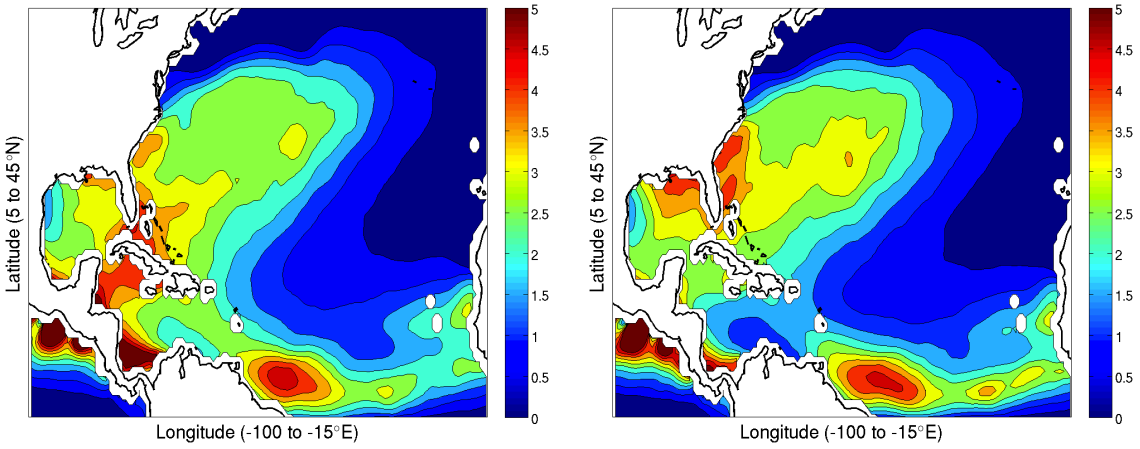

(c) GPI Difference (La Niña minus Control)

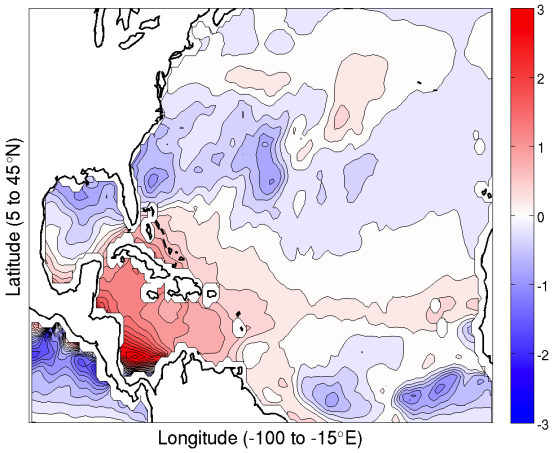

Figure 5.8: Genesis potential index for the months of August through October, for (a) the perpetual La Niña interannually invariant simulation, (b) the control interannually invariant simulation, and (c) the difference, i.e., the control GPI subtracted from the perpetual La Niña GPI.

The GPI in the La Niña simulation is predominantly elevated in the MDR (see Figure 5.8). The basin-wide average GPI is 4.8% greater in the perpetual La Niña simulation when compared with the control, and 22.5% greater in the MDR. This is also evident in the spatial distribution of genesis events shown in Figure 5.9, with a 44.4% increase in TCs developing in the MDR, a 19.5% increase outside of the MDR, and a total increase of 31.4%. As discussed in Section 5.2, although there is no significant change in the AEW activity or the degree of covariance between AEW count and TC count, the percent of TCs with African origins increases from 67.6% in the control simulation to 74.1% in the perpetual La Niña simulation.

5.3.3 Significance of ENSO Phase

There is no significant difference in AEW activity or seasonal cycle between the perpetual La Niña and the control simulations, regardless of whether diagnosed through count or spectral statistics. There is a difference in the *magnitude* of the seasonal cycle of developing AEW count, African TC count, and TC count signals for the perpetual La Niña simulation, although the general distribution of events within the seasonal cycle is the same as for the control simulation. These differences in magnitude present clearly in the August through October total counts of developing AEWs, African TCs, and TCs, each of which shows a statistically significant increase from the control to the perpetual La Niña simulation.

While these simulations suggest that AEW count is not strongly dependent on ENSO state, the number of waves that *develop* clearly is, likely owing to changes in the large-scale favorability. In the perpetual La Niña simulation, GPI increases are especially concentrated in the MDR, and more TCs form there accordingly. Although the perpetual La Niña simulation does not produce statistically significantly more AEWs, a larger portion of TCs have their origins in AEWs. The percentage of AEWs that develop is not fixed, nor do a certain percentage of TCs form from AEWs

(a) La Niña

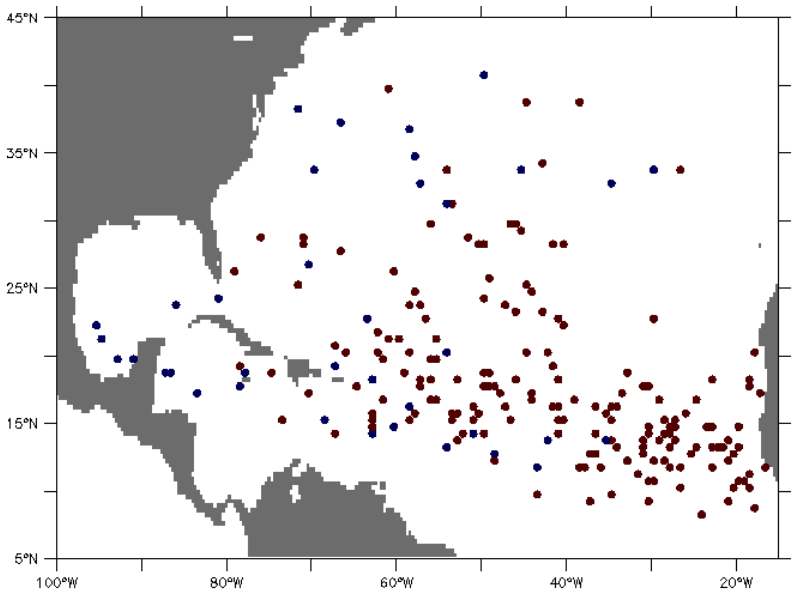

(b) Control

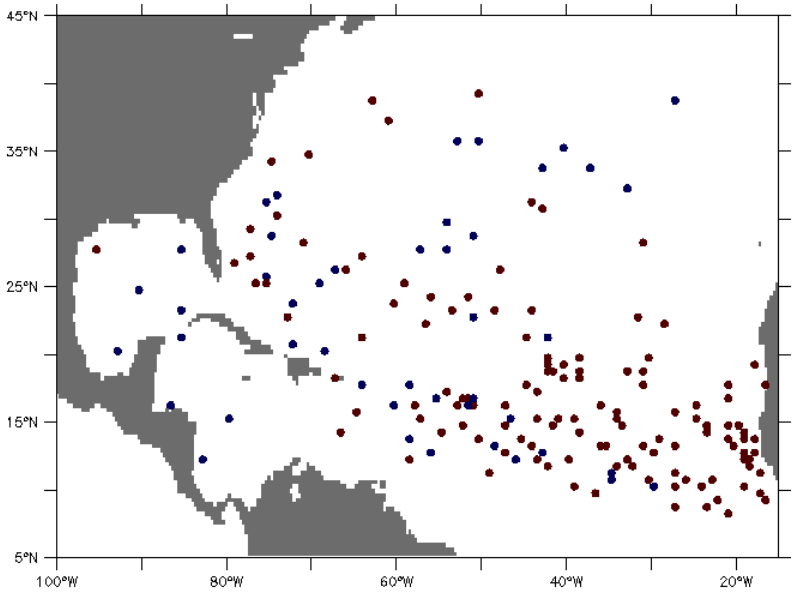

Figure 5.9: Tropical storm origins for the months of August through October for twenty model years, for (a) the perpetual La Niña interannually invariant simulation, and (b) the control interannually invariant simulation. Genesis points of storms spawned by AEWs are shown as red dots, non-African storms as blue dots.

regardless of the large-scale conditions. To the contrary, these simulations show that environmental favorability can indeed be a limiting factor in the number of AEWs that develop into TCs.

5.4 Summary

One theory in the existing literature is that AEW and TC count are both primarily determined by environmental factors, and any covariance between the two is simply due to the influence of changes in large-scale favorability (Caron and Jones, 2011). However, the evidence shown above clearly demonstrates that this is not the case in the HiRAM simulations, further strengthening the argument that AEWs play an active role in determining TC variability.

The presence of TC count covariance coupled with the lack of covariance in AEW count between climatological ensemble members, forced with identical historical SST boundary conditions, indicates that there is significant AEW variability that is independent of the large-scale forcing. Separating the interannual variability of the climatological simulations into that more closely linked with environmental fluctuations (the ensemble average) and the stochastic component (the perturbation from the ensemble average), the stochastic component of AEW variability shows significant positive correlation with the corresponding TC variability. This provides further evidence that variations in AEW count may explain a component of the TC variability that remains unexplained by known environmental factors.

That is not to say that environmental factors are unimportant. The fact that a statistically significant change in climatologically average TC count is evident between simulations with the same average number of AEWs, namely the perpetual La Niña and the control simulations, supports the notion that environmental factors conducive to TC development are more important than the number of AEWs in determining the

average number of TCs that form annually. Even so, the perpetual La Niña and the control simulations both exhibit the same AEW-TC covariance on interannual scales that was evident in the climatological simulations, even in the absence of interannual variability in the SST forcing. This too supports a direct connection between AEW count and TC count variability, and while this connection may be of secondary importance to large-scale conditions when it comes to climatologically average counts, it does seem to be independent of forcing via the SST boundary condition.

When the effects of interannual variability of the large-scale environment are diminished, either through considering the perturbation from the ensemble mean in climatological simulations or through examination of simulations with interannually invariant SSTs, it is clear that there is significant correlation between AEW and TC counts. Overall, the model exhibits notable internal AEW variability, which explains a significant portion of the TC variability unexplained by changes in SSTs.

Chapter 6

Results: Perturbing the Environment to Examine the Relationship between Large-Scale Favorability, AEW Activity, and TC Activity

By systematically varying the albedo of Africa, it is possible to perturb the large-scale environment beyond current climatological variability and examine how changes in AEW activity and overall environmental favorability interact and affect TC activity. The focus of this chapter is on the suite of uniform albedo simulations, which share the same control simulation as in Chapter 5. The four simulations in the suite have interannually invariant climatological SSTs, as in the control simulation, but the albedo over Africa is prescribed to be uniform. The simulations are numbered 1-4 in order of increasing albedo, with albedos of 7.5%, 15%, 30%, and 45% (see Section 2.1.2 for more information).

First, the role of African albedo is assessed in Section 6.1, through comparison with the control simulation (Section 6.1.1), an exploration of the model sensitivity to the value of the albedo parameter (Section 6.1.2), and a cursory discussion of potential physical mechanisms at work (Section 6.1.3). Next, the effects of the large-scale favorability and the AEW count on TC count are disentangled in Section 6.2, using GPI as a reference (Section 6.2.1), considering each of the components of GPI separately (Section 6.2.2), and employing multiple linear regression techniques (Sec-

tion 6.2.3). Finally, a summary of the results of the albedo simulations and their relevance for understanding the relationship between AEW and TC activity is provided in Section 6.3. As in previous chapters, unless otherwise specified, the fields and quantities discussed are averaged from August 1 through October 31 of all 20 years of the simulation to produce "annual" climatological averages.

6.1 The Role of African Albedo

The original motivation for manipulating African albedo was the idea that removing the strong gradient in surface albedo might disrupt the surface temperature gradient between the Sahara and the rainforest to its south, potentially weakening the AEJ. As described further in Section 6.1.1, removing the albedo gradient alone does not have a significant effect on the surface temperature gradient, the large-scale environment, or AEW statistics in HiRAM. While the modeled atmosphere is not sensitive to the *gradient* in the surface albedo, it is sensitive to the *magnitude* of the surface albedo. The effects of varying the value of the albedo are discussed in Section 6.1.2. Since this suite of simulations is novel, the bulk of this section is descriptive, with a preliminary physical explanation for the model behavior in Section 6.1.3.

6.1.1 Comparing Control to a Uniform Albedo Simulation

In this section, the uniform albedo simulation with 30% albedo over the entire continent of Africa is compared against the control simulation with realistic surface albedo. The surface albedos of northern Africa are shown in Figure 6.1. As noted in Section 2.1.2, the albedo over Africa is not completely "uniform" in the experimental simulations, as the soil albedo model has a dependence on azimuth angle and geographical variation in the direct to diffuse ratio of solar radiation. This accounts for the weak gradient present in Figure 6.1a, which although non-zero, is trivial in

comparison with the strong gradient in albedo between the Sahel and the Sahara in Figure 6.1b.

Despite the lack of a strong gradient in surface albedo, this uniform albedo simulation produces AEW and TC count statistics that are indistinguishable from the control simulation (see Figure 6.2). The spectral measures of AEW activity are also quite similar, with the differences in spectra shown in Figure 6.3 being largely within the range of variability observed among the climatological ensemble members (recall Figure 4.3). Although the percent of the power located in the 3-5 day band is larger for the uniform albedo simulation than the control, 64.4% and 59.4% respectively, the spectral centroid for both simulations is 3.68 days.

Figure 6.4 shows the genesis potential together with the spatial distribution of all August through October genesis events (see Section 2.2.1 for more details about GPI). By visual inspection, the differences in spatial distribution of the GPI in these two simulations are within reasonable range of the level of variability found in the climatological ensemble (recall Figure 4.7). The uniform albedo simulation does have slightly lower GPI in the MDR in comparison to the control, with values of 1.4 and 1.6, respectively. This is reflected in the relatively lower concentration of genesis events in the MDR and higher concentration in the subtropical northern Atlantic for the uniform albedo simulation. Averaging over the entire Atlantic basin, the two simulations each yield identical values of GPI (1.7) and statistically indistinguishable TC count.

The limited impact of removing the surface albedo gradient speaks to the disconnection between surface and planetary albedo, and by extension, the importance of the position and strength of the ITCZ. As the planetary albedos shown in Figure 6.5 indicate, the surface albedo in areas of convection is unimportant, because the cloud cover dominates the planetary albedo. The surface albedo over northern Africa, where there is limited cloud cover, does impact the planetary albedo, opening

(a) "Uniform Albedo" (30%) Surface Albedo

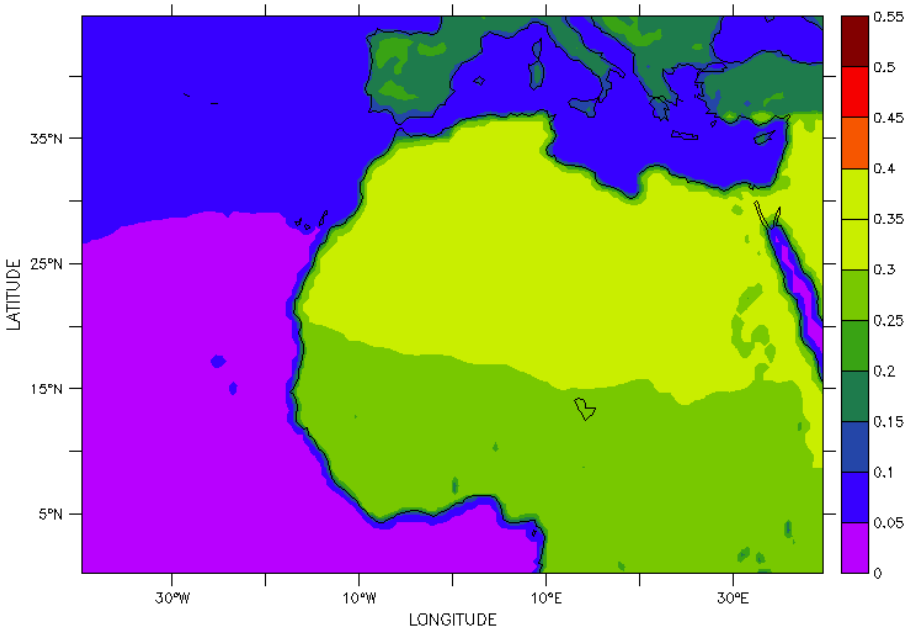

(b) Control Surface Albedo

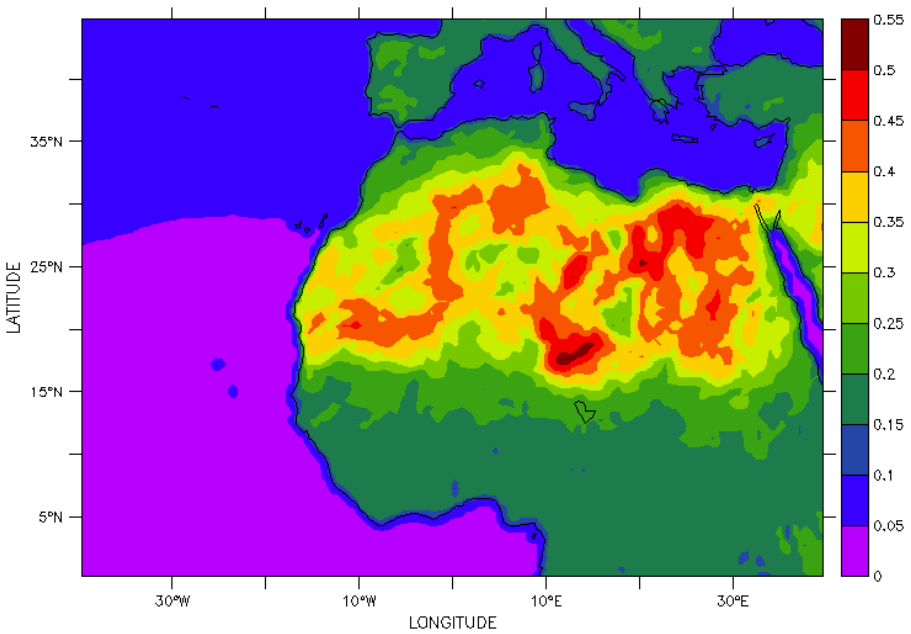

Figure 6.1: Average surface albedo for the months of August through October, for (a) the uniform African albedo simulation with 30% albedo over Africa, and (b) the control simulation with realistic African albedo.

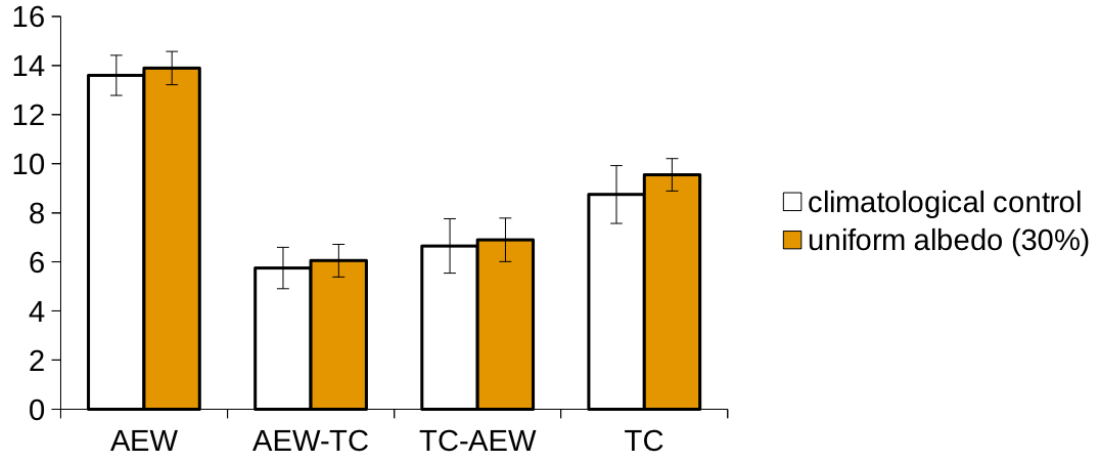

Figure 6.2: Modeled August through October average counts for African easterly waves (AEW), developing African easterly waves (AEW-TC), African tropical storms (TC-AEW), and all tropical storms (TC) for the control simulation (white) and the uniform African albedo simulation with 30% albedo (orange). Error bars denote 95% confidence intervals.

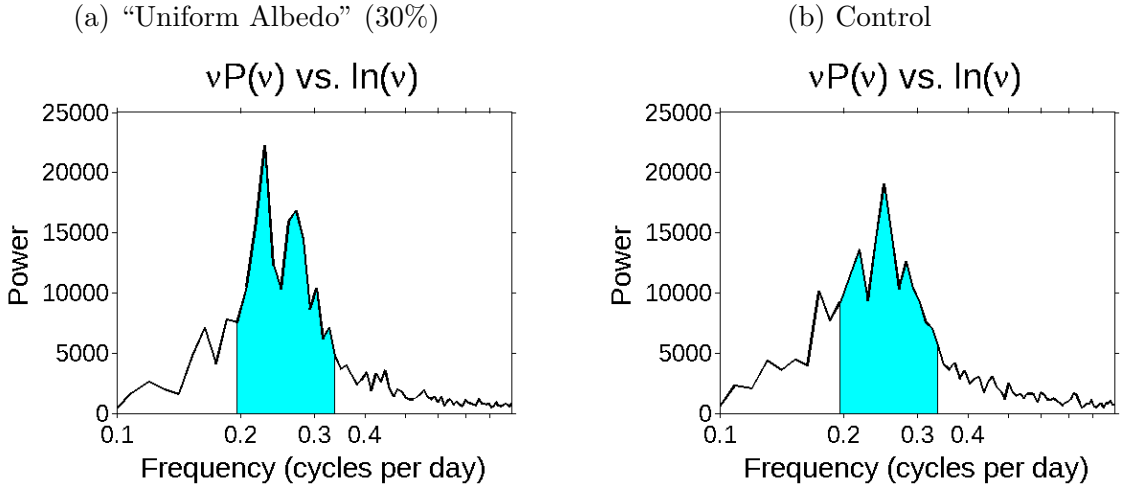

Figure 6.3: Power spectrum of 1-10 day band-pass filtered meridional wind at 850 mb, averaged between 10°N and 20°N, at the coast of Africa (15°W), for August 1 through October 31, for (a) the uniform African albedo simulation with 30% albedo over Africa, and (b) the control simulation with realistic African albedo. The 3-5 day band is highlighted in cyan.

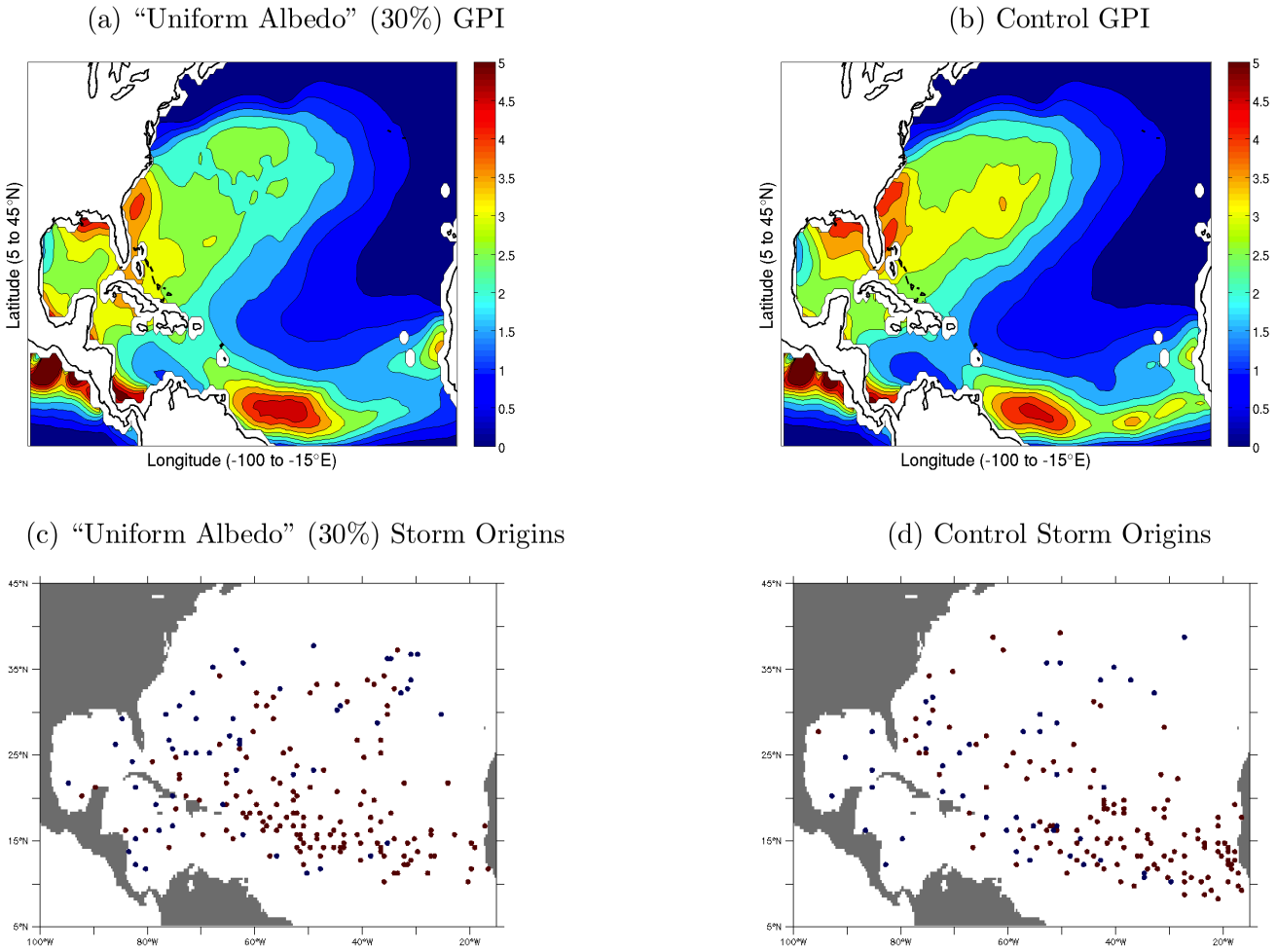

Figure 6.4: Genesis potential index (top, a and b) and tropical storm origins (bottom, c and d) for the months of August through October for twenty model years, for the uniform African albedo simulation with 30% albedo over Africa (left, a and c) and the control simulation with realistic African albedo (right, b and d). Genesis points of storms spawned by AEWs are shown as red dots, non-African storms as blue dots.

itself to manipulation as in Section 6.1.2. Despite very different surface albedo distributions, given the current magnitude of the surface albedo, the 30% uniform albedo and control simulations have strikingly similar planetary albedo.

Additional climatological fields for the uniform albedo simulation are shown with the other members of the suite, including zonal wind at 600 mb (Figure 6.10) and precipitation rate (Figure 6.11), which also show good agreement with the control for 30% albedo. To avoid belaboring the point, every field is not shown here, but visual inspection of other climatological fields, including temperature, meridional velocity, and zonal velocity, both for cross-sections at 5°E and 10°W, and at various levels over Africa and the eastern Atlantic, reveals excellent agreement between the albedo simulation with 30% albedo over the entire continent of Africa and the control simulation with realistic surface albedo.

6.1.2 Sensitivity to Value of Uniform Albedo Parameter

While the gradient in the observed surface albedo over Africa does not seem to be of critical importance due to overlying cloud cover dominating the planetary albedo in the transition zone, as shown above in Section 6.1.1, the magnitude of the albedo in the region of the Sahara does seem to impact the planetary albedo, and by extension the overall model climate. In this section, the effects of variation in the surface albedo parameter for the uniform albedo simulations are described, through examination of several fields of interest over Africa and the Atlantic: the genesis potential and associated genesis points, the zonal winds at the level of the AEJ core, and the precipitation rates. Various quantitative measures of favorability and storm activity are also discussed throughout and are summarized in Figures 6.12, 6.13, and 6.14 at the end of the section.

Spatial plots of GPI are shown in Figure 6.6, with the difference between each perturbed simulation and the control simulation shown in Figure 6.7. While it is

(a) “Uniform Albedo” (30%) Planetary Albedo

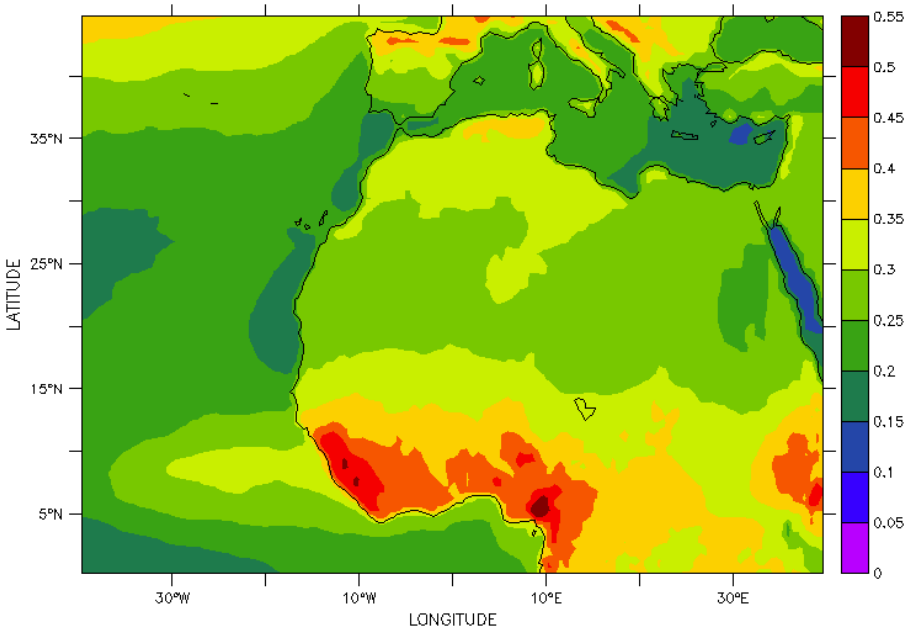

(b) Control Planetary Albedo

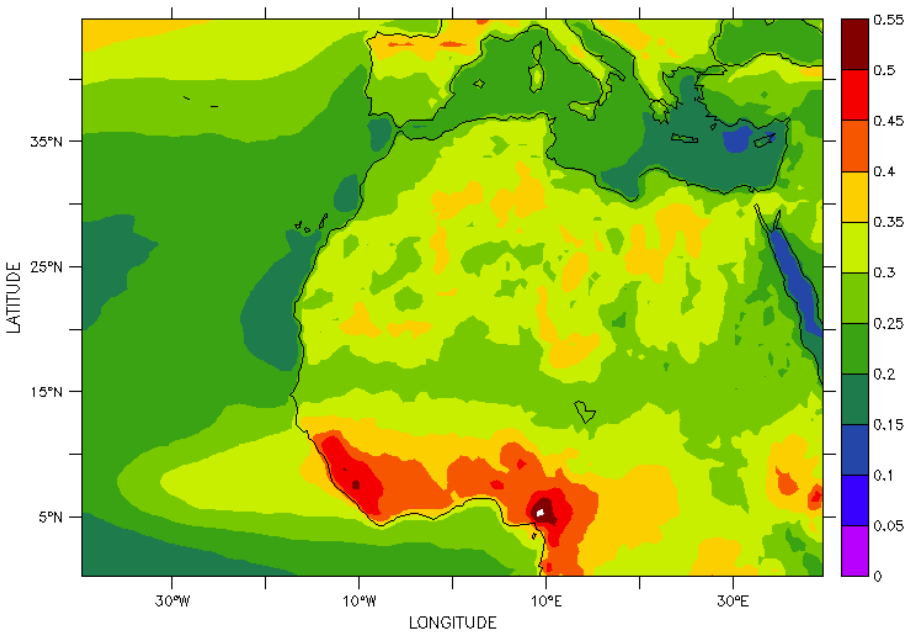

Figure 6.5: Average planetary albedo for the months of August through October, for (a) the uniform African albedo simulation with 30% albedo over Africa, and (b) the control simulation with realistic African albedo.

obvious from these figures that the basin-wide average GPI increases monotonically with increasing albedo, it is also clear that it does not do so in a spatially uniform fashion, with the MDR in particular exhibiting non-monotonic behavior. To clarify this point quantitatively, Figure 6.12a provides a plot of basin-wide average GPI as a function of albedo, and Figure 6.12b shows average GPI in the MDR, also as a function of albedo.

The TC genesis points are shown in Figure 6.8, which follow the structure of the GPI to a large extent, but also exhibit some differences. Total TC count increases with increasing albedo, although unlike the GPI, it shows some indication of leveling off (see Figure 6.14a). While the MDR GPI actually decreases from the penultimate to ultimate albedo simulation (see Figure 6.12b), the number of TCs in the MDR in the third and fourth albedo simulations are indistinguishable (see Figure 6.14b). These differences from the GPI may be due to the competing effect of the AEW count statistics, shown in Figure 6.9. While the basin-wide average GPI increases monotonically and quite linearly with albedo ($R^2 = 0.982$), the AEW count levels off and is less linear ($R^2 = 0.803$). The competing effects of GPI and AEW count are examined more closely in Section 6.2.

AEW counts seem to scale with jet strength to some extent (see Figure 6.10), the changes in which, in turn, are inversely proportional to the amount of precipitation in the tropical rain belt associated with the ITCZ (see Figure 6.11). As is apparent in Figure 6.10, with increasing albedo, the AEJ core shifts equatorward and westward, while also strengthening. The rain belt also shifts equatorward, but weakens with increasing albedo in Figure 6.11.

For brevity, spatial plots of the components of GPI are not shown here, but their average values, both in the entire Atlantic basin (left column) and in the MDR (right column), are plotted against the uniform albedo parameters in Figures 6.12 and 6.13. The components of GPI include the relative humidity at 600 mb in units of percent

(a) 7.5% Uniform African Albedo

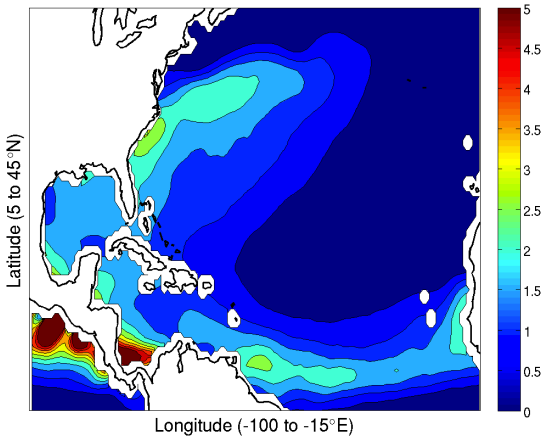

(b) 15% Uniform African Albedo

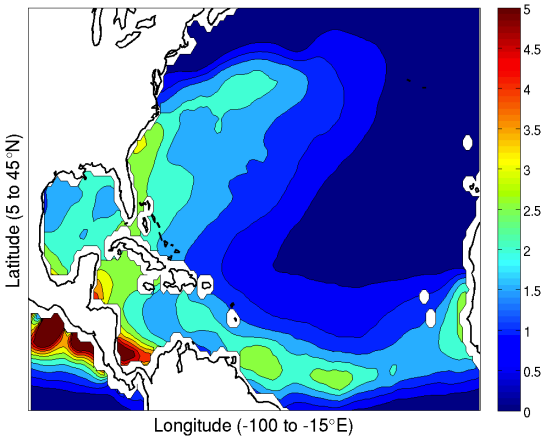

(c) 30% Uniform African Albedo

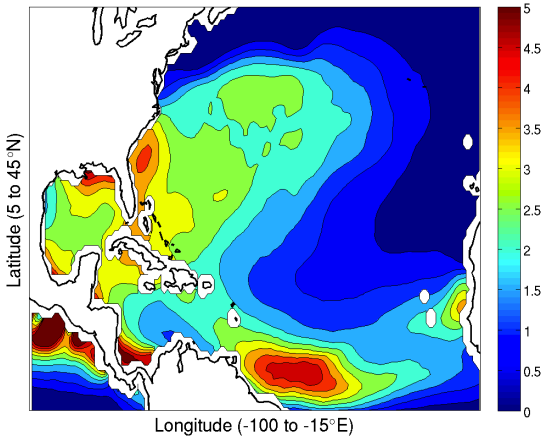

(d) 45% Uniform African Albedo

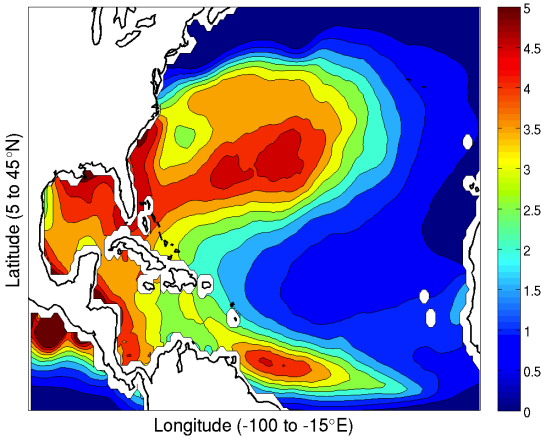

Figure 6.6: Genesis potential index for the months of August through October, for the uniform African albedo simulation with (a) 7.5% albedo, (b) 15% albedo, (c) 30% albedo, and (d) 45% albedo.

(a) 7.5% Uniform African Albedo

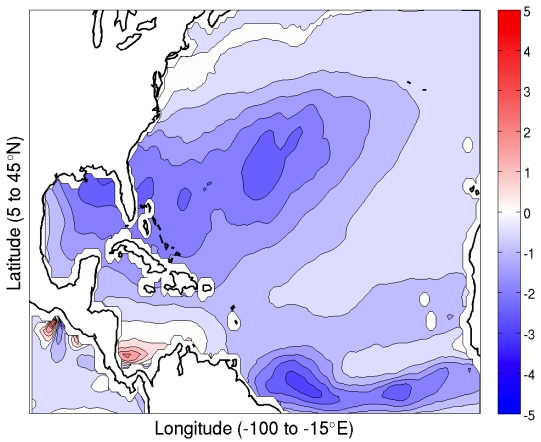

(b) 15% Uniform African Albedo

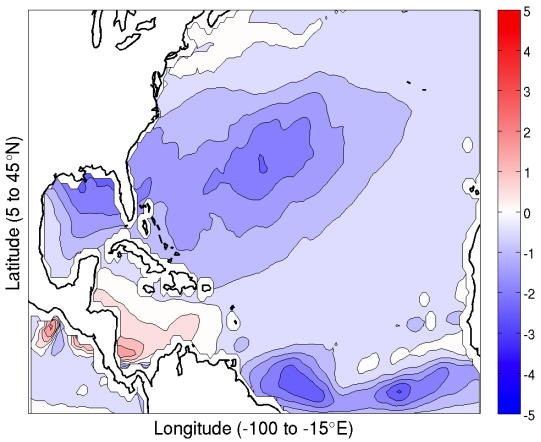

(c) 30% Uniform African Albedo

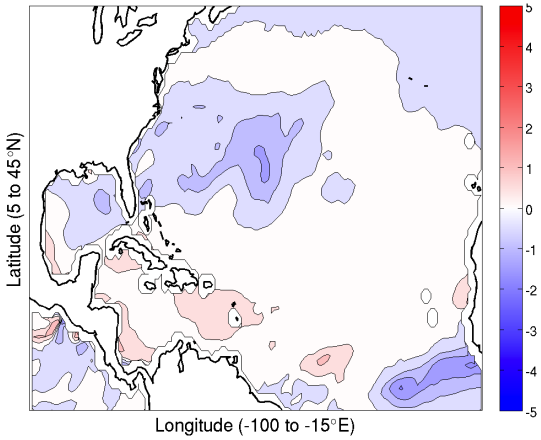

(d) 45% Uniform African Albedo

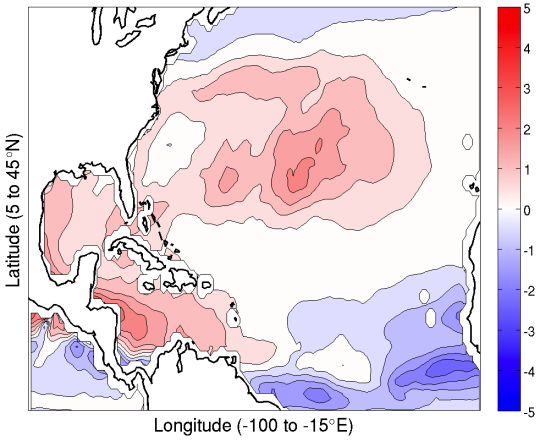

Figure 6.7: The difference between genesis potential index compared to the control simulation (see Figure 6.4b) for the months of August through October, for the uniform African albedo simulation with (a) 7.5% albedo, (b) 15% albedo, (c) 30% albedo, and (d) 45% albedo.

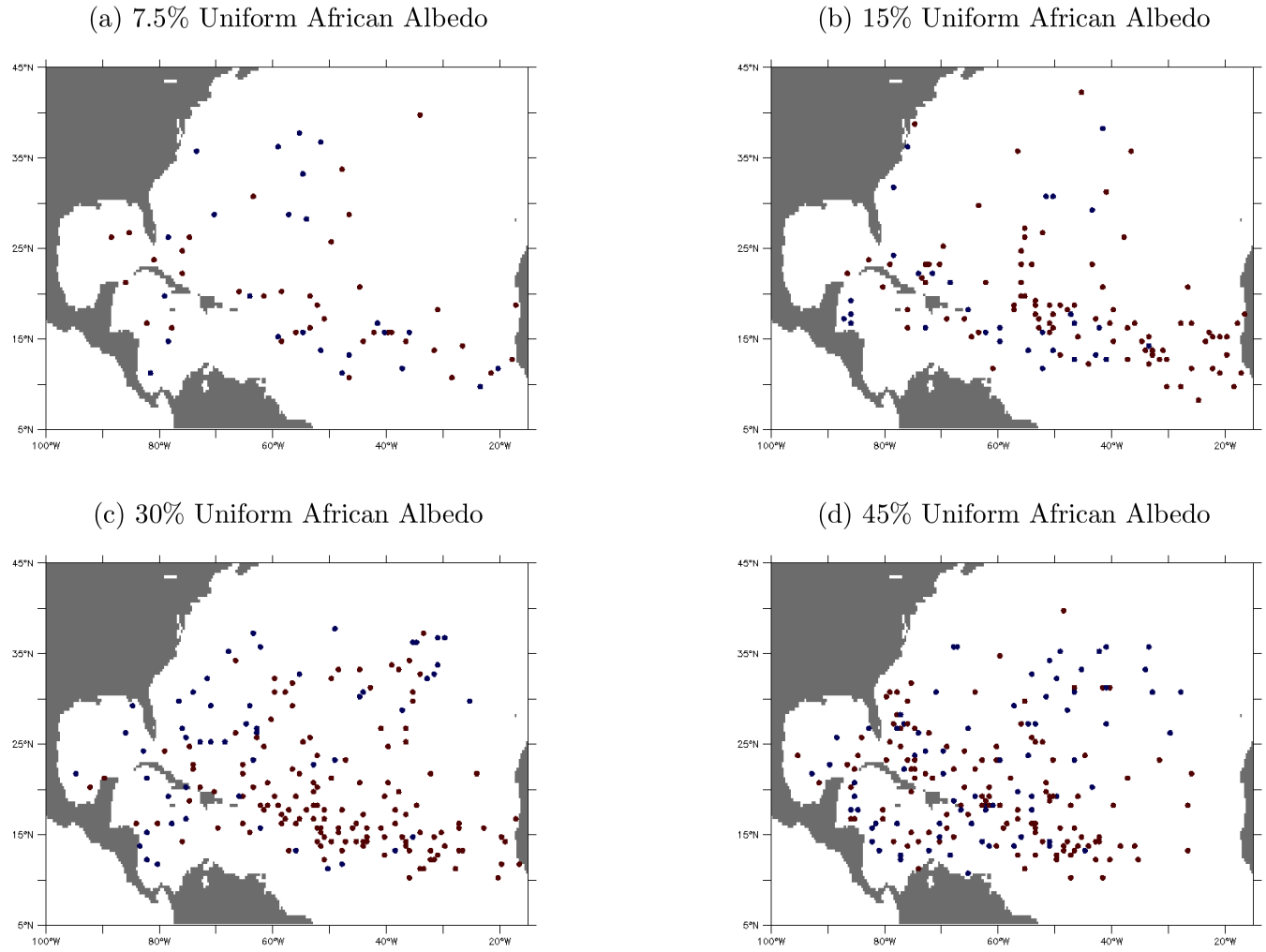

Figure 6.8: Tropical storm origins for the months of August through October for twenty model years, for the uniform African albedo simulation with (a) 7.5% albedo, (b) 15% albedo, (c) 30% albedo, and (d) 45% albedo. Genesis points of storms spawned by AEWs are shown as red dots, non-African storms as blue dots.

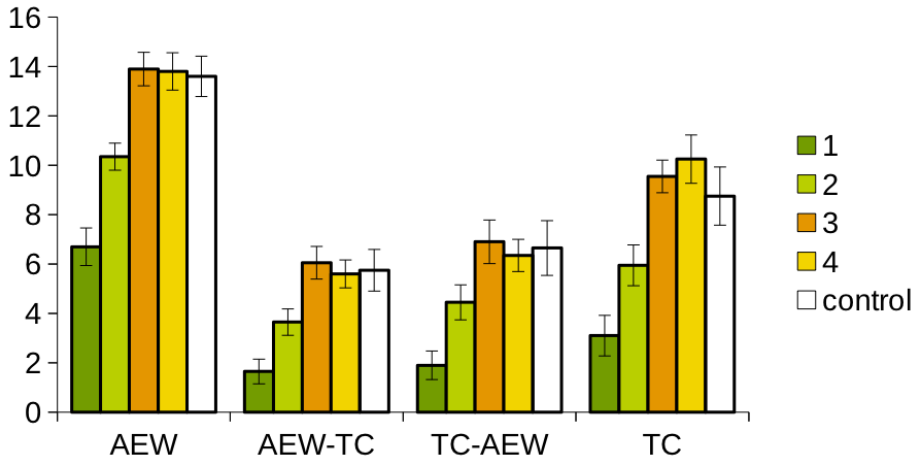

Figure 6.9: Modeled August through October average counts for African easterly waves (AEW), developing African easterly waves (AEW-TC), African tropical storms (TC-AEW), and all tropical storms (TC) for the uniform African albedo simulations, with albedos of 7.5% (dark green), 15% (light green), 30% (orange), and 45% (yellow), and the control simulation (white). Error bars denote 95% confidence intervals.

(Figure 6.12c, d), the maximum potential intensity in units of m s^{-1} (MPI; Bister and Emanuel 2002; Figure 6.12e, f), the vertical wind shear between 850 and 200 mb in units of m s^{-1} (Figure 6.13a, b), and the absolute vorticity at 850 mb in units of s^{-1} (Figure 6.13c, d). More details on these parameters and the spatial averaging can be found in Section 2.2.1.

Both the relative humidity in the entire basin and the relative humidity in the MDR have a direct relationship with African albedo (see Figure 6.12c, d). The pattern of maximum potential intensity in the Atlantic is quite different from that in the MDR, with neither showing completely monotonic response to albedo changes (see Figure 6.12e, f). The shear generally decreases with increasing albedo up through 30% albedo, but levels off in the case of the entire Atlantic, or rebounds from there in the case of the MDR (see Figure 6.13a, b). The absolute vorticity in the MDR has an inverse relationship with albedo (see Figure 6.13d), which likely reflects the weakening of the ITCZ, but shows no clear pattern for the basin-wide average (see Figure 6.13c). The explanatory power of each of these component fields in under-

(a) 7.5% Uniform African Albedo

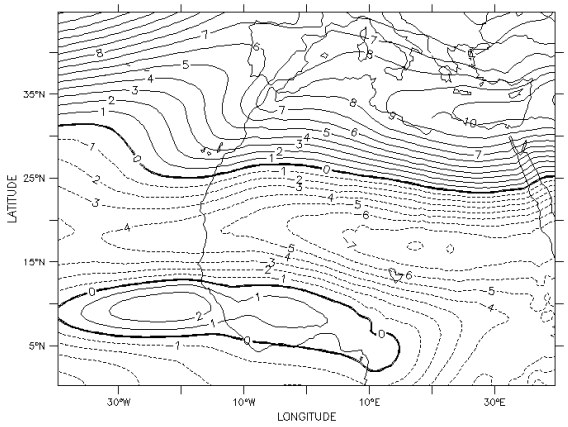

(b) 15% Uniform African Albedo

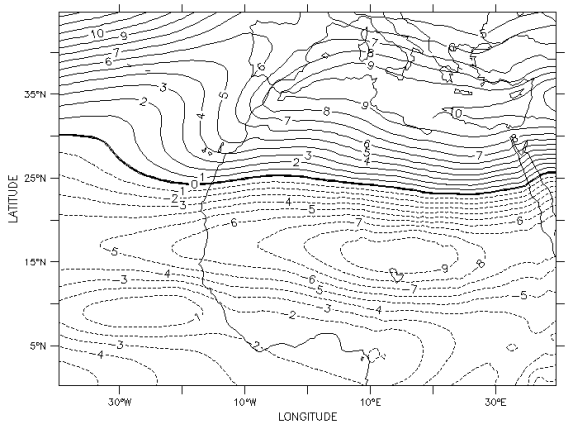

(c) 30% Uniform African Albedo

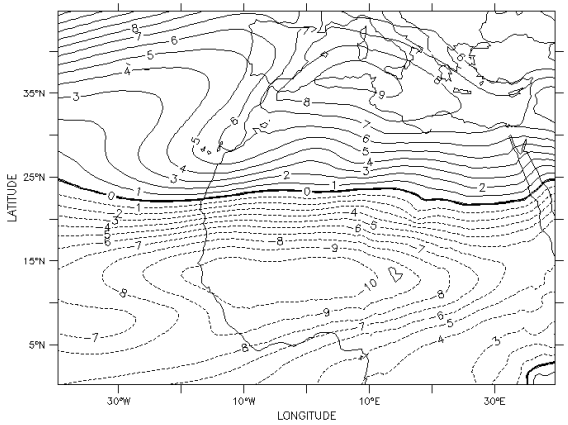

(d) 45% Uniform African Albedo

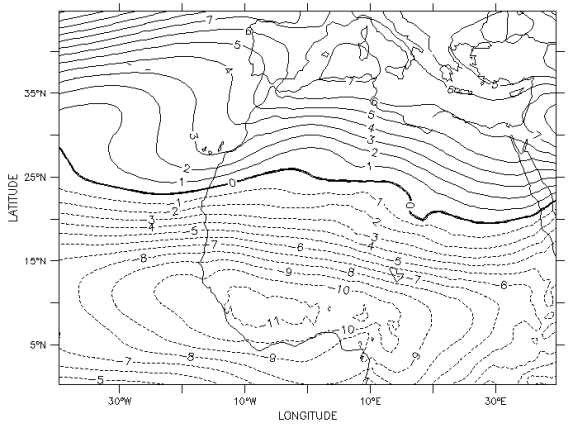

Figure 6.10: Average zonal wind at 600mb for the months of August through October for the uniform African albedo simulation with (a) 7.5% albedo, (b) 15% albedo, (c) 30% albedo, and (d) 45% albedo. Dashed contours indicate easterly winds, solid contours indicate westerly winds, and the contour interval is 1 m s^{-1}.

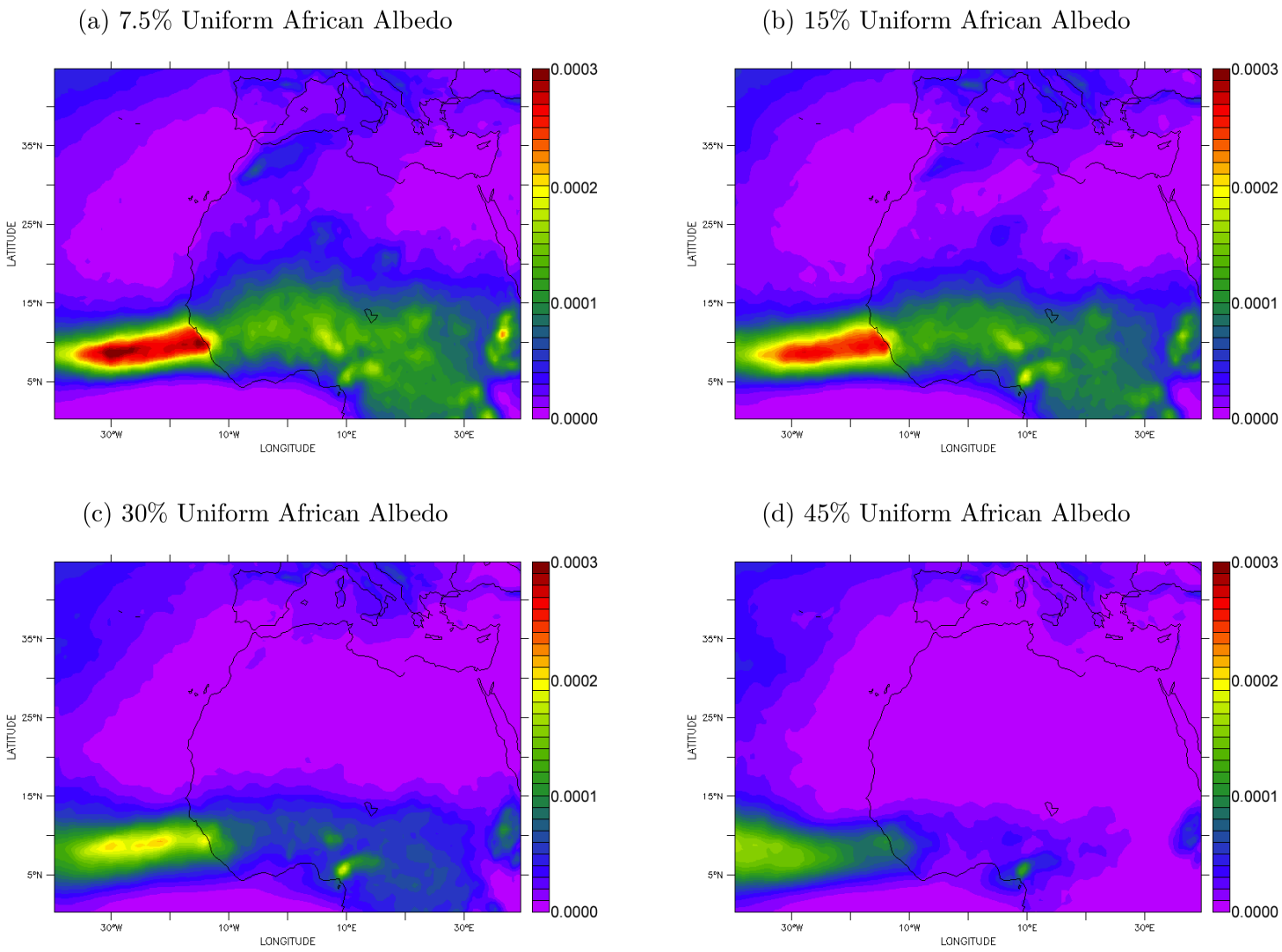

Figure 6.11: Average precipitation rate for the months of August through October for the uniform African albedo simulation with (a) 7.5% albedo, (b) 15% albedo, (c) 30% albedo, and (d) 45% albedo. Colorbar ranges from 0 to 0.0003 kg m^{-2} s^{-1}.

standing the differences in TC count variability between the members of the uniform albedo suite is diagnosed in Section 6.2.2.

6.1.3 Physical Relevance of Albedo

Much of the contemporary literature suffers from the lack of a common vernacular to discuss the relationships between tropical phenomena, with unresolvable discrepancies between the definitions of AEWs and the ITCZ in particular (Nicholson, 2009). This makes it difficult to conduct a meta-analysis to construct narratives that provide conceptual explanations of the interrelated dynamics of the AEJ, ITCZ, and AEWs. For this reason, the below explanation is fairly speculative and further study is required to understand the physical mechanism of the atmosphere's sensitivity to African albedo when it comes to AEWs. Since the potential connection between the albedo, the AEJ, and AEWs are a means to an end, this connection is only discussed briefly below.

Given the above caveats, there are two general "modes" in West Africa, namely "wet years" that are typified by a weaker and more poleward AEJ, and "dry years" typified by a stronger and more equatorward AEJ (Grist and Nicholson, 2001; Nicholson and Grist, 2001). Wet years are also associated with a stronger West African Westerly Jet (WAWJ), located around 10°N, near the surface, from the eastern Atlantic toward the West African coast (Pu and Cook, 2012). Grist et al. (2002) found that in wet years AEWs tend to be stronger but have longer periods, although the direction of causality was not clear. Relatedly, Thorncroft and Rowell (1998) found that AEW activity is positively correlated with the strength of the AEJ. These results taken together indicate that as the AEJ shifts equatorward and strengthens (as it does in the dry mode), one would expect AEW activity to increase. Although it seems the ITCZ also plays a pivotal role (Hsieh and Cook, 2005), due to incompatible definitions of the ITCZ, it is difficult to speculate precisely how. For example,

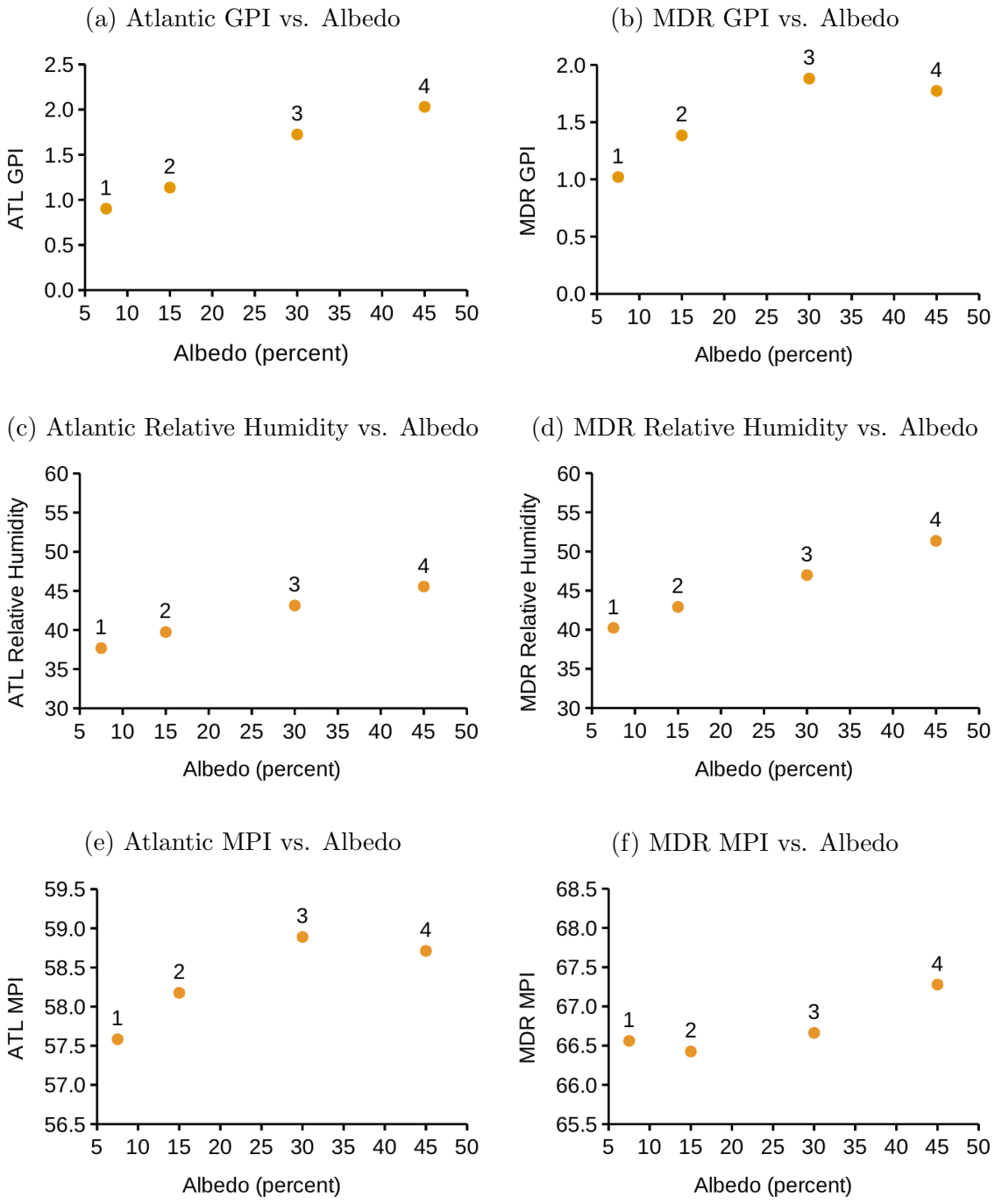

Figure 6.12: Quantitative measures of large-scale favorability, including the genesis potential index (GPI; a and b), relative humidity at 600 mb in units of percent (c and d), and maximum potential intensity in units of m s^{-1} (MPI; Bister and Emanuel, 2002; e and f), averaged over the entire Atlantic basin (left) and the MDR (right). Definitions and details of the spatial averaging can be found in Section 2.2.1.

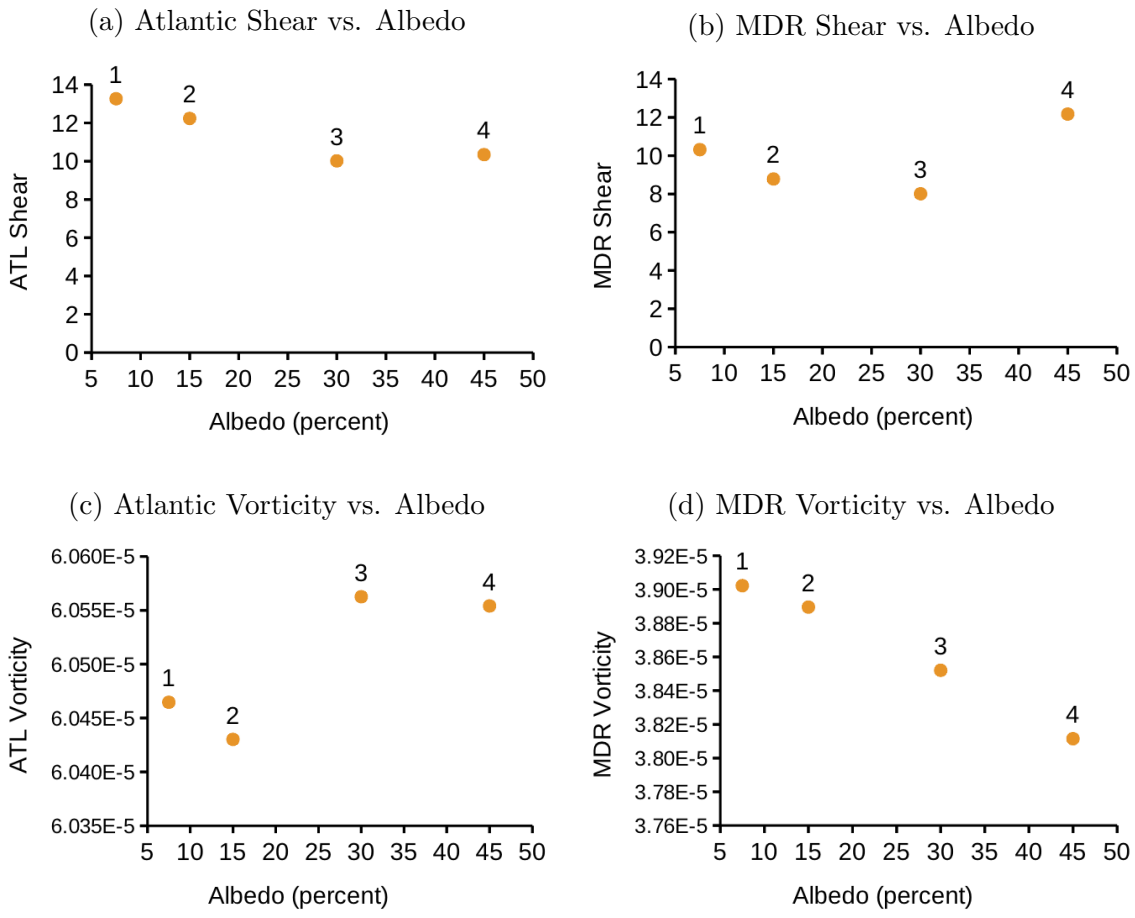

Figure 6.13: Quantitative measures of large-scale favorability, including the vertical wind shear between 850 and 200 mb in units of m s^{-1} (a and b) and absolute vorticity at 850 mb in units of s^{-1} (c and d), averaged over the entire Atlantic basin (left) and the MDR (right). Definitions and details of the spatial averaging can be found in Section 2.2.1.

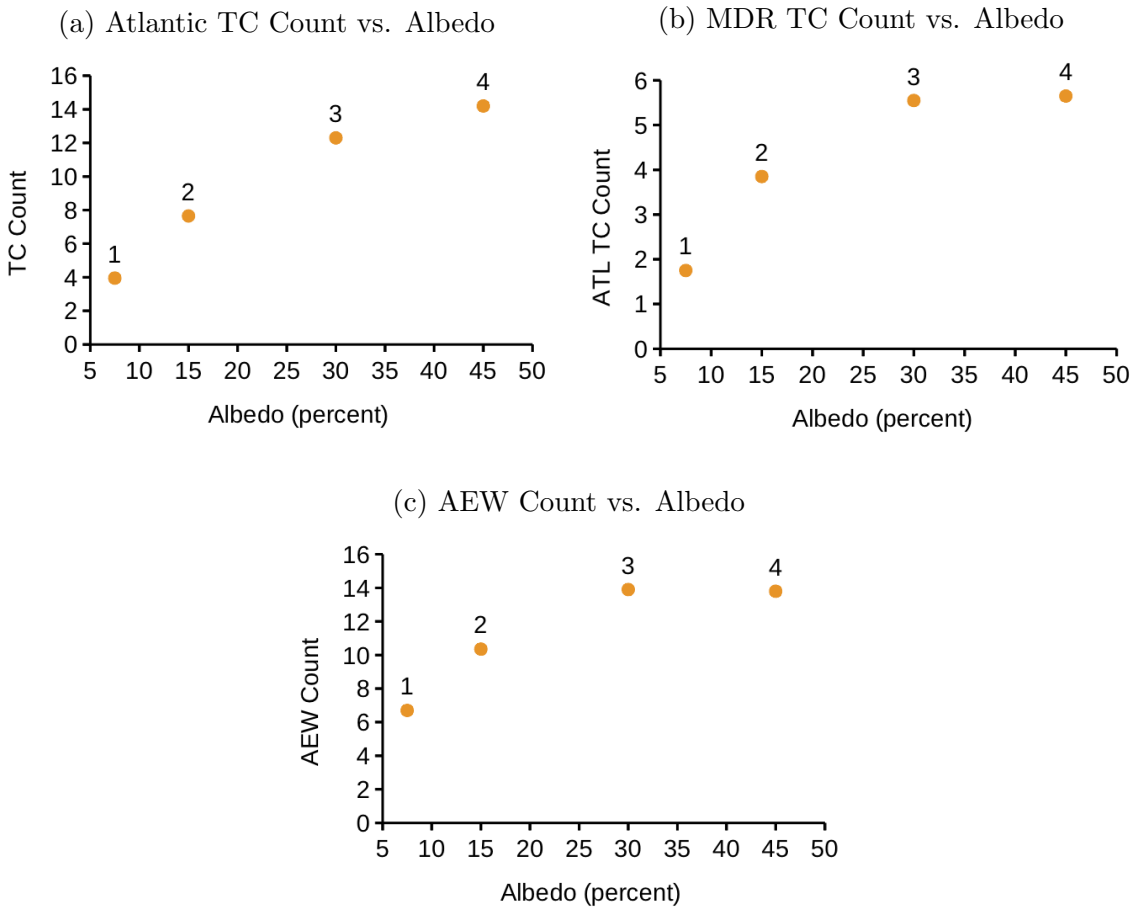

Figure 6.14: Average annual (ASO) count of (a) Atlantic TCs, (b) MDR TCs, and (c) AEWs, plotted by surface albedo value over Africa.

Nicholson and Grist (2001) found the equatorward shift of the AEJ in dry years to be associated with the equatorward shift of the ITCZ.

Similar patterns as those described above arise climatologically in the perturbed albedo simulations. In the uniform albedo simulations, there is a direct relationship between the strength of the precipitation belt associated with the ITCZ and the strength of the WAWJ, which are inversely related to the strength of the AEJ. As the albedo increases, the ITCZ shifts equatorward and weakens, the WAWJ weakens, and the AEJ shifts equatorward and strengthens in turn. As the AEJ shifts equatorward and strengthens, the AEW count increases. In general, it seems increasing the African albedo has a similar effect as transitioning from the wet mode to the dry mode. This

makes physical sense and is consistent with Charney's albedo-precipitation feedback hypothesis (Charney, 1975). Charney found that increasing the albedo of north Africa from 14% to 35% in an early GCM led to the ITCZ shifting equatorward several degrees.

The Sahel experienced extreme drought conditions in the 1970s and 1980s, and while for a time this was thought to be due to anthropogenic desertification and the albedo-precipitation feedback, the current consensus is that any desertification that may have occurred would not be enough to account for the observed changes in rainfall, and changes in ocean temperatures are more likely the primary cause (Folland et al., 1986; Nicholson et al., 1998; Giannini et al., 2003; Held et al., 2005). Whether through ocean temperature changes or land mass changes, there is a strong body of evidence supporting the notion that the ITCZ tends to be displaced toward the anomalously warm hemisphere (Broccoli et al., 2006; Kang et al., 2008, 2009; Kang and Held, 2012; Kang et al., 2014). In the uniform albedo simulations, increasing the albedo generally leads to cooling, as a greater proportion of incident radiation is reflected. This cooling is disproportionately located to the northern hemisphere, specifically northern Africa, due to differences in land mass and cloud cover. As the surface in the northern hemisphere cools, the ITCZ shifts southward due to the return flow of the anomalous Hadley circulation (Kang et al., 2009). The origins of the associated weakening of the ITCZ with its equatorward shift could be in part due to the fact that the SSTs are prescribed in the model, and so as the ITCZ shifts, it moves away from the typically collocated SST relative maximum.

While this is somewhat speculative, the preliminary explanation of the the physical relevance of the albedo is now summarized. As the African albedo increases in the uniform albedo simulations, this triggers anomalous cooling in northern Africa. Anomalous cooling in the northern hemisphere leads to a southward shift of the ITCZ. These changes are similar to moving from a climatology that resembles the wet mode

toward something resembling the dry mode, increasing the strength of the AEJ and leading to more AEW activity. Further study is necessary to better asses the validity of this explanation. This is left to future work, since the focus of this dissertation is on the relationship between AEW activity, large-scale favorability, and TC activity, not on the origins of or controls on AEWs. As detailed in the previous sections, increasing African albedo leads to increases not only in AEW activity, but also in the genesis potential of the Atlantic. The relevance of these factors to TC variability is discussed in the following section.

6.2 Importance of Large-Scale Favorability and AEW Count for TC Count

Manipulating the value of the surface albedo over Africa in the uniform albedo simulations has successfully perturbed the annual AEW count significantly beyond the interannual variability observed climatologically (recall Figure 6.9). Since this manipulation also led to significant changes in the GPI (recall Figures 6.6, 6.7, and 6.12), the ultimate changes in average TC count cannot immediately be ascribed to these changes in AEW count. This section is dedicated to disentangling and quantifying the relative importance of the AEW count and large-scale environmental factors in explaining TC count.

As shown in Figure 6.15, annual TC count is well correlated with annual AEW count across members of the uniform albedo suite, both for the total Atlantic basin TC count ($R^2 = 0.955$, $p = 0.023$), and the count of TCs that formed in the MDR ($R^2 = 0.998$, $p = 0.0012$). It is worth noting that as in all previous sections, all uniform albedo simulations also exhibit statistically significant interannual correlation between AEW count and TC count, with coefficients of determination of consistent

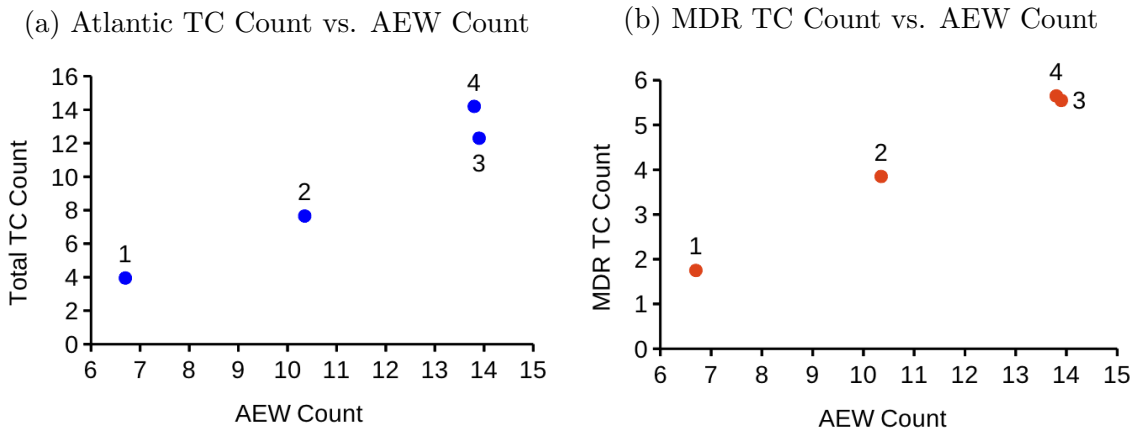

Figure 6.15: Scatterplots of uniform albedo simulation suite members' average annual (ASO) TC count versus AEW count, for (a) all Atlantic TCs, and (b) only TCs that formed in the MDR.

magnitude with the control simulation (see Section 5.2). Note too that all simulations have interannually invariant SST, like the control.

The TC count also shows correlation with GPI, both averaged over the MDR and the entire Atlantic basin. Figure 6.16 shows Atlantic TC count (a; $R^2 = 0.974$, $p = 0.013$), MDR TC count (b; $R^2 = 0.871$, $p = 0.067$), and AEW count (c; $R^2 = 0.874$, $p = 0.065$) versus Atlantic GPI. While the linear regression between Atlantic TC count and Atlantic GPI returns a statistically significant positive correlation coefficient at the 95% confidence level, the MDR TC count and AEW count correlations with the Atlantic GPI are not statistically significant. Similarly, Figure 6.17 shows Atlantic TC count (a; $R^2 = 0.921$, $p = 0.040$), MDR TC count (b; $R^2 = 0.973$, $p = 0.014$), and AEW count (c; $R^2 = 0.986$, $p = 0.0069$) versus MDR GPI, all three of which exhibit statistically significant positive correlation at the 95% confidence level.

It is reasonable that better correlations are found between MDR GPI and MDR TC and AEW counts than for the basin-wide GPI, since a greater percentage of TCs in the MDR are spawned by AEWs and are therefore more sensitive to changes in AEW count. It is worth noting that since GPI was designed to correlate with TC count, it is possible that the index itself might be contaminated by actual genesis

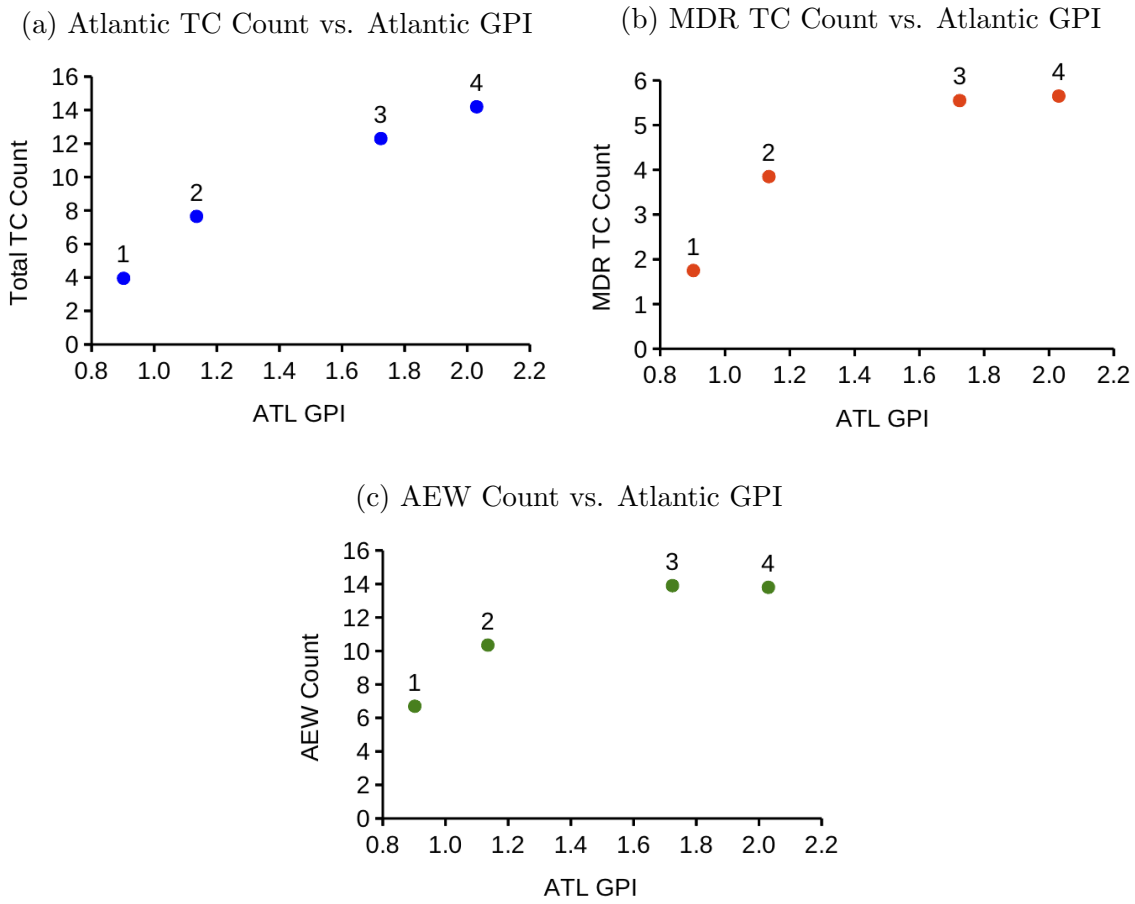

Figure 6.16: Scatterplots of average annual (ASO) count statistics versus average Atlantic GPI for the uniform albedo simulation suite, including (a) all Atlantic TCs, (b) only TCs that formed in the MDR, and (c) AEWs.

events, thereby making it impossible to observe a change in TC activity without a corresponding change in GPI.

6.2.1 Removing the Effect of GPI by Regression

Since Section 6.2 demonstrates that there are statistically significant correlations between both GPI metrics and TC count, AEW count and TC count, and even AEW count and MDR GPI, in order to discern if AEW provides any skill beyond GPI in explaining TC count, both AEW and TC average annual counts are detrended by GPI in this section, and the residuals are correlated. By similar logic as in Section 5.1.2,

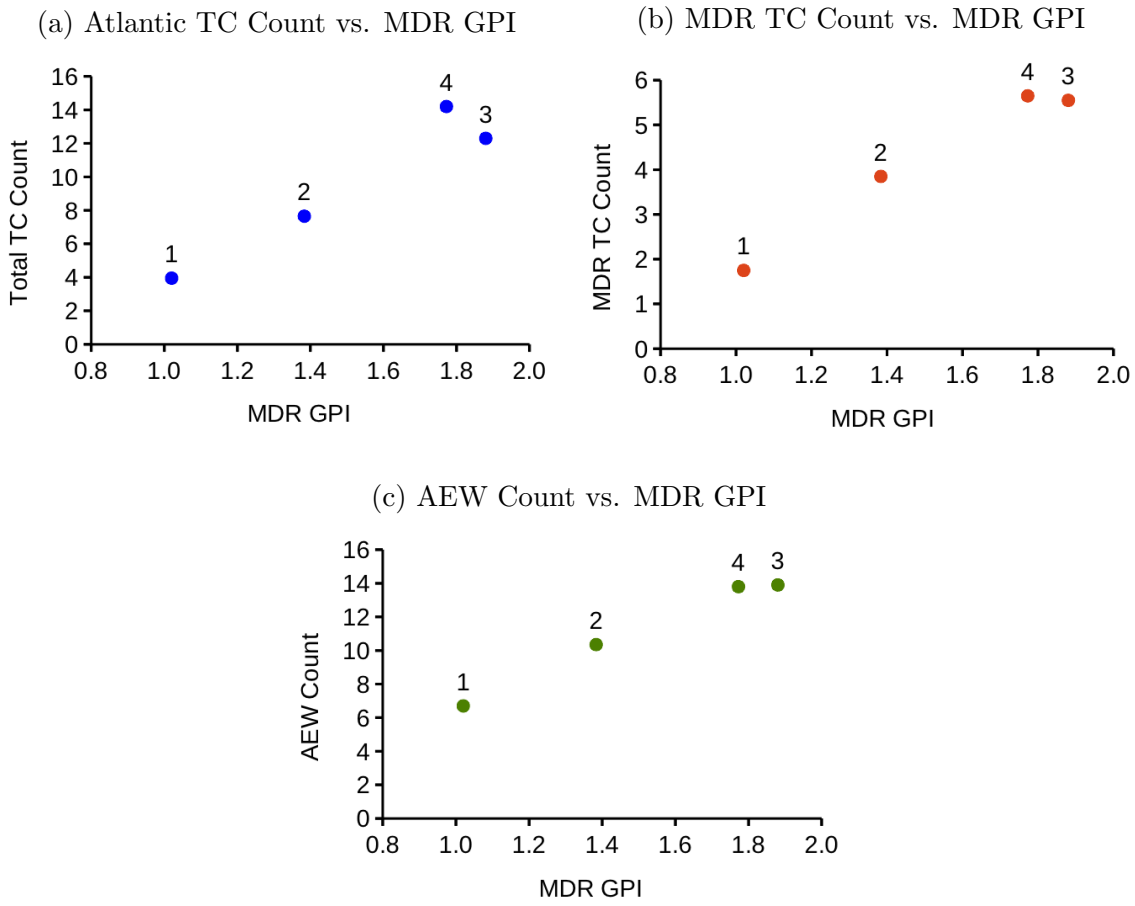

Figure 6.17: Scatterplots of average annual (ASO) count statistics versus average MDR GPI for the uniform albedo simulation suite, including (a) all Atlantic TCs, (b) only TCs that formed in the MDR, and (c) AEWs.

this isolates the AEW and TC activity signals that remain unexplained by the large-scale environment as communicated by GPI, but this time at the climatological level rather than the interannual level.

First, the AEW and TC counts are detrended by basin-wide Atlantic GPI and the residuals are plotted in Figure 6.18. For the total TC count and the AEW count residuals (Figure 6.18a), the coefficient of determination is $R^2 = 0.913$ with a p-value of $p = 0.044$, which is statistically significant at the 90% confidence level. The correlation is even stronger when considering MDR TC count and AEW count residuals (Figure 6.18b), significant at the 95% confidence level, with a coefficient of determi-

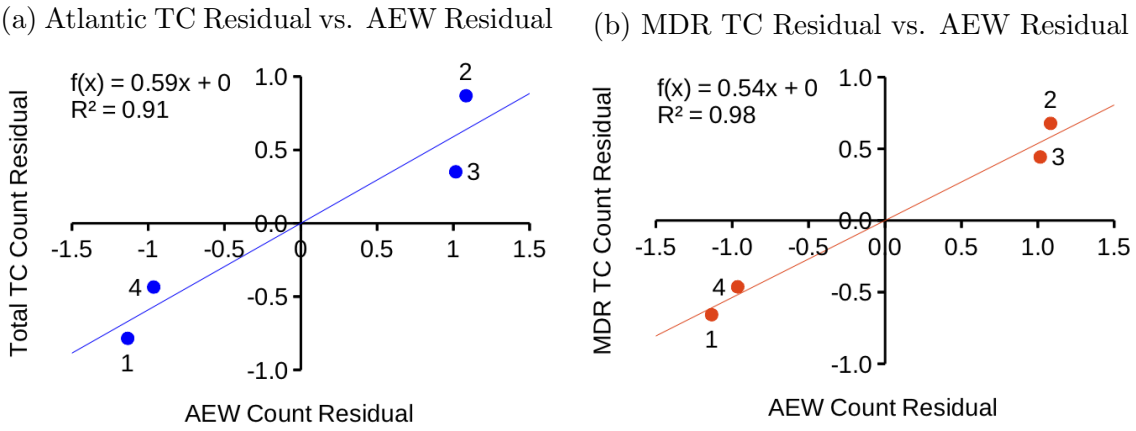

Figure 6.18: Scatterplots of average annual (ASO) TC count residuals versus AEW count residuals, detrended by Atlantic GPI, for (a) all Atlantic TCs, and (b) only TCs that formed in the MDR.

nation of $R^2 = 0.981$ and a p-value of $p = 0.0097$. To be fair, it would be surprising if AEW count did not provide skill beyond the Atlantic GPI in explaining MDR TC count, since MDR TC count is expected to scale with MDR GPI, which responded differently to the albedo changes than the basin-wide GPI (recall Figure 6.12a and b). On the other hand, it is notable that AEW count seems to provide statistically significant additional skill beyond Atlantic GPI in explaining total TC count, since Atlantic GPI is expected to correlate closely with total TC count by design.

Similarly, AEW and TC counts are detrended by MDR GPI and the residuals are plotted in Figure 6.19. Although it does not make a great deal of physical sense to detrend basin-wide TC counts by MDR GPI, this is shown for completeness in Figure 6.19a. There is no detectable correlation between Atlantic TC count and AEW count detrended by MDR GPI ($R^2 = 0.552$, $p = 0.26$). On the other hand, even though MDR GPI explains over 97% of the variance in MDR TC count, AEW and MDR TC count residuals detrended for MDR GPI (Figure 6.19b) have an impressive coefficient of determination ($R^2 = 0.994$, $p = 0.0032$), significant with over 95% confidence.

(a) Atlantic TC Residual vs. AEW Residual

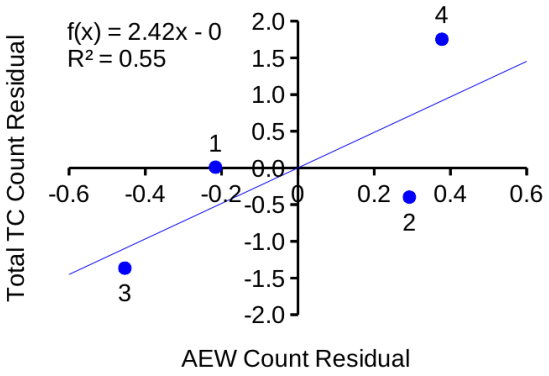

(b) MDR TC Residual vs. AEW Residual

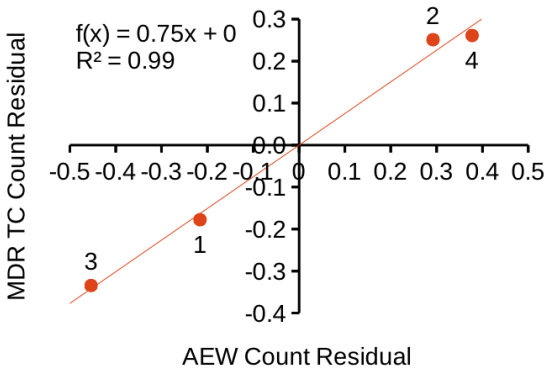

Figure 6.19: Scatterplots of average annual (ASO) TC count residuals versus AEW count residuals, detrended by MDR GPI, for (a) all Atlantic TCs, and (b) only TCs that formed in the MDR.

The above evidence suggests that AEW count may indeed provide additional skill beyond the state of the large-scale environment in explaining the climatologically average annual TC count in the uniform albedo simulations. To strengthen this argument, the components of GPI are considered separately below in Section 6.2.2.

6.2.2 Considering GPI Components Separately

Following similar procedures as above in Section 6.2.1, residuals were considered for all favorability indicators detrended by GPI, for both the MDR and the basin-wide averages. Of AEW count, absolute vorticity, relative humidity, potential intensity, and vertical wind shear (see Section 2.2.1 for definition of GPI and its components), the AEW count residuals are the only residuals to show significant correlation with TC count residuals.

The intra-simulation variance in each of the indicators of favorability is also compared directly to that of TC count, MDR TC count, and AEW count, and the coefficients of determination and p-values are shown in Table 6.1 for the basin-wide averages. Statistical significance at the 95% confidence level is denoted with an aster-

isk, and following the correlation with the total GPI value (which was also discussed in the opening of this section above, Section 6.2), the large-scale environmental components are listed in order of decreasing importance. The coefficients of determination and p-values for the total TC count are shown in bold, since averaging indicators of large-scale environmental favorability over the entire Atlantic basin makes them the most relevant.

Table 6.1: Linear Correlation between Atlantic GPI Components and Counts

	Total TC Count		MDR TC Count		AEW Count	
Component of GPI	**R^2**	**p-value**	**R^2**	**p-value**	**R^2**	**p-value**
Total Atlantic GPI	**0.974***	**0.013**	0.871	0.067	0.874	0.065
Relative Humidity $\mathcal{H}$	**0.979***	**0.010**	0.882	0.061	0.878	0.063
Wind Shear V_{shear}	**0.933***	**0.034**	0.945*	0.028	0.964*	0.018
Potential Intensity V_{pot}	**0.909***	**0.046**	0.975*	0.013	0.987*	0.007
Absolute Vorticity η	**0.493**	**0.298**	0.359	0.401	0.394	0.372

* *asterisk denotes statistically significant with 95% confidence*

The relative humidity exhibits the strongest covariance, even compared with the total GPI, although the confidence intervals overlap with those of GPI. Notably, while all the other components of GPI (humidity, shear, and potential intensity) show statistically significant correlation with total TC count, the absolute vorticity shows no correlation with TC or AEW counts.

Similar to Table 6.1, intra-simulation variance for indicators of favorability averaged over just the MDR are compared to count variance in Table 6.2. This time, the coefficients of determination and p-values for the MDR TC count are shown in bold, since averaging indicators of large-scale environmental favorability over the MDR makes these most relevant. Statistical significance at the 95% confidence level is denoted with an asterisk, and following the correlation with the MDR GPI value (which was also discussed above in Section 6.2) the large-scale environmental components are listed in order of decreasing importance.

Table 6.2: Linear Correlation between MDR GPI Components and Counts

	Total TC Count		MDR TC Count		AEW Count	
Component of GPI	**R^2**	**p-value**	**R^2**	**p-value**	**R^2**	**p-value**
Total MDR GPI	0.921*	0.040	**0.973***	**0.014**	0.986*	0.007
Relative Humidity $\mathcal{H}$	0.950*	0.025	**0.829**	**0.089**	0.821	0.094
Absolute Vorticity η	0.898	0.052	**0.742**	**0.139**	0.739	0.140
Potential Intensity V_{pot}	0.554	0.256	**0.351**	**0.408**	0.344	0.414
Wind Shear V_{shear}	0.041	0.798	**0.000**	**0.998**	0.000	0.994

* *asterisk denotes statistically significant with 95% confidence*

With the exception of MDR GPI, none of the individual indicators of large-scale favorability in the MDR show statistically significant covariance with MDR TC count. Relative humidity comes closest, with a 95% confidence interval of -0.404 $<$ R $<$ 0.998. Due to the small sample size, correlations must be very strong in order to achieve statistical significance with so few degrees of freedom. Similar to Section 6.2.1, detrending AEW and TC counts for MDR relative humidity in place of GPI, the residual AEW and TC counts exhibit statistically significant covariance, both for MDR TC count ($R^2 = 0.987$, $p = 0.007$) and total TC count ($R^2 = 0.993$, $p = 0.003$).

It is not possible to determine whether any of these large-scale environmental favorability measures could be contaminated by the TCs or AEWs themselves, which could account for a portion of the covariance between the indicators of favorability and the TC activity, but AEW count has again been shown to add additional skill. Although not presented in detail above, regardless of which large-scale favorability factor is chosen to detrend for environmental impacts, AEW and TC count residuals show statistically significant positive correlation, either for MDR totals, the entire basin, or both. This is taken a step further in the next section, in which stepwise linear models are constructed using environmental favorability metrics and AEW count as predictors for TC counts.

6.2.3 Multiple Linear Regression of TC Count

Since the above sections demonstrate that AEW count, GPI, and the components of GPI all covary with climatological TC count across the uniform albedo suite of simulations, and there is evidence that AEW count provides skill above and beyond the environmental factors, the focus of this section is quantifying this level of skill using multiple linear regression. When given the option of all possible predictors, AEW count, and both MDR and basin-wide GPI, relative humidity, potential intensity, shear, and absolute vorticity, a stepwise linear regression model chooses only AEW count for the MDR TC count predictand, and both relative humidity (RH) and AEW count for the basin-wide TC count predictand.

As mentioned above in the opening of Section 6.2, the coefficient of determination for a linear model of MDR TC count versus AEW count is $R^2 = 0.998$, with a corresponding p-value of $p = 0.0012$. Although other predictors show correlation with MDR TC count individually, AEW count alone is the best predictor of climatological MDR TC count across these uniform albedo simulations. For the total Atlantic TC count, a linear model of the form $TC \sim 1 + RH + AEW$ yields an adjusted $R^2 = 0.99997$, with $p = 0.0034$. The coefficients of the resulting linear model are discussed in Section 7.2. For reference, relative humidity alone yields an adjusted $R^2 = 0.969$ ($p = 0.010$) and the AEW count alone yields an adjusted $R^2 = 0.933$ ($p = 0.023$). The p-value to accept AEW count as an additional predictor in the stepwise model is $p = 0.015$, which demonstrates that AEW count provides a statistically significant improvement over relative humidity alone.

6.3 Summary

In this chapter, the annual climatological AEW count and the large-scale environment are successfully manipulated far beyond climatological variation through the

alteration of African albedo. Somewhat surprisingly, the model is not very sensitive to the gradient in surface albedo found between the Sahara and the rainforest to its south, as a simulation with a uniform surface albedo of 30% over Africa produces results very similar to the control simulation with realistic albedo. However, there are strong sensitivities to the magnitude of the uniform albedo. These sensitivities are exploited to produce novel regimes and determine to what extent changes in TC count between these regimes might be attributed to changes in AEW count.

The suite of four uniform albedo simulations generally exhibit increased AEW activity and increased environmental favorability with increasing albedo. The changes to the large-scale environment are similar to what is expected when transitioning from a "wet mode" to a "dry mode" over western Africa. Although somewhat speculative, it seems that anomalous cooling, caused by greater reflectance of insolation in the northern hemisphere, shifts the ITCZ southward due to the return flow of the anomalous Hadley circulation, leading the AEJ to also shift southward and strengthen, producing more AEWs.

Although there are only four simulations in the uniform albedo suite, there is a statistically significant linear relationship between AEW count and TC count. However, there is also a statistically significant relationship between measures of environmental favorability and TC count, including GPI, relative humidity, vertical wind shear, and potential intensity. While GPI is commonly used as an indicator of favorability, e.g., in Caron and Jones (2011), it is an imperfect measure and there might be other environmental factors at play that could be forcing AEWs and TCs to covary. It is also possible that some of the measures of environmental favorability could be contaminated by TCs or AEWs themselves and this could account for a portion of the covariance, but through detrending and through stepwise linear regression, AEW count still shows additional skill over the metrics used here to diagnose the large-scale environment.

Chapter 7

Considering All Modeled Results Holistically

The relationship between AEWs and TCs in HiRAM is probed in various ways in Chapters 4 through 6, on multiple timescales and using a variety tools to isolate the importance of the AEW activity and separate it from the effects of the large-scale favorability on TC activity. Chapter 4 examines the climatological simulations, comparing the interannual relationship between AEW count and TC count in the model to the historical relationship determined in Chapter 3 from NCEP-NCAR II Reanalysis and IBTrACS, using ENSO phase and annual trends as a lens into interannual changes in the large-scale environment historically. In Chapter 5, the internal variability in the AEW-TC relationship is isolated by considering the interannual variation in the perturbation from the climatological ensemble mean, and analyzing control and perpetual La Niña simulations with interannually invariant SSTs. Finally, in Chapter 6 the relationship between AEW count and TC count is considered on a climatological rather than interannual timescale, using GPI and its components as indicators of the large-scale favorability in climates drastically different from the present.

All of the simulations discussed throughout Chapters 4 through 6 are considered together here, including all experiments: the climatological simulations (H1, H2, and H3), the control and perpetual La Niña simulations, and the four uniform albedo

simulations. This is done to both show consistency between and to extend the results from the preceding chapters. First, the relationship between AEW count and TC count is considered interannually, as totals from every model year are examined (Section 7.1). Next, this relationship is considered climatologically, as average annual counts from each simulation are examined (Section 7.2). Following this comprehensive assessment of the model results, the major findings are summarized briefly in Section 7.3.

7.1 The Interannual Relationship between AEW and TC Count

While each individual simulation does reveal statistically significant positive interannual correlation between AEW count and TC count, the associated lines of best fit are not well-constrained due to relatively small sample sizes, since the simulations discussed in Chapters 4 through 6 were either 20 or 28 years long and exhibit marked interannual variability. Section 5.1.2 is an exception, since there were 84 model years pooled together, as perturbations from the climatological ensemble mean were considered to evaluate the stochastic component of AEW activity. In general, the correlation coefficient between AEW count and TC count is consistently positive with 90% or greater confidence for each individual simulation, but the slope and intercept of the line of best fit varies drastically between simulations. For this reason, all model years are pooled across simulations here, to better quantify and constrain the interannual relationship between AEW and TC count.

In Section 4.4 and 4.5, it is apparent that ENSO phase as diagnosed by SST anomalies (see Appendix B) correlates with TC activity on interannual timescales in the climatological simulations, but all additional model runs (the control simulation, the perpetual La Niña simulation, and the uniform albedo simulations) have

climatologically invariant SSTs, and therefore ENSO cannot be used as an indicator of interannual variability of large-scale favorability for these simulations. Section 6.2 indicates that relative humidity in the mid-troposphere is a useful measure of climatological large-scale favorability in drastically different climates, but as Bruyère et al. (2012) show, GPI and relative humidity do not correlate well with TC activity interannually and thus may not adequately represent environmental favorability on these timescales.

In the absence of a convincing interannual measure of environmental favorability across all suites of simulations, the relationship between AEW count and TC count is considered here, without explicitly regressing out the effects of ENSO, GPI, or otherwise accounting for potential large-scale influences. This differs from Section 5.1.2, where the variance is explicitly separated into the part due to environmental variability and the stochastic component in the climatological ensemble. Figure 7.1 includes the annual (ASO) TC count versus the annual AEW count for every model year of every simulation, for a total of N = 204 model years.

Although the various simulations do not all share similar large-scale environments, the correlation between annual TC and AEW count across simulations is extremely significant, with $R^2 = 0.395$ and $p = 8.5 \times 10^{-24}$ (see Figure 7.1). In other words, about 40% of the variance in annual TC count in HiRAM simulations is explained by annual AEW count variability, although a portion of this is associated with changes in large-scale variability that affect both AEW and TC count (see Section 5.1.2). Least squares regression returns the following line of best fit:

$$\mathrm{TC} = 1.60 + 0.51 \cdot \mathrm{AEW}, \tag{7.1}$$

where TC is the annual number of TCs, and AEW is the annual number of AEWs in August through October.

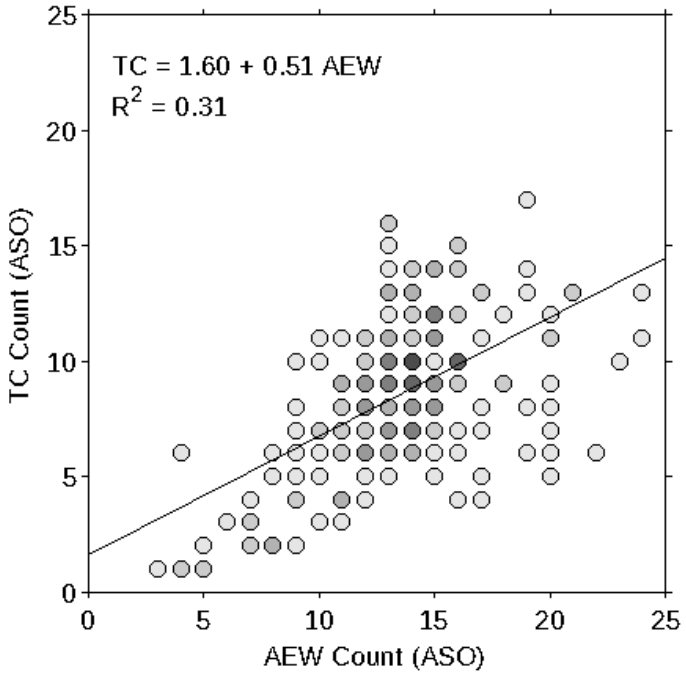

Figure 7.1: Scatterplot of annual August through October TC count versus AEW count, for every model year of every simulation discussed in any of the previous chapters, including the climatological simulations (H1, H2, and H3), the control simulation, the perpetual La Niña simulation, and the uniform albedo simulations (uniform albedo 1, 2, 3, and 4), for a total of 204 model years. The shading of the dots indicates the number of years with the given number of TCs and AEWs, ranging from one (light gray) to nine (black), with line of best fit plotted in black.

AEWs are not completely absent in any model year, but Equation 7.1 implies that if there were no AEWs in the model, there would be an average of 1.60 TCs annually. Further, for each additional AEW, there would be an average of 0.51 additional TCs annually, due to a combination of the stochastic variability in AEW count itself and covariation of AEW and TC counts forced by the environment. The analysis in Section 5.1.2 reveals that each AEW above and beyond the average number, purportedly determined by the large-scale environment, has approximately a 1 in 4 chance of developing into a TC. Applying this finding to the present analysis suggests that about half of the influence of AEW count on TC count is mediated by environmental

favorability (0.51-0.25=0.26), while the other half may be due to stochastic AEW variance.

Applying Equation 7.1 to "predict" climatological TC counts given climatological AEW counts compares favorably with the climatological simulation average TC counts and the reanalysis-derived historical record. With the average number of AEWs varying annually between 13.32 and 14.14 for the three climatological ensemble members, using Equation 7.1, one would expect between 8.39 and 8.81 TCs per year. This is within the error bars of the climatological ensemble members' annual TC counts, for which there are actually between 9.07 and 9.36 TCs, and interannual variability results in a 95% confidence interval of ± 0.90 (see Figure 4.2). Although Equation 7.1 provides a reasonable fit for climatologically average AEW and TC counts in simulations with climates similar to the present day, this relationship breaks down when applied to the perpetual La Niña and the highest uniform albedo simulation on a climatological timescale. This is likely because the changes to the large-scale environment are more drastic in these cases, and thus the influence of environmental favorability is more important than the interannual relationship between AEW and TC count.

Like Figure 7.1, Figure 7.2 also includes the annual (ASO) TC count versus the annual AEW count for every model year of every simulation, but partitioned by TC origin type, with African TC counts in Figure 7.2a and non-African TC counts in Figure7.2b. The lines of best fit for African TC count and non-African TC count versus AEW count are given by:

$$\text{African TC} = 0.12 + 0.45 \cdot \text{AEW}, \text{ and} \tag{7.2}$$

$$\text{Non-African TC} = 1.48 + 0.06 \cdot \text{AEW}, \tag{7.3}$$

where African TC is the annual number of TCs that have their origins in AEWs, Non-African TC is the annual number of TCs that do not have African origins of any kind, and AEW is the annual number of AEWs in August through October.

Annual non-African TC count is only very weakly correlated with AEW count, with a coefficient of determination of $R^2 < 0.02$, which is significantly positive at the 90% but not 95% confidence level, with $p = 0.059$. The shallow slope evident in Figure 7.2b and Equation 7.3 (for every additional AEW, one would only expect an average of 0.06 additional non-African TCs annually), demonstrates that AEW variability has little net influence on the number of TCs without African origins. There are a number of possible competing factors at play, including environmental favorability and trade-offs with African TC development. However, there is no correlation between non-African TC count and African TC count interannually across simulations ($R = -0.01$, $p = 0.78$).

Elevated AEW activity could potentially increase the total number of TCs, while also decreasing the fraction or number of TCs that do not have African origins. Although not ubiquitously (the perpetual La Niña simulation being a potential exception), increased environmental favorability is typically associated with an increase in the climatologically average level of AEW activity across simulations, so one might expect a significant positive relationship between AEW counts and any subset of TC counts, mediated by large-scale conditions. On the other hand, the impacts of changing AEW activity and environmental favorability on TC formation are not spatially uniform, as shown in Figure 6.8. In Kossin and Vimont (2007), shifts in cyclogenesis regions are shown to affect the overall number of storms. This is likely due to differences in the local environments as well as proximity to suitable seeds, such as AEWs. As is clear from Figure 4.8, African and non-African TC origin points are not concentrated in the same areas and thus are not necessarily responding to the same

(a) African TCs v. AEWs

(b) Non-African TCs v. AEWs

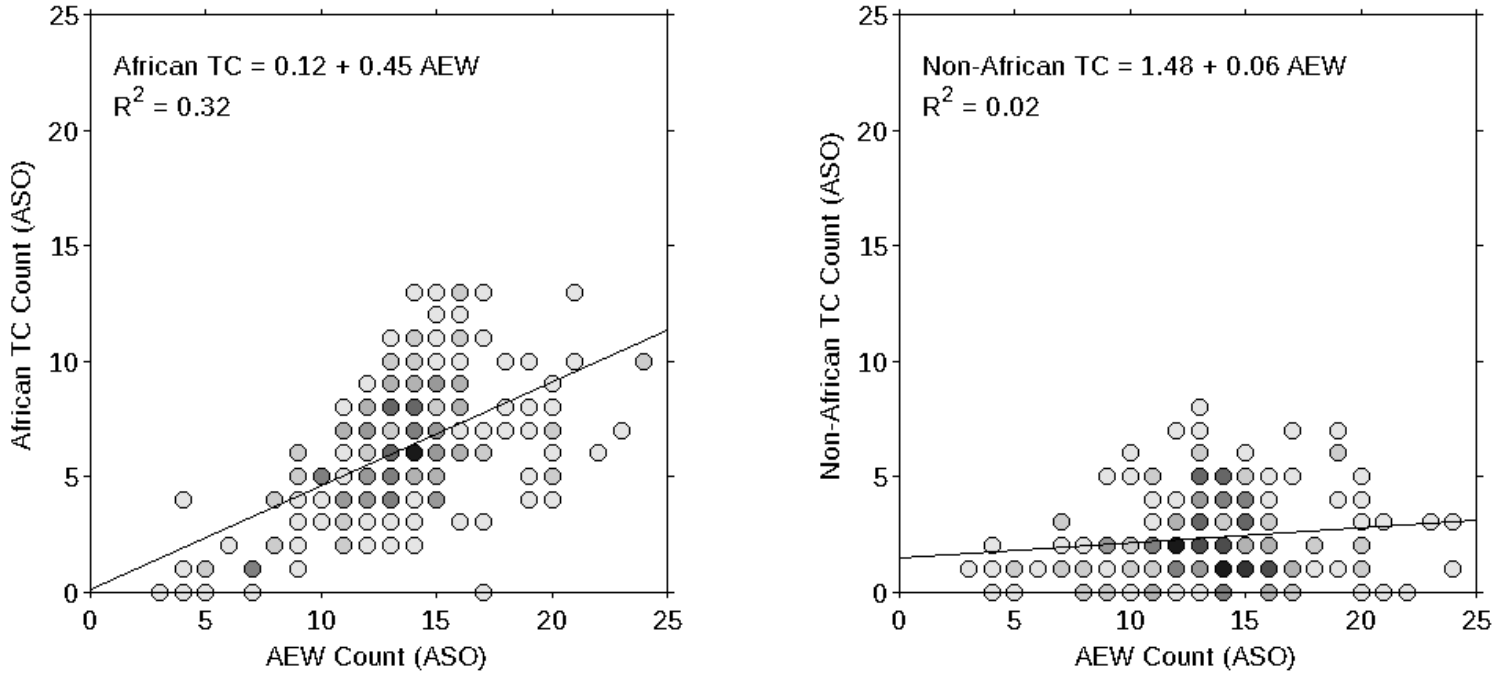

Figure 7.2: Scatterplot of annual August through October (a) African TC count versus AEW count, and (b) Non-African TC count versus AEW count, for every model year of every simulation discussed in any of the previous chapters, including the climatological simulations (H1, H2, and H3), the control simulation, the perpetual La Niña simulation, and the uniform albedo simulations (uniform albedo 1, 2, 3, and 4), for a total of 204 model years. The shading of the dots indicates the number of years with the given number of TCs and AEWs, ranging from one (light gray) to nine (black), with lines of best fit plotted in black.

environmental influences, which may contribute to the lack of correlation between the two.

Because all TCs are either African or non-African, the slopes and intercepts of the lines of best fit for African TC count versus AEW count (Equation 7.2) and non-African TC count versus AEW count (Equation 7.3) sum to that for the total TC count versus AEW count (Equation 7.1). As evident in Equations 7.2 and 7.3, the vast majority of the increase in TC count associated with increasing AEW count can be attributed to storms that have African origins.

7.2 The Climatological Relationship between AEW and TC Count

The major results originally described in Section 6.2.3 are applied here to assess whether the findings from the uniform albedo suite explain the climatological average AEW and TC counts in all of the simulations explored in Chapters 4 through 6. Figure 7.3 shows the average annual (ASO) TC count versus the average annual AEW count for each simulation, including error bars denoting 95% confidence intervals on both counts, which give an indication of the level of interannual variability within each simulation.

Unfortunately, pooling all of the simulations together in this fashion does not provide new insight above and beyond the conclusions drawn from the uniform albedo simulations alone in Chapter 6, because there is strong overlap in the AEW and TC count error bars for the climatological simulations, the control simulation, the perpetual La Niña simulation, and two of the uniform albedo simulations (See Figure 7.3). The multiple linear regression in Section 6.2.3 yields the following model:

$$\mathrm{TC} = 4.13 + 0.80 \cdot (\mathrm{RH} - \mathrm{RH_c}) + 0.56 \cdot \mathrm{AEW}, \tag{7.4}$$

where TC is the average annual number of TCs in August through October, RH is the basin-wide climatologically average August through October relative humidity at 600 mb in percent, RH_c is RH for the control simulation, and AEW is the average annual number of AEWs in August through October.

Even though constructed using only the uniform albedo simulations, Equation 7.4 provides a good fit for the climatologically average counts in all simulations. The TC counts predicted by Equation 7.4 exhibit strong correlation with the actual TC counts in the simulations, with $R^2 = 0.933$ and $p = 1.7 \times 10^{-3}$. Although it is clear that environmental favorability, as communicated through relative humidity, plays an important role in determining average TC count in HiRAM, the direct relationship between AEW count and TC count itself in Figure 7.3 is striking. Correlating the climatologically average TC counts and the AEW counts across simulations yields a coefficient of determination of $R^2 = 0.918$ ($p = 2.6 \times 10^{-3}$).

Equation 7.4 implies that if relative humidity is the same as in the control simulation and there are no AEWs, there would still be an average of 4.13 TCs per year. This is greater than the corresponding value from the interannual regression (the intercept of Equation 7.1), perhaps due to the implicit connection between AEW count and relative humidity. If Atlantic relative humidity and AEW count are linked to some degree, it would be unlikely to have zero AEWs without a corresponding decrease in relative humidity. This would lead to fewer than 4.13 TCs per year in the limiting case with zero AEWs. While this interpretation may strengthen the argument that AEW count and relative humidity covary, this does not imply that the AEW-TC relationship is necessarily fully determined by environmental favorability. As discussed in Sections 6.2.2 and 6.2.3, AEW count does indeed provide additional information beyond the large-scale environment as diagnosed by Atlantic basin relative humidity.

All else equal, Equation 7.4 also implies that the number of additional TCs expected for a climate with an average increase of one AEW per year is 0.56. This

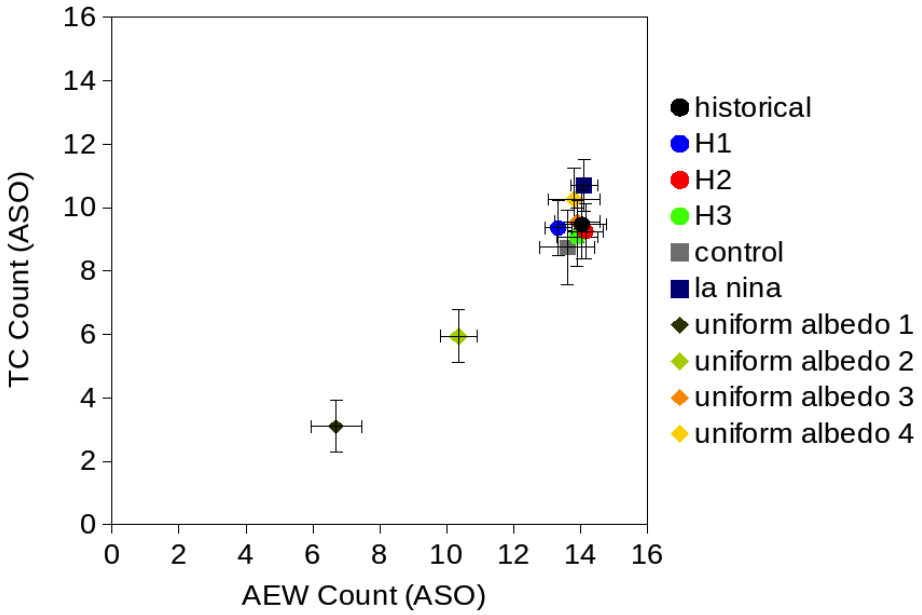

Figure 7.3: Scatterpot of climatologically average annual August through October TC count versus AEW count for the reanalysis-derived historical record and for each of the simulations discussed in any of the previous chapters, including the climatological simulations (H1, H2, and H3), the control simulation, the perpetual La Niña simulation, and the uniform albedo simulations (uniform albedo 1, 2, 3, and 4). Error bars denote 95% confidence intervals.

compares well with the results from the interannual analysis in Section 7.1, in which Equation 7.1 implies that there would be an average of 0.51 additional TCs annually for each additional AEW. In both cases, a portion of this number is likely mediated by changes in environmental favorability, but as argued in Section 7.1 using the analysis from Section 5.1.2, as much as half of the influence of AEW count on TC count may be due to stochastic AEW variance.

7.3 Summary

In this chapter, the simulations examined in Chapters 4 through 6 are considered together as a comprehensive unit, showing consistency between simulations and extending key results discussed in earlier chapters. Count totals from every model year

are examined to quantify the interannual relationship between AEW count and TC count, and climatological averages from each simulation are examined to quantify the contribution of relative humidity and AEW count in determining average TC count.

Without correcting for the effects of the environmental favorability, on average 1 in 2 AEWs contribute an additional TC annually across simulations, due to a combination of stochastic interannual variability in AEW count itself and the covariation between AEW and TC count forced by the environment. Considering this together with the result from Section 5.1.2, that each AEW above and beyond the number determined by the large-scale environment has a 1 in 4 chance of developing into a TC in the climatological simulations, suggests that about half of the influence of AEW count on TC count is mediated by environmental favorability and half is due to stochastic AEW variability in the model. Further, almost all of the net change in TC count associated with AEW count changes can be attributed to storms that have African origins. AEW variance has very little net effect on the number of storms that do not have origins associated with AEWs.

The result originally described in Section 6.2.3, the multiple linear regression model of TC count with relative humidity and AEW count serving as predictors for the uniform albedo simulations, shows skill when applied to the climatologically average AEW and TC counts across simulations. Unfortunately, the addition of the climatological, control, and perpetual La Niña simulations does not provide new insight above and beyond the original result, since there is strong overlap in AEW and TC count error bars. Comparing this climatological model (Equation 7.4) to the interannual model (Equation 7.1) provides further evidence that AEW count and relative humidity covary, but that AEW count provides additional skill over basin-wide average relative humidity in predicting climatologically average TC count.

Chapter 8

Conclusion

The major findings of this study are summarized briefly in Section 8.1, followed by possible directions for future work in Section 8.2. It is argued that the evidence presented strongly supports the notion that not only does African easterly wave (AEW) activity exhibit variance on interannual and climatological timescales that is correlated with Atlantic tropical storm (TC) activity variance, but the relevance of AEW count to TC count is not exclusively determined by large-scale environmental factors.

8.1 Summary

After reviewing the state of the field and motivating the study of the relationship between AEW and TC variability in Chapter 1, novel analysis techniques were designed, tested, and justified in Chapter 2, based on the current literature. The historical AEW record was then revisited, applying these analysis techniques to NCEP-NCAR II reanalysis in Chapter 3, comparing updated AEW counts with past studies and examining potential explanations for differences. In Chapter 4, this newly-developed historical record was used to legitimize the Geophysical Fluid Dynamic Laboratory's (GFDL's) High Resolution Atmospheric Model (HiRAM) for the study of the relationship between AEWs and TCs, comparing an ensemble of three climatological simulations to the historical record.

The model was then used to isolate the internal variability of AEW activity in Chapter 5, both by taking advantage of the multiple historical realizations produced by the climatological suite of simulations and by examining additional simulations forced by interannually invariant prescribed sea surface temperature (SST), including a control simulation with climatologically average SSTs and a perpetual La Niña simulation with composite SSTs from strong La Niña years (see Appendix B). In Chapter 6, the large-scale environment was drastically altered through the manipulation of African albedo, and the resulting climatologies were examined to disentangle the effects of environmental favorability and AEW activity levels on TC activity. Finally, the results from the various simulations were analyzed comprehensively in Chapter 7, on both interannual and climatological timescales. The key results pertaining to the relationship between AEWs and Atlantic TCs from Chapters 3 through 7 are highlighted and synthesized here.

The AEW historical record produced with the current methodology as applied to NCEP-NCAR II reanalysis does not exhibit statistically significant correlation with any past studies of the interannual variability of AEW count and its potential relationship with TC count (Avila et al., 2000; Thorncroft and Hodges, 2001; Hopsch et al., 2007). This is not surprising, as none of the past studies correlate with each other. Upon further scrutiny, these past studies do not agree on total annual AEW count, the degree of AEW variability, or the relationship between AEW and TC counts. The methodology employed in the present study is more robust than in past studies, in that the present techniques are designed to target and count relevant AEWs that originate over Africa and make it to the MDR. This methodology also links individual AEWs and TCs, strengthening the argument that there is a causal relationship between AEW and TC count, rather than simply a similar degree of variance in two independent fields giving the illusion of a relationship. It is heartening that the reanalysis-derived historical record developed with the novel analysis

techniques employed here shows good agreement with the seasonal cycle and spectral statistics of AEW activity put forth in past studies and with modeled-derived AEW activity in climatological HiRAM simulations.

The historical AEW count record derived from NCEP-NCAR II reanalysis exhibits marked interannual variability and statistically significant correlation with TC count. Although such a relationship between AEWs and TCs has been suggested by others in the literature (e.g., Thorncroft and Hodges, 2001), this is the first rigorous quantitative evidence of such a linkage. The correlation between AEW and TC count is slightly weaker in the model-derived than in the reanalysis-derived historical record, but is still significant. When minimizing the confounding influence of environmental favorability by subtracting the effects attributed to ENSO phase and annual trend from the counts, the AEW residuals explain a statistically significant amount of the TC residual interannual variability, namely, 10% in the climatological simulations and 40% in the reanalysis-derived historical record.

The climatological ensemble of HiRAM simulations shows reasonable agreement with the reanalysis-derived AEW record overall, producing average annual AEW and TC counts that are indistinguishable from the historical record. The ensemble average model-derived AEW counts covary with the reanalysis-derived historical counts interannually, but the individual ensemble members do not exhibit statistically significant correlation with reanalysis-derived historical AEW variability. On the other hand, both ensemble average and the individual ensemble member model-derived TC counts correlate well with the reanalysis-derived historical TC counts. This implies that AEW activity is at least partially determined by the prescribed SST, but to a lesser extent than TC activity, so a significant portion of the AEW variability is independent of the large-scale forcing.

Since ensemble averaging helps isolate the effects of the large-scale forcing, the interannual variability of the model-derived historical AEW and TC counts may be

separated into environmental fluctuations (the ensemble mean) and stochastic variability (the perturbation from the ensemble mean). These perturbation AEW and TC counts are well-correlated interannually for the climatological ensemble members. Although much of the TC variability is constrained by the favorability of the large-scale conditions, this supports the idea that variability in AEW count may explain the component of the TC variability that remains unexplained by known environmental factors. Specifically, a linear regression model of perturbation TC count reveals that an average of one in four additional AEWs, above and beyond the average determined by environmental factors, contributes an additional TC.

Another way to examine the importance of AEW variability above and beyond that determined by the large-scale favorability is by examining simulations forced by interannually invariant SSTs. In these cases, there simply is no interannual variability in the forcing, minimizing the associated variation of the large-scale environment. Both a control and a perpetual La Niña simulation with seasonally varying but interannually invariant forcing exhibit covariance between AEW and TC counts on interannual scales, demonstrating that there is significant internal variability in AEW activity in the atmosphere, and that this internal AEW variability has relevance to TC variability beyond the covariance in both due to large-scale forcing as communicated through the prescribed SSTs.

Although AEW count and TC count covary interannually to a degree beyond what would be expected due to environmental forcing alone, the large-scale environment can be more important than the number of AEWs in determining the climatologically average number of TCs that form annually, as evidenced by the control and the perpetual La Niña simulations. These two simulations have statistically significantly different climatologically average TC count, despite having statistically indistinguishable average AEW counts. This increase in TC activity is associated with an increase

in the genesis potential index (GPI; Emanuel and Nolan, 2004) in the Atlantic due to La Niña.

This interplay between large-scale favorability and AEW activity level in determining the climatologically average TC count is examined further through a suite of four simulations with prescribed uniform albedo over Africa. Through the alteration of the magnitude of the uniform African albedo, the environmental favorability and AEW activity is varied significantly beyond the range naturally occurring in the current climate on interannual scales. Both the large-scale favorability as determined by GPI and the AEW count generally increase with increasing albedo, as the model exhibits behavior similar to that expected in a transition from a "wet mode" to a "dry mode" over western Africa. There is a statistically significant relationship between both GPI and climatological TC count, as well as climatological AEW count and TC count in the uniform albedo simulations. Statistical tests show that AEW count demonstrates additional skill over, and is not simply responding to, the environmental changes that also affect TC count, as communicated by GPI and its components, absolute vorticity, relative humidity, potential intensity, and vertical wind shear.

Across both the reanalysis-derived historical record and all model simulations, there is a statistically significant correlation between AEW count and TC count. Considering AEW and TC count totals from every model year across all simulations, without correcting for the effects of differences in large-scale favorability, an average of approximately 1 in 2 AEWs contribute an additional TC annually. This effect can be partitioned into the part due to the covariation between AEW and TC count that is forced by the environment, and the stochastic variability of AEW count itself. Since the latter accounts for approximately 1 in 4 AEWs contributing an additional TC annually, it seems that about half of the influence of AEW count on TC count stems from covariation due to environmental favorability, and half due to internal AEW variability.

Given the results of interannual and climatological detrending, multiple linear regression models, and ensemble averaging, it is unlikely that the relationship between AEW count and TC count is simply controlled by the large-scale environmental favorability. AEWs seem to play an active role in determining TC count, as the internal atmospheric variability in AEW count explains a component of the TC variability unexplained by known indicators of environmental favorability.

8.2 Future Work

The rich datasets developed here to determine whether AEWs influence Atlantic TC activity contain several yet unexplored facets, such as regional impacts on TC genesis, landfall potential, TC strength, and the percent of African TCs. With the principal relationship between AEWs and TCs newly established, these datasets could be applied to address a great number of secondary research questions.

It is argued above that the stochastic component of AEW count provides skill above and beyond what can be easily deduced from the large-scale environmental favorability, both in the reanalysis-derived historical record and in the model, warranting further study of the sources of this AEW variability. Coupled with the results presented here, a better understanding of the physical mechanisms at work in determining AEW activity level would have applications in TC predictability. Analyzing fluctuations in the modeled African Easterly Jet on various timescales, both its strength and location, could be an interesting starting point.

In any study of AEW activity, the length of the observational record is a severely limiting factor, necessitating the use of modeling techniques for some applications. Unfortunately, since the correlation between AEW count and TC count is found to be weaker in HiRAM than in the historical record produced using NCEP-NCAR II and IBTrACS, the model may not capture the full extent of the AEW variability and

the associated TC variability in the real world. If AEWs are resolvable, it would be useful to corroborate and possibly extend the reanalysis-derived historical record produced here, perhaps using the Twentieth Century Reanalysis (20CR) from Compo et al. (2011). The 20CR dataset exclusively assimilates surface-based observations of sea level pressure and temperature (SLP and SST), eliminating the observational biases inherent in upper-level observations and providing a longer record with fewer assimilation discontinuities than contemporary reanalyses. Comparing with the historical record produced here using NCEP-NCAR II, the trade-off in surface-only data assimilation could be evaluated to determine whether 20CR would be a useful tool for studying AEW variability. More generally, it would be productive to compare multiple reanalyses, to better constrain the level of uncertainty in historical AEW variability, establish whether there is an overall trend in AEW count, and evaluate the fidelity of the climatological HiRAM simulations.

As well as applying the present analysis techniques to multiple reanalyses, it would also be telling to use multiple genesis potential indices to corroborate or qualify the conclusions drawn above. Using multiple measures of environmental favorability could strengthen the argument that AEW count does indeed influence TC activity, exhibiting skill above and beyond the state of the large-scale environmental conditions. Systematic study of measures of genesis potential and their constituent components could also provide insight on the potential level of contamination in these metrics, diagnosing the extent to which AEW and TC activity itself might influence measures of the large-scale favorability.

Finally, it would be useful to either use an extended reanalysis-derived historical record or to produce additional simulation years to better ascertain the typical level of AEW activity in La Niña conditions, as well as in El Niño conditions. Although there was no statistically significant difference in AEW count in the simulation forced with composited La Niña SSTs and the simulation forced with climatologically average

SSTs, there may have been a difference that was simply too small to detect. This could have implications for the results presented about the relevance of ENSO phase.

Appendix A

Some Useful Acronyms

The following acronyms are used throughout this dissertation.

AEW	African Easterly Wave
AEJ	African Easterly Jet
AEJ_N	Northern African Easterly Jet (see Figure 1.1)
AEJ_S	Southern African Easterly Jet (see Figure 1.1)
AGCM	Atmospheric General Circulation Model
AM2.1	Atmospheric Model v 2.1 from GFDL (Anderson et al., 2004)
AMIP-II	Atmospheric Model Intercomparison Project
AMMA	African Monsoon Multidisciplinary Analyses
AOS	Atmospheric and Oceanic Sciences
AR5	The Fifth Assessment Report of the IPCC
BRDF	Bidirectional Reflectance Distribution Function
DOE	Department of Energy
ECMWF	European Centre for Medium-Range Weather Forecasts
ENSO	El Niño-Southern Oscillation
EOF	Empirical Orthogonal Functions
ERA-40	European Centre for Medium-Range Weather Forecasts (ECMWF) Reanalysis (Uppala et al., 2005)
ERA-Interim	European Centre for Medium-Range Weather Forecasts (ECMWF) Reanalysis (Dee et al., 2011)
GARP	Global Atmospheric Research Program
GATE	GARP Atlantic Tropical Experiment (Kuettner, 1974)
GCM	General Circulation Model
GFDL	NOAA's Geophysical Fluid Dynamics Laboratory
GPI	Genesis Potential Index (Emanuel and Nolan, 2004)
HadISST	Hadley Centre Global Sea Ice and Sea Surface Temperature Dataset (Rayner et al., 2003)
HEART	Hard Equations and Rational Thinking
HiRAM	High Resolution Atmospheric Model from GFDL

IBTrACS	International Best Track Archive for Climate Stewardship (Knapp et al., 2010)
IPCC	Intergovernmental Panel on Climate Change
ITCZ	Intertropical Convergence Zone
MDR	Main Development Region
MJO	Madden-Julian Oscillation
MODIS	MODerate Resolution Imaging Spectroradiometer
MPI	Maximum Potential Intensity (Bister and Emanuel, 2002)
NAMMA	National Aeronautics and Space Administration (NASA) African Monsoon Multidisciplinary Analyses (AMMA) (Zipser et al., 2009)
NASA	National Aeronautics and Space Administration
NCAR	National Center for Atmospheric Research
NCEP	National Centers for Environmental Prediction
NCEP-NCAR I	National Centers for Environmental Prediction (NCEP)-National Center for Atmospheric Research (NCAR) Reanalysis (Kalnay et al., 1996)
NCEP-NCAR II	National Centers for Environmental Prediction (NCEP)-Department of Energy (DOE) Atmospheric Model Intercomparison Project (AMIP II) Reanalysis (Kanamitsu et al., 2002)
NOAA	National Oceanic and Atmospheric Administration
OLR	Outgoing Longwave Radiation
ONI	Oceanic Niño Index (NOAA/NWS Cold and Warm Episodes by Season, 2014)
SAL	Saharan Air Layer
SST	Sea Surface Temperature
TC	Tropical Cyclone; all intensities of cyclones detected by the tracking algorithm are included (see Section 2.2.2), and are referred to interchangeably as "tropical storms" and "TCs," regardless of strength
TEJ	Tropical Easterly Jet
WAWJ	West African Westerly Jet

Appendix B

ENSO Classification

The Oceanic Niño Index (ONI) consists of a three-month running average of SST anomalies in the region from 5°S to 5°N and 120°W to 170°W (NOAA/NWS Cold and Warm Episodes by Season, 2014). ONI is used to classify years by ENSO phase throughout this dissertation and is partially reproduced here. Relevant ONI values for June through August (JJA), July through September (JAS), August through October (ASO), and September through November (SON) are shown below, along with the average of these four values (JJASON Average), for the years 1967 through 2012 (although no individual simulation or historical study spans the entire period).

Years from historical simulations and past studies are classified based on the JJASON Average; years in which the JJASON Average is greater than 0.5 are considered El Niño years (e.g., 1982, 1986, 1987, 1991, 1994, 1997, 2002, 2004, 2006, 2009); years in which the JJASON Average is less than -0.5 are considered La Niña years (e.g., 1985, 1988, 1995, 1998, 1999, 2000, 2007, 2010, 2011). The JJASON Average is also used for multiple regressions that include ENSO phase as a predictor (e.g., Sections 3.2.4 and 4.5).

The La Niña composite for the perpetual La Niña simulation (see Section 2.1.2 and Chapter 5) was produced from years after 1982 for which the ONI index for both JAS and ASO is less than -0.5 (i.e., 1985, 1988, 1998, 1999, and 2000). This

was finalized before this version of ONI and the associated JJASON averages were considered, but is compatible with the definitions given here.

Year	JJA	JAS	ASO	SON	JJASON Average	ENSO Phase
1967	0.1	-0.1	-0.3	-0.3	-0.2	
1968	0.4	0.5	0.5	0.6	0.5	El Niño
1969	0.5	0.5	0.8	0.9	0.7	El Niño
1970	-0.5	-0.7	-0.7	-0.7	-0.7	La Niña
1971	-0.7	-0.7	-0.7	-0.8	-0.7	La Niña
1972	1.1	1.4	1.6	1.9	1.5	El Niño
1973	-1.0	-1.2	-1.3	-1.6	-1.3	La Niña
1974	-0.5	-0.4	-0.4	-0.6	-0.5	La Niña
1975	-1.1	-1.2	-1.4	-1.5	-1.3	La Niña
1976	0.2	0.4	0.6	0.7	0.5	El Niño
1977	0.4	0.4	0.4	0.7	0.5	El Niño
1978	-0.3	-0.4	-0.4	-0.3	-0.4	
1979	0.0	0.2	0.3	0.5	0.3	
1980	0.3	0.1	-0.1	0.0	0.1	
1981	-0.4	-0.4	-0.3	-0.2	-0.3	
1982	0.7	1.0	1.5	1.9	1.3	El Niño
1983	0.2	-0.2	-0.5	-0.8	-0.3	
1984	-0.3	-0.2	-0.3	-0.6	-0.4	
1985	-0.5	-0.5	-0.5	-0.4	-0.5	La Niña
1986	0.3	0.5	0.7	0.9	0.6	El Niño
1987	1.4	1.6	1.6	1.5	1.5	El Niño
1988	-1.3	-1.2	-1.3	-1.6	-1.4	La Niña
1989	-0.3	-0.3	-0.3	-0.3	-0.3	
1990	0.3	0.3	0.4	0.3	0.3	
1991	0.8	0.7	0.7	0.8	0.8	El Niño
1992	0.3	0.0	-0.2	-0.3	-0.1	
1993	0.3	0.2	0.2	0.2	0.2	
1994	0.4	0.4	0.5	0.7	0.5	El Niño
1995	-0.2	-0.4	-0.7	-0.8	-0.5	La Niña
1996	-0.2	-0.3	-0.3	-0.3	-0.3	
1997	1.5	1.8	2.1	2.3	1.9	El Niño
1998	-0.7	-1.0	-1.2	-1.3	-1.1	La Niña
1999	-1.0	-1.1	-1.1	-1.3	-1.1	La Niña
2000	-0.6	-0.5	-0.6	-0.6	-0.6	La Niña
2001	0.0	0.0	-0.1	-0.2	-0.1	
2002	0.8	0.8	0.9	1.2	0.9	El Niño
2003	0.2	0.4	0.4	0.4	0.4	

Year	JJA	JAS	ASO	SON	JJASON Average	ENSO Phase
2004	0.5	0.7	0.8	0.7	0.7	El Niño
2005	0.2	0.1	0.0	-0.2	0.0	
2006	0.2	0.3	0.5	0.8	0.5	El Niño
2007	-0.4	-0.6	-0.8	-1.1	-0.7	La Niña
2008	-0.3	-0.2	-0.1	-0.2	-0.2	
2009	0.5	0.6	0.8	1.1	0.8	El Niño
2010	-0.9	-1.2	-1.4	-1.5	-1.3	La Niña
2011	-0.2	-0.4	-0.6	-0.8	-0.5	La Niña
2012	0.1	0.4	0.5	0.6	0.4	

Bibliography

Agudelo, P. A., C. D. Hoyos, J. A. Curry, and P. J. Webster, 2011: Probabilistic discrimination between large-scale environments of intensifying and decaying African Easterly Waves. *Clim. Dynam.*, **36**, 1379–1401. [3, 5, 11, 38, 39, 41, 76, 87, 91]

Aiyyer, A. R. and C. Thorncroft, 2006: Climatology of vertical wind shear over the tropical Atlantic. *J. Climate*, **19**, 2969–2983. [3, 15]

Albignat, J. P. and R. J. Reed, 1980: The origin of African wave disturbances during Phase III of GATE. *Mon. Wea. Rev.*, **108**, 1827–1839. [3, 4, 7, 9, 38, 78, 87, 94]

Anderson, J. et al., 2004: The new GFDL global atmosphere and land model AM2/LM2: Evaluation with prescribed SST simulations. *J. Climate*, **17**, 4641–4673. [30, 176]

Avila, L. A. and G. B. Clark, 1989: Atlantic tropical systems of 1988. *Mon. Wea. Rev.*, **117**, 2260–2265. [3, 6, 13, 38, 64, 65]

Avila, L. A. and R. J. Pasch, 1992: Atlantic tropical systems of 1991. *Mon. Wea. Rev.*, **120**, 2688–2696. [3, 13, 64]

Avila, L. A., R. J. Pasch, and J. G. Jiing, 2000: Atlantic tropical systems of 1996 and 1997: Years of contrasts. *Mon. Wea. Rev.*, **128**, 3695–3706. [1, 2, 3, 6, 13, 38, 39, 62, 63, 64, 65, 66, 72, 73, 75, 78, 79, 80, 81, 83, 84, 86, 87, 88, 169]

Bain, C. L., D. J. Parker, N. Dixon, A. H. Fink, C. M. Taylor, B. Brooks, and S. F. Milton, 2011: Anatomy of an observed African easterly wave in July 2006. *Quart. J. Roy. Meteor. Soc.*, **137**, 923–933. [3, 38]

Bain, C. L., K. D. Williams, S. F. Milton, and J. T. Heming, 2014: Objective tracking of African Easterly Waves in Met Office models. *Quart. J. Roy. Meteor. Soc.*, **140**, 47–57. [38, 39, 40]

Belanger, J. I., J. A. Curry, and P. J. Webster, 2010: Predictability of North Atlantic tropical cyclone activity on intraseasonal time scales. *Mon. Wea. Rev.*, **138**, 4362–4374. [2, 16]

Bender, M., I. Ginis, and Y. Kurihara, 1993: Numerical simulations of tropical cyclone-ocean interaction with a high-resolution coupled model. *J. Geophys. Res.*, **98**, 23,245–23,263. [17, 18]

Bengtsson, L., K. Hodges, and M. Esch, 2007a: Tropical cyclones in a T159 resolution global climate model: comparison with observations and re-analyses. *Tellus A*, **59**, 396–416. [17, 18]

Bengtsson, L., K. I. Hodges, M. Esch, N. Keenlyside, L. Kornblueh, J. Luo, and T. Yamagata, 2007b: How may tropical cyclones change in a warmer climate? *Tellus A*, **59**, 539–561. [17, 18]

Berry, G. J. and C. Thorncroft, 2005: Case study of an intense African easterly wave. *Mon. Wea. Rev.*, **133**, 752–766. [3, 5, 10]

Bister, M. and K. A. Emanuel, 2002: Low frequency variability of tropical cyclone potential intensity. 1. Interannual to interdecadal variability. *J. Geophys. Res.*, **107**, 4801. [99, 177]

Briegleb, B. P., P. Minnis, V. Ramanathan, and E. Harrison, 1986: Comparison of regional clear-sky albedos inferred from satellite observations and model computations. *J. Climate Appl. Meteor.*, **25**, 214–226. [29]

Broccoli, A. J., K. A. Dahl, and R. J. Stouffer, 2006: Response of the ITCZ to Northern Hemisphere cooling. *Geophys. Res. Lett.*, **33**, L01 702. [146]

Bruyère, C. L., G. J. Holland, and E. Towler, 2012: Investigating the use of a genesis potential index for tropical cyclones in the North Atlantic basin. *J. Climate*, **25**, 8611–8626. [37, 53, 54, 55, 159]

Burpee, R. W., 1972: The origin and structure of easterly waves in the lower troposphere of North Africa. *J. Atmos. Sci.*, **29**, 77–90. [3, 4, 6, 7, 8, 38, 96]

Burpee, R. W., 1974: Characteristics of North African easterly waves during the summers of 1968 and 1969. *J. Atmos. Sci.*, **31**, 1556–1570. [3, 4, 7, 38]

Bye, J. and K. Keay, 2008: A new hurricane index for the Caribbean. *Interciencia*, **33**, 556–560. [52]

Camargo, S. J., K. A. Emanuel, and A. H. Sobel, 2007a: Use of a genesis potential index to diagnose ENSO effects on tropical cyclone genesis. *J. Climate*, **20**, 4819–4834. [37, 52, 53, 121]

Camargo, S. J., A. H. Sobel, A. G. Barnston, and K. A. Emanuel, 2007b: Tropical cyclone genesis potential index in climate models. *Tellus A*, **59**, 428–443. [37, 52, 53]

Camargo, S. J., M. C. Wheeler, and A. H. Sobel, 2009: Diagnosis of the MJO modulation of tropical cyclogenesis using an empirical index. *J. Atmos. Sci.*, **66**, 3061–3074. [37, 53]

Carlson, T. N., 1969a: Synoptic histories of three African disturbances that developed into Atlantic hurricanes. *Mon. Wea. Rev.*, **97**, 256–276. [3, 4, 11, 38]

Carlson, T. N., 1969b: Some remarks on African disturbances and their progress over the tropical Atlantic. *Mon. Wea. Rev.*, **97**, 716–726. [3, 4, 38]

Caron, L. P. and C. G. Jones, 2011: Understanding and simulating the link between African easterly waves and Atlantic tropical cyclones using a regional climate model: the role of domain size and lateral boundary conditions. *Clim. Dynam.*, **39**, 113–135. [2, 13, 14, 17, 53, 54, 125, 156]

Caron, L. P., C. G. Jones, and K. Winger, 2010: Impact of resolution and downscaling technique in simulating recent Atlantic tropical cylone activity. *Clim. Dynam.*, **37**, 869–892. [13, 17, 38]

Chang, C. B., 1993: Impact of desert environment on the genesis of African wave disturbances. *J. Atmos. Sci.*, **50**, 2137–2145. [6]

Charney, J. G., 1975: Dynamics of deserts and drought in the Sahel. *Quart. J. Roy. Meteor. Soc.*, **101**, 193–202. [146]

Charney, J. G. and M. E. Stern, 1962: On the stability of internal baroclinic jets in a rotating atmosphere. *J. Atmos. Sci.*, **19**, 159–172. [6]

Chen, T. C., 2006: Characteristics of African easterly waves depicted by ECMWF reanalyses for 1991-2000. *Mon. Wea. Rev.*, **134**, 3539–3566. [5, 7, 8, 9, 12, 38]

Chen, T. C., S. Y. Wang, and A. J. Clark, 2008: North Atlantic hurricanes contributed by African easterly waves north and south of the African easterly jet. *J. Climate*, **21**, 6767–6776. [7, 12]

Compo, G. P., et al., 2011: The twentieth century reanalysis project. *Quart. J. Roy. Meteor. Soc.*, **137**, 1–28. [174]

Cook, K. H., 1999: Generation of the African easterly jet and its role in determining West African precipitation. *J. Climate*, **12**, 1165–1184. [11, 96]

Dee, D. P., et al., 2011: The ERA-Interim reanalysis: Configuration and performance of the data assimilation system. *Quart. J. Roy. Meteor. Soc.*, **137**, 553–597. [49, 50, 52, 176]

Diedhiou, A., S. Janicot, A. Viltard, P. deFelice, and H. Laurent, 1999: Easterly wave regimes and associated convection over West Africa and tropical Atlantic: results from the NCEP/NCAR and ECMWF reanalyses. *Clim. Dynam.*, **15**, 795–822. [3, 5, 38]

Douville, H., 2005: Limitations of time-slice experiments for predicting regional climate change over South Asia. *Clim. Dynam.*, **24**, 373–391. [18]

Dunion, J. P. and C. S. Velden, 2004: The impact of the Saharan air layer on Atlantic tropical cyclone activity. *Bull. Amer. Meteor. Soc.*, **85**, 353–365. [14]

Duvel, J. P., 1990: Convection over tropical Africa and the Atlantic Ocean during northern summer. Part II: Modulation by easterly waves. *Mon. Wea. Rev.*, **118**, 1855–1868. [3, 5, 9, 38]

Emanuel, K., 2010: Tropical cyclone activity downscaled from NOAA-CIRES reanalysis, 1908–1958. *J. Adv. Model. Earth Syst.*, **2**. [37, 52, 54, 55]

Emanuel, K., 2011: Global warming effects on US hurricane damage. *Wea. Climate Soc.*, **3**, 261–268. [1]

Emanuel, K., R. Sundararajan, and J. Williams, 2008: Hurricanes and global warming. *Bull. Amer. Meteor. Soc.*, **89**, 347–367. [1, 17]

Emanuel, K. A., 1989: The finite-amplitude nature of tropical cyclogenesis. *J. Atmos. Sci.*, **46**, 3431–3456. [12]

Emanuel, K. A., 2014: *MATLAB script for calculating TC maximum intensity*. ftp://texmex.mit.edu/pub/emanuel/TCMAX/, Massachusetts Institute of Technology. [36]

Emanuel, K. A. and D. S. Nolan, 2004: Tropical cyclone activity and the global climate system. *Preprints, 26th Conf. on Hurricanes and Tropical Meteorology, Miami, FL, Amer. Meteor. Soc.* [36, 37, 52, 54, 99, 101, 176]

Fink, A. H. and A. Reiner, 2003: Spatiotemporal variability of the relation between African easterly waves and West African squall lines in 1998 and 1999. *J. Geophys. Res.*, **108**, 4332. [5, 7, 8, 38]

Fink, A. H., J. M. Schrage, and S. Kotthaus, 2010: On the potential causes of the nonstationary correlations between West African precipitation and Atlantic hurricane activity. *J. Climate*, **23**, 5437–5456. [5, 15]

Fink, A. H., D. G. Vincent, P. M. Reiner, and P. Speth, 2004: Mean state and wave disturbances during phases I, II, and III of GATE based on ERA-40. *Mon. Wea. Rev.*, **132**, 1661–1683. [5, 7, 8, 9, 12, 38, 40, 41, 81]

Folland, C. K., T. N. Palmer, and D. E. Parker, 1986: Sahel rainfall and worldwide sea temperatures, 1901–85. *Nature*, **320**, 602–607. [146]

Frank, N. L., 1970: Atlantic tropical systems of 1969. *Mon. Wea. Rev.*, **98**, 307–314. [3]

Frank, W. M. and P. E. Roundy, 2006: The role of tropical waves in tropical cyclogenesis. *Mon. Wea. Rev.*, **134**, 2397–2417. [2, 3, 16, 76, 87, 91]

Garner, S. T., I. M. Held, T. Knutson, and J. Sirutis, 2009: The roles of wind shear and thermal stratification in past and projected changes of Atlantic tropical cyclone activity. *J. Climate*, **22**, 4723–4734. [17, 107]

GFDL Global Atmospheric Model Development Team, 2004: The new GFDL global atmosphere and land model AM2–LM2: Evaluation with prescribed SST simulations. *J. Climate*, **17**, 4641–4673. [31, 33]

Giannini, A., R. Saravanan, and P. Chang, 2003: Oceanic forcing of Sahel rainfall on interannual to interdecadal time scales. *Science*, **302**, 1027–1030. [146]

Gibson, J. K., 1997: ECMWF re-analysis project report series: ERA description. Tech. rep., European Centre for Medium-Range Weather Forecasts. [66, 68]

Goldenberg, S. B., C. W. Landsea, A. M. Mestas-Nuñez, and W. M. Gray, 2001: The recent increase in Atlantic hurricane activity: Causes and implications. *Science*, **293**, 474–479. [2]

Goldenberg, S. B. and L. J. Shapiro, 1996: Physical mechanisms for the association of El Niño and West African rainfall with Atlantic major hurricane activity. *J. Climate*, **9**, 1169–1187. [14]

Gray, W. M., 1979: Hurricanes: Their formation, structure and likely role in the tropical circulation. *Meteorology over the tropical oceans*, **19**, 155–218. [36, 52]

Greenfield, R. S. and J. S. Fein, 1979: The Global Atmospheric Research Program's Atlantic Tropical Experiment. *Reviews of Geophysics*, **17**, 1762–1772. [4]

Grist, J. P. and S. E. Nicholson, 2001: A study of the dynamic factors influencing the rainfall variability in the West African Sahel. *J. Climate*, **14**, 1337–1359. [142]

Grist, J. P., S. E. Nicholson, and A. I. Barcilon, 2002: Easterly waves over Africa. Part II: Observed and modeled contrasts between wet and dry years. *Mon. Wea. Rev.*, **130**, 212–225. [6, 14, 142]

Gualdi, S., E. Scoccimarro, and A. Navarra, 2008: Changes in tropical cyclone activity due to global warming: Results from a high-resolution coupled general circulation model. *J. Climate*, **21**, 5204–5228. [17]

Hall, N. M. J., G. N. Kiladis, and C. D. Thorncroft, 2006: Three-dimensional structure and dynamics of African easterly waves. Part II: Dynamical modes. *J. Atmos. Sci.*, **63**, 2231–2245. [5, 10]

Held, I. M., T. L. Delworth, J. Lu, K. L. Findell, and T. R. Knutson, 2005: Simulation of Sahel drought in the 20th and 21st centuries. *Proc. Natl. Acad. Sci. USA*, **102**, 17 891–17 896. [146]

Held, I. M. and M. Zhao, 2011: The response of tropical cyclone statistics to an increase in CO_2 with fixed sea surface temperatures. *J. Climate*, **24**, 5353–5364. [17, 22, 23]

Hodges, K. I., 1995: Feature tracking on the unit sphere. *Mon. Wea. Rev.*, **123**, 3458–3465. [39]

Hopsch, S. B., C. D. Thorncroft, K. Hodges, and A. Aiyyer, 2007: West African storm tracks and their relationship to Atlantic tropical cyclones. *J. Climate*, **20**, 2468–2483. [2, 5, 6, 7, 12, 15, 16, 38, 55, 62, 66, 67, 68, 69, 70, 71, 72, 73, 74, 75, 76, 78, 80, 81, 86, 87, 88, 91, 169]

Hopsch, S. B., C. D. Thorncroft, and K. R. Tyle, 2010: Analysis of African easterly wave structures and their role in influencing tropical cyclogenesis. *Mon. Wea. Rev.*, **138**, 1399–1419. [3, 5, 11]

Hsieh, J.-S. and K. H. Cook, 2005: Generation of African easterly wave disturbances: Relationship to the African easterly jet. *Mon. Wea. Rev.*, **133**, 1311–1327. [11, 99, 142]

Hsieh, J.-S. and K. H. Cook, 2008: On the instability of the African easterly jet and the generation of African waves: reversals of the potential vorticity gradient. *J. Atmos. Sci.*, **65**, 2130–2151. [10]

Kalnay, E., et al., 1996: The NCEP/NCAR 40-year reanalysis project. *Bull. Amer. Meteor. Soc.*, **77**, 437–471. [29, 37, 49, 177]

Kanamitsu, M., W. Ebisuzaki, J. Woollen, S.-K. Yang, J. Hnilo, M. Fiorino, and G. Potter, 2002: NCEP-DOE AMIP-II reanalysis (R-2). *Bull. Amer. Meteor. Soc.*, **83**, 1631–1643. [29, 49, 50, 52, 90, 99, 177]

Kang, S. M., D. M. W. Frierson, and I. M. Held, 2009: The tropical response to extratropical thermal forcing in an idealized GCM: The importance of radiative feedbacks and convective parameterization. *J. Atmos. Sci.*, **66**, 2812–2827. [146]

Kang, S. M. and I. M. Held, 2012: Tropical precipitation, SSTs and the surface energy budget: a zonally symmetric perspective. *Clim. Dynam.*, **38**, 1917–1924. [146]

Kang, S. M., I. M. Held, D. M. W. Frierson, and M. Zhao, 2008: The response of the ITCZ to extratropical thermal forcing: Idealized slab-ocean experiments with a GCM. *J. Climate*, **21**, 3521–3532. [146]

Kang, S. M., I. M. Held, and S.-P. Xie, 2014: Contrasting the tropical responses to zonally asymmetric extratropical and tropical thermal forcing. *Clim. Dynam.*, **42**, 2033–2043. [146]

Karyampudi, V. M. and T. N. Carlson, 1988: Analysis and numerical simulations of the Saharan air layer and its effect on easterly wave disturbances. *J. Atmos. Sci.*, **45**, 3102–3136. [11]

Karyampudi, V. M. and H. F. Pierce, 2002: Synoptic-scale influence of the Saharan air layer on tropical cyclogenesis over the eastern Atlantic. *Mon. Wea. Rev.*, **130**, 3100–3128. [3, 5]

Kerns, B., K. Greene, and E. Zipser, 2008: Four years of tropical ERA-40 vorticity maxima tracks. Part I: Climatology and vertical vorticity structure. *Mon. Wea. Rev.*, **136**, 4301–4319. [38]

Kiladis, G. N., C. D. Thorncroft, and N. M. J. Hall, 2006: Three-dimensional structure and dynamics of African easterly waves. Part I: Observations. *J. Atmos. Sci.*, **63**, 2212–2230. [3, 5]

Kistler, R., et al., 2001: The NCEP-NCAR 50-year reanalysis: Monthly means CD-ROM and documentation. *Bull. Amer. Meteor. Soc.*, **82**, 247–267. [29]

Knapp, K. R., M. C. Kruk, D. H. Levinson, H. J. Diamond, and C. J. Neumann, 2010: The international best track archive for climate stewardship (IBTrACS). *Bull. Amer. Meteor. Soc.*, **91**, 363–376. [19, 44, 102, 177]

Knutson, T. R., J. J. Sirutis, S. T. Garner, I. M. Held, and R. E. Tuleya, 2007: Simulation of the recent multidecadal increase of Atlantic hurricane activity using an 18-km-grid regional model. *Bull. Amer. Meteor. Soc.*, **88**, 1549–1565. [1]

Knutson, T. R., J. J. Sirutis, S. T. Garner, G. A. Vecchi, and I. M. Held, 2008: Simulated reduction in Atlantic hurricane frequency under twenty-first-century warming conditions. *Nature Geos.*, **1**, 359–364. [17]

Knutson, T. R., R. E. Tuleya, and Y. Kurihara, 1998: Simulated increase of hurricane intensities in a CO_2-warmed climate. *Science*, **279**, 1018. [17]

Kossin, J. P., S. J. Camargo, and M. Sitkowski, 2010: Climate modulation of North Atlantic hurricane tracks. *J. Climate*, **23**, 3057–3076. [1, 12]

Kossin, J. P. and D. J. Vimont, 2007: A more general framework for understanding Atlantic hurricane variability and trends. *Bull. Amer. Meteor. Soc.*, **88**, 1767–1781. [85, 162]

Kruk, M. C., K. R. Knapp, and D. H. Levinson, 2010: A technique for combining global tropical cyclone best track data. *J. Atmos. Oceanic Technol.*, **27**, 680–692. [21, 44]

Kuettner, J. P., 1974: General description and central program of GATE. *Bull. Amer. Meteor. Soc.*, **55**, 712–719. [4, 176]

Kwon, H. J., 1989: A reexamination of the genesis of African waves. *J. Atmos. Sci.*, **46**, 3621–3631. [6]

Kwon, H. J. and M. Mak, 1990: A study of the structural transformation of the African easterly waves. *J. Atmos. Sci.*, **47**, 277–292. [11]

Landsea, C. W., 1993: A climatology of intense (or major) Atlantic hurricanes. *Mon. Wea. Rev.*, **121**, 1703–1713. [1]

Landsea, C. W. and E. S. Blake, 2014: Hurricane Humberto (AL092013) Tropical Cyclone Report. Tech. rep., National Hurricane Center. [45, 59]

Landsea, C. W. and W. M. Gray, 1992: The strong association between Western Sahelian monsoon rainfall and intense Atlantic hurricanes. *J. Climate*, **5**, 435–453. [14]

LaRow, T. E., Y.-K. Lim, D. W. Shin, E. P. Chassignet, and S. Cocke, 2008: Atlantic basin seasonal hurricane simulations. *J. Climate*, **21**, 3191–3206. [17]

Lau, K.-H. and N.-C. Lau, 1990: Observed structure and propagation characteristics of tropical summertime synoptic scale disturbances. *Mon. Wea. Rev.*, **118**, 1888–1913. [3, 5, 7, 8, 38, 55, 78, 87, 94]

Leroux, S. and N. M. J. Hall, 2009: On the relationship between African easterly waves and the African easterly jet. *J. Atmos. Sci.*, **66**, 2303–2316. [10, 96]

Leroux, S., N. M. J. Hall, and G. N. Kiladis, 2010: A climatological study of transient–mean-flow interactions over West Africa. *Quart. J. Roy. Meteor. Soc.*, **136**, 397–410. [5]

Leroux, S., N. M. J. Hall, and G. N. Kiladis, 2011: Intermittent African Easterly Wave activity in a dry atmospheric model: influence of the extratropics. *J. Climate*, **24**, 5378–5396. [10]

Manganello, J. V., et al., 2012: Tropical cyclone climatology in a 10-km global atmospheric GCM: Toward weather-resolving climate modeling. *J. Climate*, **25**, 3867–3893. [17]

Mass, C., 1979: A linear primitive equation model of African wave disturbances. *J. Atmos. Sci.*, **36**, 2075–2092. [6]

Matthews, A. J., 2004: Intraseasonal variability over tropical African during northern summer. *J. Climate*, **17**, 2427–2440. [5]

McGauley, M. G. and D. S. Nolan, 2011: Measuring environmental favorability for tropical cyclogenesis by statistical analysis of threshold parameters. *J. Climate*, **24**, 5968–5997. [37, 53, 54]

Mekonnen, A., C. D. Thorncroft, and A. R. Aiyyer, 2006: Analysis of convection and its association with African easterly waves. *J. Climate*, **19**, 5405–5421. [3, 5, 10]

Murakami, H., R. Mizuta, and E. Shindo, 2012: Future changes in tropical cyclone activity projected by multi-physics and multi-SST ensemble experiments using the 60-km-mesh MRI-AGCM. *Clim. Dynam.*, **39**, 2569–2584. [17]

NHC Data Archive, 2014: Tropical cyclone reports. *National Hurricane Center*, http://www.nhc.noaa.gov/data/. [55, 60]

Nicholson, S. E., 2009: A revised picture of the structure of the monsoon and land ITCZ over West Africa. *Clim. Dynam.*, **32**, 1155–1171. [142]

Nicholson, S. E. and J. P. Grist, 2001: A conceptual model for understanding rainfall variability in the West African Sahel on interannual and interdecadal timescales. *Int. J. Climatol.*, **21**, 1733–1757. [99, 142, 145]

Nicholson, S. E., C. J. Tucker, and M. B. Ba, 1998: Desertification, drought, and surface vegetation: An example from the West African Sahel. *Bull. Amer. Meteor. Soc.*, **79**, 815–829. [146]

Nitta, T. and Y. Takayabu, 1985: Global analysis of the lower tropospheric disturbances in the tropics during the northern summer of the FGGE year. Part II: Regional characteristics of the disturbances. *Pure Appl. Geophys.*, **123**, 272–292. [3, 5, 7, 9]

NOAA/NWS Cold and Warm Episodes by Season, 2014: Historical El Niño/La Niña episodes. *Climate Prediction Center*, http://www.cpc.ncep.noaa.gov/products/analysis_monitoring/ensostuff/ensoyears.shtml. [31, 177, 178]

Norquist, D. C., E. E. Recker, and R. J. Reed, 1977: The energetics of African wave disturbances as observed during phase III of GATE. *Mon. Wea. Rev.*, **105**, 334–342. [3, 4, 9]

Oouchi, K., J. Yoshimura, H. Yoshimura, R. Mizuta, S. Kusunoki, and A. Noda, 2006: Tropical cyclone climatology in a global-warming climate as simulated in a 20 km-mesh global atmospheric model: Frequency and wind intensity analyses. *J. Meteor. Soc. Japan*, **84**, 259–276. [17]

Paradis, D., J. P. Lafore, J. L. Redelsperger, and V. Balaji, 1995: African easterly waves and convection. I: Linear simulations. *J. Atmos. Sci.*, **52**, 1657–1679. [6, 10]

Peng, M. S., B. Fu, T. Li, and D. E. Stevens, 2011: Developing versus non-developing disturbances for tropical cyclone formation, Part I: North Atlantic. *Mon. Wea. Rev.*, **140**, 1047–1066. [3, 5, 12]

Pu, B. and K. H. Cook, 2012: Role of the West African westerly jet in Sahel rainfall variations. *J. Climate*, **25**, 2880–2896. [142]

Putman, W. M. and S. J. Lin, 2007: Finite-volume transport on various cubed-sphere grids. *J. Comput. Phys.*, **227**, 55–78. [30]

Pytharoulis, I. and C. Thorncroft, 1999: The low-level structure of African easterly waves in 1995. *Mon. Wea. Rev.*, **127**, 2266–2280. [3, 5, 8, 38]

Rayner, N. A., D. E. Parker, E. B. Horton, C. K. Folland, L. V. Alexander, D. P. Rowell, E. C. Kent, and A. Kaplan, 2003: Global analyses of sea surface temperature, sea ice, and night marine air temperature since the late nineteenth century. *J. Geophys. Res.*, **108**, 4407. [19, 20, 31, 32, 90, 176]

Reed, R. J., A. Hollingsworth, W. A. Heckley, and F. Delsol, 1988a: An evaluation of the performance of the ECMWF operational system in analyzing and forecasting easterly wave disturbances over Africa and the tropical Atlantic. *Mon. Wea. Rev.*, **116**, 824–865. [3, 5, 7, 38]

Reed, R. J., E. Klinker, and A. Hollingsworth, 1988b: The structure and characteristics of African easterly wave disturbances as determined from the ECMWF operational analysis/forecast system. *Meteor. Atmos. Phys.*, **38**, 22–33. [3, 5, 9]

Reed, R. J., D. C. Norquist, and E. E. Recker, 1977: The structure and properties of African wave disturbances as observed during phase III of GATE. *Mon. Wea. Rev.*, **105**, 317–333. [3, 4, 7, 8, 9]

Reed, R. J. and E. E. Recker, 1971: Structure and properties of synoptic-scale wave disturbances in the equatorial western Pacific. *J. Atmos. Sci.*, **28**, 1117–1133. [3]

Rennick, M. A., 1976: The generation of African waves. *J. Atmos. Sci.*, **33**, 1955–1969. [6]

Ross, R. S., 1991: Energetics of African wave disturbances derived from the FSU global spectral model. *Meteor. Atmos. Phys.*, **45**, 139–158. [7]

Ross, R. S. and T. N. Krishnamurti, 2007: Low-level African easterly wave activity and its relation to Atlantic tropical cyclogenesis in 2001. *Mon. Wea. Rev.*, **135**, 3950–3964. [3, 5, 7, 8, 9, 38]

Royer, J. F., F. Chauvin, B. Timbal, P. Araspin, and D. Grimal, 1998: A GCM study of the impact of greenhouse gas increase on the frequency of occurrence of tropical cyclones. *Climatic Change*, **38**, 307–343. [53]

Ryan, B. F., I. G. Watterson, and J. L. Evans, 1992: Tropical cyclone frequencies inferred from Gray's yearly genesis parameter: Validation of GCM tropical climates. *Geophys. Res. Lett.*, **19**, 1831–1834. [53]

Sall, S. M., H. Sauvageot, A. T. Gaye, A. Viltard, and P. de Felice, 2006: A cyclogenesis index for tropical Atlantic off the African coasts. *Atmos. Res.*, **79**, 123–147. [52]

Satoh, M., et al., 2011: The intra-seasonal oscillation and its control of tropical cyclones simulated by high-resolution global atmospheric models. *Clim. Dynam.*, **39**, 2185–2206. [17]

Schaaf, C. B., et al., 2002: First operational BRDF, albedo nadir reflectance products from MODIS. *Remote Sensing of Environment*, **83**, 135–148. [34, 35]

Schade, L. and K. Emanuel, 1999: The ocean's effect on the intensity of tropical cyclones: Results from a simple coupled atmosphere-ocean model. *J. Atmos. Sci.*, **56**, 642–651. [18]

Schenkel, B. A. and R. E. Hart, 2012: An examination of tropical cyclone position, intensity, and intensity life cycle within atmospheric reanalysis datasets. *J. Climate*, **25**, 3453–3475. [51]

Simmons, A. J., 1977: A note on the instability of the African easterly jet. *J. Atmos. Sci.*, **34**, 1670–1674. [6]

Snyder, A. D., Z. Pu, and Y. Zhu, 2010: Tracking and verification of East Atlantic tropical cyclone genesis in the NCEP global ensemble: Case studies during the NASA African monsoon multidisciplinary analyses. *Wea. Forecasting*, **25**, 1397–1411. [38]

Sugi, M., H. Murakami, and J. Yoshimura, 2009: A reduction in global tropical cyclone frequency due to global warming. *SOLA*, **5**, 164–167. [17]

Thompson, R. M., S. W. Payne, E. E. Recker, and R. J. Reed, 1979: Structure and properties of synoptic-scale wave disturbances in the intertropical convergence zone of the eastern Atlantic. *J. Atmos. Sci.*, **36**, 53–72. [3, 4, 9]

Thorncroft, C. and K. Hodges, 2001: African easterly wave variability and its relationship to Atlantic tropical cyclone activity. *J. Climate*, **14**, 1166–1179. [2, 5, 6, 7, 12, 15, 16, 38, 39, 41, 62, 66, 67, 68, 70, 72, 73, 74, 75, 76, 78, 80, 81, 84, 86, 87, 88, 91, 169]

Thorncroft, C. D., 1995: An idealized study of African easterly waves. III: More realistic basic states. *Quart. J. Roy. Meteor. Soc.*, **121**, 1589–1614. [6, 7]

Thorncroft, C. D. and M. Blackburn, 1999: Maintenance of the African easterly jet. *Quart. J. Roy. Meteor. Soc.*, **125**, 763–786. [11]

Thorncroft, C. D., N. M. J. Hall, and G. N. Kiladis, 2008: Three-dimensional structure and dynamics of African easterly waves. Part III: Genesis. *J. Atmos. Sci.*, **65**, 3596–3607. [10]

Thorncroft, C. D. and B. J. Hoskins, 1994a: An idealized study of African easterly waves. I: A linear view. *Quart. J. Roy. Meteor. Soc.*, **120**, 953–982. [6, 7, 8, 10, 11]

Thorncroft, C. D. and B. J. Hoskins, 1994b: An idealized study of African easterly waves. II: A nonlinear view. *Quart. J. Roy. Meteor. Soc.*, **120**, 983–1015. [6, 10]

Thorncroft, C. D. and D. P. Rowell, 1998: Interannual variability of African wave activity in a general circulation model. *Int. J. Climatol.*, **18**, 1305–1323. [3, 6, 14, 38, 78, 87, 94, 142]

Thorncroft, C. D., et al., 2003: The JET2000 project: Aircraft observations of the African easterly jet and African easterly waves. *Bull. Amer. Meteor. Soc.*, **84**, 337–351. [5]

Tippett, M. K., S. J. Camargo, and A. H. Sobel, 2011: A Poisson regression index for tropical cyclone genesis and the role of large-scale vorticity in genesis. *J. Climate*, **24**, 2335–2357. [37, 52, 54, 55]

Trenberth, K. E., D. P. Stepaniak, J. W. Hurrell, and M. Fiorino, 2001: Quality of reanalyses in the tropics. *J. Climate*, **14**, 1499–1510. [29, 49]

Uppala, S. M., et al., 2005: The ERA-40 re-analysis. *Quart. J. Roy. Meteor. Soc.*, **131**, 2961–3012. [68, 176]

Ventrice, M. J., C. D. Thorncroft, and P. E. Roundy, 2011: The Madden-Julian oscillation's influence on African easterly waves and downstream tropical cyclogenesis. *Mon. Wea. Rev.*, **139**, 2704–2722. [5, 14, 38]

Vitart, F., 2006: Seasonal forecasting of tropical storm frequency using a multi-model ensemble. *Quart. J. Roy. Meteor. Soc.*, **132**, 647–666. [17]

Vitart, F., J. L. Anderson, and W. F. Stern, 1997: Simulation of interannual variability of tropical storm frequency in an ensemble of GCM integrations. *J. Climate*, **10**, 745–760. [17]

Waliser, D. E., K. M. Lau, and J.-H. Kim, 1999: The influence of coupled sea surface temperatures on the Madden-Julian oscillation: A model perturbation experiment. *J. Atmos. Sci.*, **56**, 333–358. [18]

Walsh, K. J. E., M. Fiorino, C. W. Landsea, and K. L. McInnes, 2007: Objectively determined resolution-dependent threshold criteria for the detection of tropical cyclones in climate models and reanalyses. *J. Climate*, **20**, 2307–2314. [18, 44]

Xie, P. and P. A. Arkin, 1997: Global precipitation: A 17-year monthly analysis based on gauge observations, satellite estimates, and numerical model outputs. *Bull. Amer. Meteor. Soc.*, **78**, 2539–2558. [29]

Zangvil, A., 1977: On the presentation and interpretation of spectra of large-scale disturbances. *Mon. Wea. Rev.*, **105**, 1469–1472. [56]

Zawislak, J. and E. J. Zipser, 2010: Observations of seven African easterly waves in the east Atlantic during 2006. *J. Atmos. Sci.*, **67**, 26–43. [3, 11, 38]

Zhao, M. and I. M. Held, 2012: TC-permitting GCM simulations of hurricane frequency response to sea surface temperature anomalies projected for the late-twenty-first century. *J. Climate*, **25**, 2995–3009. [22, 23]

Zhao, M., I. M. Held, and S.-J. Lin, 2012: Some counter-intuitive dependencies of tropical cyclone frequency on parameters in a GCM. *J. Atmos. Sci.*, **69**, 2272–2283. [19, 30, 31, 40, 42]

Zhao, M., I. M. Held, S.-J. Lin, and G. A. Vecchi, 2009: Simulations of global hurricane climatology, interannual variability, and response to global warming using a 50-km resolution GCM. *J. Climate*, **22**, 6653–6678. [19, 20, 21, 22, 23, 30, 31, 40, 42, 103]

Zhao, M., I. M. Held, and G. A. Vecchi, 2010: Retrospective forecasts of the hurricane season using a global atmospheric model assuming persistence of SST anomalies. *Mon. Wea. Rev.*, **138**, 3858–3868. [22, 23]

Zipser, E., et al., 2009: The Saharan air layer and the fate of African easterly waves: NASA's AMMA field study of tropical cyclogenesis. *Bull. Amer. Meteor. Soc.*, **90**, 1137–1156. [5, 11, 177]